THE IMPLEMENTATION OF PHOTON POLARIZATION INTO THE MERCURY TRANSPORT CODE

A Thesis

by

ETHAN CHARLES WINDSOR

Submitted to the Office of Graduate and Professional Studies of
Texas A&M University
in partial fulfillment of the requirements for the degree of

MASTER OF SCIENCE

Chair of Committee,	Marvin Adams
Committee Members,	Patrick Brantley
	Ryan McClarren
	George Kattawar
Head of Department,	Yassin Hassan

August 2014

Major Subject: Nuclear Engineering

ABSTRACT

Polarization effects have been ignored in most photon transport codes to date, but new technology has created a need for portable, massively parallel, versatile transport codes that include the effects of polarization. In this project, the effects of both linear and elliptic polarization on the angular distribution of coherently and incoherently scattered photons are incorporated into the Monte Carlo transport code Mercury. In Mercury, photons are given a polarization fraction, polarization direction, and a polarization ellipticity. These new variables are tracked throughout each particle's history. They impact and are impacted by interactions with the medium. The determination of how these variables affect the photon's interactions with the medium uses Stokes vectors and the Mueller matrices for coherent and incoherent scattering events. Verification studies were performed comparing results from Mercury against analytical, experimental, and computational results. In all cases, Mercury showed agreement with the expected results. It was also shown that polarization effects are present and potentially significant even in cases where an initial beam is completely unpolarized. Adding polarization effects slowed the code between 10-50% depending on the particular problem. Mercury can now accurately model polarized light.

ACKNOWLEDGEMENTS

I would like to thank several people for their assistance with this project and my college career as a whole. I would like to thank my chair Dr. Adams, who provided me with guidance and direction. I would also like to thank the other members of my committee: Dr. Brantley, Dr. Kattawar, and Dr. McClarren. Next, I would like to thank my fellow classmates for all of the assistance they've given me over the years. Lastly I would like to thank my friends and family for all of their support and for making my college experience an enjoyable one.

TABLE OF CONTENTS

Page

LIST OF FIGURES

Page

LIST OF TABLES

Page

CHAPTER I

INTRODUCTION

Electromagnetic radiation is characterized by a travelling wave in the electric and magnetic fields. The orientation of the electric field vector as it travels through time and space defines the polarization of the wave. The polarization state of a photon can have a significant effect on the way it interacts with matter—largely in the angular distribution of scattering events. An unpolarized beam consists of photons with a random distribution of polarization states, so the polarization effects of each individual photon are averaged out over the whole beam. However, a polarized beam consists, at least partly, of photons with the same polarization state. Because of this, the polarization effects are visible and can be significant.

Few radiation transport codes that treat x-rays and gammas consider the effects of polarization. Treating all photons as unpolarized has been sufficient for most applications in the past. However, with the development of new technologies in photon generation, imaging, and detection, polarization effects have become important even in some applications involving MeV-range photons.

The initial motivation for this project was the development and application of MEGa-ray (Mono Energetic Gamma-ray) sources, which has been pioneered at LLNL (Lawrence Livermore National Lab). This new technology can produce polarized gamma rays in a narrow, tunable energy range, which could be used to identify specific radionuclides by tuning the beam to a specific nuclear resonance frequency. However,

since the beam is polarized, any computer simulation that wishes to accurately model these MEGa-rays must model polarized photon beams.

The objectives of this study are to investigate past research on polarization effects on radiation transport and to implement the known physics into Mercury, a Monte Carlo transport code developed at LLNL. Monte Carlo methods simulate individual histories of many particles using random numbers and statistical distributions. If enough particles are simulated, the average behavior of the simulated particles will be indicative of that in the simulated system.

CHAPTER II

LITERATURE REVIEW

In 1852, Stokes [1] defined four parameters that are needed to fully characterize the polarization state of a beam of light. Those parameters were expressed in a geometrical notation by van de Hulst [2] and are given below.

$$\overrightarrow{S_S} = \begin{bmatrix} I \\ Q \\ U \\ V \end{bmatrix} = \begin{bmatrix} I \\ I\,P\,cos2\beta\,cos2\chi \\ I\,P\,cos2\beta\,sin2\chi \\ I\,P\,sin2\beta \end{bmatrix}; \qquad \text{Eq. 1}$$

where I is the intensity of the beam and has units of power per unit area, P is a unitless number between 0 and 1 that describes the fraction of the beam that is polarized, and χ and β are angles defined by the picture below.

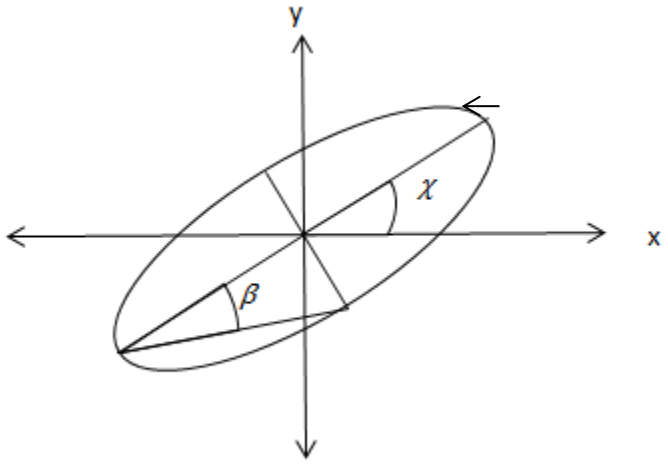

Figure 1. A diagram displaying the definition of angles χ and β. The z-axis is along the direction of photon travel (out of the paper), and the choice of the x-axis is arbitrary. The ellipse in the figure depicts the path traced out by the electric field vector of a photon as

it travels in the positive z-direction. In the case of a linearly polarized beam, β is 0, and therefore V is also 0. In the case of a circularly polarized beam, β is π/4 and Q=U=0.

Elliptical polarization can be referred to as right-handed or left-handed depending on which way the electric field vector rotates. Right-handed corresponds to a positive value of β. There are conflicting conventions defining handedness though. Typically the engineering community uses the convention that handedness is determined by pointing the thumb on the right or left hand in the same direction as the wave is travelling, and matching the curl of the fingers to the direction of rotation of the electric field vector [3]. In other words by this convention, the polarization ellipse described in Figure 1 would be right-handed and β would be positive. The optics community typically uses the opposite convention where the thumb would point anti-parallel to the travelling wave [4]. By this convention, Figure 1 describes a left-handed polarization and β would be negative. In this project, the first convention will be used.

J.E. Fernandez and J.H. Hubbel [5] describe polarization effects on multiple scattering events. They focus on the difference between the scalar transport equation and the vector transport equation. The steady state scalar transport equation is given below [6].

$$\vec{\Omega} \cdot \vec{\nabla} I(\vec{r}, \vec{\Omega}, E) + \sigma_t I(\vec{r}, \vec{\Omega}, E) = \int_0^\infty dE' \int_{4\pi} d\Omega' \, \sigma_s(\vec{\Omega}', \vec{\Omega}, E', E) I(\vec{r}, \vec{\Omega}', E') + \Gamma(\vec{r}, \vec{\Omega}, E) \quad \text{Eq. 2}$$

where σ_t is the total photon opacity, $\sigma_s(\vec{\Omega}', \vec{\Omega}, E', E)$ is the scattering kernel, Γ is a source term, and I now has units of power per unit area per unit solid angle.

The vector transport equation is similar to the scalar transport equation except the intensity and source terms are replaced by four-vectors. Each element in these vectors corresponds to a Stokes parameter. The scattering kernel is also replaced with a kernel matrix. The vector transport equation is given below [7].

$$\vec{\Omega}\cdot\vec{\nabla}\boldsymbol{I}(\vec{r},\vec{\Omega},E)+\ \sigma_t\boldsymbol{I}(\vec{r},\vec{\Omega},E)$$

$$=\int_0^\infty dE'\int_{4\pi}d\Omega'\,\boldsymbol{H}(\vec{\Omega}',\vec{\Omega},E',E)\boldsymbol{I}(\vec{r},\vec{\Omega}',E')\ +\ \boldsymbol{\Gamma}(\vec{r},\vec{\Omega},E) \qquad \text{Eq. 3}$$

where $\boldsymbol{I}$ and $\boldsymbol{\Gamma}$ are defined below.

$$\boldsymbol{I}=\begin{bmatrix}I\\Q\\U\\V\end{bmatrix} \qquad \text{Eq. 4}$$

$$\boldsymbol{\Gamma}=\begin{bmatrix}\Gamma_I\\\Gamma_Q\\\Gamma_U\\\Gamma_V\end{bmatrix} \qquad \text{Eq. 5}$$

The kernel matrix $\boldsymbol{H}$ is defined by the expression below.

$$\boldsymbol{H}(\vec{\Omega}',\vec{\Omega},E',E)=\boldsymbol{L}(-\Psi)\boldsymbol{M}(\vec{\Omega}',\vec{\Omega},E',E)\boldsymbol{L}(-\Psi'), \qquad \text{Eq. 6}$$

where $\boldsymbol{L}$ is a rotation matrix defined as

$$\boldsymbol{L}(a)=\begin{bmatrix}1&0&0&0\\0&\cos(2a)&\sin(2a)&0\\0&-\sin(2a)&\cos(2a)&0\\0&0&0&1\end{bmatrix}. \qquad \text{Eq. 7}$$

This rotation matrix rotates the vector $\boldsymbol{I}$ by angle a in the counterclockwise direction when looking along the direction of the beam. The Mueller matrix, $\boldsymbol{M}$, operates in the plane formed by the incident and scattered photon direction vectors (scattering

plane), so $\boldsymbol{L}$ is needed to rotate the vector $\boldsymbol{I}$ from the local meridian plane to the scattering plane and then back again after the transformation. The Mueller matrix is dependent on the characteristics of the photon, the target, and the type of interaction. The elements of $\boldsymbol{M}$ for a general scattering interaction with a single atom can be seen below.

$$\boldsymbol{M}_{(scat)}\left(\vec{\Omega}',\vec{\Omega},E',E\right)=\left(\frac{\sigma_s\left(\vec{\Omega}',\vec{\Omega},E',E\right)}{\frac{E}{E'}+\frac{E'}{E}+\left(\vec{\Omega}\cdot\vec{\Omega}'\right)^2-1}\right)\times$$

$$\begin{bmatrix}\frac{E}{E'}+\frac{E'}{E}+\left(\vec{\Omega}\cdot\vec{\Omega}'\right)^2-1 & \left(\vec{\Omega}\cdot\vec{\Omega}'\right)^2-1 & 0 & 0\\ \left(\vec{\Omega}\cdot\vec{\Omega}'\right)^2-1 & \left(\vec{\Omega}\cdot\vec{\Omega}'\right)^2+1 & 0 & 0\\ 0 & 0 & 2\left(\vec{\Omega}\cdot\vec{\Omega}'\right) & 0\\ 0 & 0 & 0 & \left(\frac{E}{E'}+\frac{E'}{E}\right)\left(\vec{\Omega}\cdot\vec{\Omega}'\right)\end{bmatrix} \quad \text{Eq. 8}$$

All primed quantities represent the incident photon and unprimed quantities represent the scattered photon. The function $\sigma_s\left(\vec{\Omega}',\vec{\Omega},E',E\right)$ is given in Eq. 9.

$$\sigma_s\left(\vec{\Omega}',\vec{\Omega},E',E\right)$$

$$=\begin{cases}\frac{1}{2}r_0^2\left(\frac{E}{E'}\right)^2 S(x,Z)\left(\frac{E}{E'}+\frac{E'}{E}+\left(\vec{\Omega}\cdot\vec{\Omega}'\right)^2-1\right), Incoherent,\\ \frac{1}{2}r_0^2F^2(x,Z)\left(1+\left(\vec{\Omega}\cdot\vec{\Omega}'\right)^2\right), Coherent.\end{cases} \quad \text{Eq. 9}$$

Here, r_0 is the classical electron radius, $S(x,Z)$ is the incoherent scattering function, $F(x,Z)$ is the atomic form factor, $x=\frac{E'}{hc}sin\left(\frac{\theta}{2}\right)$, θ is the polar scattering angle, and Z is the atomic number of the target atom. Tabulated values and analytic expressions for $S(x,Z)$ and $F(x,Z)$ can be found in a paper by Hubbell *et al.* [8]

The angles Ψ' and Ψ are the angles between the scattering plane and the meridian plane of the incident beam and outgoing beams, respectively, and they are found using the equations below.

$$\cos(\Psi') = \frac{\mu\sqrt{1-\mu'^2} - \mu'\sqrt{1-\mu^2}\cos(\phi-\phi')}{\sqrt{1-\left(\vec{\Omega}\cdot\vec{\Omega}'\right)^2}} \quad \text{Eq. 10}$$

$$\cos(\Psi) = \frac{\mu'\sqrt{1-\mu^2} - \mu\sqrt{1-\mu'^2}\cos(\phi-\phi')}{\sqrt{1-\left(\vec{\Omega}\cdot\vec{\Omega}'\right)^2}} \quad \text{Eq. 11}$$

Here μ is the cosine of the polar angle in spherical coordinates and φ is the azimuthal angle; both of these angles are measured in the lab frame. Fernandez [5] solves the vector transport equation in specific simplified cases and gives the Mueller matrices for several types of interactions including Compton and Rayleigh scattering.

Fernandez also described implementation of linear polarization effects into a Monte Carlo code [9]. One feature of photon polarization that is beneficial to implementing into a Monte Carlo code is that the polarization state of a photon does not affect the probability of a scattering interaction taking place; it affects only the angle at which the photon scatters. Even further, the polarization affects only the azimuthal angle of scattering. The polar angle of scattering is unchanged by the polarization state of the photon.

The reason this is so beneficial is because most existing Monte Carlo codes first sample the type of interaction, then if it is a scattering event, the code samples the polar scattering angle, and then it samples the azimuthal scattering angle. Since the polarization affects only one part of that process, the majority of the code can be left

unchanged. The only changes that need to be made are to the sampling of the azimuthal angle. If polarization is not included in the code, then the azimuthal angle is uniformly sampled. If polarization is included, then the way to sample that angle comes out of the kernel matrix operating on the Stokes vector.

One useful result that can be extracted out of this math is the differential scattering cross section for a scattering event. The differential scattering cross section can be found by dividing the first component of the Stokes vector after interaction by the original first component of the Stokes vector. This can be seen in Eq. 12-Eq. 15. With no loss of generality, the initial photon can be assumed to be traveling in the positive z-direction and the x-axis can be taken to point in the direction of the initial polarization vector. In this case $\mu' = 1$, $\phi' = 0$, and $\chi' = 0$.

$$\begin{bmatrix} I \\ Q \\ U \\ V \end{bmatrix} = \boldsymbol{H}_{(scat)} \begin{bmatrix} I_0 \\ Q_0 \\ U_0 \\ V_0 \end{bmatrix} = L(-\Psi) M_{(scat)} L(-\Psi') \begin{bmatrix} I_0 \\ I_0\, P_0\, cos2\beta'\, cos2\chi' \\ I_0\, P_0\, cos2\beta'\, sin2\chi' \\ I_0\, P_0\, sin2\beta' \end{bmatrix}$$

$$\xrightarrow[chosen\ axes]{} \boldsymbol{L}(0)\boldsymbol{M}_{(scat)}\boldsymbol{L}(\phi - \pi) \begin{bmatrix} I_0 \\ I_0\, P_0\, cos2\beta' \\ 0 \\ I_0\, P_0\, sin2\beta' \end{bmatrix}; \qquad \text{Eq. 12}$$

$$I = I_0 * \sigma_s\left(\vec{\Omega}', \vec{\Omega}, E', E\right)$$

$$\times \left[1 + \left(\frac{\left(\vec{\Omega} \cdot \vec{\Omega}'\right)^2 - 1}{\frac{E}{E'} + \frac{E'}{E} + \left(\vec{\Omega} \cdot \vec{\Omega}'\right)^2 - 1}\right) P_0\, cos2\beta' \cos(2\phi)\right] \qquad \text{Eq. 13}$$

$$= I_0 * \sigma_s\left(\vec{\Omega}', \vec{\Omega}, E', E\right)\left[1 + \left(\frac{-sin^2\theta}{\frac{E}{E'} + \frac{E'}{E} - sin^2\theta}\right) P_0\, cos2\beta'\, cos2\phi\right]$$

$$\left(\frac{d\sigma}{d\Omega}\right)_s = \frac{I}{I_0} = \sigma_s\left(\vec{\Omega}', \vec{\Omega}, E', E\right)\left[1 + \left(\frac{-sin^2\theta}{\frac{E}{E'} + \frac{E'}{E} - sin^2\theta}\right) P_0\, cos2\beta'\, cos2\phi\right] \quad \text{Eq. 14}$$

$$\left(\frac{d\sigma}{d\Omega}\right)_s = \frac{\sigma_s\left(\vec{\Omega}', \vec{\Omega}, E', E\right)}{\frac{E}{E'} + \frac{E'}{E} - sin^2\theta}\left[\frac{E}{E'} + \frac{E'}{E} + sin^2\theta(P_0\, cos2\beta'(1 - 2cos^2\phi) - 1)\right] \quad \text{Eq. 15}$$

Here, θ is the polar angle of scattering; it is the angle between the incident and outgoing photon's direction vectors, and ϕ is the azimuthal angle of scattering. The angles θ and ϕ in this case are in reference to the coordinate system defined by the photon's direction vector and the polarization vector. For any individual particle, as long as the direction vector, the polarization vector, θ, and ϕ are known then the outgoing direction vector can be calculated.

Carrying out the algebra further gives the following values for the rest of the Stokes parameters and the expressions for the new values of P, β, and χ.

$$Q = I_0[-sin^2\theta + P_0 cos2\beta' cos2\phi(cos^2\theta + 1)] \quad \text{Eq. 16}$$

$$U = -2I_0 P_0 cos\theta cos2\beta' sin2\phi \quad \text{Eq. 17}$$

$$V = \left(\frac{E}{E'} + \frac{E'}{E}\right) I_0 P_0 sin2\beta' \quad \text{Eq. 18}$$

$$P = \frac{\sqrt{Q^2 + U^2 + V^2}}{I} \quad \text{Eq. 19}$$

$$cos2\chi = \frac{Q}{\sqrt{Q^2 + U^2}} \quad \text{Eq. 20}$$

$$sin2\chi = \frac{U}{\sqrt{Q^2 + U^2}} \quad \text{Eq. 21}$$

$$cos2\beta = \frac{\sqrt{Q^2 + U^2}}{\sqrt{Q^2 + U^2 + V^2}} \quad \text{Eq. 22}$$

$$sin2\beta = \frac{V}{\sqrt{Q^2 + U^2 + V^2}} \quad \text{Eq. 23}$$

Several other Monte Carlo codes have been adapted to incorporate photon polarization [10][11][12][13], and it is from papers written on these topics that a large amount of the work for adapting Mercury is drawn. It is worth noting that all the implementations found to this point deal with only linearly polarized photons, whereas this project addresses the more general elliptically polarized photons.

The EGS4 [14] code is a general purpose Monte-Carlo electron-photon transport code. The predecessor, EGS3, was developed by SLAC [15] at Stanford for radiation transport-shower simulations. The SLAC team later joined with other researchers to produce EGS4, which was designed to be useful for medical-physics calculations in addition to the higher energy applications of EGS3. The code simulates the cascade phenomena caused by high energy electrons travelling through matter. Because photons are produced by electron decelerations and they in turn launch electrons, photons need to be properly modeled in most electron-transport calculations. Y. Namito [14] details how the polarization effects of photon interactions were incorporated into EGS4.

Namito does not deal with the Stokes parameters. Instead he deals solely with the Klein-Nishina formula [16].

$$\left(\frac{d\sigma}{d\Omega}\right)_{KN} = \frac{1}{4}r_0^2\left(\frac{E}{E'}\right)^2\left(\frac{E}{E'} + \frac{E'}{E} - 2 + 4(\vec{e}' \cdot \vec{e})^2\right) \quad \text{Eq. 24}$$

Here, r_0 is the classical electron radius, $\vec{e}'$ is the incident polarization vector and $\vec{e}$ is the scattered polarization vector. The scattered polarization vector can be decomposed into two components, $\vec{e_\parallel}$ and $\vec{e_\perp}$. $\vec{e_\parallel}$ lies in the plane formed by $\vec{e}'$ and $\vec{\Omega}$ and is perpendicular to $\vec{\Omega}$, and $\vec{e_\perp} = \vec{\Omega} \times \vec{e_\parallel}$. The formulas for $\vec{e_\parallel}$ and $\vec{e_\perp}$ are given below as functions of the spherical coordinates θ and ϕ for the case that $\vec{e}' = \vec{e_x}$ and $\vec{\Omega'} = \vec{e_z}$. No generality will be lost in the end result by assuming this case.

$$\vec{e_\parallel} = \left(\sqrt{cos^2\theta\, cos^2\phi + sin^2\phi}\right)\vec{e_x} - \left(\frac{sin^2\theta\, cos\phi\, sin\phi}{\sqrt{cos^2\theta\, cos^2\phi + sin^2\phi}}\right)\vec{e_y} - \left(\frac{cos\theta\, sin\theta\, cos\phi}{\sqrt{cos^2\theta\, cos^2\phi + sin^2\phi}}\right)\vec{e_z} \quad \text{Eq. 25}$$

$$\vec{e_\perp} = \left(\frac{cos\theta}{\sqrt{cos^2\theta\, cos^2\phi + sin^2\phi}}\right)\vec{e_y} - \left(\frac{sin\theta\, sin\phi}{\sqrt{cos^2\theta\, cos^2\phi + sin^2\phi}}\right)\vec{e_z} \quad \text{Eq. 26}$$

Eq. 24 can now be broken down into parallel and perpendicular components.

$$\left(\frac{d\sigma}{d\Omega}\right)_\parallel = \frac{1}{4}r_0^2\left(\frac{E}{E'}\right)^2\left(\frac{E}{E'} + \frac{E'}{E} - 2 + 4(cos^2\theta\, cos^2\phi + sin^2\phi)\right) = \frac{1}{4}r_0^2\left(\frac{E}{E'}\right)^2\left(\frac{E}{E'} + \frac{E'}{E} + 2 - 4sin^2\theta\, cos^2\phi\right) \quad \text{Eq. 27}$$

$$\left(\frac{d\sigma}{d\Omega}\right)_\perp = \frac{1}{4}r_0^2\left(\frac{E}{E'}\right)^2\left(\frac{E}{E'} + \frac{E'}{E} - 2\right) \quad \text{Eq. 28}$$

Adding Eq. 27 and Eq. 28 gives us the full differential cross section for a linearly polarized photon.

$$\left(\frac{d\sigma}{d\Omega}\right)_{KN} = \frac{1}{2}r_0^2\left(\frac{E}{E'}\right)^2\left(\frac{E}{E'} + \frac{E'}{E} - 2sin^2\theta\, cos^2\phi\right) \quad \text{Eq. 29}$$

It should be noted that in the general case, the angles θ and ϕ are with respect to the meridian reference frame and not the lab frame. Namito then shows that in the Thomson limit where $E = E'$, the differential cross section reduces to the equation below.

$$\left(\frac{d\sigma}{d\Omega}\right)_{T} = r_0^2(1 - sin^2\theta\, cos^2\phi) \quad \text{Eq. 30}$$

The Klein-Nishina equation deals with a scatter off of an unbound electron. In order to get the differential scattering cross section for bound electrons an incoherent scattering function needs to be introduced.

$$\left(\frac{d\sigma}{d\Omega}\right)_{Compton} = S(x, Z)\left(\frac{d\sigma}{d\Omega}\right)_{KN} \quad \text{Eq. 31}$$

$$\left(\frac{d\sigma}{d\Omega}\right)_{Rayleigh} = F^2(x, Z)\left(\frac{d\sigma}{d\Omega}\right)_{T} \quad \text{Eq. 32}$$

It should be noted that Eq. 31 and Eq. 32 agree with Eq. 15 in the specific case that $P_0 = 1$ and $\beta = 0$, which corresponds to the fully linearly polarized photon that Namito was dealing with.

Eq. 31 and Eq. 32 can be used to sample the direction of the scattered photon using rejection sampling. Namito discusses how he deals with the polarization state of the scattered photon. In Namito's routine, every photon is fully polarized. He represents an unpolarized beam by uniformly sampling the polarization vector of each individual photon. This is what physically makes up an unpolarized beam in reality. When a

polarized photon scatters it may become depolarized. If the photon remains polarized then the new polarization vector will be the unit vector described by Eq. 25. If the photon is depolarized, then the new polarization vector is randomly selected from the plane perpendicular to the photon's direction of travel.

The depolarization probability, (1-P), is found by dividing Eq. 28 by Eq. 29.

$$(1-P) = \left(\frac{d\sigma}{d\Omega}\right)_{\perp} \Big/ \left(\frac{d\sigma}{d\Omega}\right)_{KN} = \frac{\frac{E}{E'} + \frac{E'}{E} - 2}{\frac{E}{E'} + \frac{E'}{E} - 2sin^2\theta\, cos^2\phi} \qquad \text{Eq. 33}$$

Namito then compares the results of his modification to the EGS4 code to a benchmark experiment performed with a linearly polarized photon source. His simulation results show reasonable agreement with the experimental results [17]. Figure 2 below shows the setup and the results from this experiment.

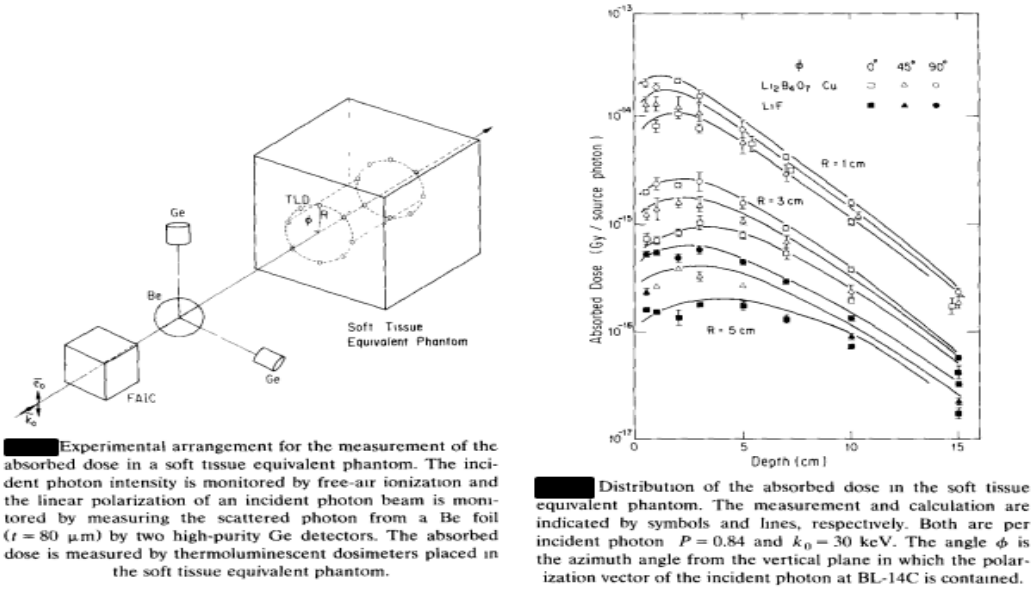

Experimental arrangement for the measurement of the absorbed dose in a soft tissue equivalent phantom. The incident photon intensity is monitored by free-air ionization and the linear polarization of an incident photon beam is monitored by measuring the scattered photon from a Be foil ($t = 80$ μm) by two high-purity Ge detectors. The absorbed dose is measured by thermoluminescent dosimeters placed in the soft tissue equivalent phantom.

Distribution of the absorbed dose in the soft tissue equivalent phantom. The measurement and calculation are indicated by symbols and lines, respectively. Both are per incident photon $P = 0.84$ and $k_0 = 30$ keV. The angle ϕ is the azimuth angle from the vertical plane in which the polarization vector of the incident photon at BL-14C is contained.

Figure 2. The experimental setup and the results from the validation experiment performed by Namito *et al.*

Giorgio Matt [18] goes into great detail about the implementation of the polarization physics into a computational model, and his writing is useful for a general outline of the procedure to follow; however, the way he deals with partially polarized beams is not as efficient as the way that it is dealt with by Fernandez [7]. Matt's model is similar to the model described by Namito except he does not go into as much detail on the derivation of the differential cross section. He does not use the Stokes parameters in his code; instead, he stores the polarization vector. This is similar to how Mercury will model polarization, but Matt treats photons as either completely linearly polarized or completely unpolarized. The unpolarized fraction of a beam will have polarization vectors that point in random directions in the plane perpendicular to the direction of travel.

Even though this is physically what is taking place it causes a problem because in order to properly represent the unpolarized portion of the beam a large number of particles must be simulated. A more efficient way of modeling partially polarized photon is to treat each photon itself as partially polarized and to use a weighted average of its distribution of outcomes. This is the approach that Fernandez uses and it is the approach that will be used in Mercury. Although it was Matt's intention to get his work incorporated into newer versions of MCNP, the current versions of MCNP still do not include polarization effects [19].

CHAPTER III

METHODOLOGY

Mercury is a general-purpose Monte Carlo radiation transport code developed at LLNL. It is a massively parallel code written in C++ and is intended to be the next generation transport code for the lab [20]. The code uses a collision kinematics library called MCAPM to perform the nuclear reaction physics [21]. MCAPM was not altered in this project because the effects of polarization do not change the inputs or outputs of MCAPM.

Including polarization physics into the code requires additional information to be calculated after MCAPM has completed its task. Mercury works by tracking a particle through a particular geometry and sampling when a reaction will take place. After Mercury determines a reaction will take place it sends MCAPM the information about the particle and the target atoms in the cell. MCAPM then returns the type of interaction, the properties of any resulting particles, the isotope with which the interaction occurs, and, in the event of a scatter, the polar angle of scattering. Because Mercury only concerned itself with unpolarized transport before, there was no need to return an azimuthal angle of scattering because it could just be uniformly sampled from $[0, 2\pi]$. Sampling an azimuthal angle based on the polarization state of the photon is where the majority of the changes in the physics package of the code were required by this project.

It is important to note that Mercury does not store the Stokes parameters of each particle. Instead the modified code stores the three components of a unit polarization

vector, a polarization fraction variable, and the variable β explained in Chapter II. Because the polarization vector is a unit vector, it would be possible to represent it with only two numbers instead of its three Cartesian components. However, the Cartesian components are convenient and the additional number is not a significant storage burden.

After MCAPM returns the type of interaction, the polar angle of scattering, and the outgoing particle's energy, Eq. 15 is used to sample the azimuthal angle of scattering. In particular only the bracketed portion of Eq. 15 is needed since it is the only portion that has a dependency on ϕ. Since MCAPM already returns the type of interaction and the polar angle of scattering and β is known beforehand, the equation has only one unknown, ϕ, and it can be easily and efficiently sampled through the rejection technique. The rejection technique is efficient for this distribution because the lowest efficiency scenario takes place when $P_0 = 1$, $\beta' = 0$, and $\theta = 90°$, which corresponds to an efficiency of 0.50. Another method that could be implemented at a later date is to uniformly sample ϕ, but alter the weight of each particle according to the probability of each particle's value of ϕ.

After the scattering angles are known, the new direction vector can be calculated. The geometry is easier to understand if the new direction vector is first calculated in terms of the old direction vector ($\vec{\Omega}'$), the old polarization vector ($\vec{e'}$), and the cross product of the two ($\vec{\Omega}' \times \vec{e'}$). This intermediate step is useful because the scattering angles are in reference to this coordinate system. Recall that $cos\theta = \vec{\Omega}' \cdot \vec{\Omega}$, and that ϕ

is the angle between $\overrightarrow{e'}$ and the scattering plane. Eq. 34 gives the new direction vector ($\vec{\Omega}$) in terms of ($\vec{\Omega}'$), ($\overrightarrow{e'}$), ($\vec{\Omega}' \times \overrightarrow{e'}$), θ, and ϕ.

$$\vec{\Omega} = cos\theta\ \vec{\Omega}' + sin\theta cos\phi\ \overrightarrow{e'} + \ sin\theta sin\phi\ (\vec{\Omega}' \times \overrightarrow{e'}) \qquad \text{Eq. 34}$$

Eq. 34 can be expanded into three equations that give the x, y, and z components of $\vec{\Omega}$ in the global reference frame. These are the three variables stored by the code for the direction of the outgoing particle.

$$\Omega_x = cos\theta\ \Omega'_x + sin\theta cos\phi\ e'_x + \ sin\theta sin\phi\ (\Omega'_y e'_z - \ \Omega'_z e'_y) \qquad \text{Eq. 35}$$

$$\Omega_y = cos\theta\ \Omega'_y + sin\theta cos\phi\ e'_y + \ sin\theta sin\phi\ (\Omega'_z e'_x - \ \Omega'_x e'_z) \qquad \text{Eq. 36}$$

$$\Omega_z = cos\theta\ \Omega'_z + sin\theta cos\phi\ e'_z + \ sin\theta sin\phi\ (\Omega'_x e'_y - \ \Omega'_y e'_x) \qquad \text{Eq. 37}$$

The next step in the implementation is to calculate P using Eq. 16-Eq. 19. This is a straightforward calculation and requires no geometrical transformations or rotations. Then using Eq. 16-Eq. 21, χ can be calculated. Eq. 38 shows how to calculate χ from the values of $cos2\chi$ and $sin2\chi$.

$$if\ sin2\chi > 0, then\ \chi = \frac{acos[cos2\chi]}{2},$$
$$if\ sin2\chi < 0, then\ \chi = -\frac{acos[cos2\chi]}{2}, \qquad \text{Eq. 38}$$

Calculating the new polarization vector requires more complicated geometry. The components for the new polarization vector need to be expressed in terms of θ, ϕ, χ, and properties of the incident particle. The first step is to create a set of orthonormal unit vectors that describe the reference frame characterized by the new direction vector and the scattering plane. Obviously the first unit vector will simply be the new direction

vector ($\vec{\Omega}$). The next unit vector must be perpendicular to the scattering plane and the new direction vector. This unit vector will be called $\vec{\eta}$ and is characterized by Eq. 39.

$$\vec{\eta} = \frac{\vec{\Omega}' \times \vec{\Omega}}{\left|\vec{\Omega}' \times \vec{\Omega}\right|} = \frac{\vec{\Omega}' \times \vec{\Omega}}{sin\theta} \quad \text{Eq. 39}$$

Eq. 40-Eq. 45 go through the algebra for calculating the x-component of $\vec{\eta}$.

$$\eta_x = \frac{\Omega'_y \Omega_z - \Omega'_z \Omega_y}{sin\theta} \quad \text{Eq. 40}$$

$$\eta_x = \frac{1}{sin\theta}\left[\Omega'_y\left(cos\theta\ \Omega'_z + sin\theta cos\phi\ e'_z + sin\theta sin\phi\ \left(\Omega'_x e'_y - \Omega'_y e'_x\right)\right)\right. \quad \text{Eq. 41}$$
$$\left. -\Omega'_z\left(cos\theta\ \Omega'_y + sin\theta cos\phi\ e'_y + sin\theta sin\phi\ (\Omega'_z e'_x - \Omega'_x e'_z)\right)\right]$$

$$\eta_x = cos\phi\left(\Omega'_y e'_z - \Omega'_z e'_y\right) \quad \text{Eq. 42}$$
$$- sin\phi\ \left(e'_x\left(\Omega'^2_y + \Omega'^2_z\right) - \Omega'_x\left(\Omega'_y e'_y + \Omega'_z e'_z\right)\right)$$

$$\eta_x = cos\phi\left(\vec{\Omega'} \times \vec{e'}\right)_x - sin\phi\ \left(\left(\Omega'^2_y + \Omega'^2_z + \Omega'^2_x\right)e'_x\right. \quad \text{Eq. 43}$$
$$\left. -\ \Omega'_x\left(\Omega'_y e'_y\ +\ \Omega'_z e'_z + \Omega'_x e'_x\right)\right)$$

$$\eta_x = \left[cos\phi\left(\vec{\Omega'} \times \vec{e'}\right)_x - sin\phi\ \left(e'_x - \Omega'_x\left(\vec{\Omega'} \cdot \vec{e'}\right)\right)\right] \quad \text{Eq. 44}$$

$$\eta_x = \left[cos\phi\left(\vec{\Omega'} \times \vec{e'}\right)_x - sin\phi\ e'_x\right] \quad \text{Eq. 45}$$

Eq. 45 can be generalized to give the equation for $\vec{\eta}$.

$$\vec{\eta} = cos\phi\left(\vec{\Omega}' \times \vec{e'}\right) + sin\phi\ \vec{e'} \quad \text{Eq. 46}$$

Now the last unit vector needs to be determined. This last unit vector ($\vec{\gamma}$) will lie within the scattering plane and be perpendicular to $\vec{\Omega}$. Eq. 47-Eq. 53 will go through the algebra for the x-component of $\vec{\gamma}$.

$$\vec{\gamma} = \vec{\eta} \times \vec{\Omega} \quad \text{Eq. 47}$$

$$\gamma_x = \eta_y \Omega_z - \eta_z \Omega_y \quad \text{Eq. 48}$$

$$\begin{aligned}\gamma_x = {} & \left[\left(cos\phi(\Omega'_z e'_x - \Omega'_x e'_z) - sin\phi\, e'_y\right)\left(cos\theta\, \Omega'_z + sin\theta cos\phi\, e'_z\right.\right. \\ & \left.\left. + sin\theta sin\phi\, (\Omega'_x e'_y - \Omega'_y e'_x)\right)\right] \\ & - \left[\left(cos\phi\left(\Omega'_x e'_y - \Omega'_y e'_x\right) - sin\phi\, e'_z\right)\left(cos\theta\, \Omega'_y\right.\right. \\ & \left.\left. + sin\theta cos\phi\, e'_y + sin\theta sin\phi\, (\Omega'_z e'_x - \Omega'_x e'_z)\right)\right]\end{aligned} \quad \text{Eq. 49}$$

$$\begin{aligned}\gamma_x = cos\theta\Big[cos\phi\Big(e'_x\left(\Omega'^2_z + \Omega'^2_y\right) - \Omega'_x(\Omega'_y e'_y + \Omega'_z e'_z)\Big) + sin\phi(\Omega'_y e'_z \\ - \Omega'_z e'_y)\Big] - sin\theta\Big[cos^2\phi\left(\left(e'^2_z + e'^2_y\right)\Omega'_x\right. \\ \left. - e'_x(\Omega'_y e'_y + \Omega'_z e'_z)\right) + sin^2\phi\left(\left(e'^2_z + e'^2_y\right)\Omega'_x\right. \\ \left. - e'_x(\Omega'_y e'_y + \Omega'_z e'_z)\right)\Big]\end{aligned} \quad \text{Eq. 50}$$

$$\begin{aligned}\gamma_x = cos\theta\Big[cos\phi\left(e'_x\left(\Omega'^2_z + \Omega'^2_y + \Omega'^2_x\right)\right. \\ \left. - \Omega'_x\left(\Omega'_y e'_y + \Omega'_z e'_z + \Omega'_x e'_x\right)\right) + sin\phi\left(\overrightarrow{\Omega'} \times \overrightarrow{e'}\right)_x\Big] \\ - sin\theta\left[\Omega'_x\left(e'^2_z + e'^2_y + e'^2_x\right) - e'_x(\Omega'_y e'_y + \Omega'_z e'_z\right. \\ \left. + \Omega'_x e'_x)\right]\end{aligned} \quad \text{Eq. 51}$$

$$\begin{aligned}\gamma_x = cos\theta\left[cos\phi\left(e'_x - \Omega'_x(\overrightarrow{\Omega'} \cdot \overrightarrow{e'})\right) + sin\phi\left(\overrightarrow{\Omega'} \times \overrightarrow{e'}\right)_x\right] \\ - sin\theta\left[\Omega'_x - e'_x(\overrightarrow{\Omega'} \cdot \overrightarrow{e'})\right]\end{aligned} \quad \text{Eq. 52}$$

$$\gamma_x = cos\theta cos\phi e'_x + cos\theta sin\phi\left(\overrightarrow{\Omega'} \times \overrightarrow{e'}\right)_x - sin\theta\, \Omega'_x \quad \text{Eq. 53}$$

Now Eq. 53 can be generalized to give an expression for $\vec{\gamma}$

$$\vec{\gamma} = cos\theta cos\phi\overrightarrow{e'} + cos\theta sin\phi\left(\overrightarrow{\Omega'} \times \overrightarrow{e'}\right) - sin\theta\overrightarrow{\Omega'} \quad \text{Eq. 54}$$

With the orthonormal set of unit vectors $\vec{\gamma}, \vec{\eta}$, and $\vec{\Omega}$, the new polarization vector can be expressed.

$$\vec{e} = cos\chi\,\vec{\gamma} + sin\chi\vec{\eta} \quad \text{Eq. 55}$$

$$\vec{e} = cos\chi\,\left(cos\theta cos\phi\overrightarrow{e'} + cos\theta sin\phi\left(\vec{\Omega}' \times \overrightarrow{e'}\right) - sin\theta\vec{\Omega}'\right) \quad \text{Eq. 56}$$

$$+ sin\chi\left(cos\phi\left(\vec{\Omega}' \times \overrightarrow{e'}\right) - sin\phi\,\overrightarrow{e'}\right)$$

$$\vec{e} = -sin\theta cos\chi\vec{\Omega}' + \,(cos\theta cos\phi cos\chi - sin\phi sin\chi\,)\,\overrightarrow{e'} \quad \text{Eq. 57}$$

$$+ (cos\theta sin\phi cos\chi + cos\phi sin\chi)\left(\vec{\Omega}' \times \overrightarrow{e'}\right)$$

$$e_x = -sin\theta cos\chi\Omega'_x + \,(cos\theta cos\phi cos\chi - sin\phi sin\chi\,)e'_x \quad \text{Eq. 58}$$

$$+ (cos\theta sin\phi cos\chi + cos\phi sin\chi)\left(\Omega'_y e'_z - \Omega'_z e'_y\right)$$

$$e_y = -sin\theta cos\chi\Omega'_y + \,(cos\theta cos\phi cos\chi - sin\phi sin\chi\,)e'_y \quad \text{Eq. 59}$$

$$+ (cos\theta sin\phi cos\chi + cos\phi sin\chi)(\Omega'_z e'_x - \Omega'_x e'_z)$$

$$e_z = -sin\theta cos\chi\Omega'_z + \,(cos\theta cos\phi cos\chi - sin\phi sin\chi\,)e'_z \quad \text{Eq. 60}$$

$$+ (cos\theta sin\phi cos\chi + cos\phi sin\chi)\left(\Omega'_x e'_y - \Omega'_y e'_z\right)$$

The last parameter that needs to be calculated is β. A few important characteristics about β are that it ranges from [-π/4,π/4]. This means that $sin2\beta$ is sufficient information to calculate β. Also the sign of β corresponds to the helicity of the polarization ellipse. So a positive β indicates a right handed rotation about the direction of travel, and a negative β indicates a left handed rotation about the direction of travel.

Eq. 16-Eq. 18, and Eq. 23 give the new value of β, and no rotations or transformations need to be performed on this parameter, so it can simply be stored.

At this point all of the mathematics describing the polarization physics has been described. Once these manipulations are complete, the particle can be released to travel through the problem space and undergo subsequent interactions.

Another capability this project added to the code is some useful polarization-related tallies. Five additional tallies were added to the code: the polarization fraction, the polarization ellipticity, and the 2nd, 3rd, and 4th Stokes parameters. The 1st Stokes parameter is already present in the code because it is simply the intensity.

Adding the polarization fraction tally is the simplest and perhaps most useful of the five new tallies. The purpose of this tally is to determine the average polarization fraction of all of the particles that pass through a given surface. The way that this is done is that a cumulative sum of the polarization fraction multiplied by the weight of the particle is stored by the code. This sum is what is returned by the code, however in order to calculate the actual average polarization fraction passing through that surface, the returned tally has to be divided by the total weight of the particles passing through that surface. Fortunately there is already a tally for the total weight passing through a surface. Eq. 61 and Eq. 62 show how the tally works.

$$P_{tally} = \sum P_i * w_i \qquad \text{Eq. 61}$$

$$P_{average} = \frac{P_{tally}}{w_{tally}} = \frac{\sum P_i * w_i}{\sum w_i} \quad \text{Eq. 62}$$

Here, P_{tally} is the value returned by the polarization fraction tally, w_{tally} is the value returned by the weight tally, P_i is the polarization fraction of the i-th particle, w_i is the weight of the i-th particle, and $P_{average}$ is the average polarization fraction through the surface over which the tally is taken.

The polarization ellipticity tally works in much the same way as the polarization fraction tally. As particles pass through a surface, a cumulative sum of the polarization ellipticity multiplied by the particle weight is stored. The cumulative sum divided by the total weight of the particles passing through the surface will give the average ellipticity of the particles. Eq. 63 and Eq. 64 show how the tally works.

$$\beta_{tally} = \sum \beta_i * w_i \quad \text{Eq. 63}$$

$$\beta_{average} = \frac{\beta_{tally}}{w_{tally}} = \frac{\sum \beta_i * w_i}{\sum w_i} \quad \text{Eq. 64}$$

Here, β_{tally} is the value returned by the polarization fraction tally, β_i is the polarization fraction of the i-th particle, and $\beta_{average}$ is the average polarization fraction through that surface.

The three Stokes parameter tallies are more complicated because they involve some geometry. First of all the Stokes parameters have a meaning only when they are specified for a certain direction. Therefore, the equivalent of the scalar flux from neutronics would not be a useful quantity when dealing with the Stokes parameters. For a particular direction, the Stokes parameters are defined in the frame of reference where

the z-axis defined as the direction of travel and the x-z plane is defined as the meridian plane. x^*, y^*, and z^* will be used to characterize the axes of this frame of reference. If the direction of travel is defined by a polar angle, θ, and an azimuthal angle, ϕ, then $\hat{x}^*, \hat{y}^*$, and $\hat{z}^*$ are defined by the spherical unit vectors corresponding to those angles. Figure 3 graphically shows the directions. Note that $\hat{z}^*$ is along the direction of travel.

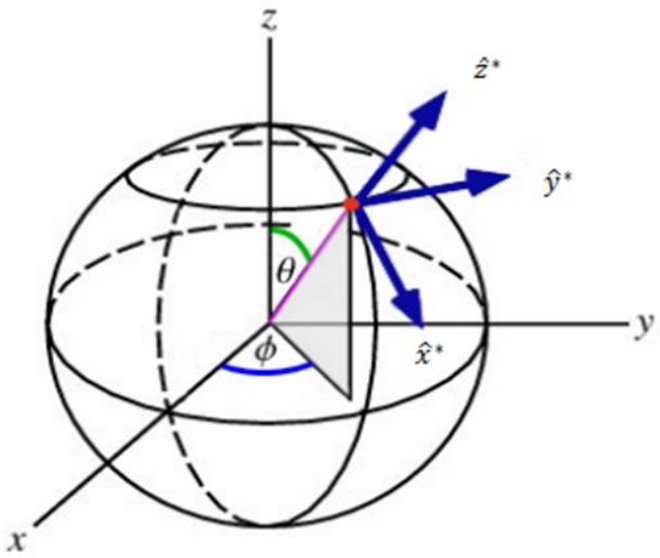

Figure 3. A depiction of the coordinate system with respect to which the Stokes parameters are calculated.

Mathematical expressions for the direction vectors are given by Eq. 65-Eq. 67. It is important to note that in these equations (unlike previous equations), θ and ϕ are in reference to a fixed global frame.

$$\hat{x}^* = cos\theta cos\phi\ \hat{x} + cos\theta sin\phi\ \hat{y} - sin\theta\hat{z} \qquad \text{Eq. 65}$$

$$\hat{y}^* = -sin\phi\ \hat{x} + cos\phi\ \hat{y} \quad \text{Eq. 66}$$

$$\hat{z}^* = sin\theta cos\phi\ \hat{x} + sin\theta sin\phi\ \hat{y} + cos\theta\hat{z} \quad \text{Eq. 67}$$

In the scenario where θ is 0 or π, we adopt the convention that ϕ equals 0. Under this scenario $\hat{x}^*, \hat{y}^*$, and $\hat{z}^*$ would simply equal $\hat{x}, \hat{y}$, and $\hat{z}$ respectively. Using these expressions for x^*, y^*, and z^*, the polarization vector will now lie in the x^*- y^* plane and χ will be the angle between the polarization vector and the x^* axis as can be seen in figure 4.

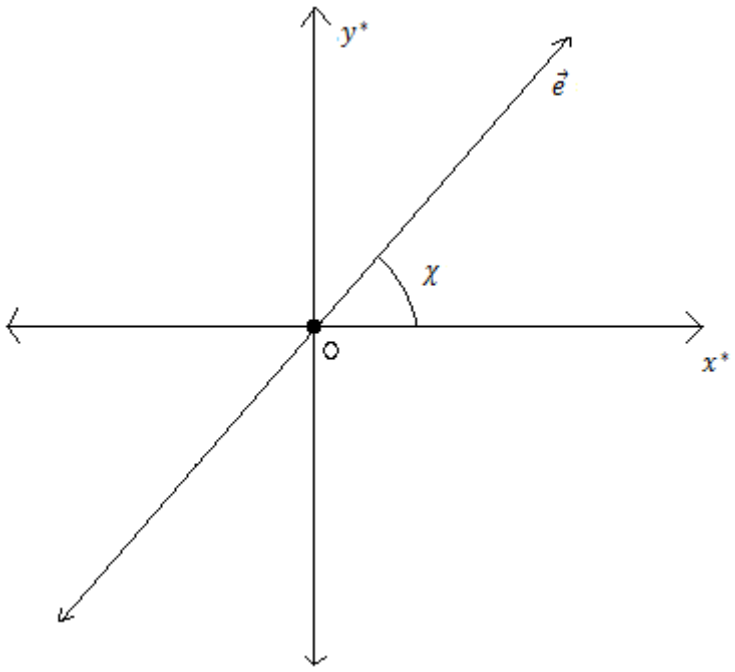

Figure 4. The polarization vector is shown in relation to the $\boldsymbol{x^*}$-$\boldsymbol{y^*}$ plane

Using this notation Eq. 1 can be rewritten as follows.

$$\begin{bmatrix} I \\ Q \\ U \\ V \end{bmatrix} = \begin{bmatrix} I \\ I\ P\ cos2\beta\ (2cos^2\chi - 1) \\ I\ P\ cos2\beta(2sin\chi cos\chi) \\ I\ P\ sin2\beta \end{bmatrix} = \begin{bmatrix} I \\ I\ P\ cos2\beta\ (2(\hat{x}^* \cdot \vec{e})^2 - 1) \\ I\ P\ cos2\beta(2(\hat{y}^* \cdot \vec{e})(\hat{x}^* \cdot \vec{e})) \\ I\ P\ sin2\beta \end{bmatrix} \quad \text{Eq. 68}$$

Another way to write Eq. 65 and Eq. 66 is to express them in terms of the components of the photon's direction vector. This will be useful because these are the values that the code will have access to.

$$\hat{x}^* = \frac{\Omega_z \Omega_x}{\sqrt[2]{1-\Omega_z^2}}\,\hat{x} + \frac{\Omega_z \Omega_y}{\sqrt[2]{1-\Omega_z^2}}\,\hat{y} - \sqrt[2]{1-\Omega_z^2}\,\hat{z} \quad \text{Eq. 69}$$

$$\hat{y}^* = -\frac{\Omega_y}{\sqrt[2]{1-\Omega_z^2}}\,\hat{x} + \frac{\Omega_x}{\sqrt[2]{1-\Omega_z^2}}\,\hat{y} \quad \text{Eq. 70}$$

Using Eq. 68-Eq. 70, expressions for the tallies of the 2nd-4th Stokes parameters can be found using the equations below.

$$Q_{tally} = \sum \left\{ w_i * P_i * cos2\beta_i * \left[2\left(\frac{\Omega_z \Omega_x e_x}{\sqrt[2]{1-\Omega_z^2}} + \frac{\Omega_z \Omega_y e_y}{\sqrt[2]{1-\Omega_z^2}} - e_z \sqrt[2]{1-\Omega_z^2} \right)_i^2 - 1 \right] \right\} \quad \text{Eq. 71}$$

$$U_{tally} = \sum \left\{ w_i * P_i * cos2\beta_i * 2\left(\frac{\Omega_z \Omega_x e_x}{\sqrt[2]{1-\Omega_z^2}} + \frac{\Omega_z \Omega_y e_y}{\sqrt[2]{1-\Omega_z^2}} - e_z \sqrt[2]{1-\Omega_z^2} \right)_i * \left(\frac{-\Omega_y e_x}{\sqrt[2]{1-\Omega_z^2}} + \frac{\Omega_x e_y}{\sqrt[2]{1-\Omega_z^2}} \right)_i \right\} \quad \text{Eq. 72}$$

$$V_{tally} = \sum \{ w_i * P_i * sin2\beta_i \} \quad \text{Eq. 73}$$

With the addition of these tallies, the implementation of polarization effects into Mercury is complete.

CHAPTER IV

RESULTS

Complex problems are difficult if not impossible to solve analytically, but one simple problem that is worth considering is the broomstick problem. In this problem, a photon beam is incident upon the bottom of a long, thin cylinder (i.e. a broomstick), pointed along the z axis. The "broomstick" is defined to be optically thin enough that essentially any photon that is scattered into a different direction will immediately exit the broomstick. It is useful to make the broomstick long, so that all of the photons will eventually interact with the material instead of simply streaming through the geometry. While this is not completely necessary, it helps with the statistics of the problem. The geometry can be seen below in Figure 5.

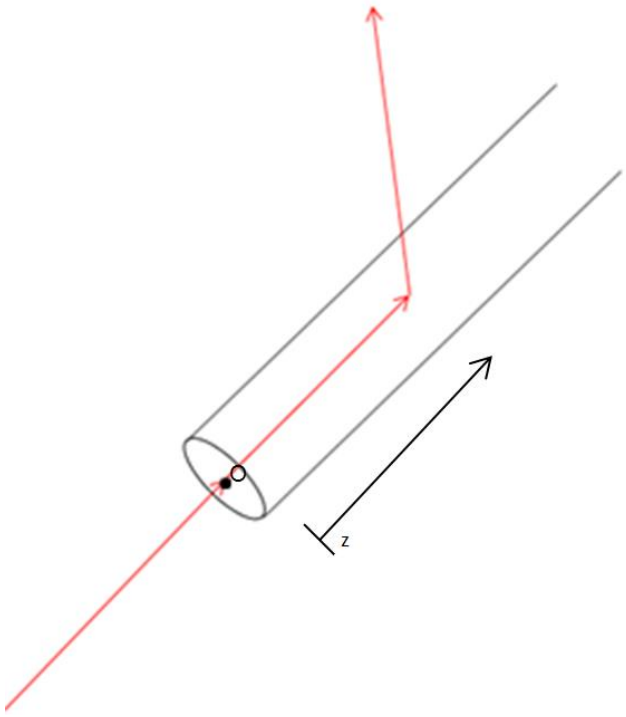

Figure 5. A broomstick geometry that is used to get single-scatter results.

In this problem, any photons that undergo a scattering event will escape the broomstick and can be tallied. Mercury has the capability to compute tallies based on the direction that the particle is travelling and the types of interaction it has undergone. Therefore, the angular distribution of the scattered particles can be compared to analytical results for both coherent and incoherent scattering.

Using Eq. **3** as a starting point, a solution for the intensity of single scattered photons can be found by first considering the intensity of unscattered photons.

$$\mu \frac{\partial}{\partial z} \boldsymbol{I}^{(0)}\left(z, \vec{\Omega}, E\right) + \sigma_t \boldsymbol{I}^{(0)}\left(z, \vec{\Omega}, E\right) = \boldsymbol{\Gamma}\left(z, \vec{\Omega}, E\right) \quad \text{Eq. 74}$$

The problem can be considered 1D because the broomstick is infinitesimally thin and the photons will be tallied immediately upon leaving the geometry. The superscripts present in Eq. 74 indicate the number of scatters that the photons have undergone. There is no scattering term because obviously a photon cannot be scattered into the unscattered portion of the beam. In the case of this problem the source will have the form seen below.

$$\boldsymbol{\Gamma}\left(\vec{r},\vec{\Omega},E\right)=\begin{bmatrix}\varphi_I\\ \varphi_Q\\ \varphi_U\\ \varphi_V\end{bmatrix}\delta(x)\delta(y)\delta(z)\delta(\mu-1)\delta(\phi)\delta(E-E^*) \qquad \text{Eq. 75}$$

Here, δ is the Dirac delta function, and E^* is the energy of the photon beam. The function $\delta(\mu-1)$ is a one-sided delta function, so that the integral of $\delta(\mu-1)$ up to the endpoint ($\mu=1$) is 1 not 0.5. Using Eq. 74 and Eq. 75, an expression for $\boldsymbol{I}^{(0)}\left(z,\vec{\Omega},E\right)$ can be found.

$$\boldsymbol{I}^{(0)}\left(z,\vec{\Omega},E\right)=\begin{bmatrix}\varphi_I\\ \varphi_Q\\ \varphi_U\\ \varphi_V\end{bmatrix}\frac{\delta(x)\delta(y)\Theta(z)\delta(\mu-1)\delta(\phi)\delta(E-E^*)}{\mu}exp\left(\frac{-\sigma_t z}{\mu}\right) \qquad \text{Eq. 76}$$

Here Θ is the Heaviside function. Since polarization does not affect the frequency of interactions in an isotropic medium, the quantities of interest are the angular distribution of the scattered photons and the polarization tallies of those photons. The scattered photons immediately exit the cylinder, and only scattered photons will exit the cylinder. This means that intensity of photons exiting the cylinder is equal to the integral of the scattering term.

$$\boldsymbol{I}_{exit}(\vec{\Omega}, E) = \int_{-\infty}^{\infty} dz' \int_{0}^{\infty} dE' \int_{4\pi} d\Omega' \, \boldsymbol{H}(\vec{\Omega}', \vec{\Omega}, E', E) \boldsymbol{I}^{(0)}(z', \vec{\Omega}', E') \quad \text{Eq. 77}$$

Solving this equation gives the following solution for $\boldsymbol{I}_{exit}(\vec{\Omega}, E)$.

$$\boldsymbol{I}_{exit}(\vec{\Omega}, E) = \frac{\boldsymbol{H}(\hat{z}, \vec{\Omega}, E^*, E)}{\sigma_{\boldsymbol{t}}} \begin{bmatrix} \Gamma_I \\ \Gamma_Q \\ \Gamma_U \\ \Gamma_V \end{bmatrix} \quad \text{Eq. 78}$$

If $\boldsymbol{H}(\hat{z}, \vec{\Omega}, E^*, E)$ is expanded into the Mueller matrix and the rotation matrices, this gives the following expression.

$$\boldsymbol{I}_{exit}(\vec{\Omega}, E) = \frac{\boldsymbol{L}(0) \, \boldsymbol{M}(\hat{z}, \vec{\Omega}, E^*, E) \boldsymbol{L}(\pi - \phi)}{\sigma_{\boldsymbol{t}}} \begin{bmatrix} \Gamma_I \\ \Gamma_Q \\ \Gamma_U \\ \Gamma_V \end{bmatrix} \quad \text{Eq. 79}$$

The Mueller matrix can be expressed simply and analytically for hydrogen [8]. The expressions for the Atomic Form Factor and the Incoherent Scattering Function of hydrogen can be seen in Eq. 80 and Eq. 81.

$$F(x, H) = [1 + 4\pi^2 {a_0}^2 x^2]^{-2} \quad \text{Eq. 80}$$

$$S(x, H) = 1 - [F(x, H)]^2 \quad \text{Eq. 81}$$

Here H indicates that these equations only hold for hydrogen, a_0 is the first Bohr radius, and $x = \frac{E'}{hc} sin\left(\frac{\theta}{2}\right)$ where h is planck's constant, c is the speed of light, E' is the incident photon energy, and θ is the polar scattering angle.

Using Eq. 8, Eq. 9, and Eq. 79-Eq. 81 the analytic solutions can be found for each Stokes parameter.

$$I_{exit,Coh}(\vec{\Omega},E)=\frac{{r_0}^2\,F^2(x,H)}{2\sigma_t}\left[\varphi_I(cos^2\theta+1)+\varphi_Q cos2\phi(cos^2\theta-1)\right.$$
$$\left.-\varphi_U sin2\phi(cos^2\theta-1)\right] \quad \text{Eq. 82}$$

$$Q_{exit,Coh}(\vec{\Omega},E)=\frac{{r_0}^2\,F^2(x,H)}{2\sigma_t}\left[\varphi_I(cos^2\theta-1)+\varphi_Q cos2\phi(cos^2\theta+1)\right.$$
$$\left.-\varphi_U sin2\phi(cos^2\theta+1)\right] \quad \text{Eq. 83}$$

$$U_{exit,Coh}(\vec{\Omega},E)=\frac{{r_0}^2\,F^2(x,H)}{2\sigma_t}\left[2\varphi_Q sin2\phi cos\theta+2\varphi_U cos2\phi cos\theta\right] \quad \text{Eq. 84}$$

$$V_{exit,Coh}(\vec{\Omega},E)=\frac{{r_0}^2\,F^2(x,H)}{2\sigma_t}\left[2\varphi_V cos\theta\right] \quad \text{Eq. 85}$$

$$I_{exit,Incoh}(\vec{\Omega},E)=\frac{{r_0}^2\,S(x,H)}{2\sigma_t}\left(\frac{E}{E'}\right)^2\left[\varphi_I\left(\frac{E}{E'}+\frac{E'}{E}+cos^2\theta-1\right)\right.$$
$$\left.+\varphi_Q cos2\phi(cos^2\theta-1)-\varphi_U sin2\phi(cos^2\theta-1)\right] \quad \text{Eq. 86}$$

$$Q_{exit,Incoh}(\vec{\Omega},E)=\frac{{r_0}^2\,S(x,H)}{2\sigma_t}\left(\frac{E}{E'}\right)^2\left[\varphi_I(cos^2\theta-1)\right.$$
$$\left.+\varphi_Q cos2\phi(cos^2\theta+1)-\ \varphi_U sin2\phi(cos^2\theta+1)\right] \quad \text{Eq. 87}$$

$$U_{exit,Incoh}(\vec{\Omega},E)=\frac{{r_0}^2\,S(x,H)}{2\sigma_t}\left(\frac{E}{E'}\right)^2\left[2\varphi_Q sin2\phi cos\theta+2\varphi_U cos2\phi cos\theta\right] \quad \text{Eq. 88}$$

$$V_{exit,Incoh}(\vec{\Omega},E)=\frac{{r_0}^2\,S(x,H)}{2\sigma_t}\left(\frac{E}{E'}\right)^2\left[\left(\frac{E}{E'}+\frac{E'}{E}\right)\varphi_V cos\theta\right] \quad \text{Eq. 89}$$

The solutions in Eq. 82-Eq. 89 can be compared with the solution obtained from Mercury using a variety of input photon beams. The figures below show comparisons between the analytic results and the results obtained by Mercury for a variety of different

photon energies and input Stokes Parameters. It is important to note that the solutions in Eq. 82-Eq. 89 are per steradian, but the tallies in Mercury will be for a finite solid angle window. Therefore, the solutions produced by Mercury were divided by the size of the solid angle range used in the simulation. In the case of these simulations that value was 0.0043633 steradians (0.05 in $cos\theta$ and $\frac{\pi}{36}$ in ϕ) when ϕ was fixed and θ was varied, and 0.0087266 steradians (0.05 in $cos\theta$ and $\frac{\pi}{18}$ in ϕ) when ϕ was varied and θ was fixed. Figure 6-Figure 29 show the results for a photon beam with an energy of 5 keV and $[\varphi_I, \varphi_Q, \varphi_U, \varphi_V] = [1,0.5,0.5,0.5]$. Both coherent and incoherent scattering results are shown since at this energy they both have significant cross sections. All of the "broomstick" problems simulated 5x10^9 particles.

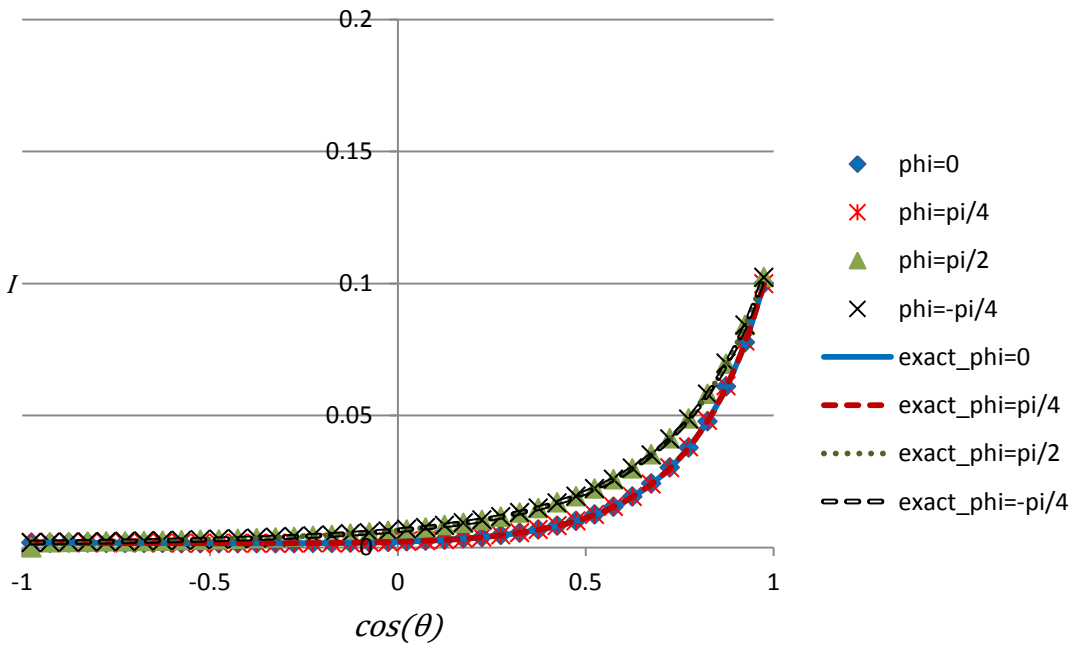

Figure 6. *I* for the coherently scattered portion of a 5 keV photon beam with a source Stokes vector of $[\varphi_I, \varphi_Q, \varphi_U, \varphi_V] = [1,0.5,0.5,0.5]$.

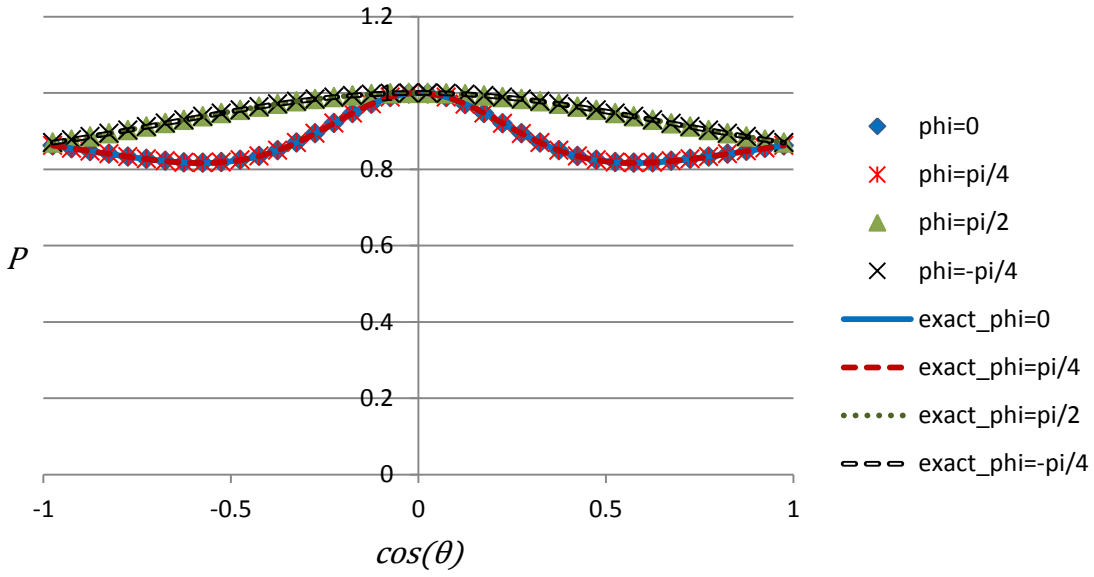

Figure 7. P for the coherently scattered portion of a 5 keV photon beam with a source Stokes vector of $[\varphi_I, \varphi_Q, \varphi_U, \varphi_V] = [1,0.5,0.5,0.5]$.

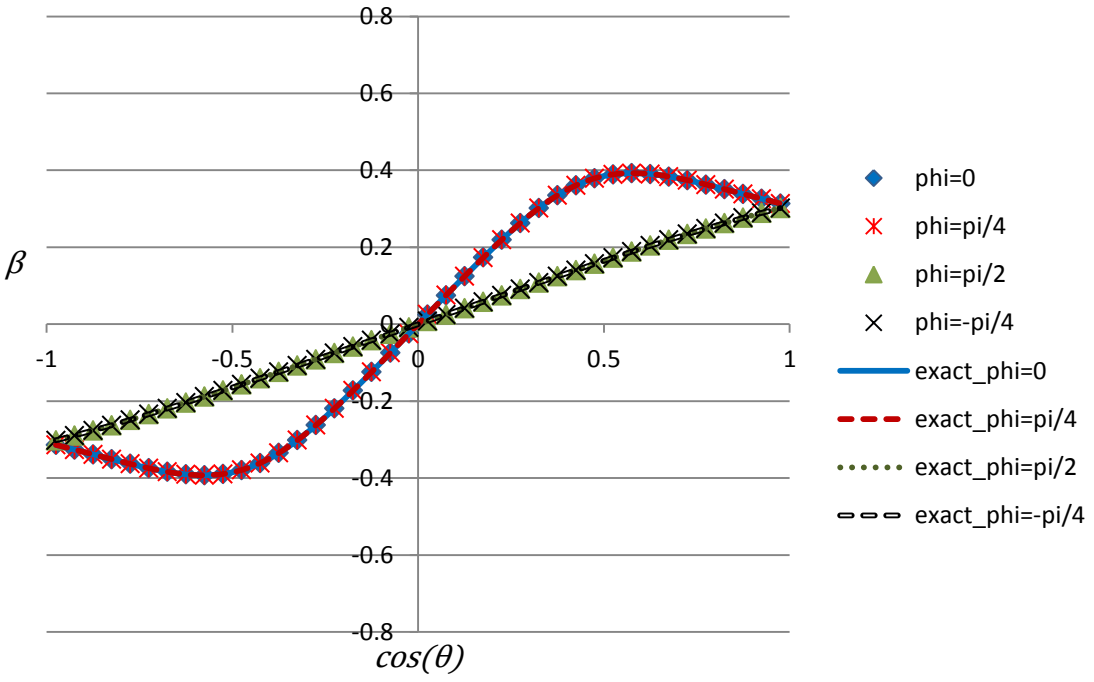

Figure 8. β for the coherently scattered portion of a 5 keV photon beam with a source Stokes vector of $[\varphi_I, \varphi_Q, \varphi_U, \varphi_V] = [1,0.5,0.5,0.5]$.

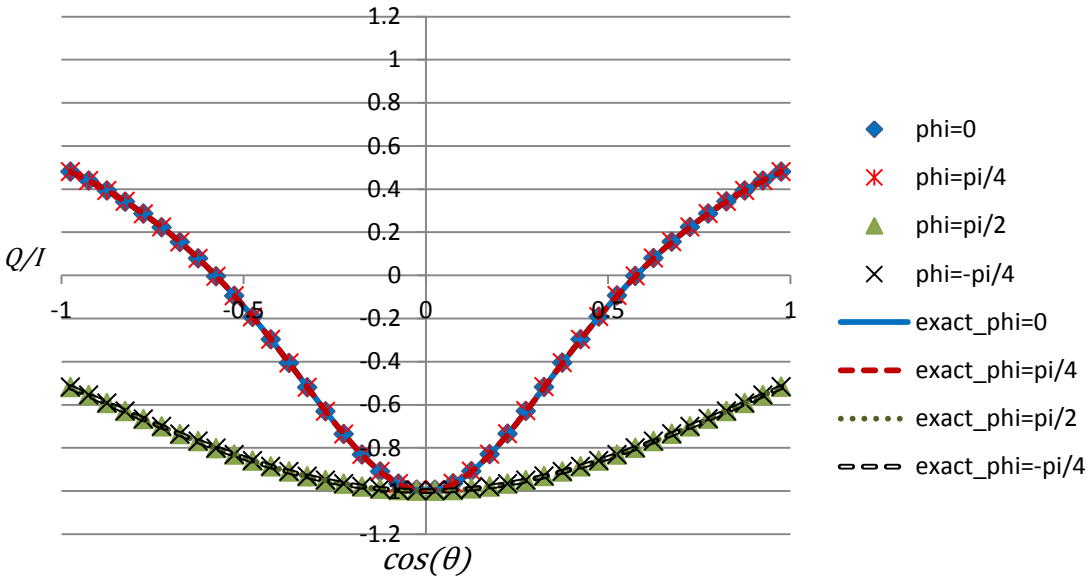

Figure 9. Q/I for the coherently scattered portion of a 5 keV photon beam with a source Stokes vector of $[\varphi_I, \varphi_Q, \varphi_U, \varphi_V] = [1,0.5,0.5,0.5]$.

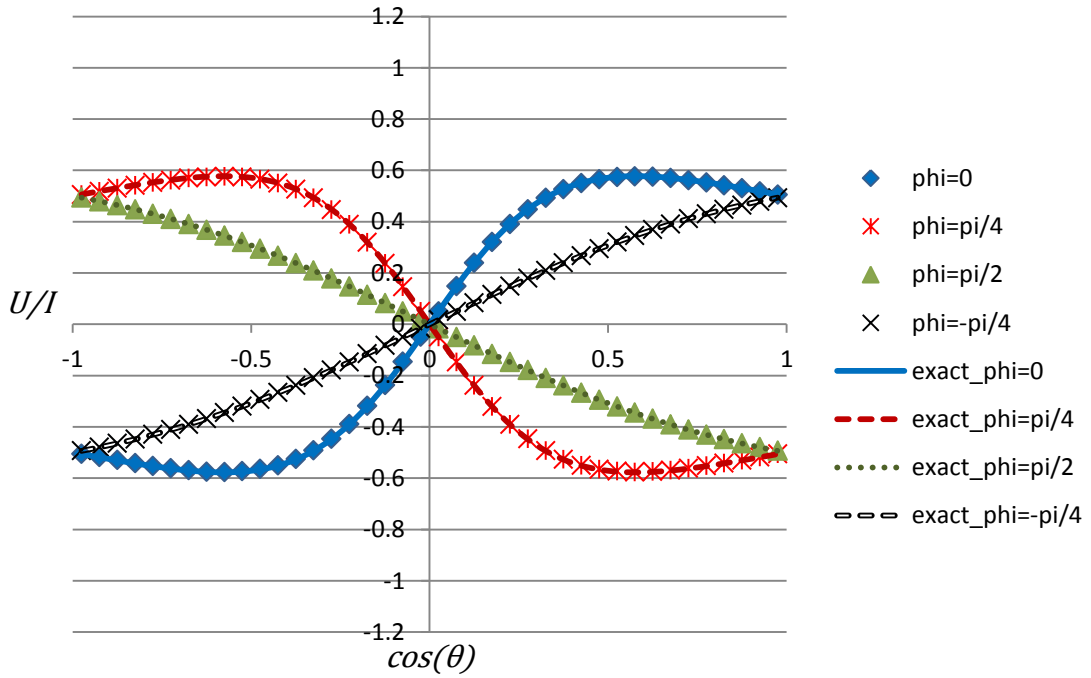

Figure 10. U/I for the coherently scattered portion of a 5 keV photon beam with a source Stokes vector of $[\varphi_I, \varphi_Q, \varphi_U, \varphi_V] = [1,0.5,0.5,0.5]$.

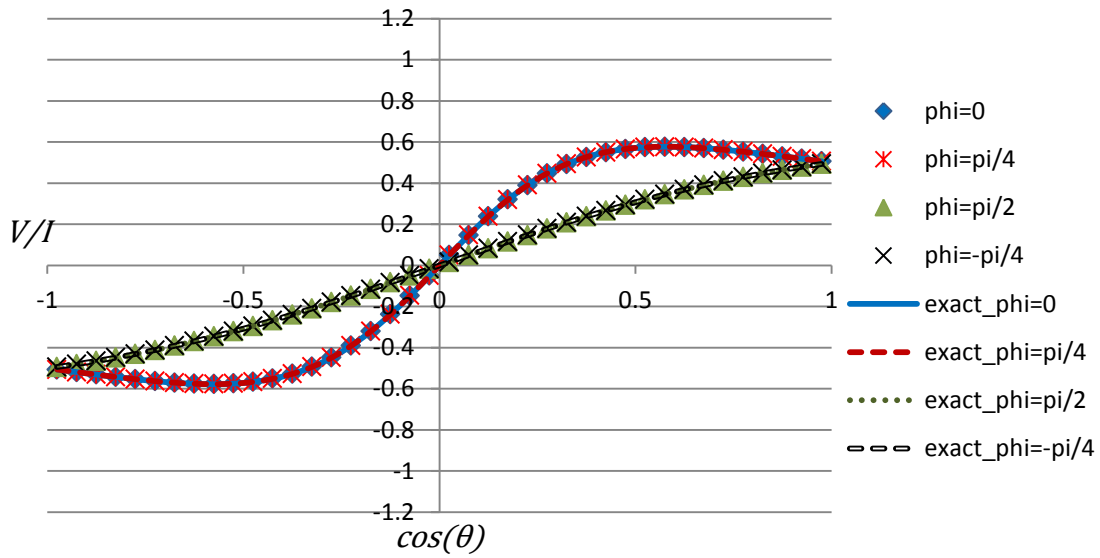

Figure 11. *V/I* for the coherently scattered portion of a 5 keV photon beam with a source Stokes vector of $[\varphi_I, \varphi_Q, \varphi_U, \varphi_V] = [1,0.5,0.5,0.5]$.

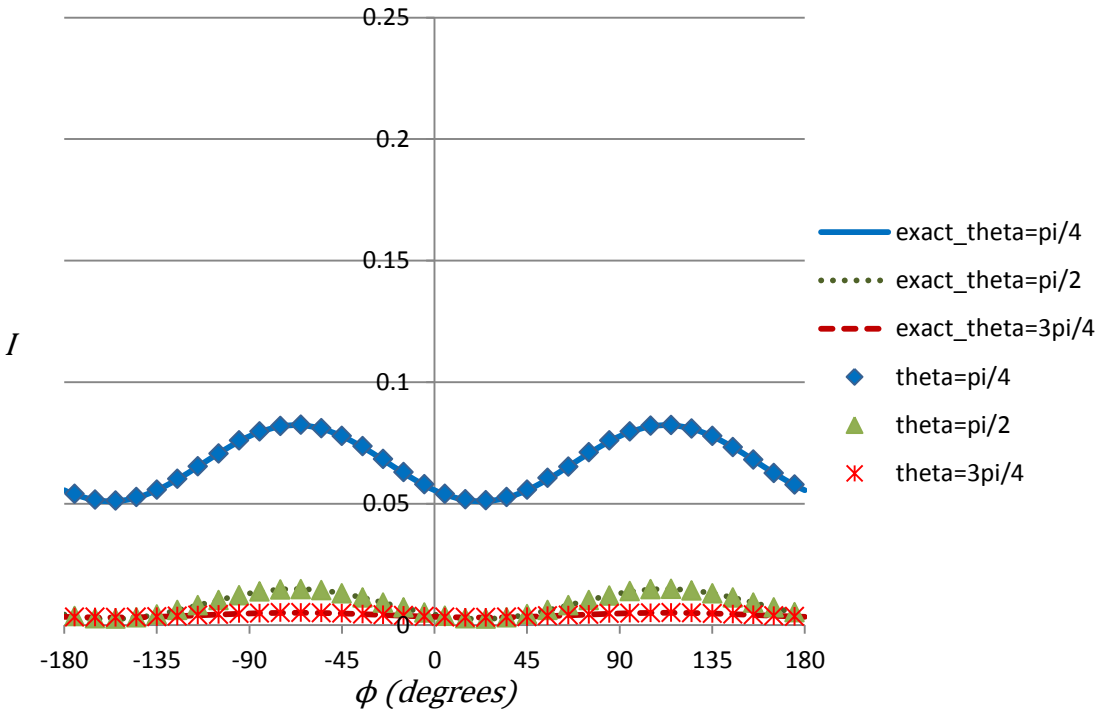

Figure 12. *I* for the coherently scattered portion of a 5 keV photon beam with a source Stokes vector of $[\varphi_I, \varphi_Q, \varphi_U, \varphi_V] = [1,0.5,0.5,0.5]$.

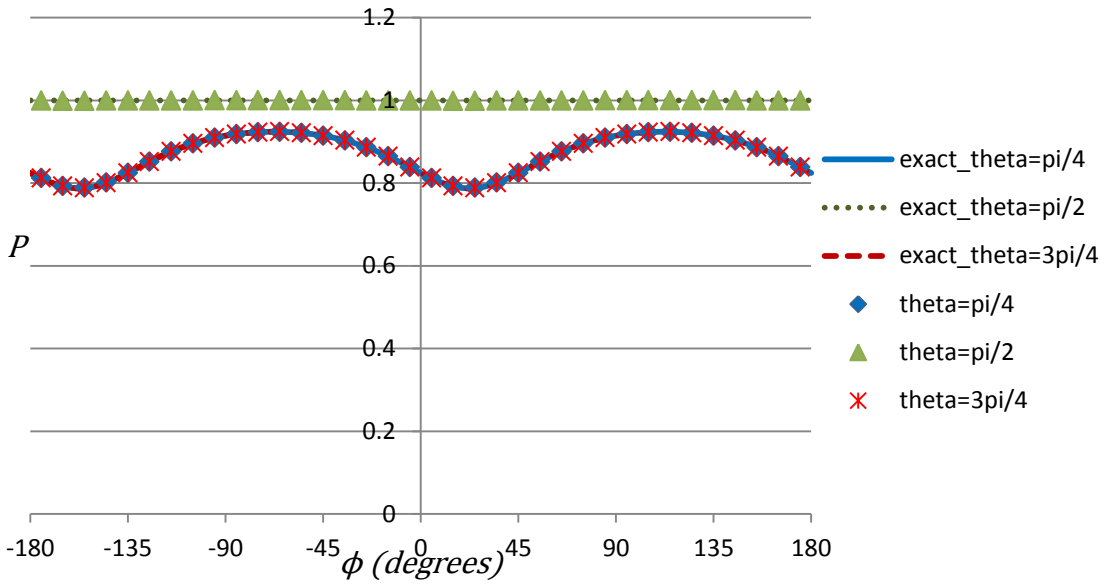

Figure 13. P for the coherently scattered portion of a 5 keV photon beam with a source Stokes vector of $[\varphi_I, \varphi_Q, \varphi_U, \varphi_V] = [1,0.5,0.5,0.5]$.

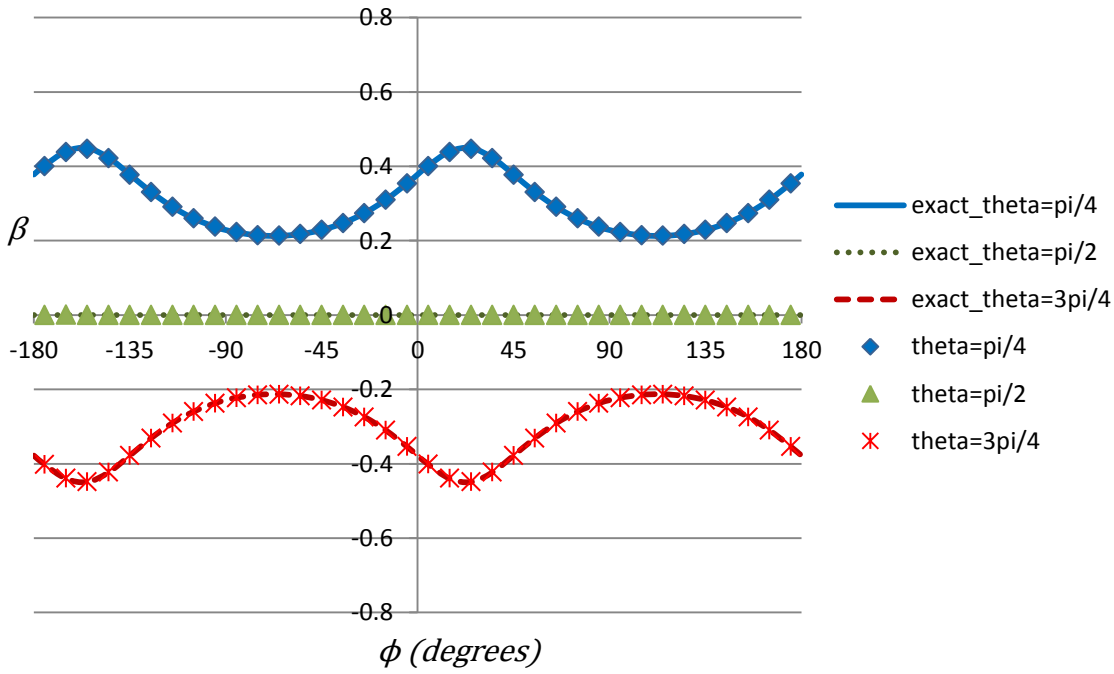

Figure 14. β for the coherently scattered portion of a 5 keV photon beam with a source Stokes vector of $[\varphi_I, \varphi_Q, \varphi_U, \varphi_V] = [1,0.5,0.5,0.5]$.

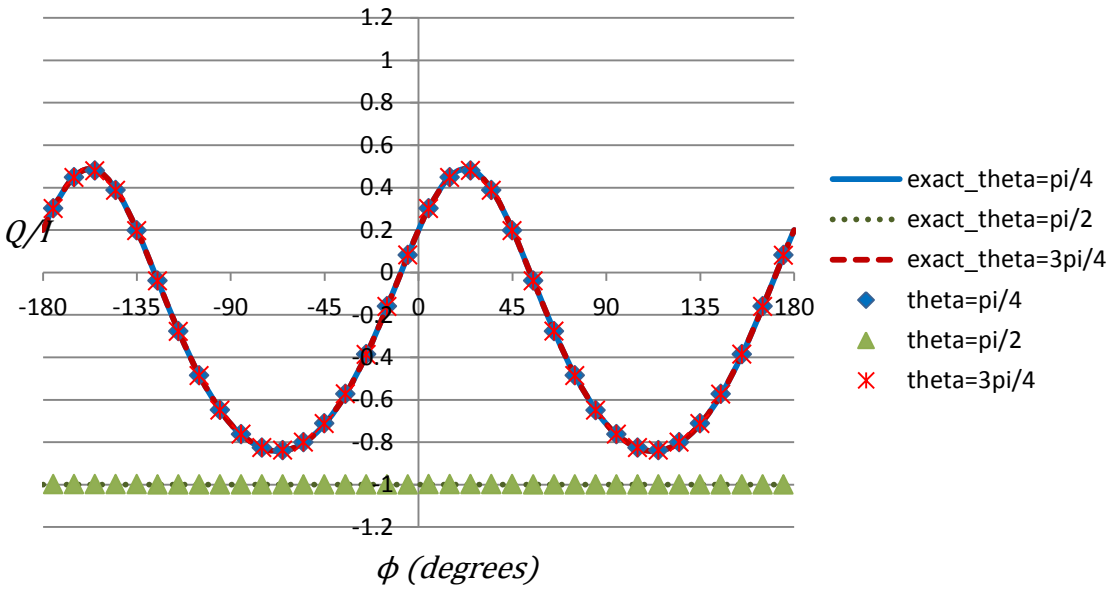

Figure 15. *Q/I* for the coherently scattered portion of a 5 keV photon beam with a source Stokes vector of $[\varphi_I, \varphi_Q, \varphi_U, \varphi_V] = [1,0.5,0.5,0.5]$.

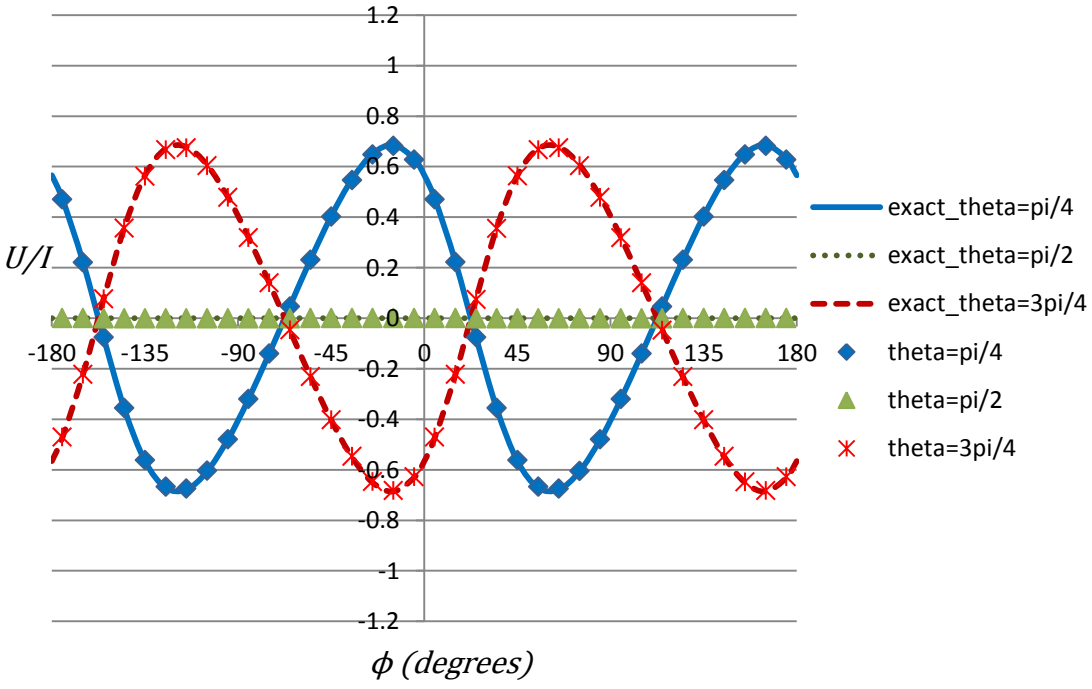

Figure 16. *U/I* for the coherently scattered portion of a 5 keV photon beam with a source Stokes vector of $[\varphi_I, \varphi_Q, \varphi_U, \varphi_V] = [1,0.5,0.5,0.5]$.

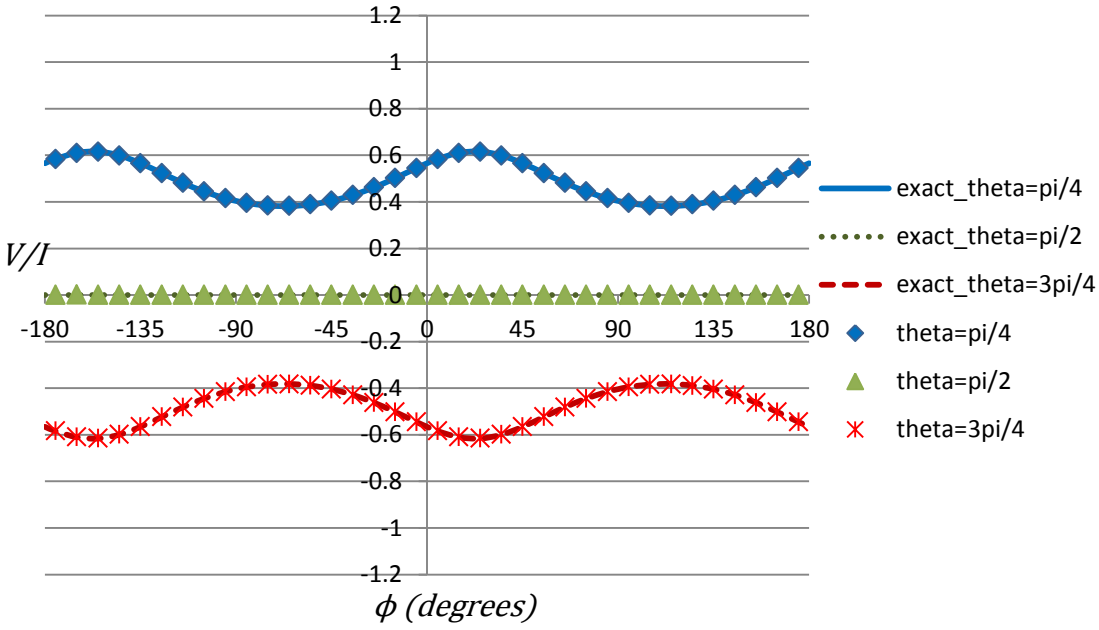

Figure 17. *V/I* for the coherently scattered portion of a 5 keV photon beam with a source Stokes vector of $[\varphi_I, \varphi_Q, \varphi_U, \varphi_V] = [1,0.5,0.5,0.5]$.

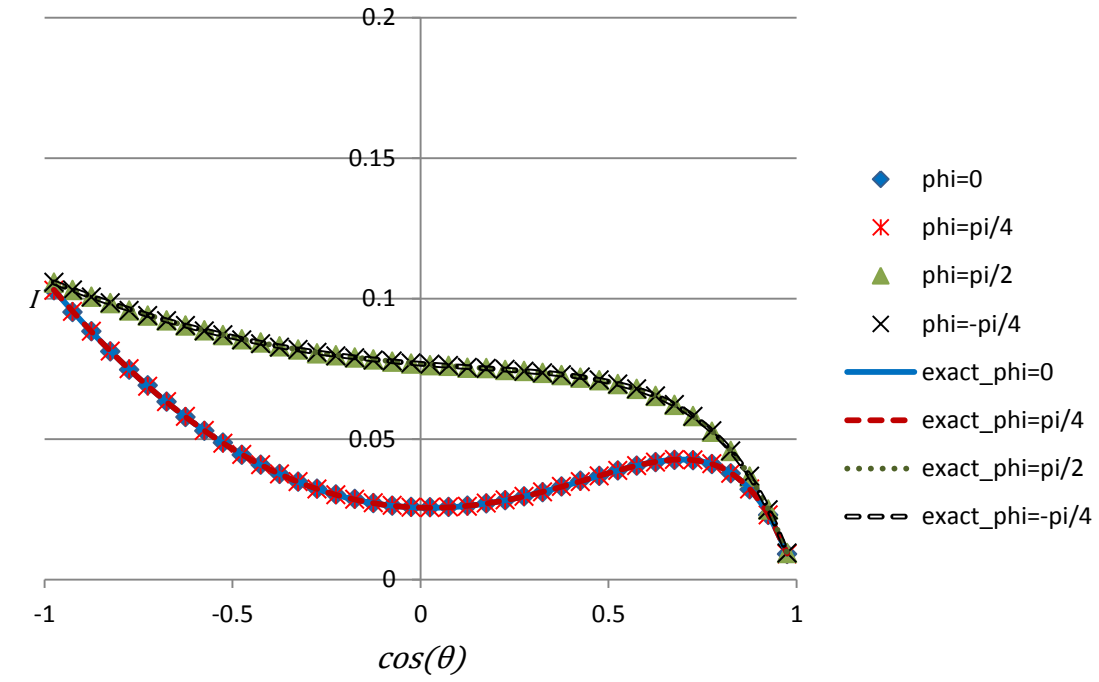

Figure 18. *I* for the incoherently scattered portion of a 5 keV photon beam with a source Stokes vector of $[\varphi_I, \varphi_Q, \varphi_U, \varphi_V] = [1,0.5,0.5,0.5]$.

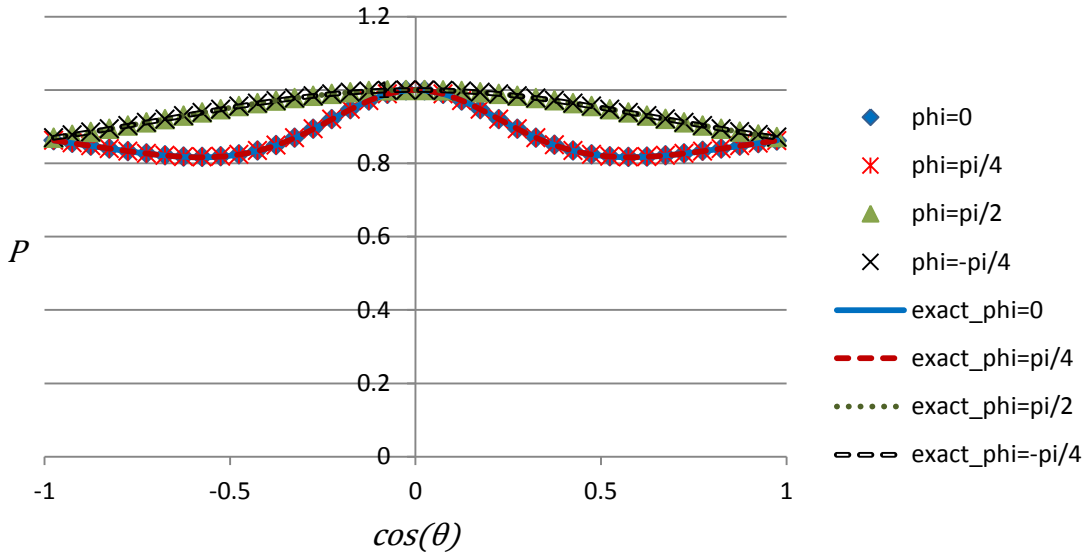

Figure 19. P for the incoherently scattered portion of a 5 keV photon beam with a source Stokes vector of $[\varphi_I, \varphi_Q, \varphi_U, \varphi_V] = [1,0.5,0.5,0.5]$.

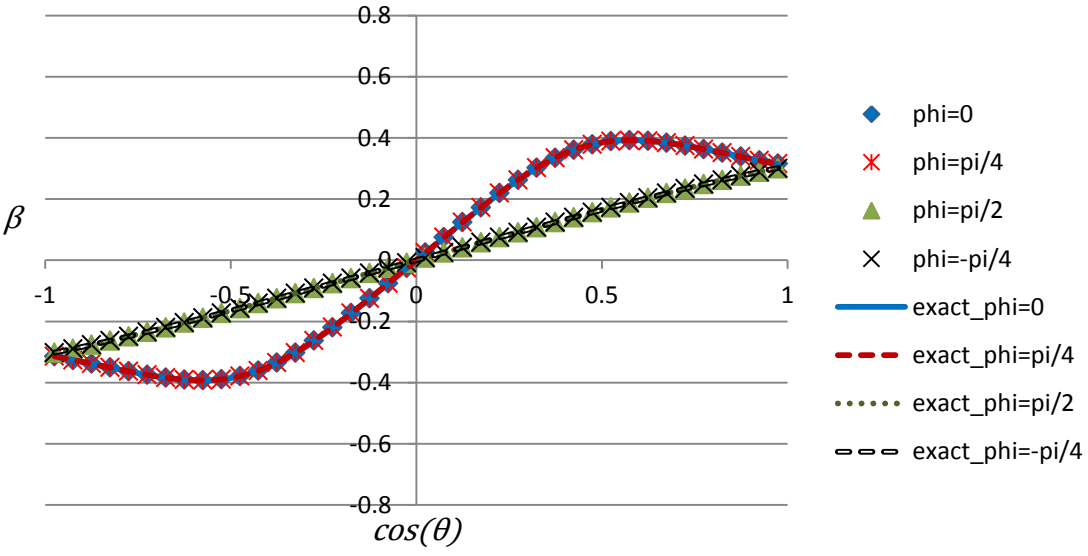

Figure 20. β for the incoherently scattered portion of a 5 keV photon beam with a source Stokes vector of $[\varphi_I, \varphi_Q, \varphi_U, \varphi_V] = [1,0.5,0.5,0.5]$.

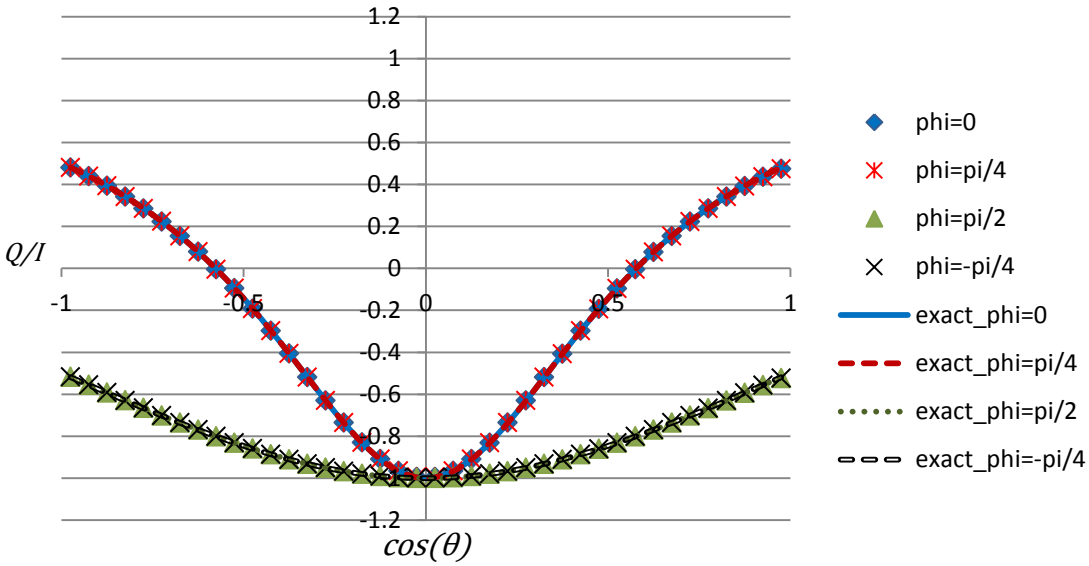

Figure 21. *Q/I* for the incoherently scattered portion of a 5 keV photon beam with a source Stokes vector of $[\varphi_I, \varphi_Q, \varphi_U, \varphi_V] = [1,0.5,0.5,0.5]$.

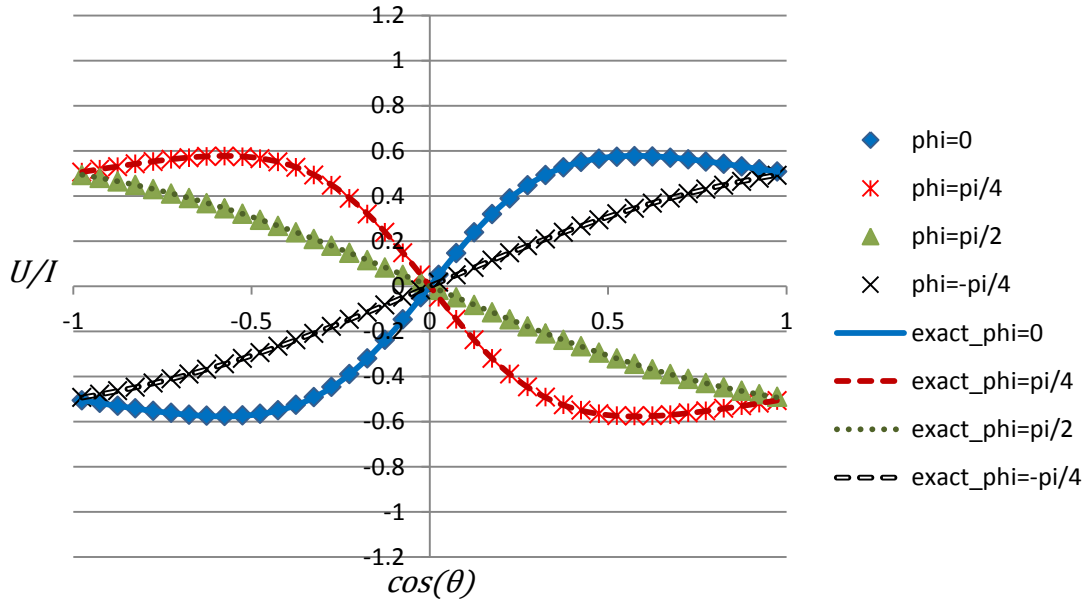

Figure 22. *U/I* for the incoherently scattered portion of a 5 keV photon beam with a source Stokes vector of $[\varphi_I, \varphi_Q, \varphi_U, \varphi_V] = [1,0.5,0.5,0.5]$.

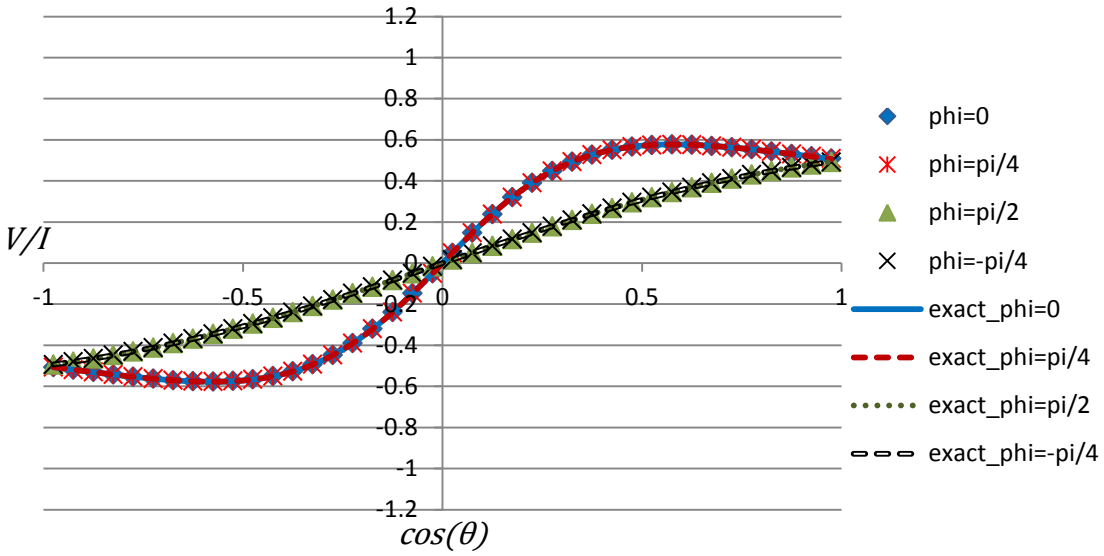

Figure 23. *V/I* for the incoherently scattered portion of a 5 keV photon beam with a source Stokes vector of $[\varphi_I, \varphi_Q, \varphi_U, \varphi_V] = [1,0.5,0.5,0.5]$.

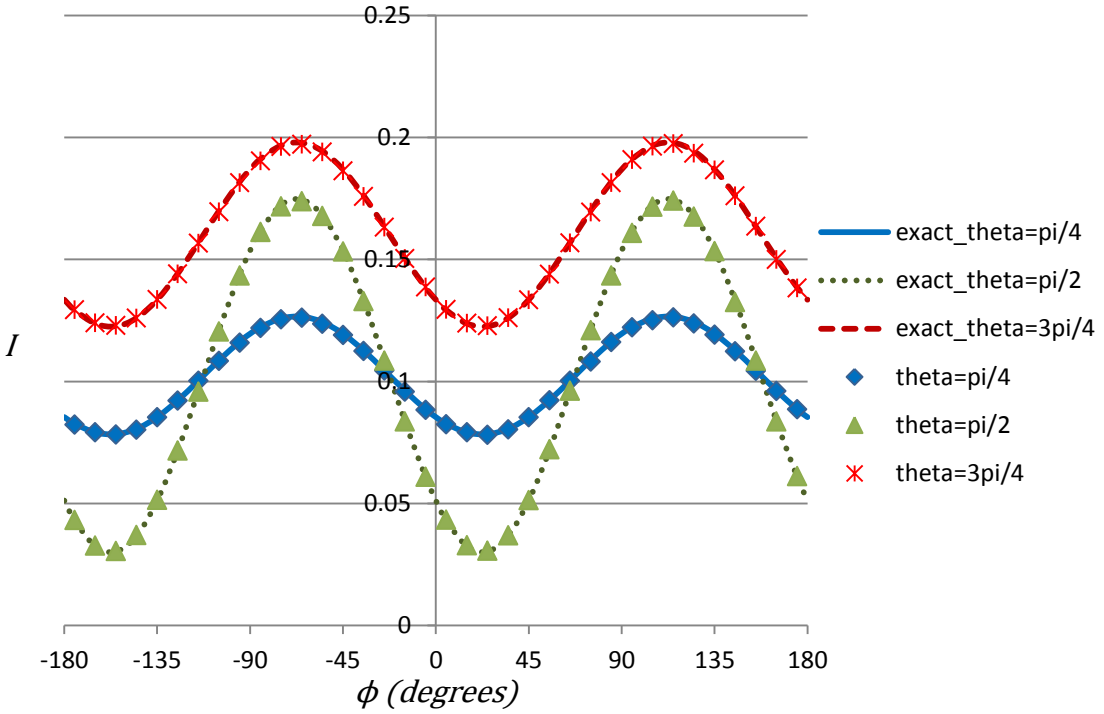

Figure 24. *I* for the incoherently scattered portion of a 5 keV photon beam with a source Stokes vector of $[\varphi_I, \varphi_Q, \varphi_U, \varphi_V] = [1,0.5,0.5,0.5]$.

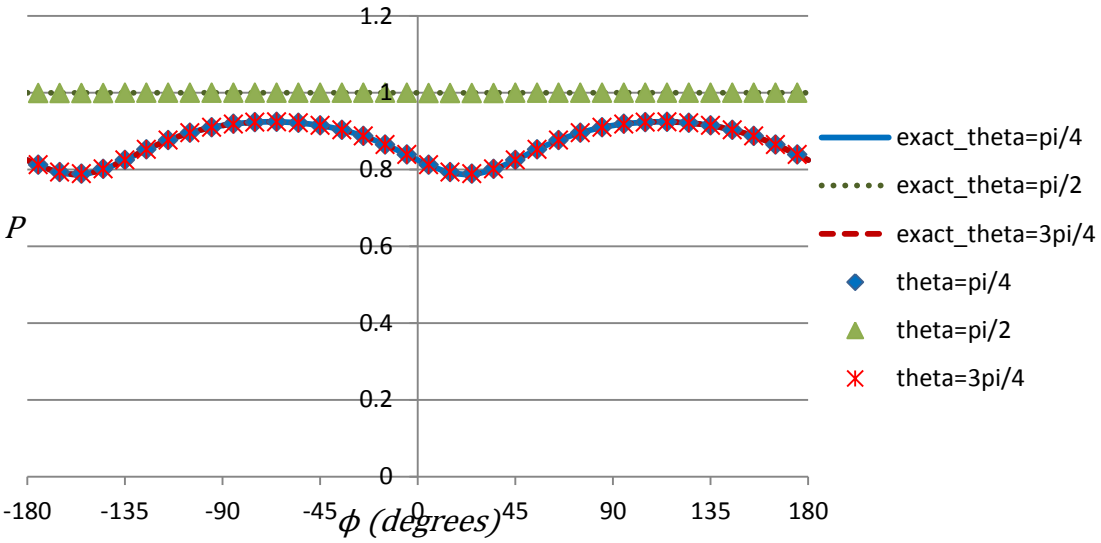

Figure 25. P for the incoherently scattered portion of a 5 keV photon beam with a source Stokes vector of $[\varphi_I, \varphi_Q, \varphi_U, \varphi_V] = [1,0.5,0.5,0.5]$.

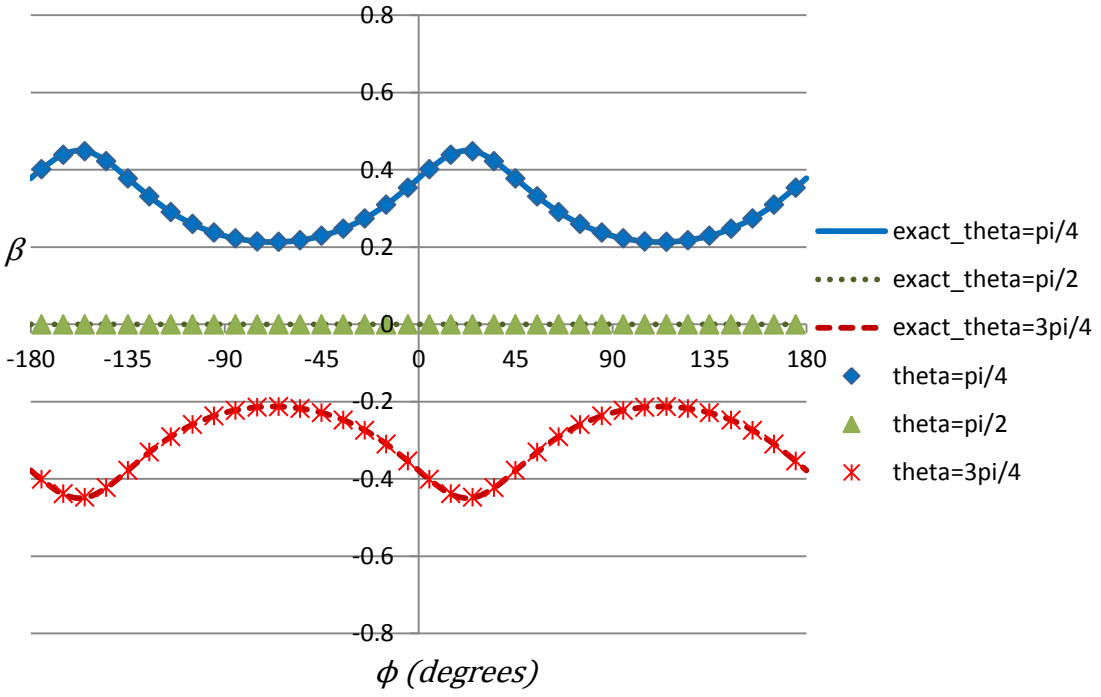

Figure 26. β for the incoherently scattered portion of a 5 keV photon beam with a source Stokes vector of $[\varphi_I, \varphi_Q, \varphi_U, \varphi_V] = [1,0.5,0.5,0.5]$.

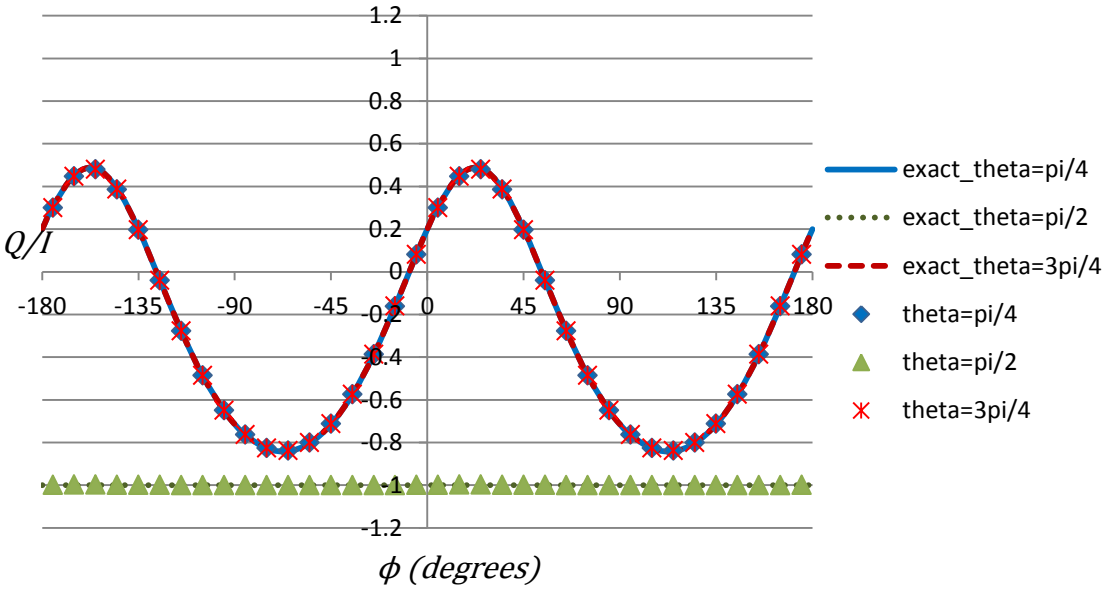

Figure 27. *Q/I* for the incoherently scattered portion of a 5 keV photon beam with a source Stokes vector of $[\varphi_I, \varphi_Q, \varphi_U, \varphi_V] = [1,0.5,0.5,0.5]$.

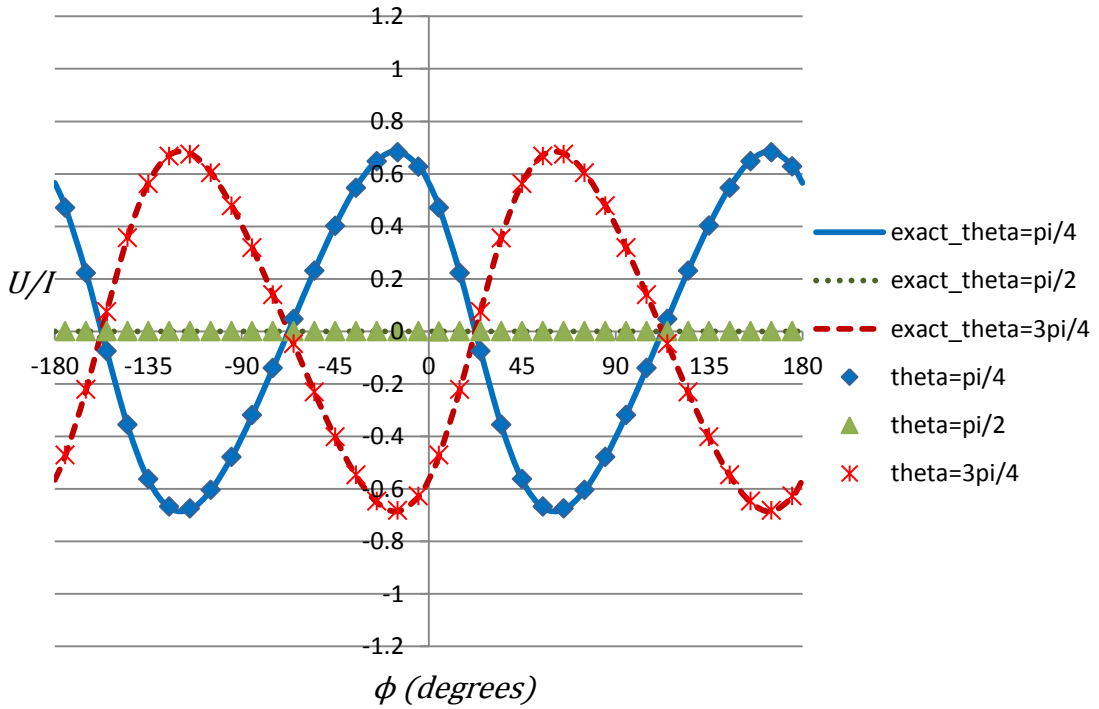

Figure 28. *U/I* for the incoherently scattered portion of a 5 keV photon beam with a source Stokes vector of $[\varphi_I, \varphi_Q, \varphi_U, \varphi_V] = [1,0.5,0.5,0.5]$.

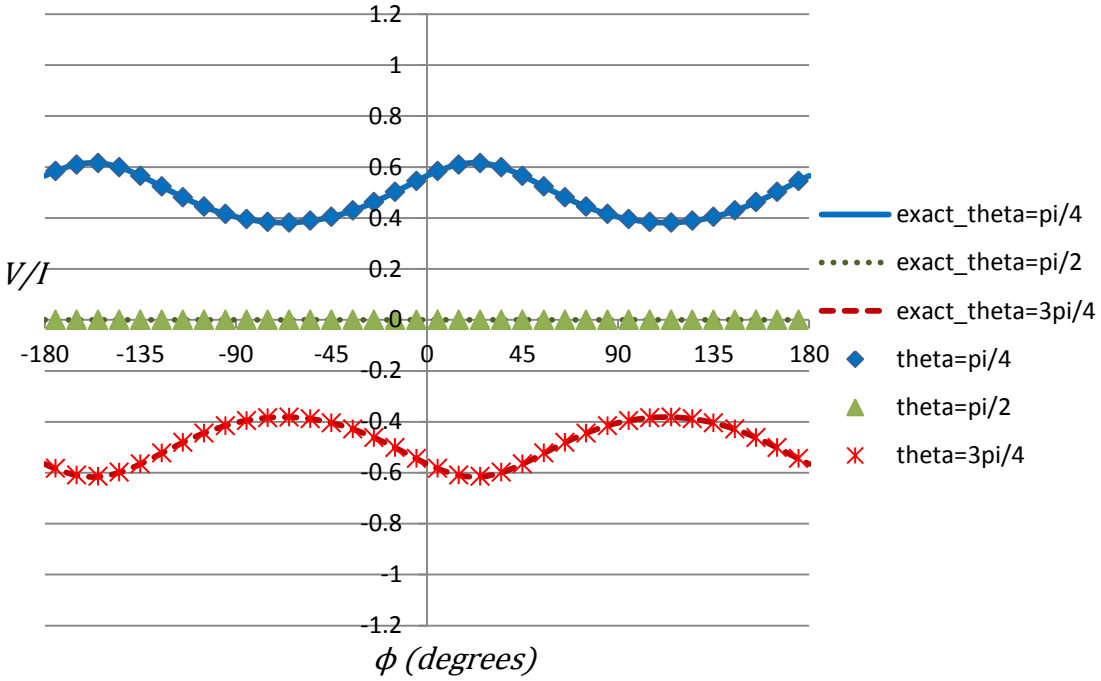

Figure 29. *V/I* for the incoherently scattered portion of a 5 keV photon beam with a source Stokes vector of $[\varphi_I, \varphi_Q, \varphi_U, \varphi_V] = [1,0.5,0.5,0.5]$.

Figure 30-Figure 41 show the results for a photon beam with the same source Stokes vector, but with an energy of 1MeV. At this energy the cross section for coherent scattering is on the order of a few microbarns and 5 orders of magnitude below the incoherent scattering cross section. For that reason, only the incoherent scattering results are shown.

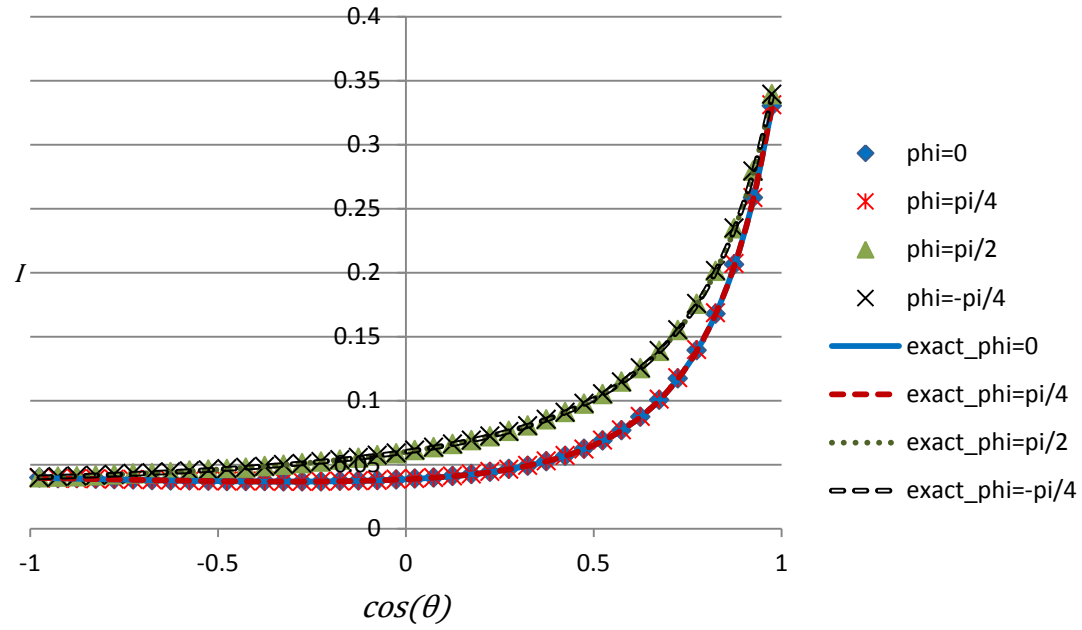

Figure 30. I for the incoherently scattered portion of a 1 MeV photon beam with a source Stokes vector of $[\varphi_I, \varphi_Q, \varphi_U, \varphi_V] = [1,0.5,0.5,0.5]$.

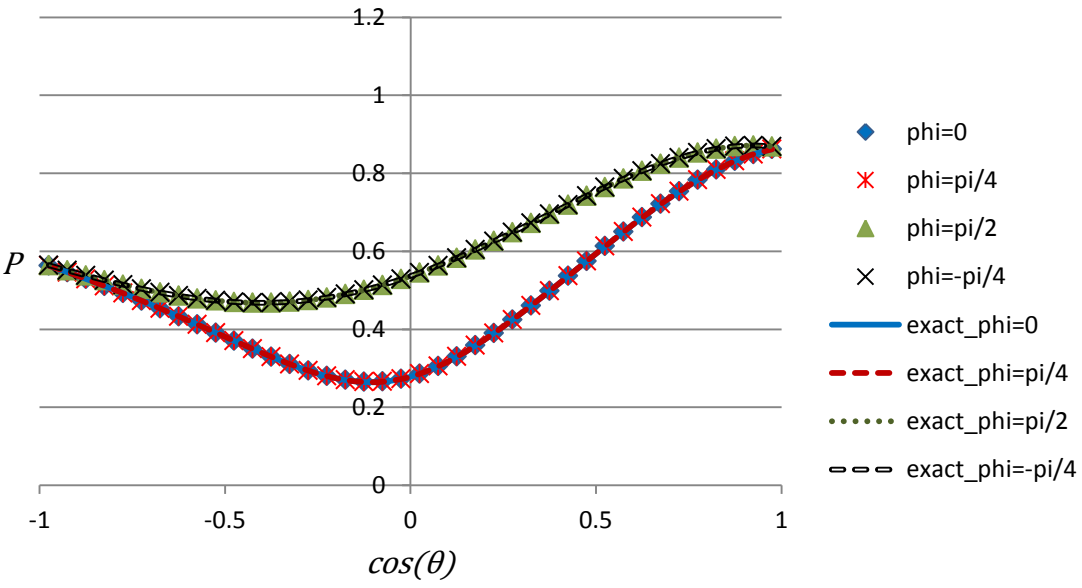

Figure 31. P for the incoherently scattered portion of a 1 MeV photon beam with a source Stokes vector of $[\varphi_I, \varphi_Q, \varphi_U, \varphi_V] = [1,0.5,0.5,0.5]$.

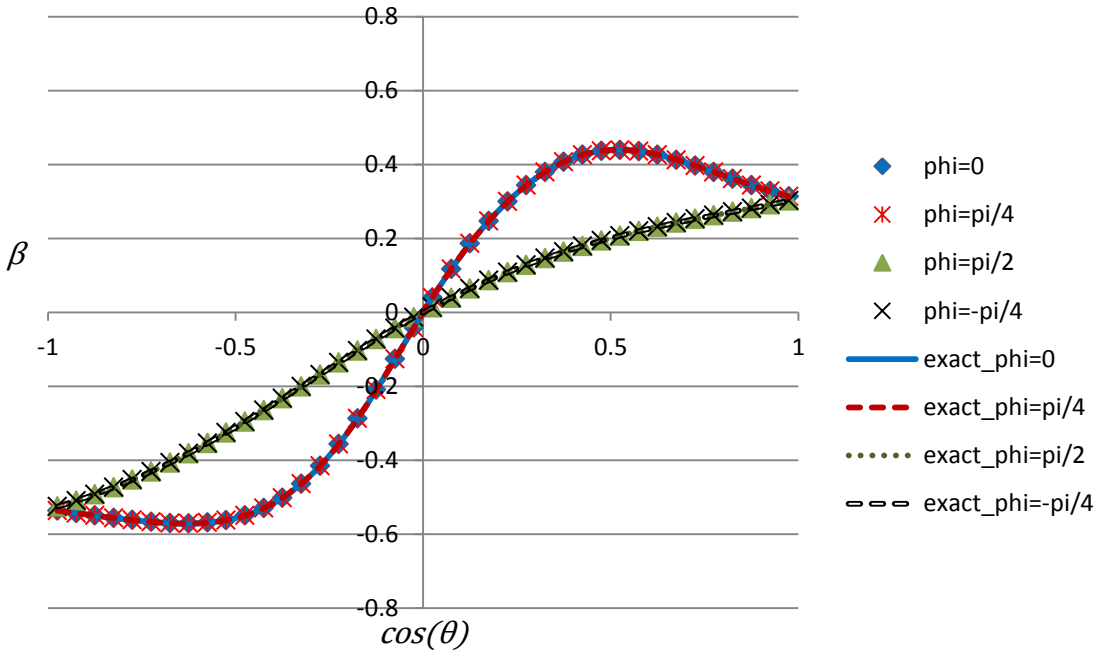

Figure 32. β for the incoherently scattered portion of a 1 MeV photon beam with a source Stokes vector of $[\varphi_I, \varphi_Q, \varphi_U, \varphi_V] = [1,0.5,0.5,0.5]$.

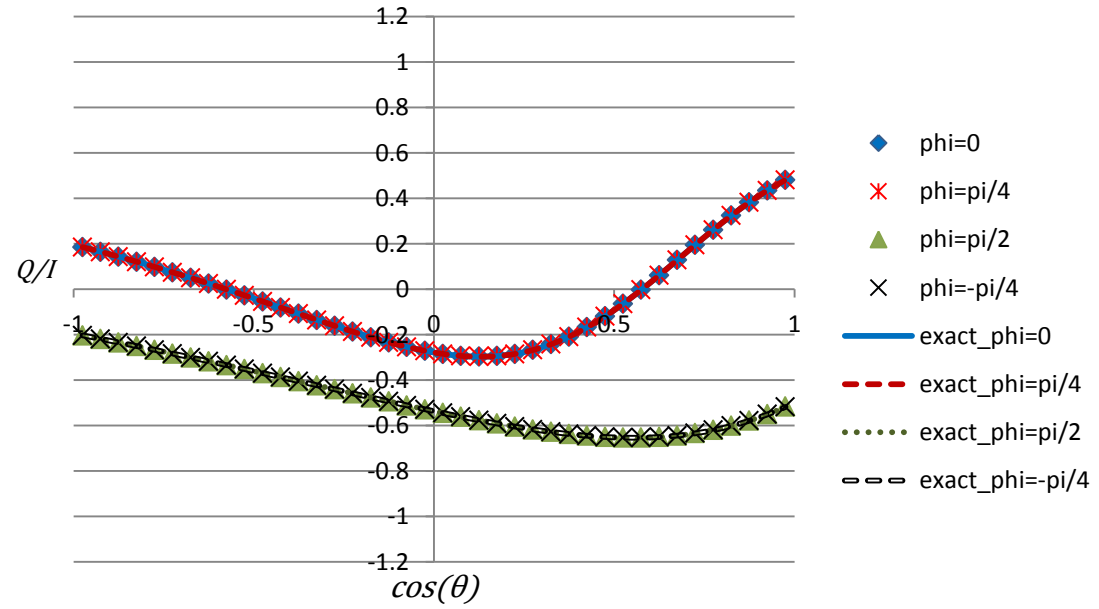

Figure 33. Q/I for the incoherently scattered portion of a 1 MeV photon beam with a source Stokes vector of $[\varphi_I, \varphi_Q, \varphi_U, \varphi_V] = [1,0.5,0.5,0.5]$.

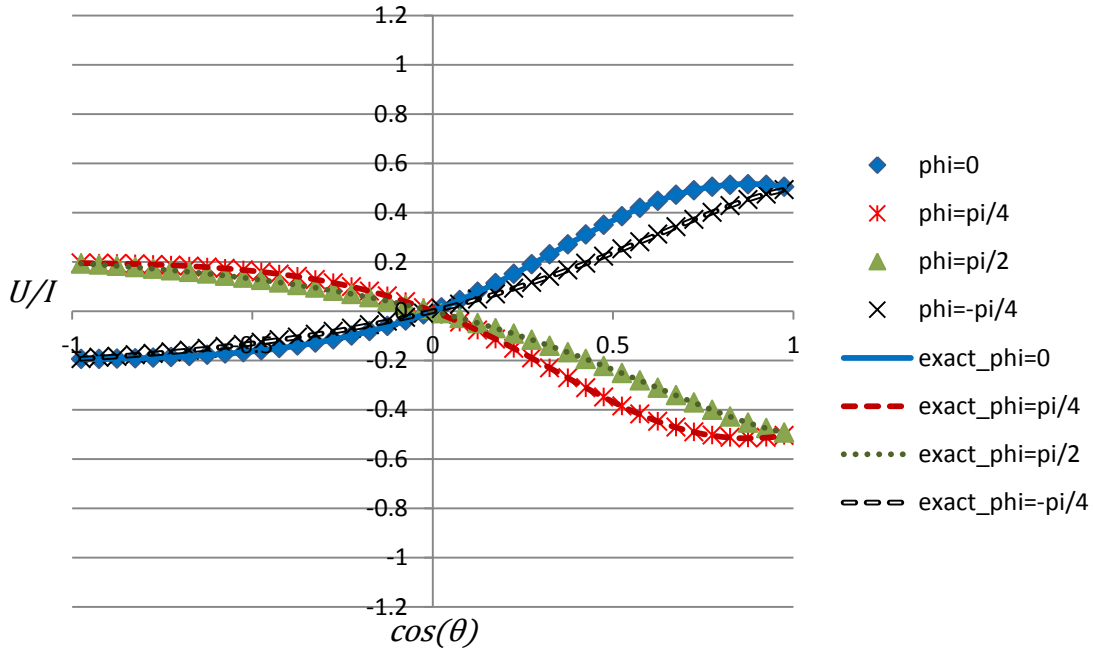

Figure 34. *U/I* for the incoherently scattered portion of a 1 MeV photon beam with a source Stokes vector of $[\varphi_I, \varphi_Q, \varphi_U, \varphi_V] = [1,0.5,0.5,0.5]$.

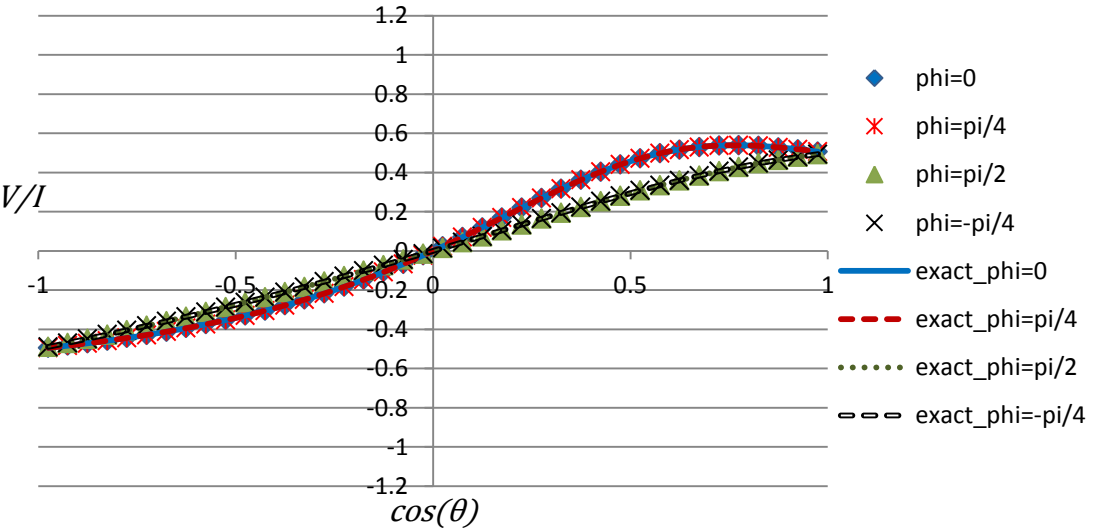

Figure 35. *V/I* for the incoherently scattered portion of a 1 MeV photon beam with a source Stokes vector of $[\varphi_I, \varphi_Q, \varphi_U, \varphi_V] = [1,0.5,0.5,0.5]$.

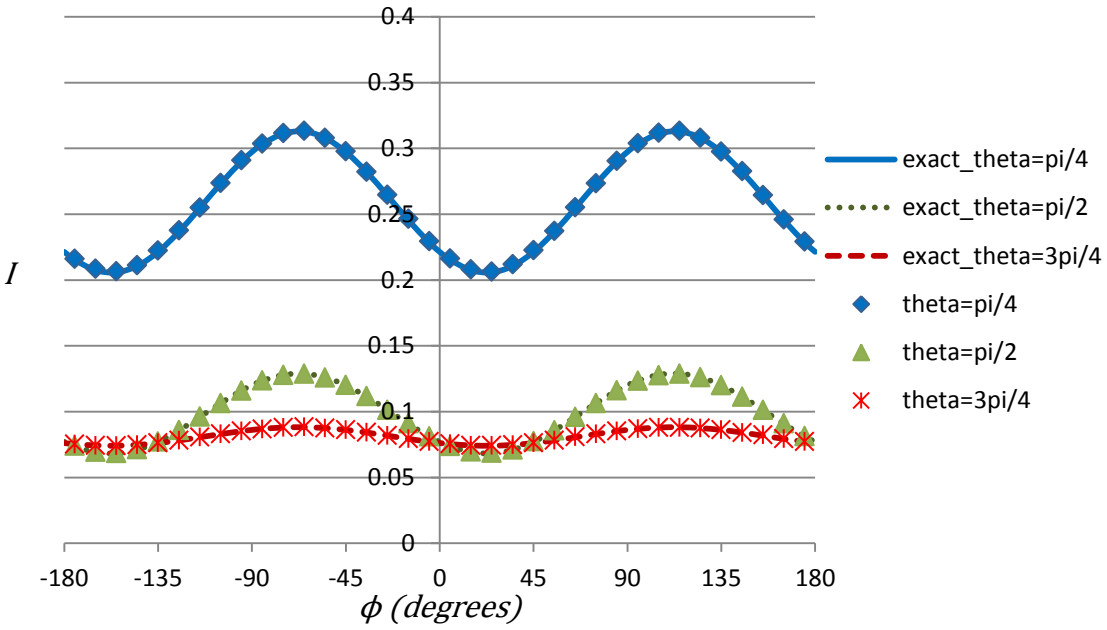

Figure 36. *I* for the incoherently scattered portion of a 1 MeV photon beam with a source Stokes vector of $[\varphi_I, \varphi_Q, \varphi_U, \varphi_V] = [1,0.5,0.5,0.5]$.

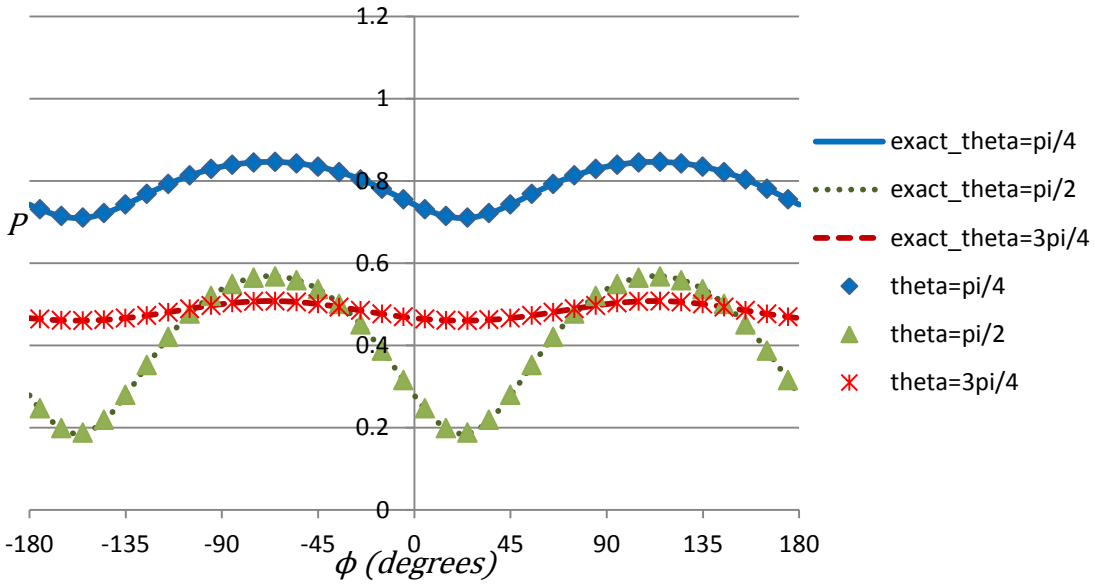

Figure 37. *P* for the incoherently scattered portion of a 1 MeV photon beam with a source Stokes vector of $[\varphi_I, \varphi_Q, \varphi_U, \varphi_V] = [1,0.5,0.5,0.5]$.

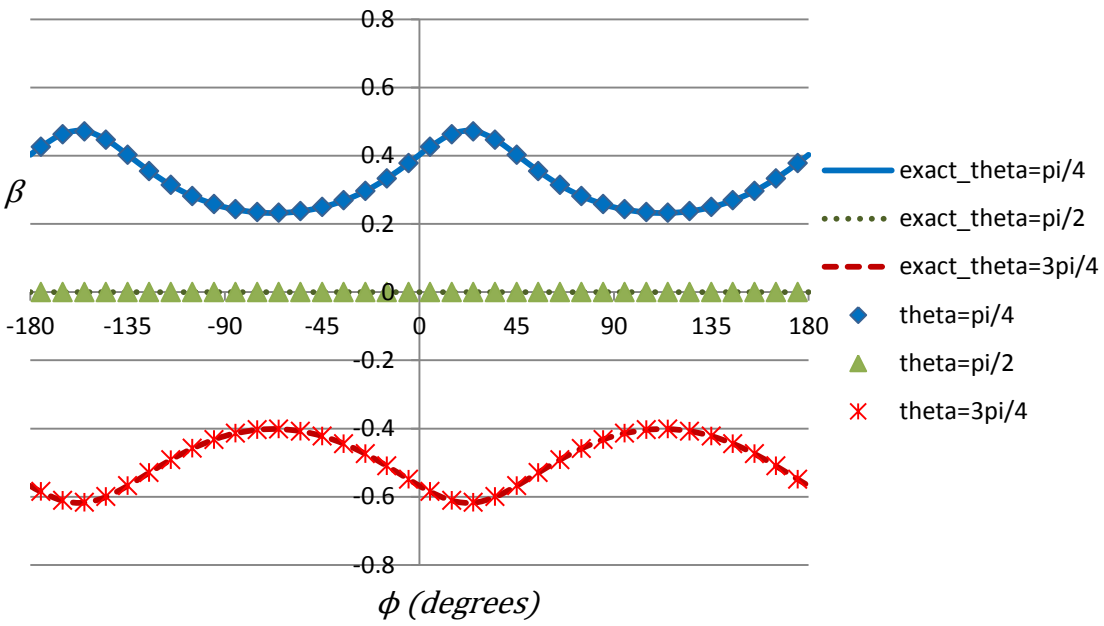

Figure 38. β for the incoherently scattered portion of a 1 MeV photon beam with a source Stokes vector of $[\varphi_I, \varphi_Q, \varphi_U, \varphi_V] = [1,0.5,0.5,0.5]$.

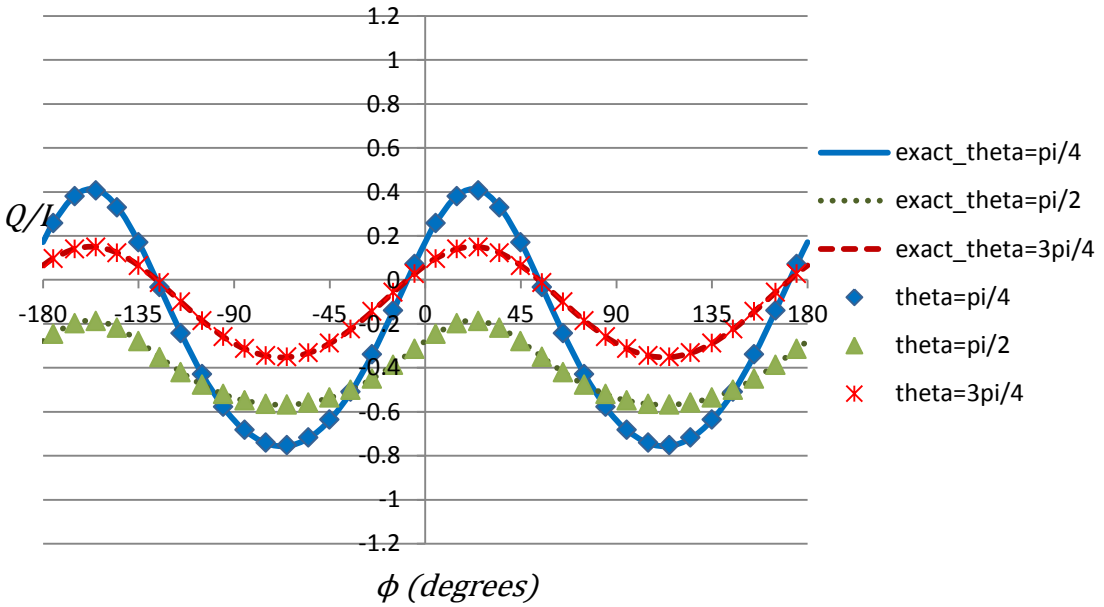

Figure 39. Q/I for the incoherently scattered portion of a 1 MeV photon beam with a source Stokes vector of $[\varphi_I, \varphi_Q, \varphi_U, \varphi_V] = [1,0.5,0.5,0.5]$.

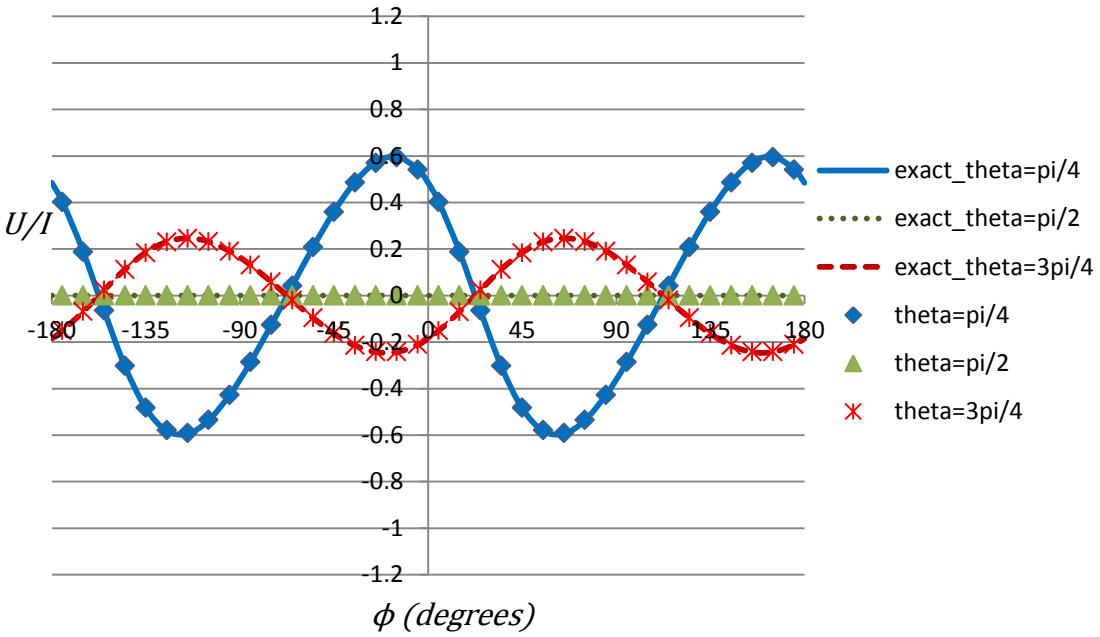

Figure 40. *U/I* for the incoherently scattered portion of a 1 MeV photon beam with a source Stokes vector of $[\varphi_I, \varphi_Q, \varphi_U, \varphi_V] = [1,0.5,0.5,0.5]$.

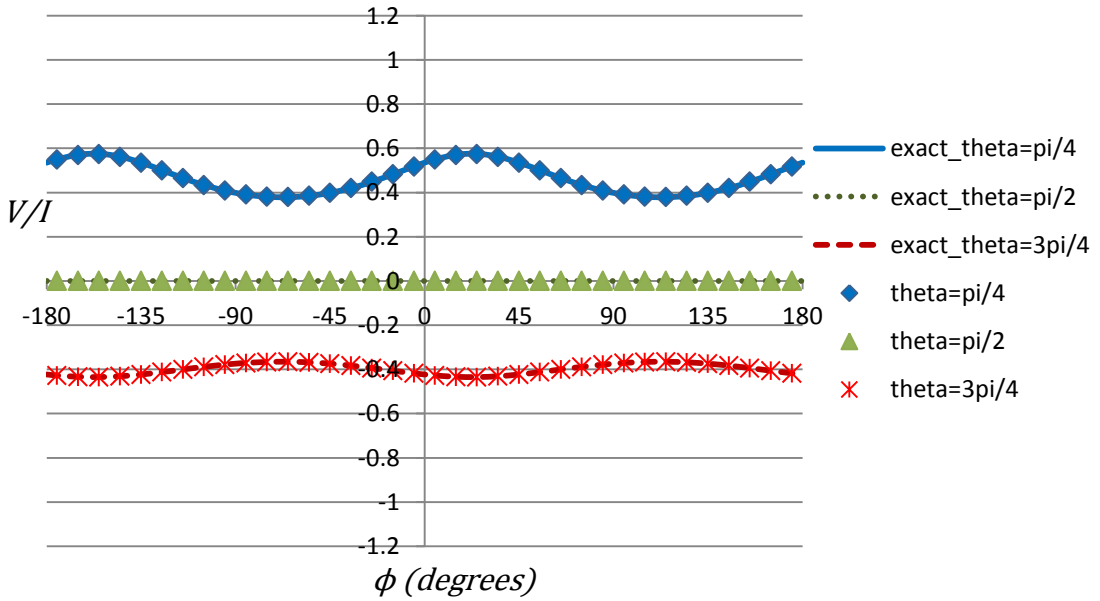

Figure 41. *V/I* for the incoherently scattered portion of a 1 MeV photon beam with a source Stokes vector of $[\varphi_I, \varphi_Q, \varphi_U, \varphi_V] = [1,0.5,0.5,0.5]$.

Figure 6-Figure 41 show that the solutions obtained by Mercury are in perfect agreement with the exact analytical solutions. Error bars are not seen on the graphs because they are so small that they are not visible. Appendix A has a more comprehensive collection of results for a variety of different source Stokes vectors. The only situations where perfect behavior is not observed are when the size of the solid angle range is large enough to cause some differences. However, even in those cases, the code results and analytic solution are still similar.

Mercury was also compared to past experimental and computational results for more complex problems. Benchmark experiments for linearly polarized photons were performed at the High Energy Accelerator Research Organization (KEK) in Japan[17].

Namito compares the results of EGS4 to the results from the experiment. The experimental setup can be seen in Figure 42, which is taken from a paper written by Namito[14].

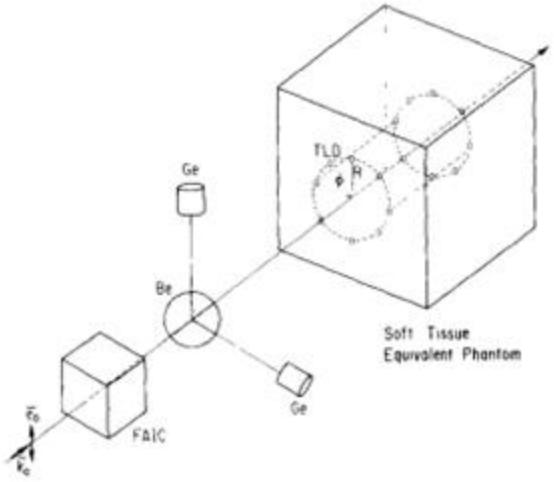

Figure 42. The setup used for the benchmark experiment. A monoenergetic (30 keV) photon beam is shot at a soft tissue equivalent phantom (30cm x 30 cm x 30 cm, ρ = 1.072 g/cm^3). The beam is linearly polarized with a polarization fraction (P) of 0.84. The phantom consists of 8.4 wt.% H, 15.5 wt.% O, 68.2 wt.% C, 3.8 wt.% N, 3.2 wt.% Cl, and 0.9 wt.% P. The absorbed dose is measured at varying depths, radial distances, and angles around the phantom.

This experiment was simulated using Mercury and the results were compared to the experimental results as well as the results found by EGS4. 1.0x10^{11} particles were simulated for the results shown in Figure 43, and the code used the ENDF/B-VI nuclear data file.

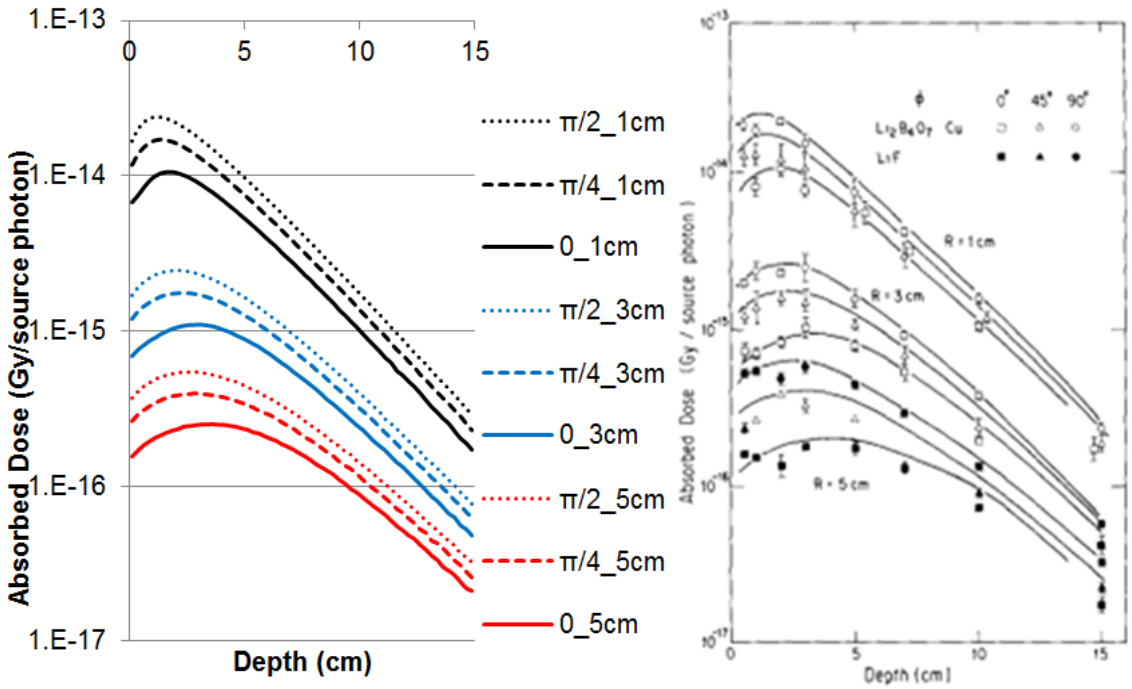

Figure 43. Absorbed dose at varying depths, radial distance away from the beam, and angles for a 30 keV beam with a polarization fraction of 0.84. On the left are the results from Mercury, and on the right are the experimental results and the results from EGS4. The maximum relative standard deviation for the Mercury results is 0.01722.

The Mercury results agree closely with the results from EGS4 and both codes agree reasonably well with the experimental results. The one place the results from the two codes slightly disagree is at small depths and larger radial distances. This small disagreement could be because of differences in cross section libraries, statistical uncertainties (no uncertainties were provided by Namito), or small differences between the actual problems being simulated. Nevertheless, Mercury's results match up well with the experimental data and the EGS4 results.

In order to test for the accuracy of elliptic polarization effects, the same problem as described in Figure 42 and Figure 43 was modeled except using different initial polarization states. The cumulative effects of multiple beams of light is equal to the effects caused by a single beam with a Stokes vector equal to the sum of the other individual beams' Stokes vectors [22]. So, if the same problem described by Namito was performed with three different photon beams with the following Stokes vectors:

$$\boldsymbol{\Gamma_1} = \frac{1}{3}\begin{bmatrix} 1 \\ 0.86 \\ -0.24 \\ 0.24 \end{bmatrix}, \qquad \boldsymbol{\Gamma_2} = \frac{1}{3}\begin{bmatrix} 1 \\ 0.9 \\ 0.1 \\ 0.32 \end{bmatrix}, \qquad \boldsymbol{\Gamma_3} = \frac{1}{3}\begin{bmatrix} 1 \\ 0.76 \\ 0.14 \\ -0.56 \end{bmatrix}, \qquad \text{Eq. 90}$$

then the combined results should be equal to a beam with the following Stokes vector:

$$\boldsymbol{\Gamma_{total}} = \boldsymbol{\Gamma_1} + \boldsymbol{\Gamma_2} + \boldsymbol{\Gamma_3} = \begin{bmatrix} 1 \\ 0.84 \\ 0 \\ 0 \end{bmatrix}. \qquad \text{Eq. 91}$$

The source Stokes vector in Eq. 91 is equal to the Stokes vector of the beam in the original simulation. Figure 44-46 show the results for the three beams described in Eq. 90 as well as the sum of the results from the three beams. When the word sum is used in these results it refers to the sum of the results of the three beams from Eq. 90 and when the word total is used it refers to the results obtained by the beam described in Eq. 91.

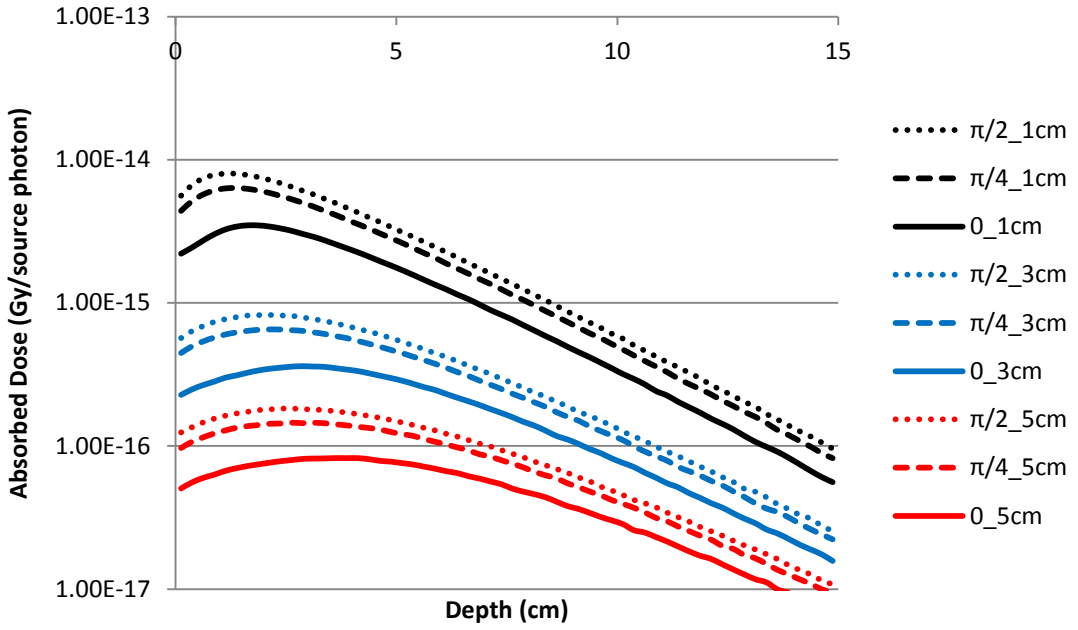

Figure 44. Absorbed dose at varying depths, radial distance away from the beam, and angles for a 30 keV beam with a Stokes vector of $^1/_3\,[1, 0.86, -0.24, 0.24]$.

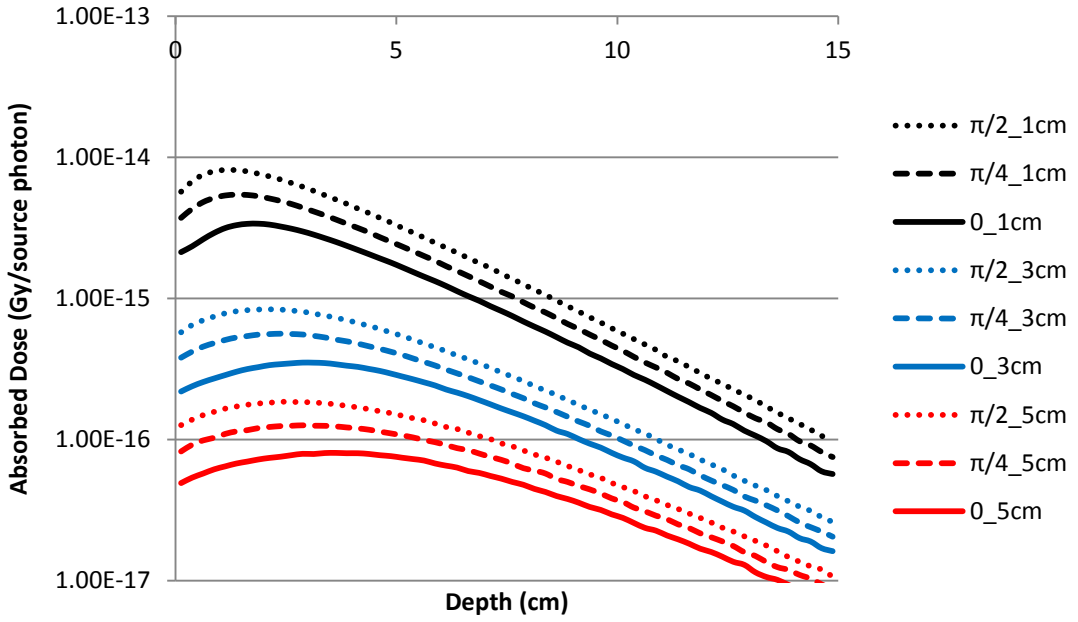

Figure 45. Absorbed dose at varying depths, radial distance away from the beam, and angles for a 30 keV beam with a Stokes vector of $^1/_3\,[1, 0.9, 0.1, 0.32]$.

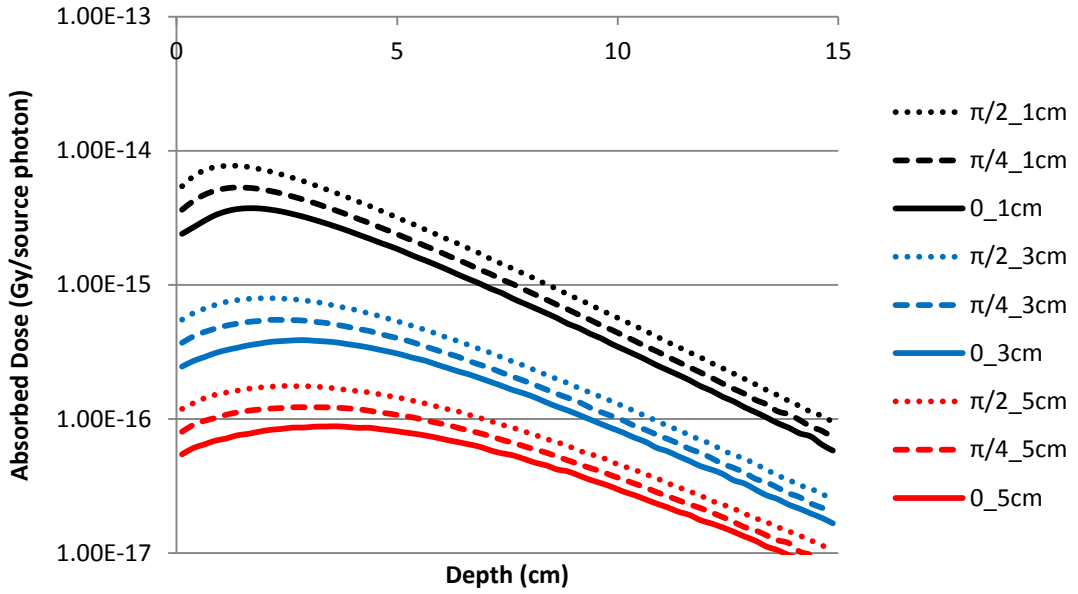

Figure 46. Absorbed dose at varying depths, radial distance away from the beam, and angles for a 30 keV beam with a Stokes vector of $^1/_3\,[1, 0.76, 0.14, -0.56]$.

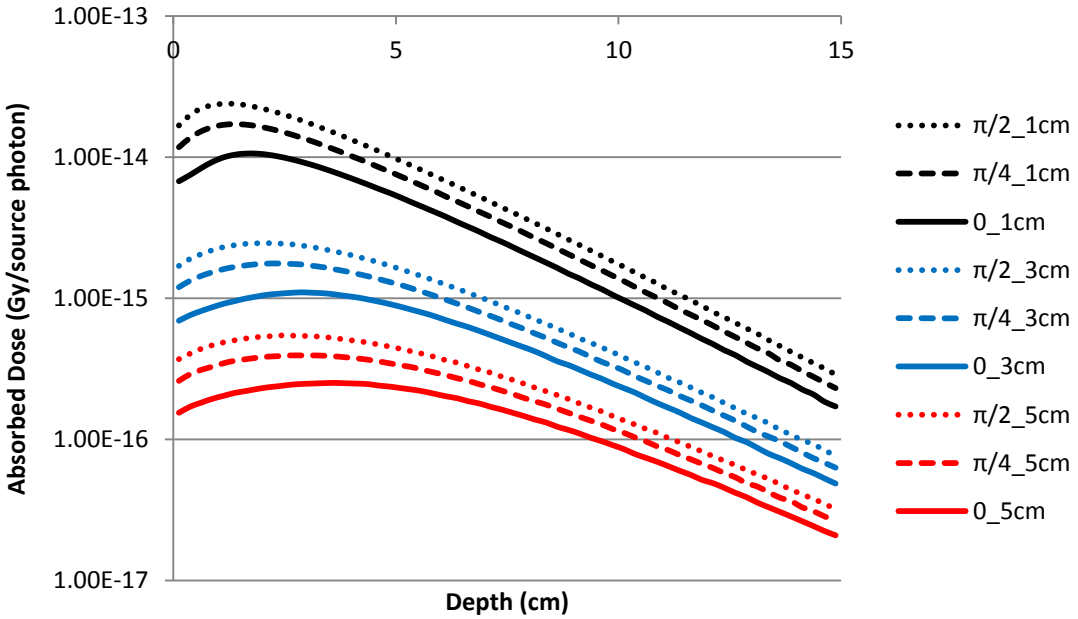

Figure 47. The combined absorbed dose at varying depths, radial distance away from the beam, and angles for three 30 keV beams with Stokes vectors of: $^1/_3\,[1, 0.86, -0.24, 0.24]$, $^1/_3\,[1, 0.9, 0.1, 0.32]$, $^1/_3\,[1, 0.76, 0.14, -0.56]$.

Figure 47 shows that the summed results of the three beams are statistically equivalent to the results achieved by the original beam as seen in Figure 43. A comparison of the relative difference between the summed results and the results from the total beam can be seen in Figure 48.

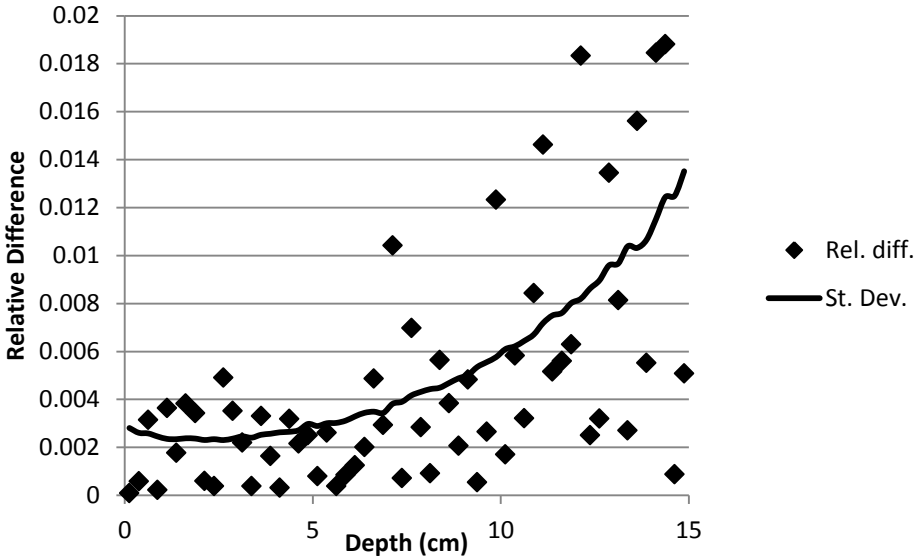

Figure 48. The relative difference between the summed results from Figure 47 and the total results from Figure 43 for a radial distance of 3 cm and an angle of 90 degrees away from the polarization direction of the total beam.

Figure 48 shows that the relative difference is within statistical uncertainties. 60% of the relative differences are within one standard deviation, 93.3% are within two standard deviations, and 100% are within three standard deviations. This is what we would expect if everything was coded perfectly. While this is not definitive proof that Mercury is accurately modeling elliptically polarized light, it does demonstrate the results are consistent with themselves. When we consider also the broomstick results

described above and in Appendix A, we consider the polarization logic in the Mercury code to be well verified.

An interesting result is that polarization effects can be observed even for unpolarized beams. Because an unpolarized beam can be polarized by scattering events, polarization effects can be seen in multiple-scatter problems. In a situation where an unpolarized beam is normal to a surface, a consideration of polarization effects will cause the multiple-scattered portion of the beam to be more skewed towards a direction parallel or antiparallel to the original beam than if polarization effects are ignored. In order to observe this phenomenon, a simulation was run where an unpolarized 50 keV beam was incident upon a slab of carbon with a thickness of 2.945 mean free paths. A tally was taken of all twice-scattered photons that exited the slab. Figure 49 shows that there is a small but clear difference between the angular distributions in the two cases. All error bars are too small to be seen on the graph.

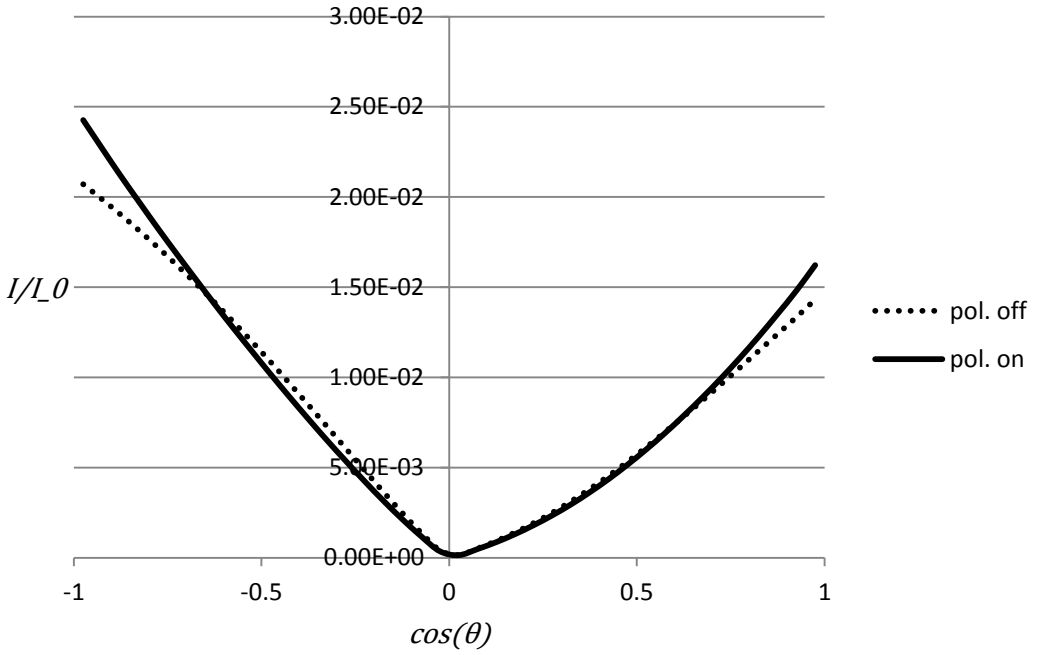

Figure 49. The angular distribution of twice scattered photons exiting a slab. The beam was incident upon the slab with an energy of 50 keV and a Stokes vector of [1, 0, 0, 0].The maximum relative uncertainty for these results is 0.0027.

There is also an effect on the portion of the beam that is reflected or transmitted through the slab. Table I below shows the transmission and reflection coefficients for this simulation.

Table I. The effect of polarization on the transmission and reflection coefficients of a 50 keV unpolarized beam on a slab of carbon with a thickness of 2.945 mean free paths.

	Transmission Coefficient	Reflection Coefficient
Polarization on	$2.24350*10^{-1}$ +/- $1.23*10^{-5}$	$3.55424*10^{-1}$ +/- $1.50*10^{-5}$
Polarization off	$2.19314*10^{-1}$ +/- $1.34*10^{-5}$	$3.49759*10^{-1}$+/- $1.48*10^{-5}$
Relative difference	$2.24472*10^{-2}$ +/- $8.11*10^{-5}$	$1.59475*10^{-2}$ +/- $5.92*10^{-5}$

Figure 49 and Table I show that polarization effects are present even in situations where the initial beam is unpolarized. The differences between considering polarization and not is small but much larger than statistical uncertainty. The effects are most evident at lower energies and in materials where scattering dominates.

Adding polarization effects does not come without a computational cost. In order to determine how much including polarization affects the run time of Mercury, the problem described in Figure 42 was run once with polarization effects turned on and once with them turned off. Both runs simulated 10^{11} particle histories on 384 cores from the same machine. With polarization enabled the simulation took 81 minutes and 7.1 seconds, and without polarization it took 68 minutes and 46 seconds. This corresponds to a slowdown of 18%. For the problem depicted in Figure 49, there was a slowdown of 43%. Scattering-dominated problems will be slowed more by enabling polarization effects than problems without many scattering events.

CHAPTER V

CONCLUSIONS

New technology in the field of gamma ray production has created the need for accurate modeling of polarized light. In this project, the capability of modeling polarized light was added to an existing massively parallel Monte Carlo transport code called Mercury. Previous implementations of polarization effects into transport codes were either done with research codes or with more narrowly focused production codes, but Mercury is a powerful and versatile modern code with an active development team.

Using the Stokes vector representation of polarized light and the vector transport equation, a method that efficiently and accurately simulates partially or fully polarized light was implemented into Mercury. Mercury now has the ability to simulate both linearly and elliptically polarized light, which is significant because previous research has primarily dealt with linearly polarized light exclusively. The ability to model elliptically polarized light beams makes Mercury unique among production transport codes although more results from experiments with elliptically polarized light would be beneficial for verification and validation.

The code was tested at low and high energies and was compared to analytical, experimental, and computational results. In all cases, Mercury showed agreement with the expected results. It was also shown that polarization effects are present and potentially significant even in cases where an initial beam is completely unpolarized. This means that any photon transport code that does not include polarization effects will

be slightly inaccurate if it does not include polarization effects, regardless of the problem being simulated.

Including polarization effects did cause significant but not crippling slowdown of the code. The simulations in this project were slowed in the range of 10-50% when polarization effects were included. Simulations with a heavy scattering component will be slowed down more than simulations in which scattering is not as prevalent.

REFERENCES

1. G. Stokes, “On the composition and resolution of streams of polarized light from different sources,” *Transactions of the Cambridge Philosophical Society,* vol. 9, pp. 399-416, 1852.

2. H. C. van de Hulst, *Light Scattering by Small Particles*, vol. 84, Courier Dover Publications, pp. 198-199, 1957.

3. S. J Orfanidis, *Electromagnetic Waves and Antennas*, Rutgers University, New Brunswick, New Jersey, 2008.

4. E. Landi Degl’Innocenti, and M. Landolfi. *Polarization in Spectral Lines,* Kluwer Academic Publishers, Dordrecht, The Netherlands, 2004.

5. J.E. Fernández, J.H. Hubbell, A.L. Hanson, L.V. Spencer, “Polarization effects on multiple scattering gamma transport,” *Radiation Physics and Chemistry*, vol. 41, pp. 579-630, April–May 1993.

6. S. Chandrasekhar, *Radiative Transfer,* Clarendon Press, Oxford, UK, 1950.

7. J. E. Fernandez, “Monte Carlo simulation of linearly polarized photons,” *Applied Radiation and Isotopes,* vol. 48, pp. 1635-1646, 1997.

8. J. H. Hubbell and I. Overbo, “Relativistic atomic form factors and photon coherent scattering cross-sections,” *Journal of Physical Chemistry*, 1979

9. J. E. Fernandez, “Polarization effects and gamma transport,” *Applied Radiation and Isotopes*, vol. 46, pp. 383-400, 1995.

10. M. C. Weisskopf, R. F. Elsner ; R. Novick ; P. Kaaret and E. Silver, “On the design of scattering polarimeters at the focus of an x-ray telescope”, *Proc. SPIE 1159, EUV, X-Ray, and Gamma-Ray Instrumentation for Astronomy and Atomic Physics*, pp. 607, November 27, 1989.

11. E Costa, M.N Cinti, M Feroci, G Matt, M Rapisarda, “Design of a scattering polarimeter for hard x-ray astronomy,” *Nuclear Instruments and Methods in Physics Research Section A: Accelerators, Spectrometers, Detectors and Associated Equipment*, vol. 366, pp. 161-172, 21 November 1995.

12. H. H. Tynes, G. W. Kattawar, E. P. Zege, I. L. Katsev, A. S. Prikhach, and L. I. Chaikovskaya, “Monte Carlo and multicomponent approximation methods for vector radiative transfer by use of effective Mueller matrix calculations,” *Appl. Opt*., vol.40, pp. 400–412, 2001.

13. Bruce M. Swinyard, Giuseppe Malaguti, Ezio Caroli, Anthony J. Dean, and Guido Di Cocco, “Spectroscopy and polarimetry capabilities of the INTEGRAL imager: Monte Carlo simulation results," *Proc. SPIE 1548, Production and Analysis of Polarized X Rays*, vol. 94, November 1, 1991.

14. Y. Namito, S. Ban, and H. Hirayama, “Implementation of linearly-polarized photon scattering into the EGS4 code,” *Nuclear Instruments and Methods in Physics Research*, vol. 332, pp. 277, 1993.

15. W. R. Nelson and Y. Namito, “The EGS4 code system: solution of gamma-ray and electron transport problems,” *SLAC Pub. 5193*, February 9, 1990.

16. O. Klein and Y. Nishina, “Iber die streuung von strahlung dutch freie elektronen nach der neuen relativistischen quantendynamik von Dirac,” *Z. Phys, vol.*52, pp. 853, 1929

17. Y. Namito, H. Hirayama, S. Ban, “Improvements of low-energy photon transport in EGS4,” *Radiation Physics and Chemistry*, vol. 53, pp. 283-294, September 1998.

18. G. Matt, M. Feroci, M. Rapisarda, and E. Costa, “Treatment of compton scattering of linearly polarized photons in Monte Carlo codes,” *Radiation Physics and Chemistry,* vol. 48, pp.403, 1996.

19. T. Goorley and A. Sood, “Using MCNP5 for medical physics applications,” Los Alamos National Laboratory Report, Los Alamos, New Mexico, LA-UR-06-2347, 2006.

20. R. J. Procassini, D. E. Cullen, G. M. Greenman, C. A. Hagmann. “Verification and Validation of MERCURY: A modern, Monte Carlo particle transport code,” Lawrence Livermore National Laboratory Report, Livermore, California, UCRL-PROC-208669, 2004.

21. B. Beck, P. Brantley, E. Brooks, F. Daffin, C. Hagmann, S. Quaglioni, J. Rathkopf, “MCAPM-C generator and collision routine (Gen2000/Bang2000) documentation,” Lawrence Livermore National Laboratory Report, Livermore, California, 2012.

22. R. C. Jones, “A new calculus for the treatment of optical systems,” *Journal of the Optical Society of America,* vol. 37, pp. 107, 1947.

APPENDIX A

ADDITIONAL RESULTS

Many more results were gained than were displayed in Chapter IV. In this appendix more results from the “broomstick” problem can be found.

A.1, $\Gamma = [1,0,0,0]$

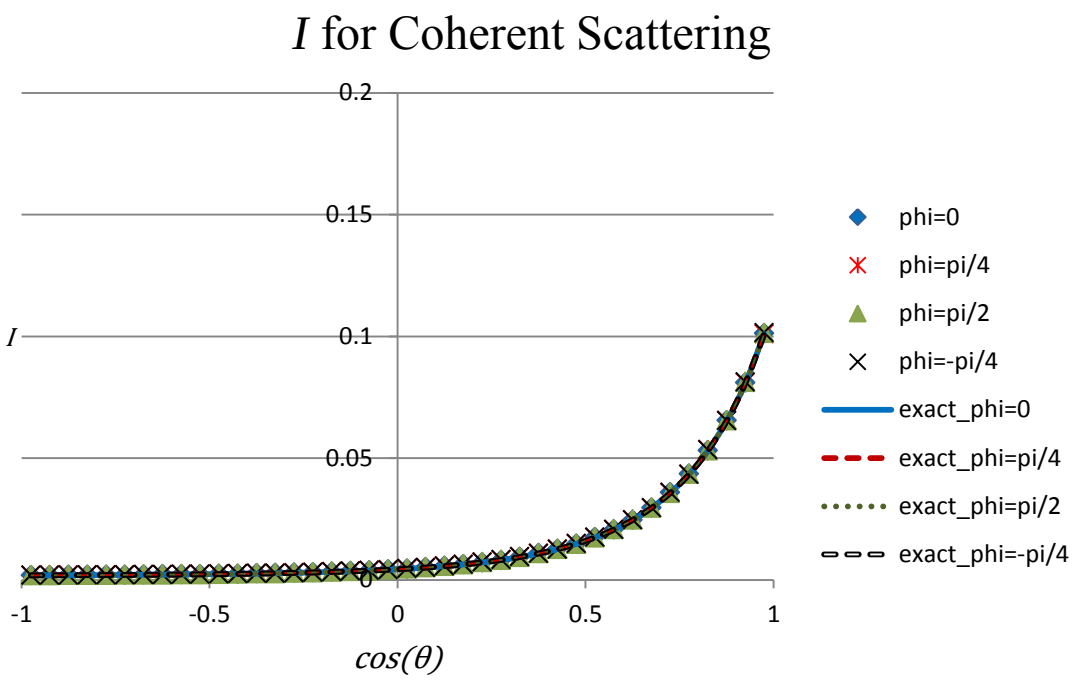

Figure A.1. I for the coherently scattered portion of a 5 keV photon beam with a source Stokes vector of $[\varphi_I, \varphi_Q, \varphi_U, \varphi_V] = [1,0,0,0]$.

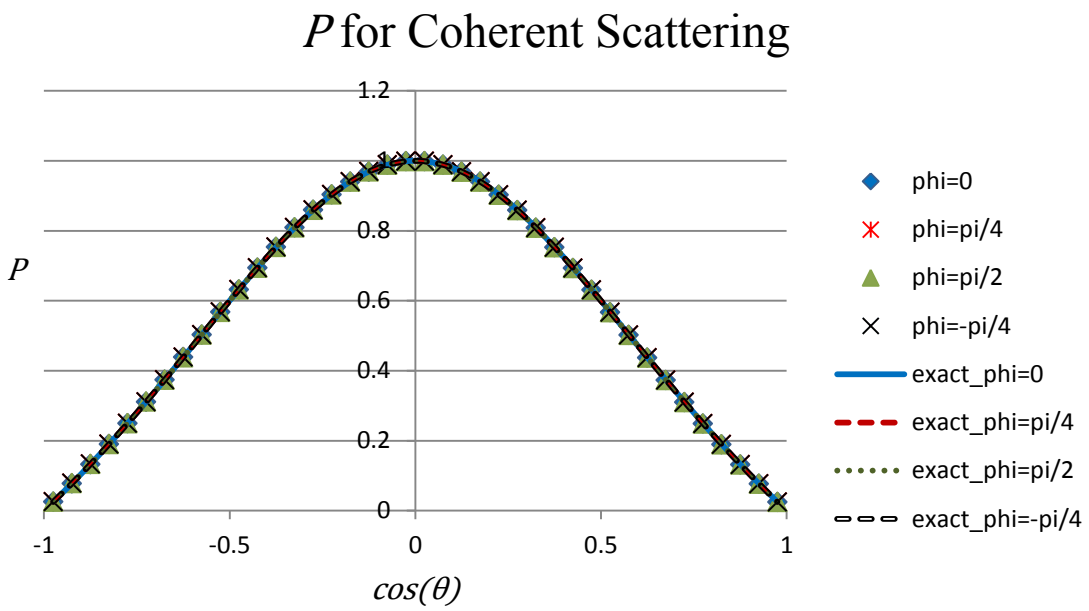

Figure A.2. P for the coherently scattered portion of a 5 keV photon beam with a source Stokes vector of $[\varphi_I, \varphi_Q, \varphi_U, \varphi_V] = [1,0,0,0]$.

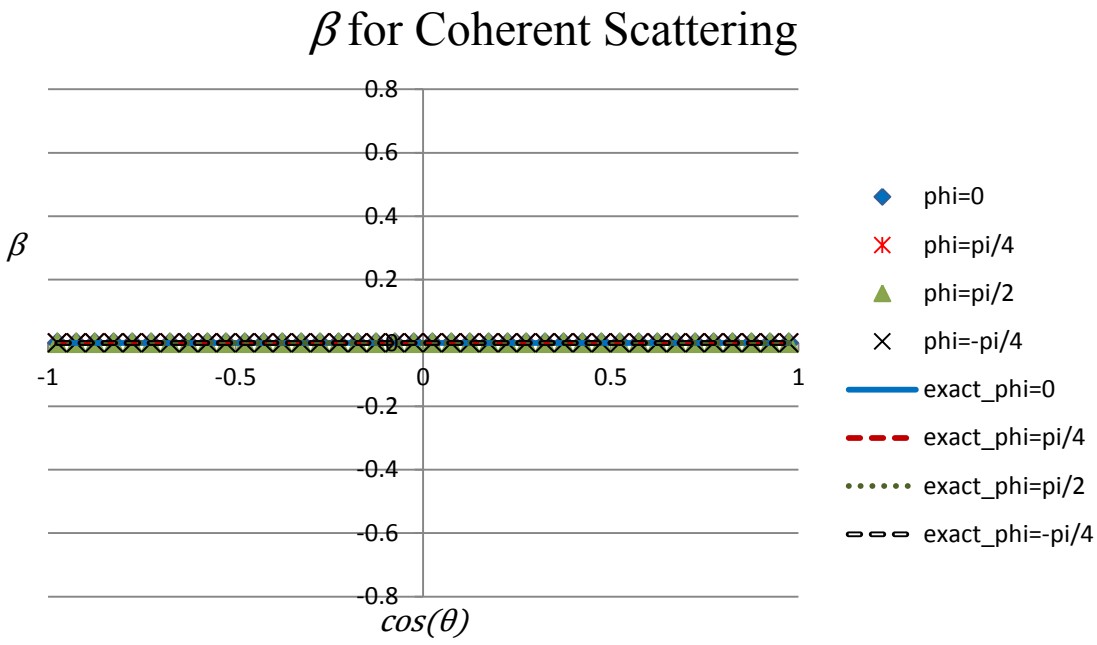

Figure A.3. β for the coherently scattered portion of a 5 keV photon beam with a source Stokes vector of $[\varphi_I, \varphi_Q, \varphi_U, \varphi_V] = [1,0,0,0]$.

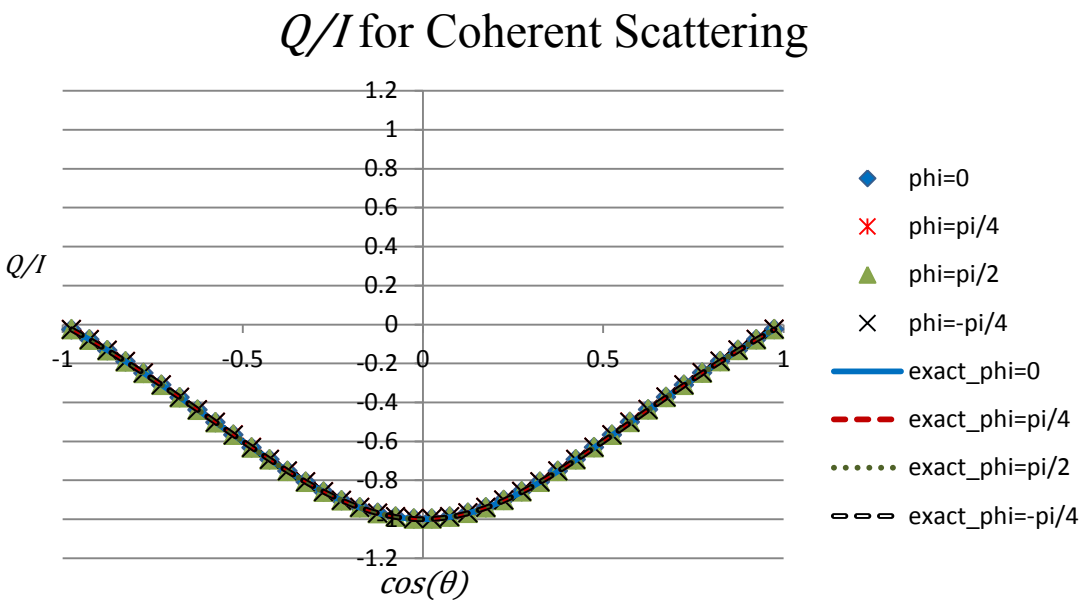

Figure A.4. *Q/I* for the coherently scattered portion of a 5 keV photon beam with a source Stokes vector of $[\varphi_I, \varphi_Q, \varphi_U, \varphi_V] = [1,0,0,0]$.

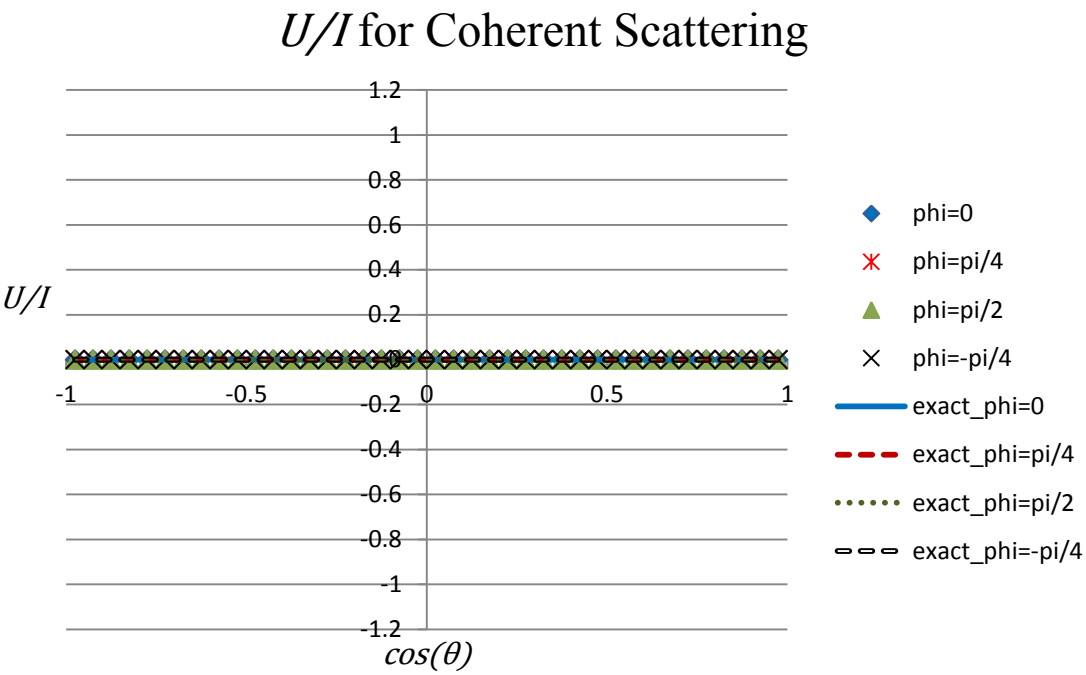

Figure A.5. *U/I* for the coherently scattered portion of a 5 keV photon beam with a source Stokes vector of $[\varphi_I, \varphi_Q, \varphi_U, \varphi_V] = [1,0,0,0]$.

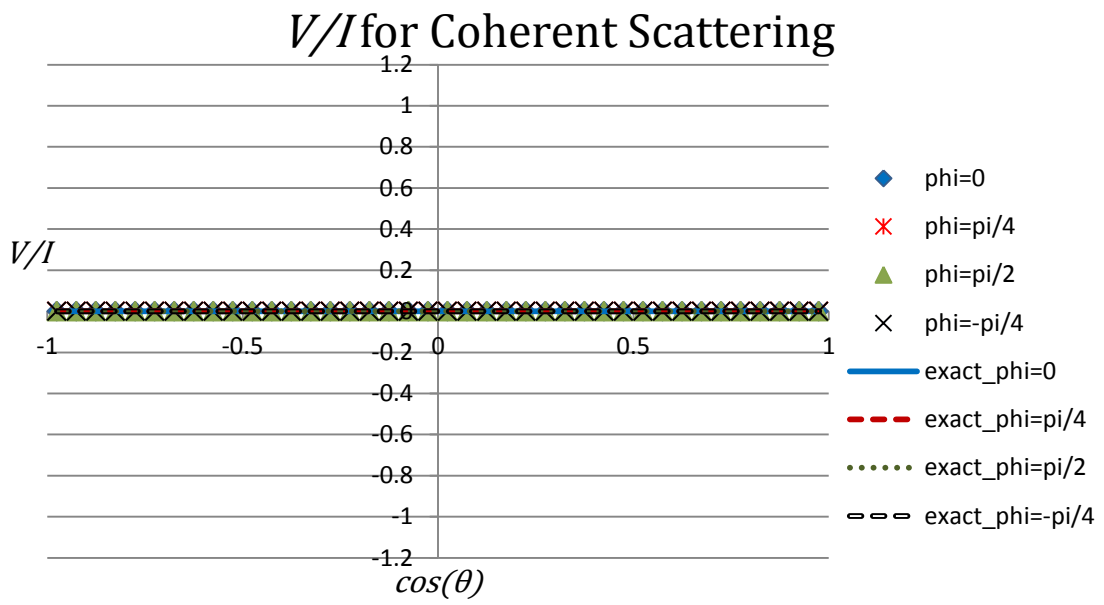

Figure A.6. V/I for the coherently scattered portion of a 5 keV photon beam with a source Stokes vector of $[\varphi_I, \varphi_Q, \varphi_U, \varphi_V] = [1,0,0,0]$.

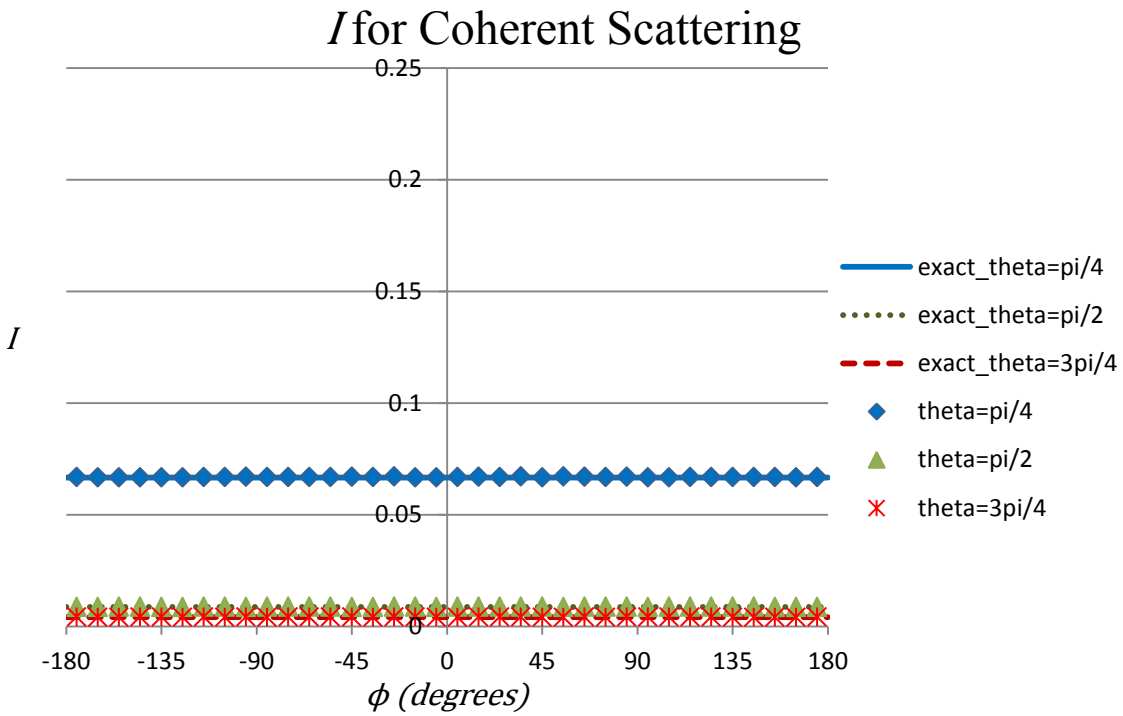

Figure A.7. I for the coherently scattered portion of a 5 keV photon beam with a source Stokes vector of $[\varphi_I, \varphi_Q, \varphi_U, \varphi_V] = [1,0,0,0]$.

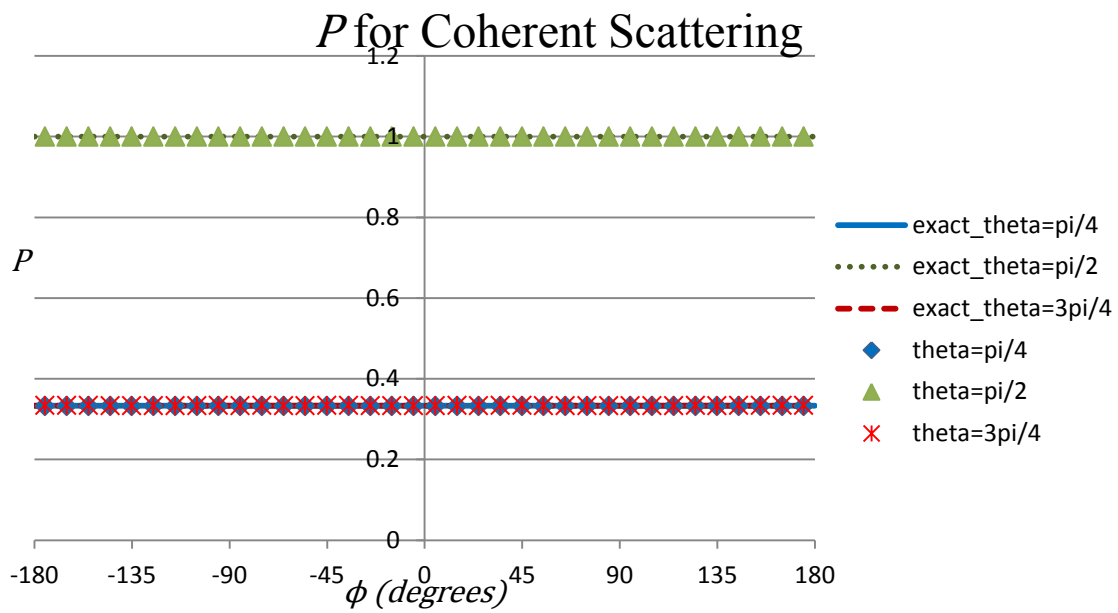

Figure A.8. P for the coherently scattered portion of a 5 keV photon beam with a source Stokes vector of $[\varphi_I, \varphi_Q, \varphi_U, \varphi_V] = [1,0,0,0]$.

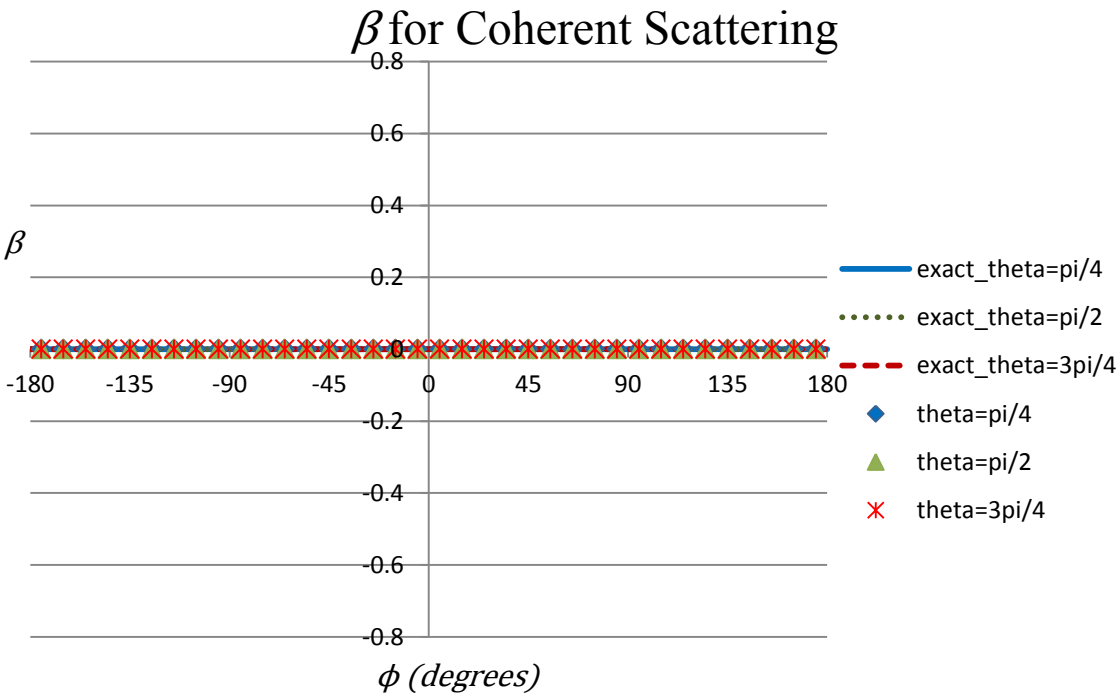

Figure A.9. β for the coherently scattered portion of a 5 keV photon beam with a source Stokes vector of $[\varphi_I, \varphi_Q, \varphi_U, \varphi_V] = [1,0,0,0]$.

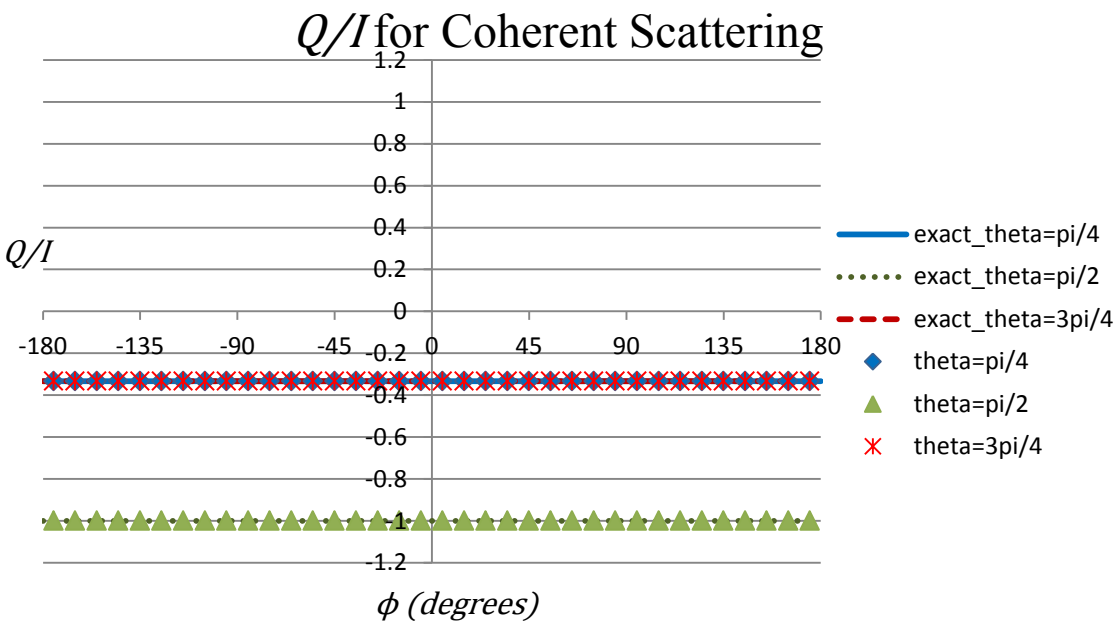

Figure A.10. Q/I for the coherently scattered portion of a 5 keV photon beam with a source Stokes vector of $[\varphi_I, \varphi_Q, \varphi_U, \varphi_V] = [1,0,0,0]$.

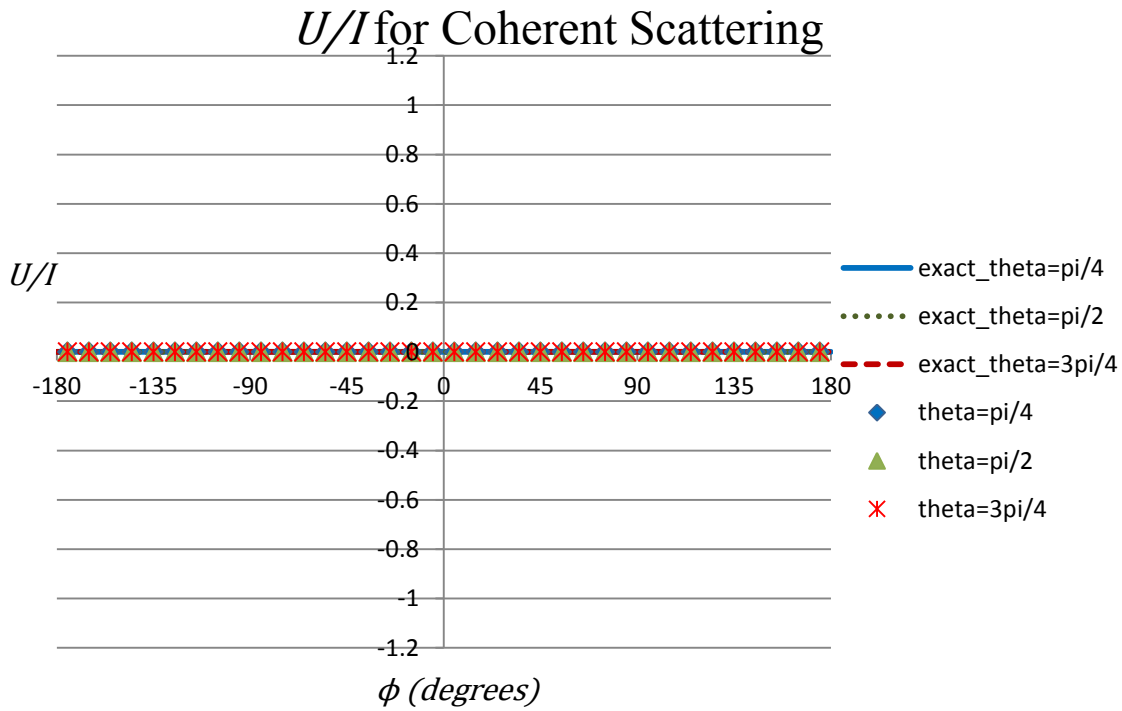

Figure A.11. U/I for the coherently scattered portion of a 5 keV photon beam with a source Stokes vector of $[\varphi_I, \varphi_Q, \varphi_U, \varphi_V] = [1,0,0,0]$.

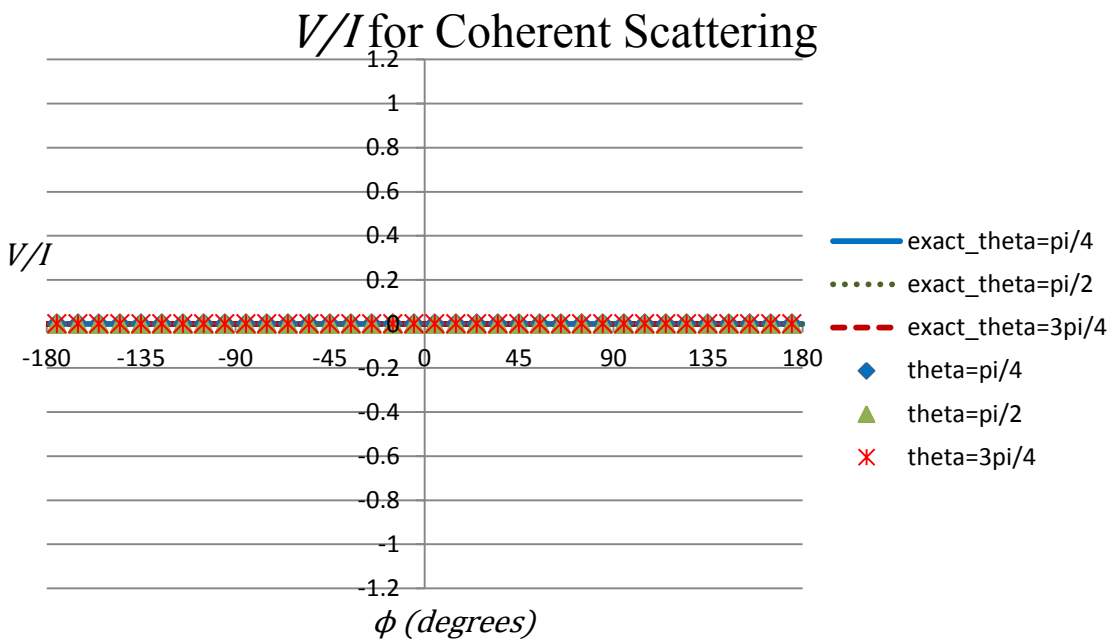

Figure A.12. *V/I* for the coherently scattered portion of a 5 keV photon beam with a source Stokes vector of $[\varphi_I, \varphi_Q, \varphi_U, \varphi_V] = [1,0,0,0]$.

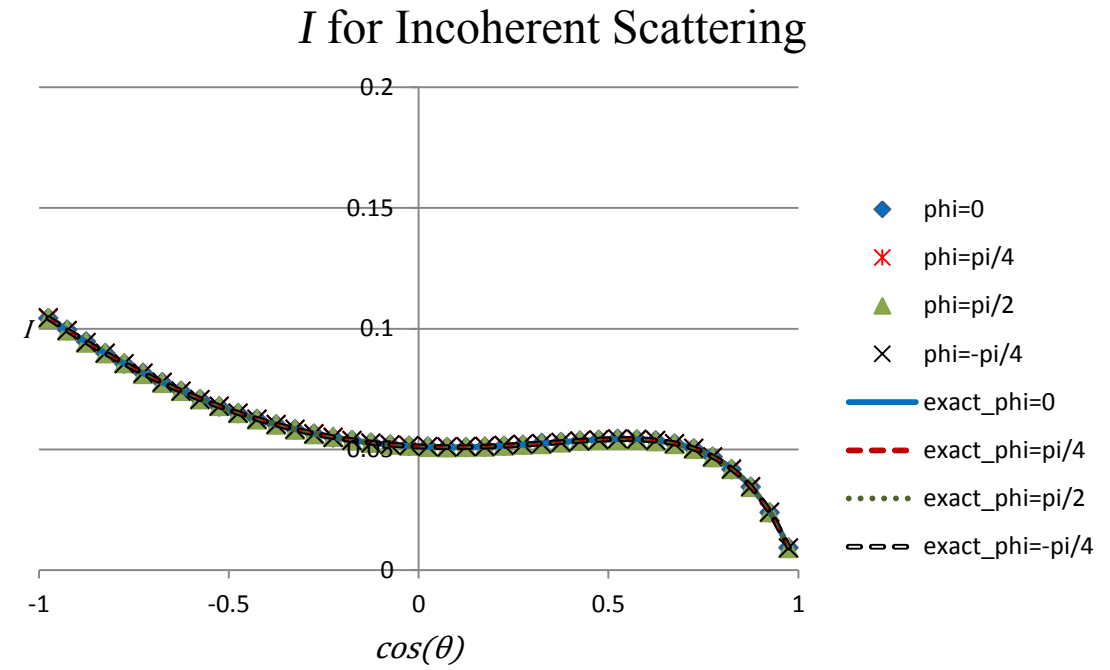

Figure A.13. *I* for the incoherently scattered portion of a 5 keV photon beam with a source Stokes vector of $[\varphi_I, \varphi_Q, \varphi_U, \varphi_V] = [1,0,0,0]$.

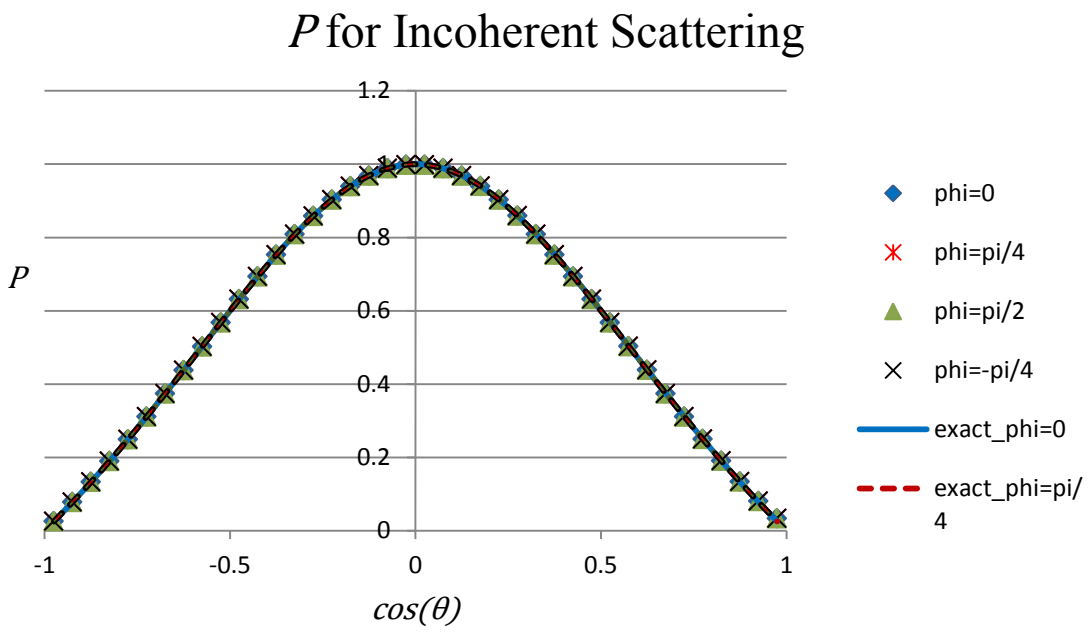

Figure A.14. P for the incoherently scattered portion of a 5 keV photon beam with a source Stokes vector of $[\varphi_I, \varphi_Q, \varphi_U, \varphi_V] = [1,0,0,0]$.

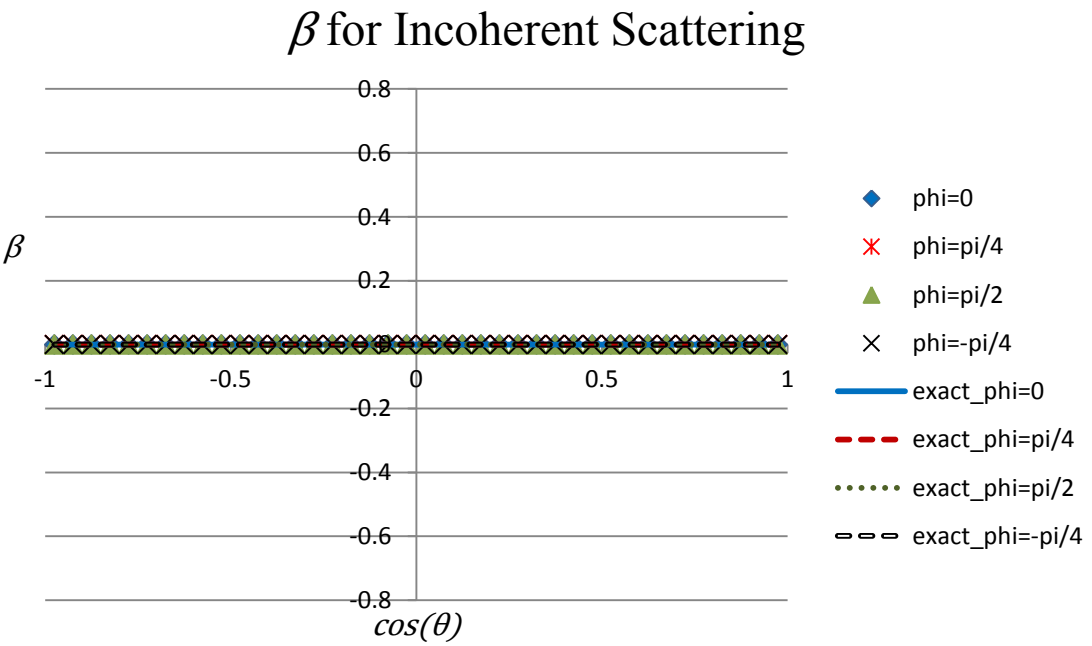

Figure A.15. β for the incoherently scattered portion of a 5 keV photon beam with a source Stokes vector of $[\varphi_I, \varphi_Q, \varphi_U, \varphi_V] = [1,0,0,0]$.

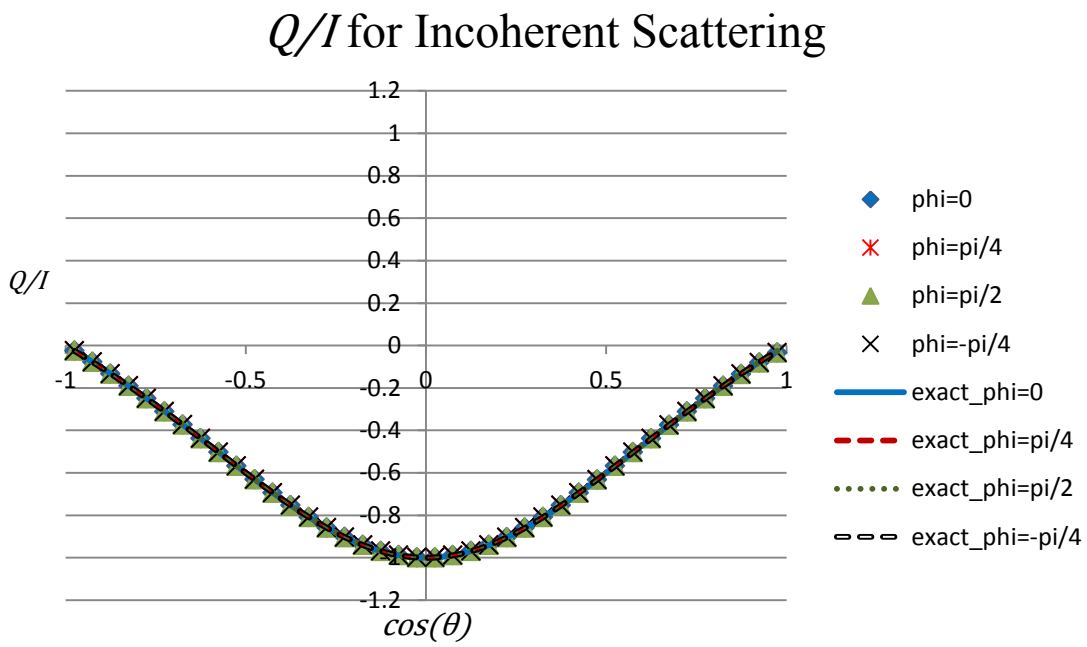

Figure A.16. *Q/I* for the incoherently scattered portion of a 5 keV photon beam with a source Stokes vector of $[\varphi_I, \varphi_Q, \varphi_U, \varphi_V] = [1,0,0,0]$.

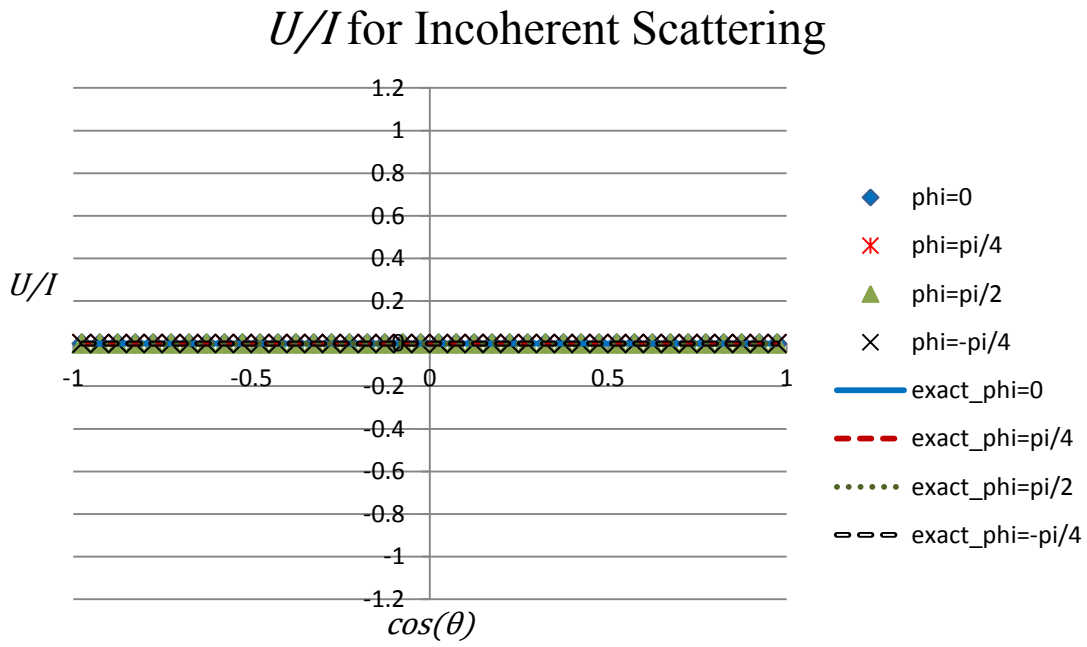

Figure A.17. *U/I* for the incoherently scattered portion of a 5 keV photon beam with a source Stokes vector of $[\varphi_I, \varphi_Q, \varphi_U, \varphi_V] = [1,0,0,0]$.

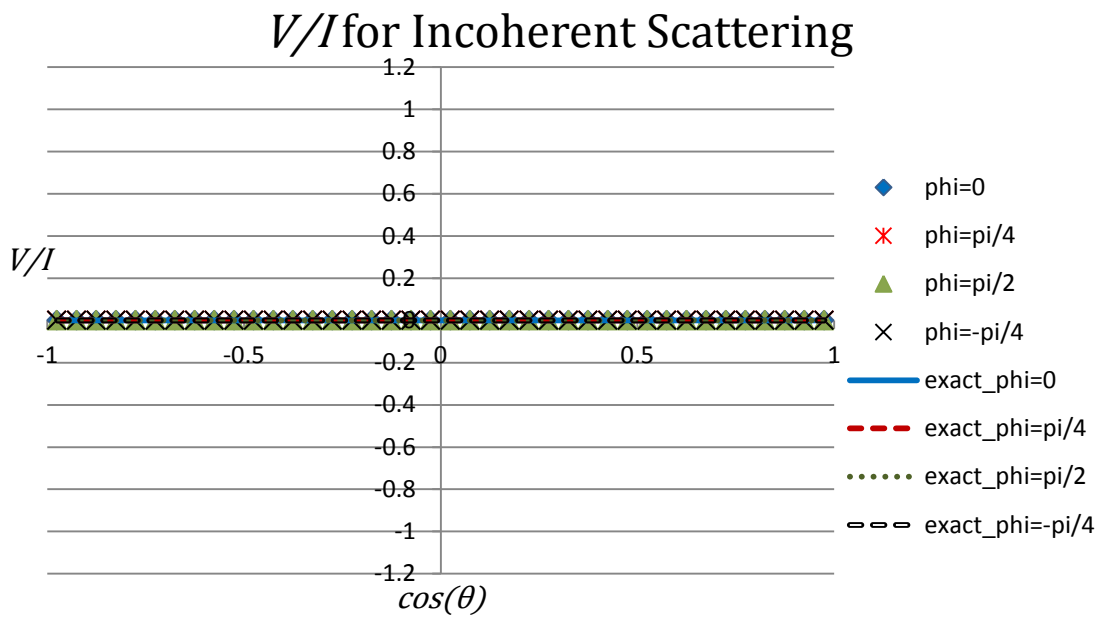

Figure A.18. *V/I* for the incoherently scattered portion of a 5 keV photon beam with a source Stokes vector of $[\varphi_I, \varphi_Q, \varphi_U, \varphi_V] = [1,0,0,0]$.

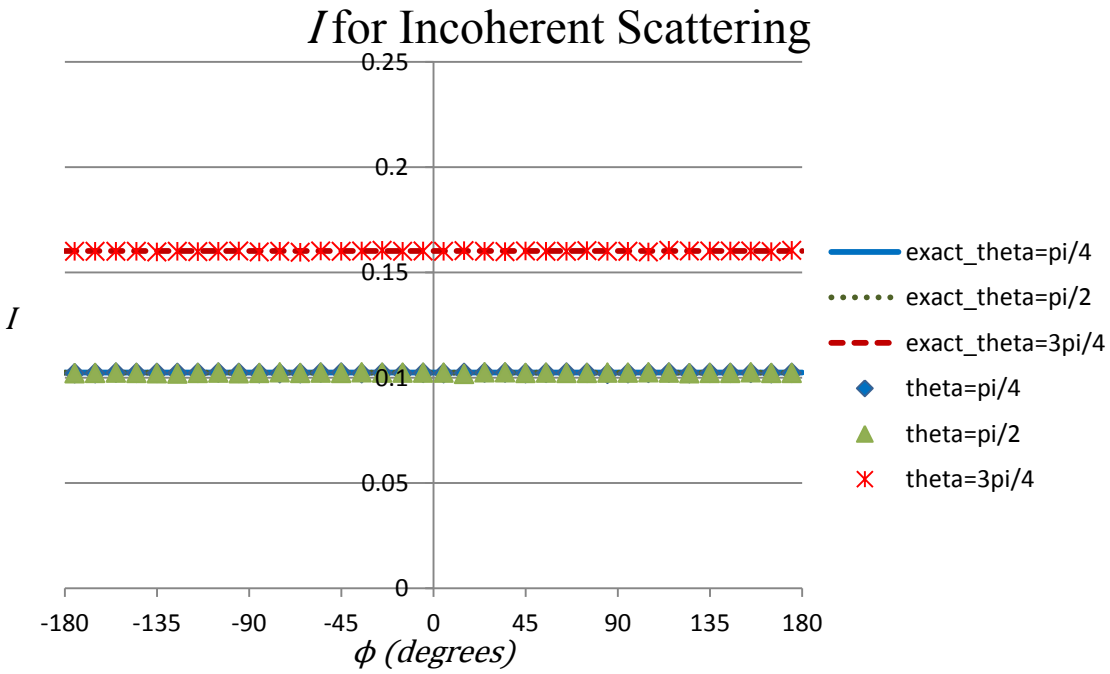

Figure A.19. *I* for the incoherently scattered portion of a 5 keV photon beam with a source Stokes vector of $[\varphi_I, \varphi_Q, \varphi_U, \varphi_V] = [1,0,0,0]$.

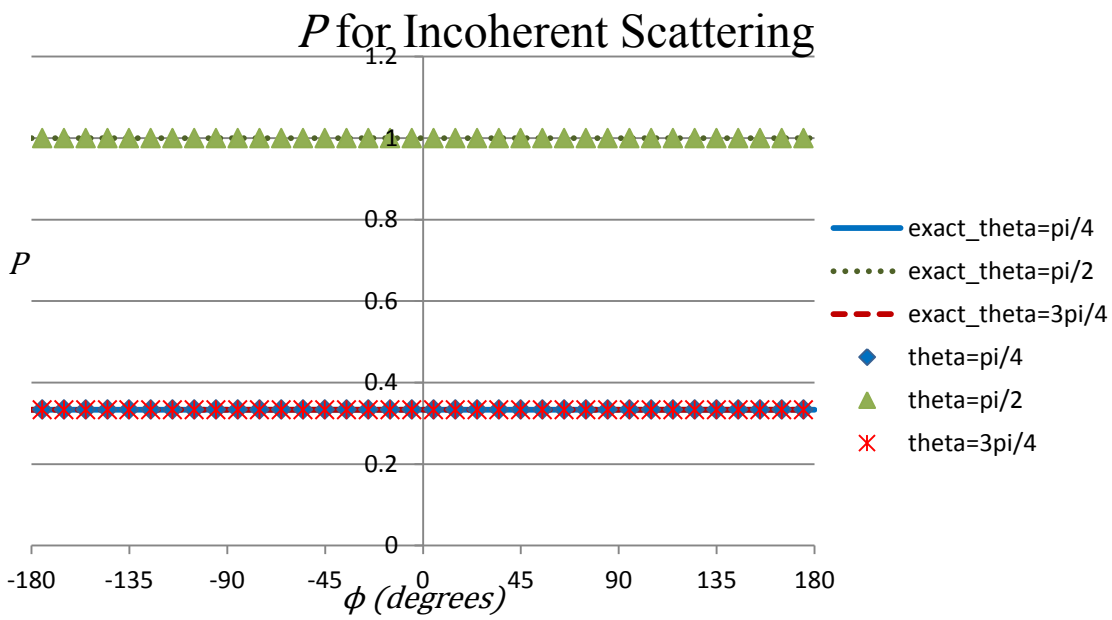

Figure A.20. P for the incoherently scattered portion of a 5 keV photon beam with a source Stokes vector of $[\varphi_I, \varphi_Q, \varphi_U, \varphi_V] = [1,0,0,0]$.

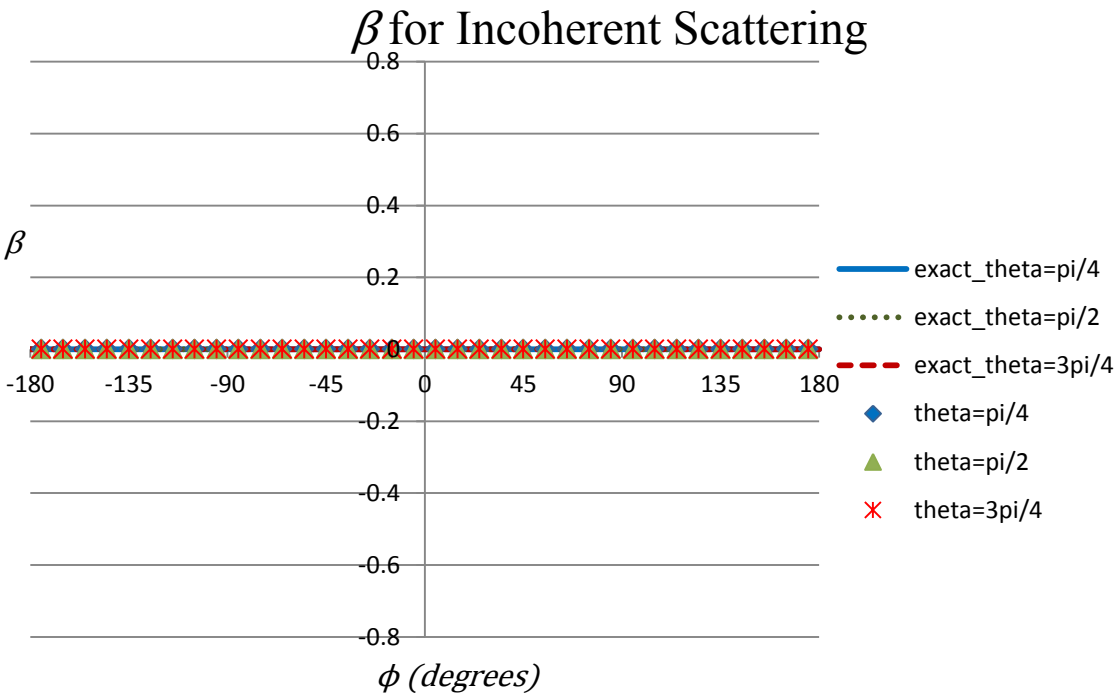

Figure A.21. β for the incoherently scattered portion of a 5 keV photon beam with a source Stokes vector of $[\varphi_I, \varphi_Q, \varphi_U, \varphi_V] = [1,0,0,0]$.

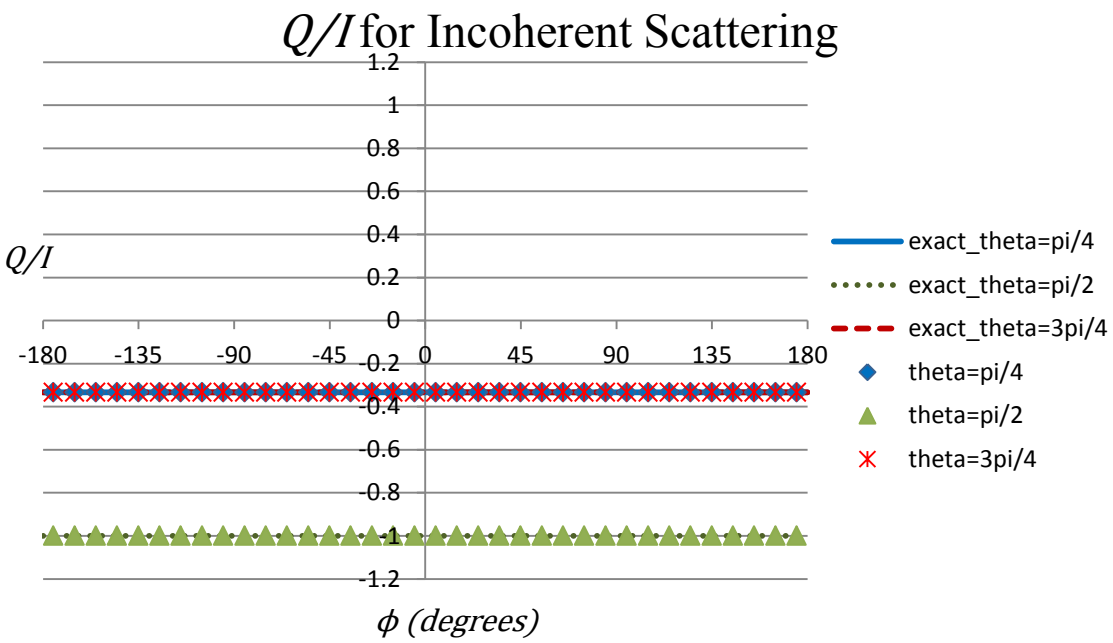

Figure A.22. Q/I for the incoherently scattered portion of a 5 keV photon beam with a source Stokes vector of $[\varphi_I, \varphi_Q, \varphi_U, \varphi_V] = [1,0,0,0]$.

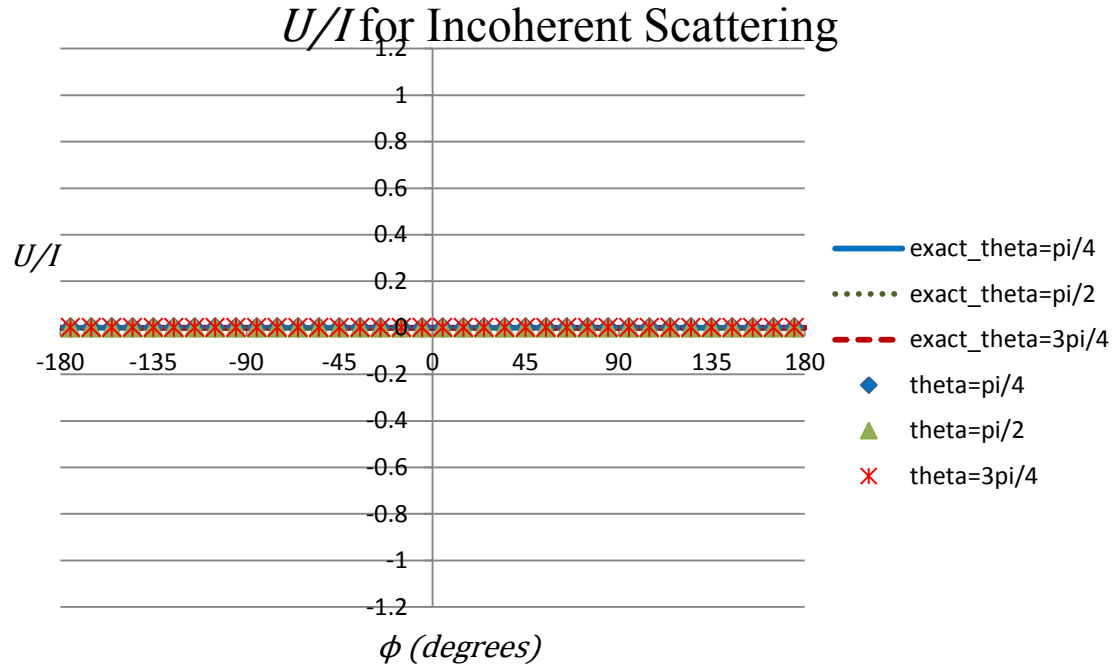

Figure A.23. U/I for the incoherently scattered portion of a 5 keV photon beam with a source Stokes vector of $[\varphi_I, \varphi_Q, \varphi_U, \varphi_V] = [1,0,0,0]$.

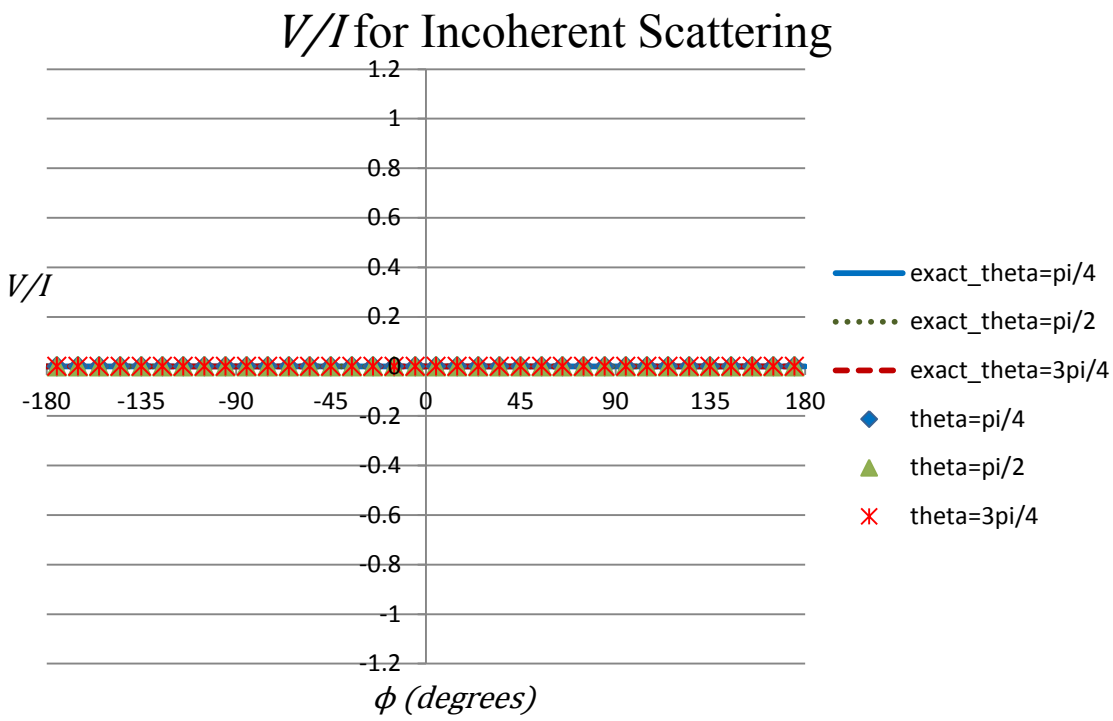

Figure A.24. *V/I* for the incoherently scattered portion of a 5 keV photon beam with a source Stokes vector of $[\varphi_I, \varphi_Q, \varphi_U, \varphi_V] = [1,0,0,0]$.

A.2, $\Gamma = [1,1,0,0]$

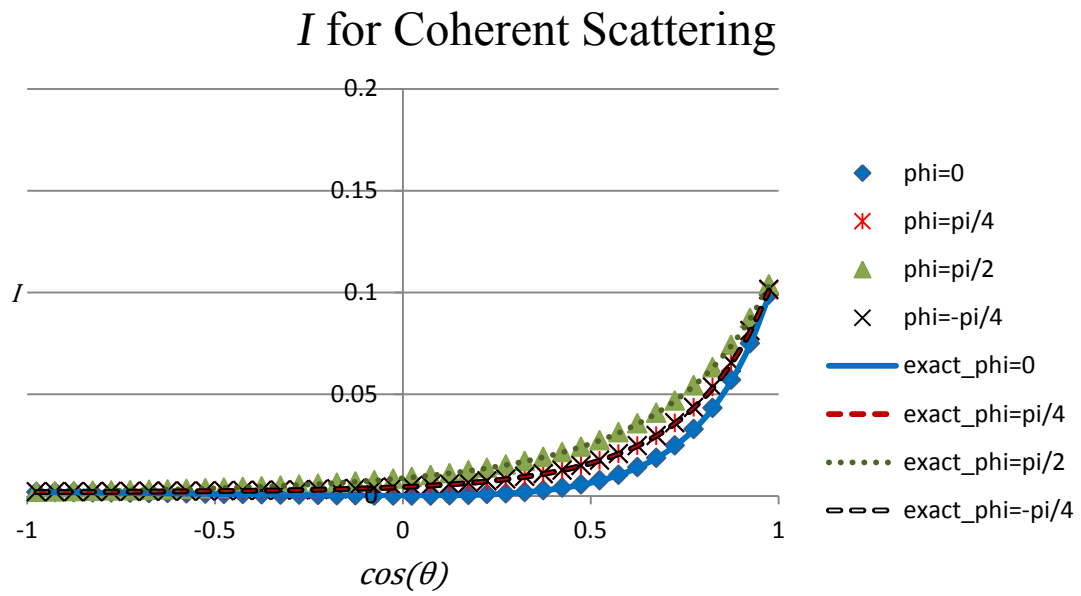

Figure A.25. *I* for the coherently scattered portion of a 5 keV photon beam with a source Stokes vector of $[\varphi_I, \varphi_Q, \varphi_U, \varphi_V] = [1,1,0,0]$.

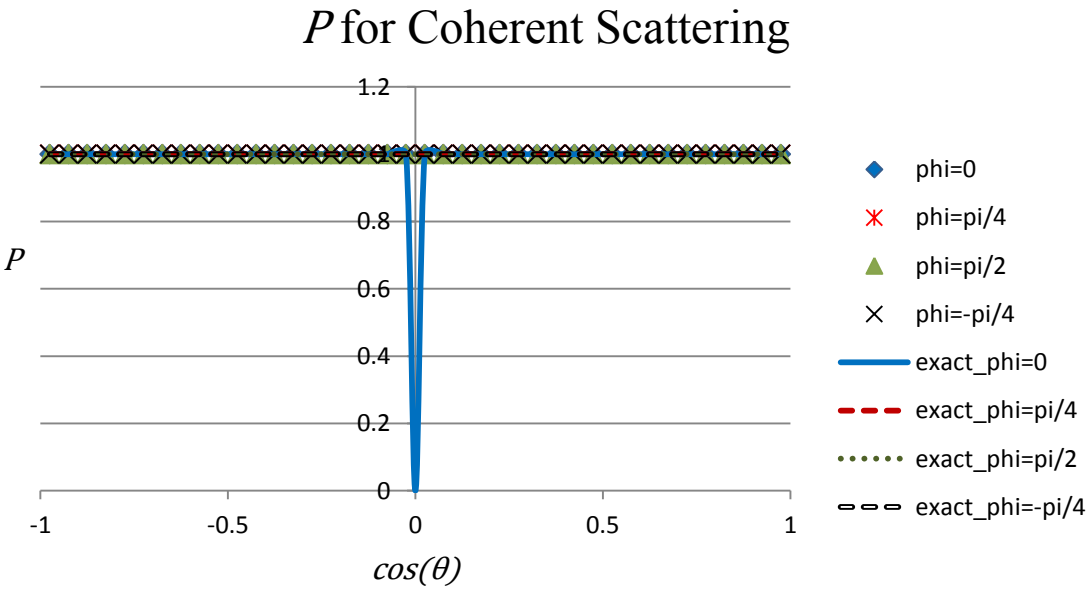

Figure A.26. *P* for the coherently scattered portion of a 5 keV photon beam with a source Stokes vector of $[\varphi_I, \varphi_Q, \varphi_U, \varphi_V] = [1,1,0,0]$.

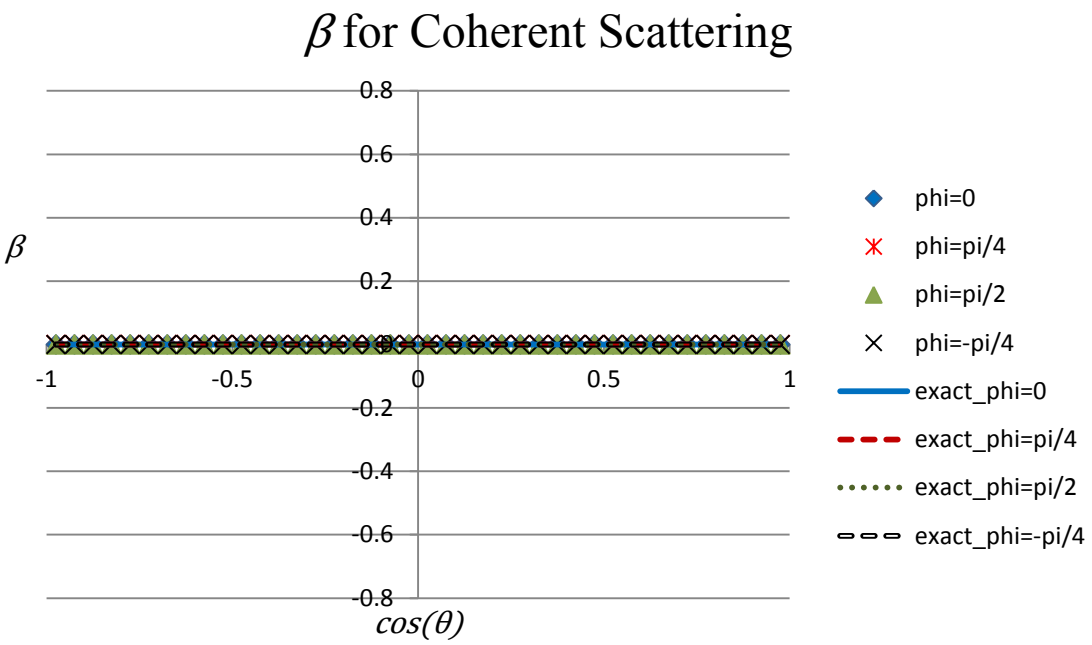

Figure A.27. β for the coherently scattered portion of a 5 keV photon beam with a source Stokes vector of $[\varphi_I, \varphi_Q, \varphi_U, \varphi_V] = [1,1,0,0]$.

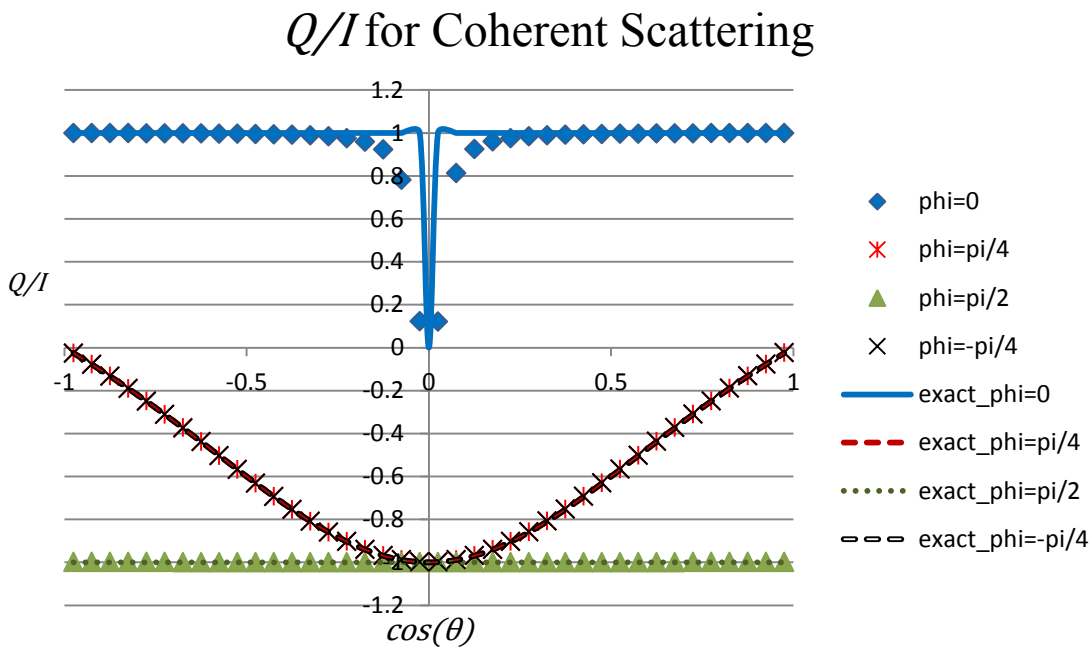

Figure A.28. *Q/I* for the coherently scattered portion of a 5 keV photon beam with a source Stokes vector of $[\varphi_I, \varphi_Q, \varphi_U, \varphi_V] = [1,1,0,0]$.

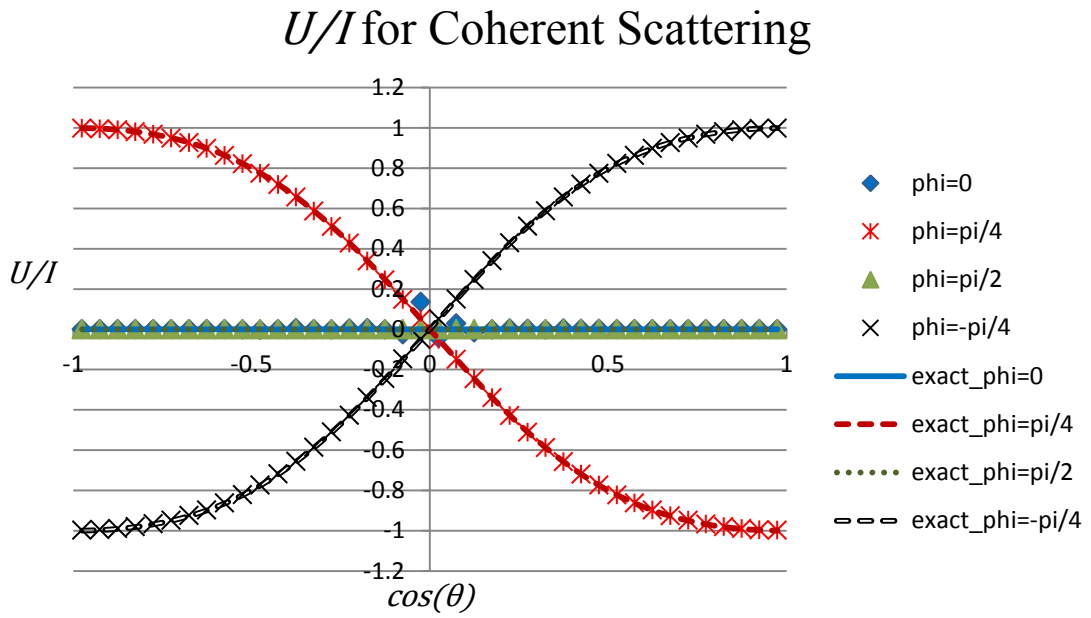

Figure A.29. *U/I* for the coherently scattered portion of a 5 keV photon beam with a source Stokes vector of $[\varphi_I, \varphi_Q, \varphi_U, \varphi_V] = [1,1,0,0]$.

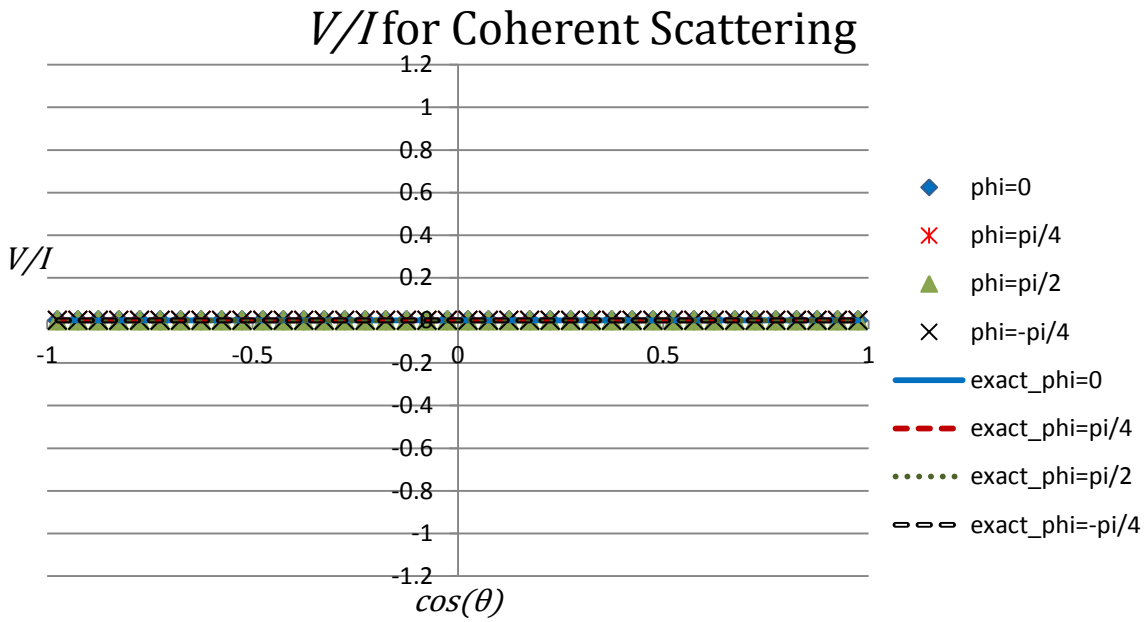

Figure A.30. *V/I* for the coherently scattered portion of a 5 keV photon beam with a source Stokes vector of $[\varphi_I, \varphi_Q, \varphi_U, \varphi_V] = [1,1,0,0]$.

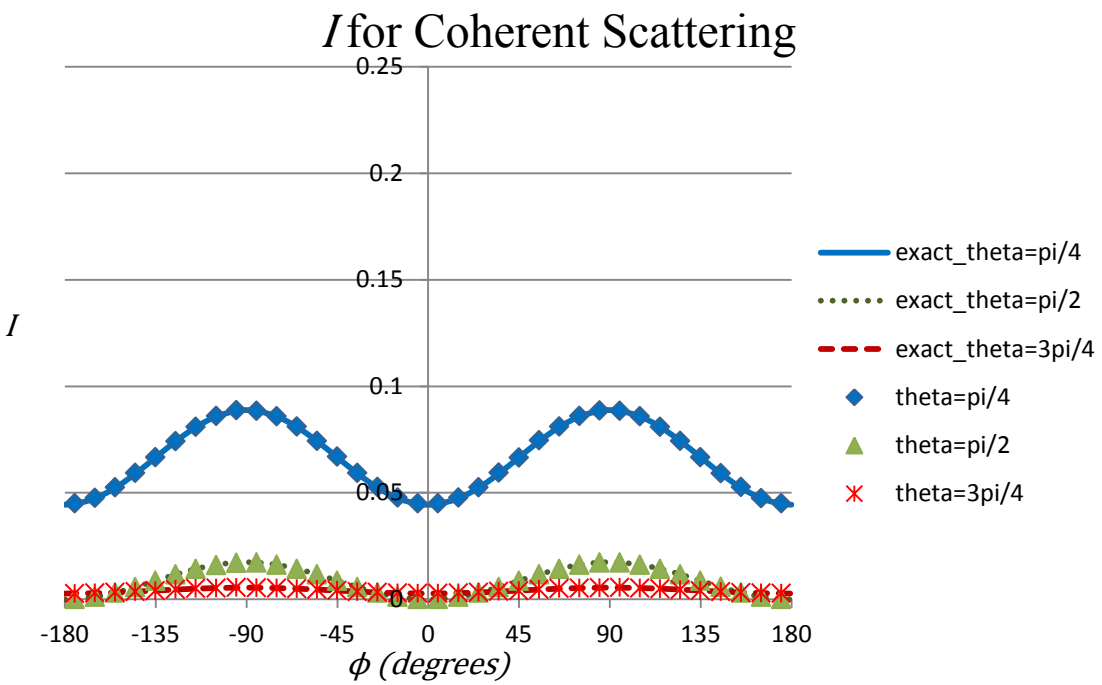

Figure A.31. *I* for the coherently scattered portion of a 5 keV photon beam with a source Stokes vector of $[\varphi_I, \varphi_Q, \varphi_U, \varphi_V] = [1,1,0,0]$.

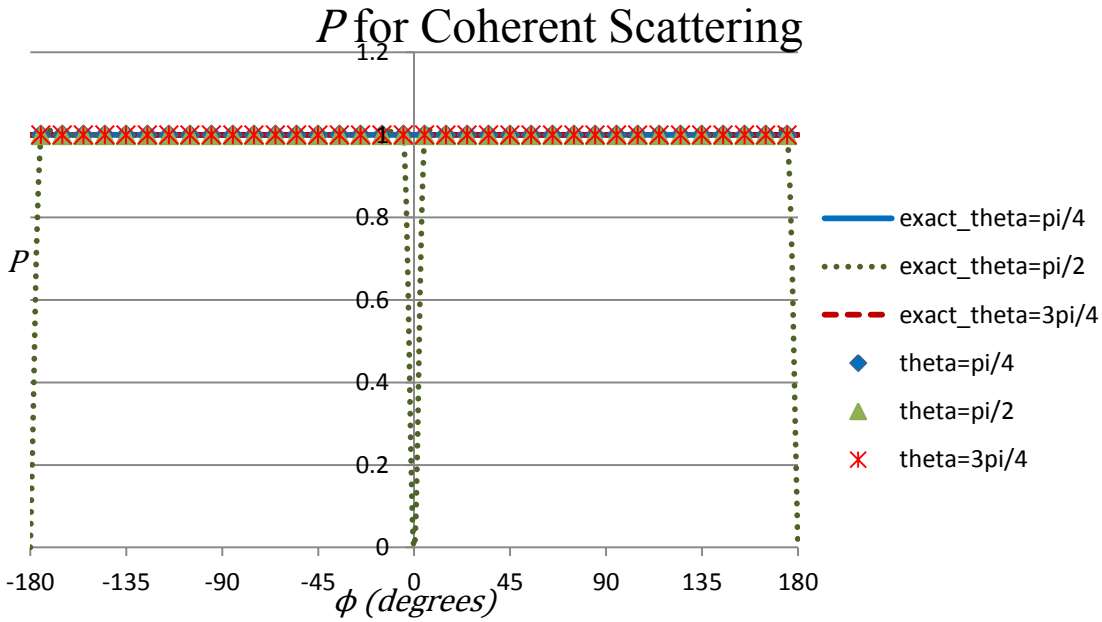

Figure A.32. *P* for the coherently scattered portion of a 5 keV photon beam with a source Stokes vector of $[\varphi_I, \varphi_Q, \varphi_U, \varphi_V] = [1,1,0,0]$.

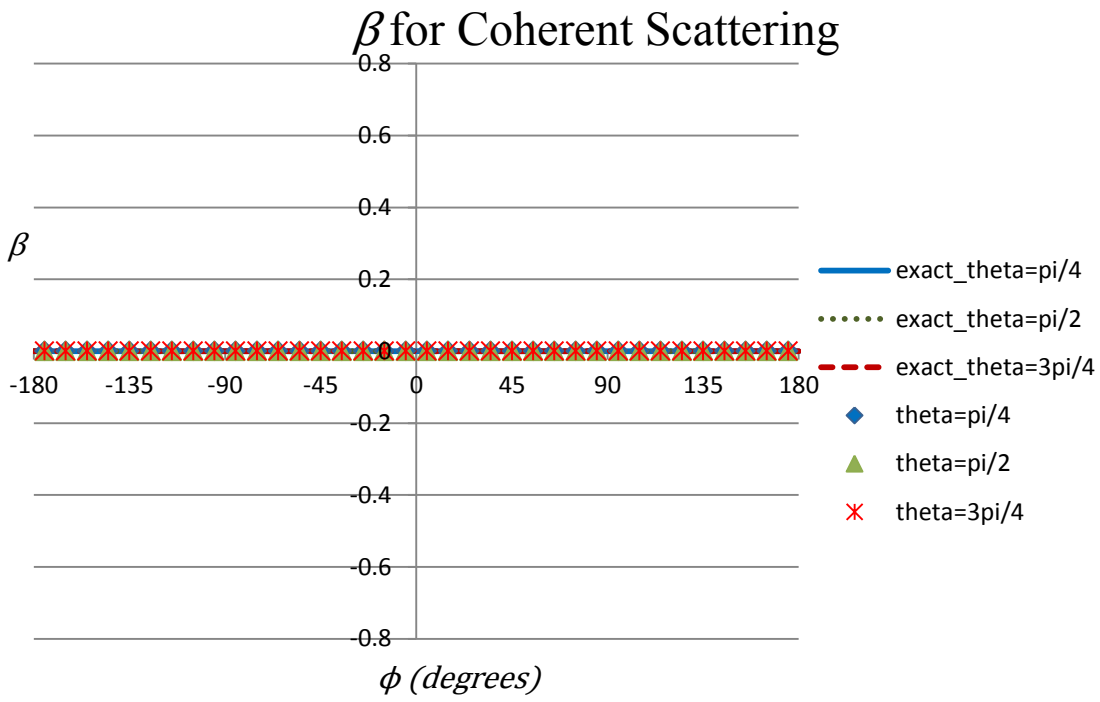

Figure A.33. β for the coherently scattered portion of a 5 keV photon beam with a source Stokes vector of $[\varphi_I, \varphi_Q, \varphi_U, \varphi_V] = [1,1,0,0]$.

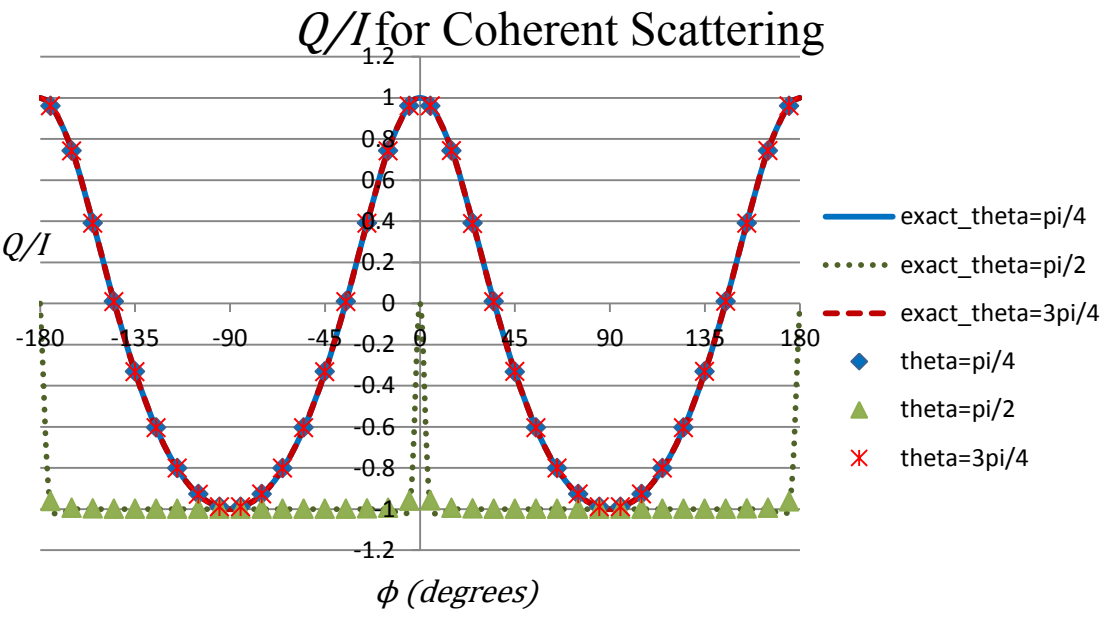

Figure A.34. Q/I for the coherently scattered portion of a 5 keV photon beam with a source Stokes vector of $[\varphi_I, \varphi_Q, \varphi_U, \varphi_V] = [1,1,0,0]$.

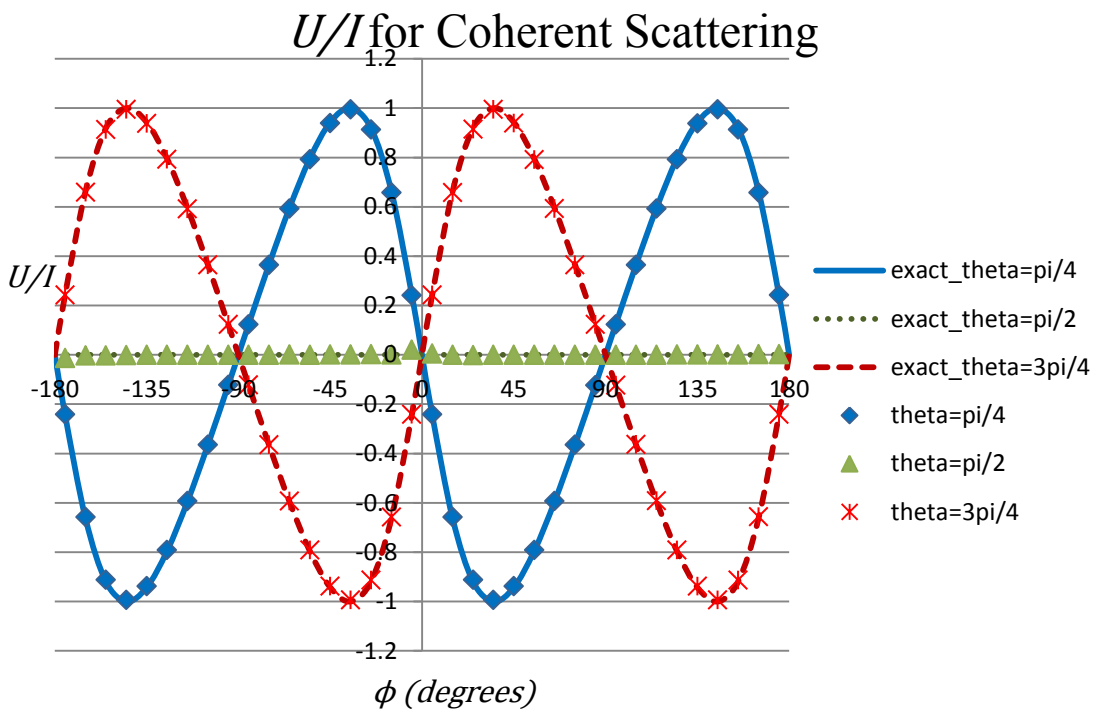

Figure A.35. *U/I* for the coherently scattered portion of a 5 keV photon beam with a source Stokes vector of $[\varphi_I, \varphi_Q, \varphi_U, \varphi_V] = [1,1,0,0]$.

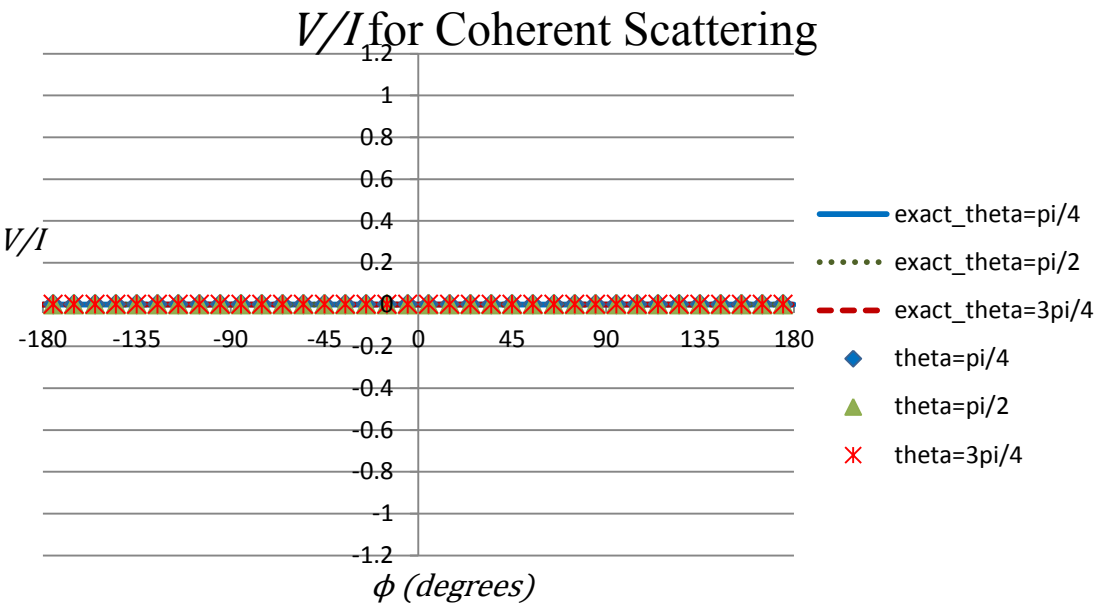

Figure A.36. *V/I* for the coherently scattered portion of a 5 keV photon beam with a source Stokes vector of $[\varphi_I, \varphi_Q, \varphi_U, \varphi_V] = [1,1,0,0]$.

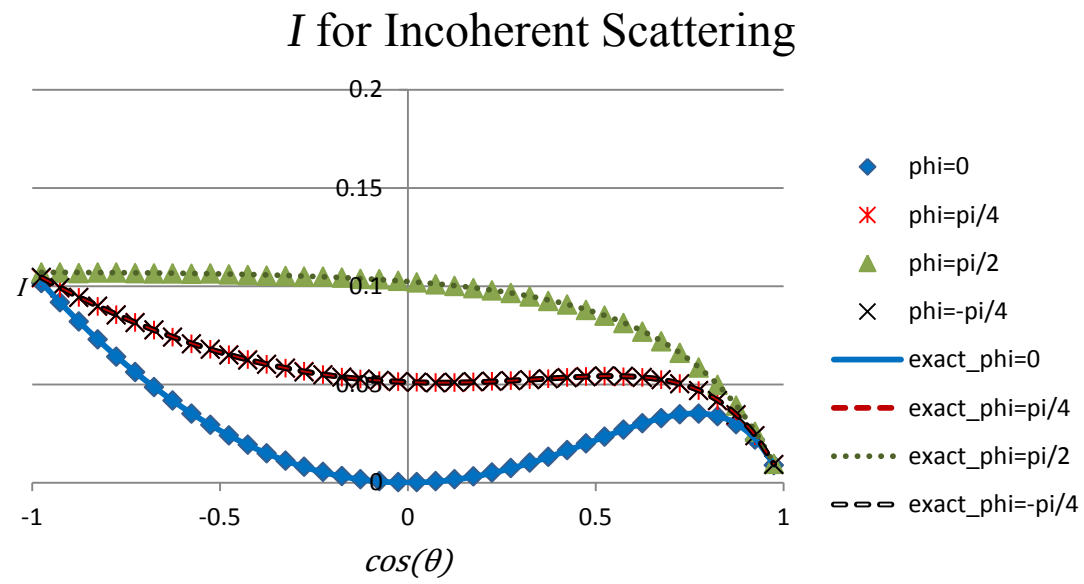

Figure A.37. *I* for the incoherently scattered portion of a 5 keV photon beam with a source Stokes vector of $[\varphi_I, \varphi_Q, \varphi_U, \varphi_V] = [1,1,0,0]$.

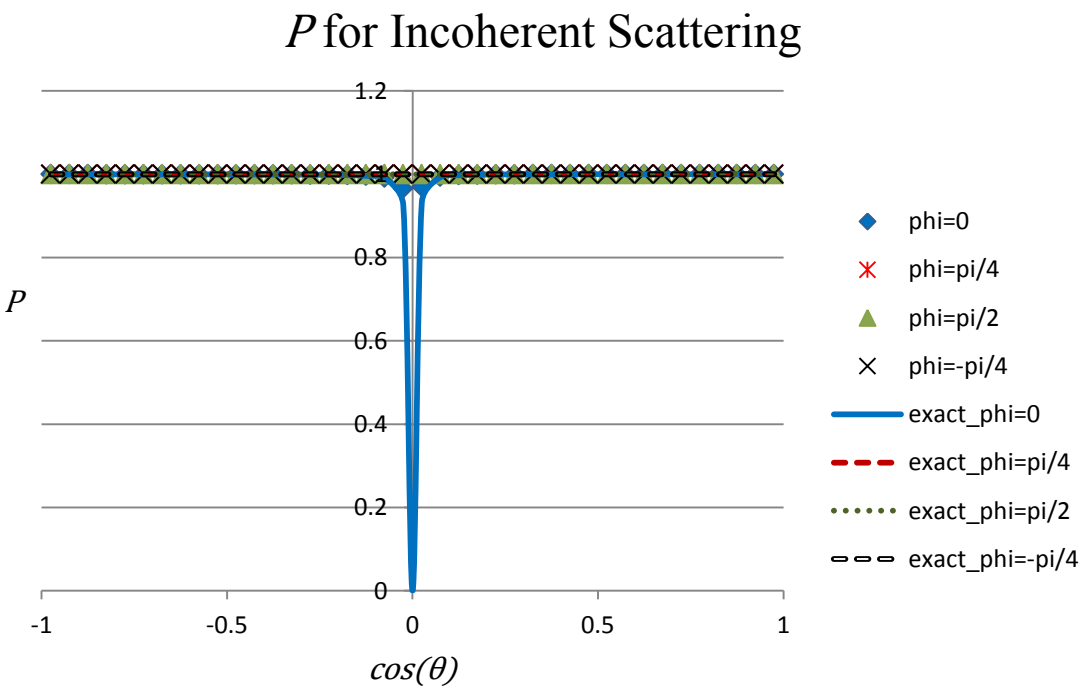

Figure A.38. *P* for the incoherently scattered portion of a 5 keV photon beam with a source Stokes vector of $[\varphi_I, \varphi_Q, \varphi_U, \varphi_V] = [1,1,0,0]$.

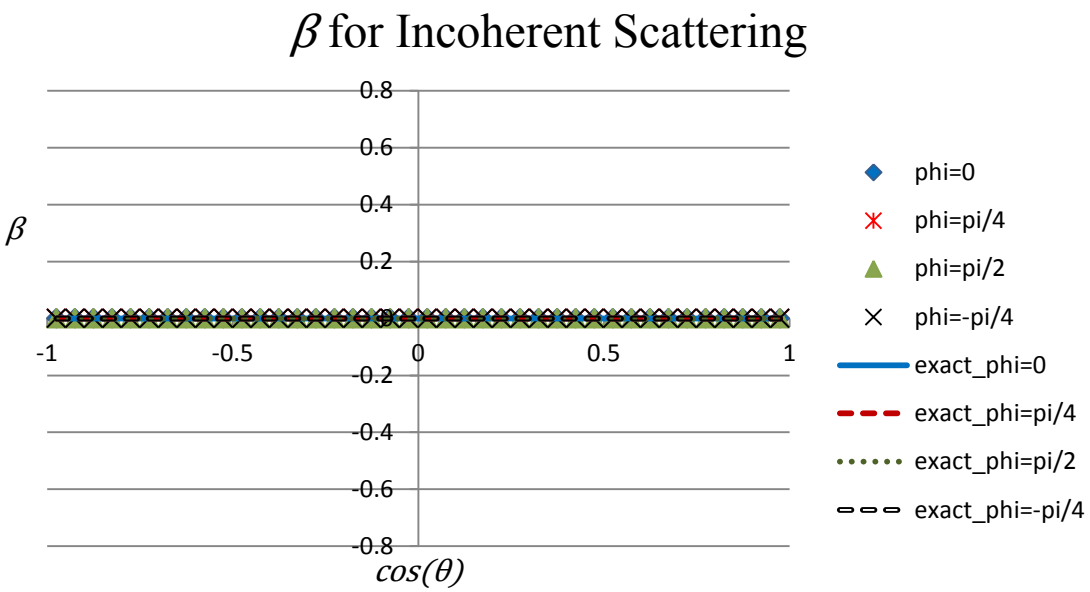

Figure A.39. β for the incoherently scattered portion of a 5 keV photon beam with a source Stokes vector of $[\varphi_I, \varphi_Q, \varphi_U, \varphi_V] = [1,1,0,0]$.

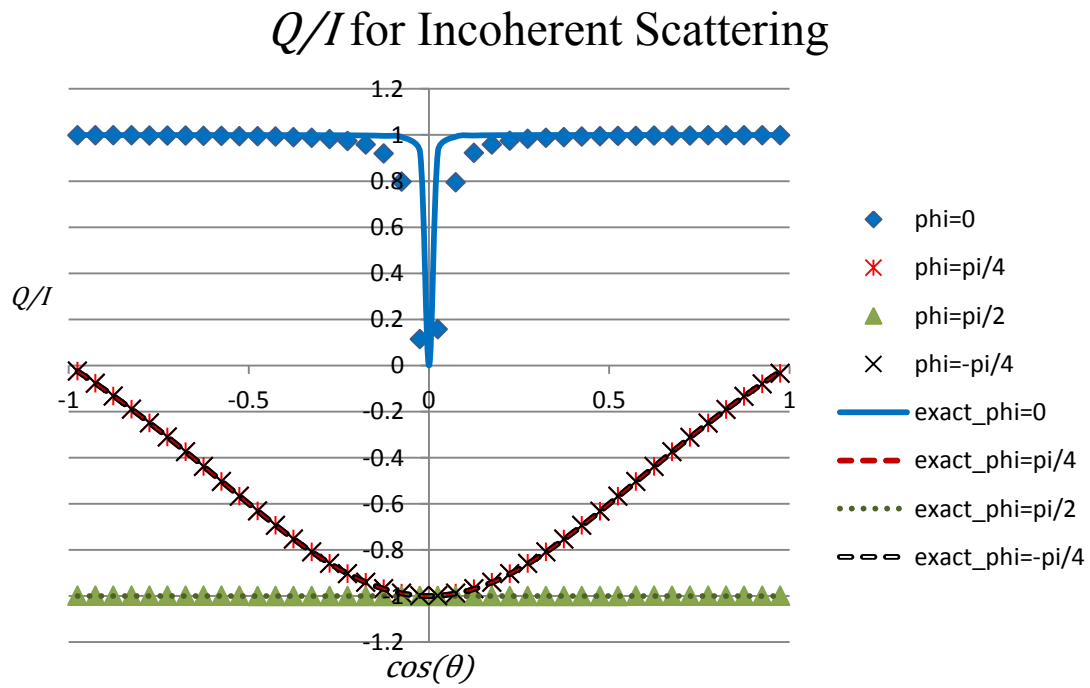

Figure A.40. Q/I for the incoherently scattered portion of a 5 keV photon beam with a source Stokes vector of $[\varphi_I, \varphi_Q, \varphi_U, \varphi_V] = [1,1,0,0]$.

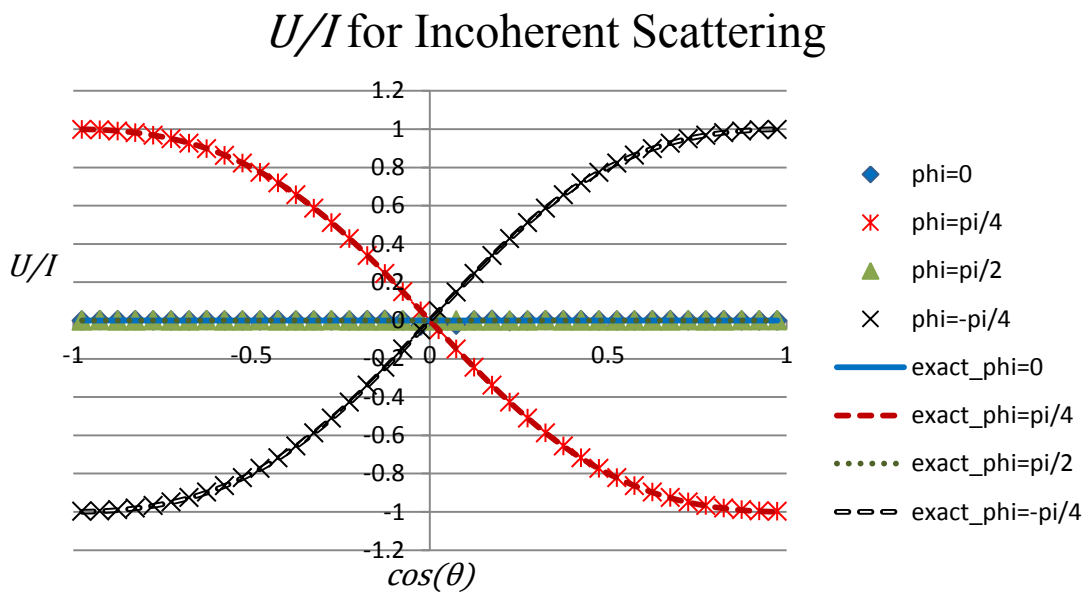

Figure A.41. *U/I* for the incoherently scattered portion of a 5 keV photon beam with a source Stokes vector of $[\varphi_I, \varphi_Q, \varphi_U, \varphi_V] = [1,1,0,0]$.

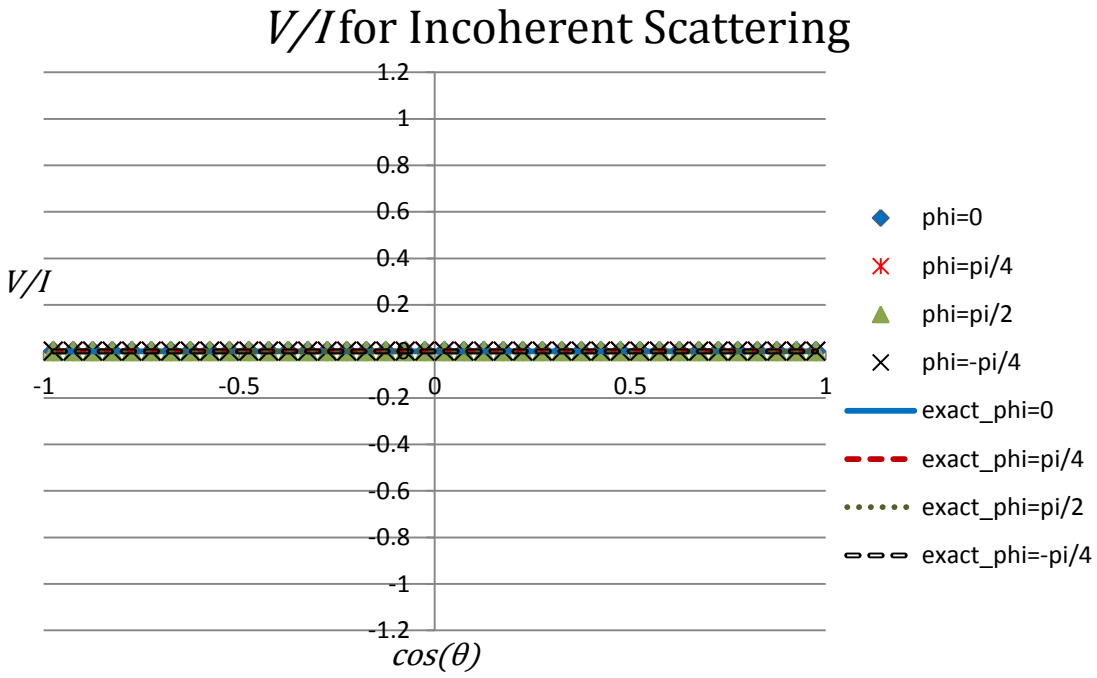

Figure A.42. *V/I* for the incoherently scattered portion of a 5 keV photon beam with a source Stokes vector of $[\varphi_I, \varphi_Q, \varphi_U, \varphi_V] = [1,1,0,0]$.

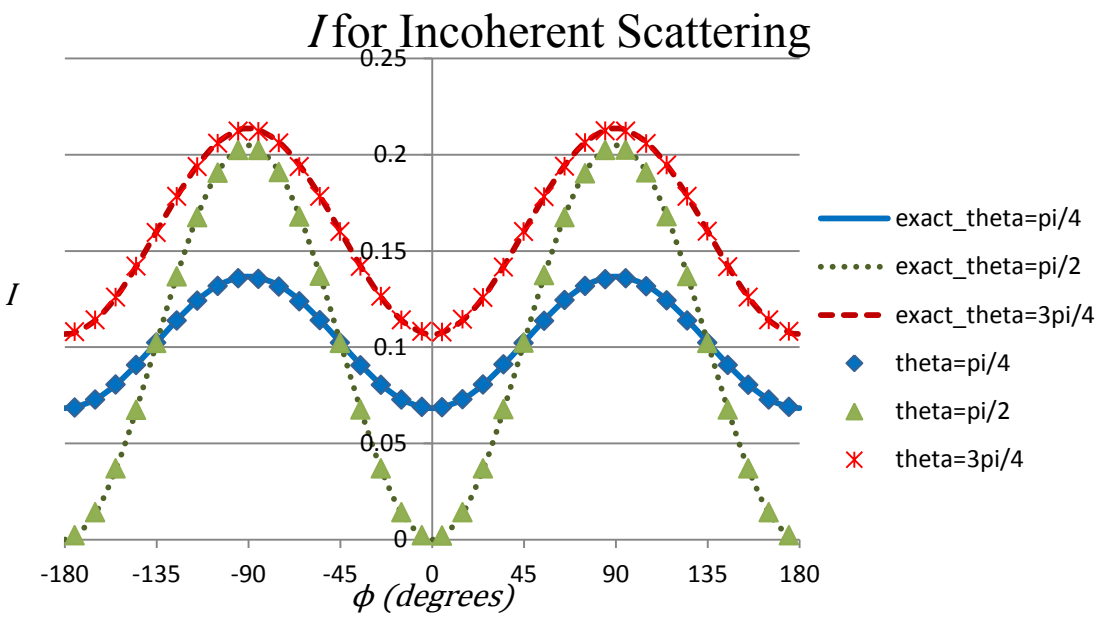

Figure A.43. *I* for the incoherently scattered portion of a 5 keV photon beam with a source Stokes vector of $[\varphi_I, \varphi_Q, \varphi_U, \varphi_V] = [1,1,0,0]$.

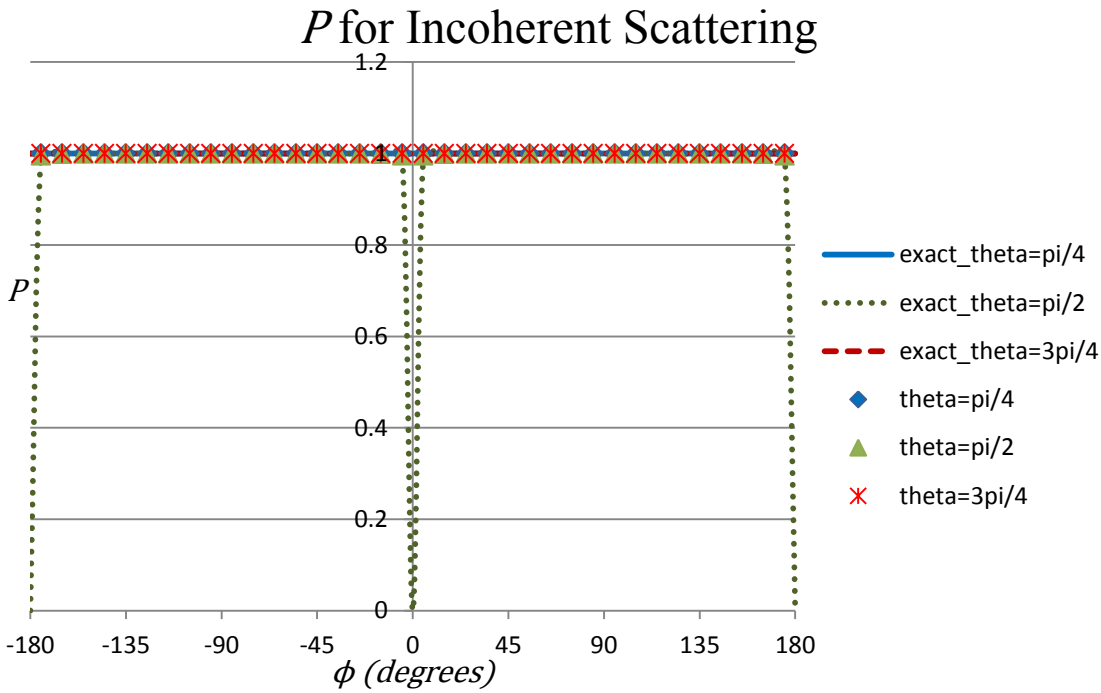

Figure A.44. *P* for the incoherently scattered portion of a 5 keV photon beam with a source Stokes vector of $[\varphi_I, \varphi_Q, \varphi_U, \varphi_V] = [1,1,0,0]$.

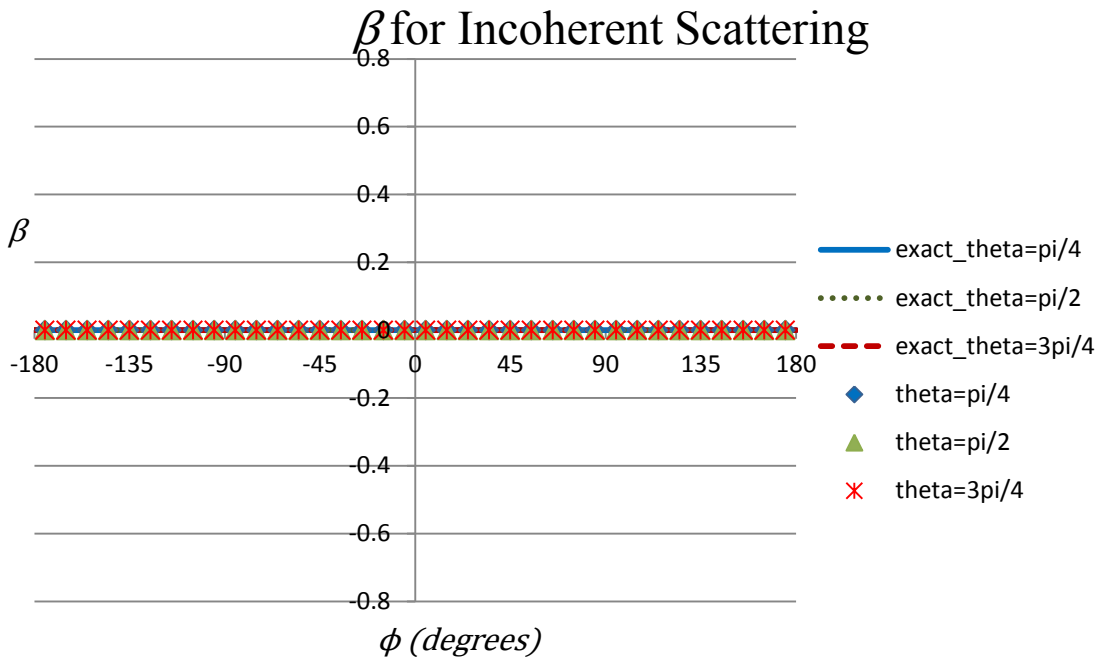

Figure A.45. β for the incoherently scattered portion of a 5 keV photon beam with a source Stokes vector of $[\varphi_I, \varphi_Q, \varphi_U, \varphi_V] = [1,1,0,0]$.

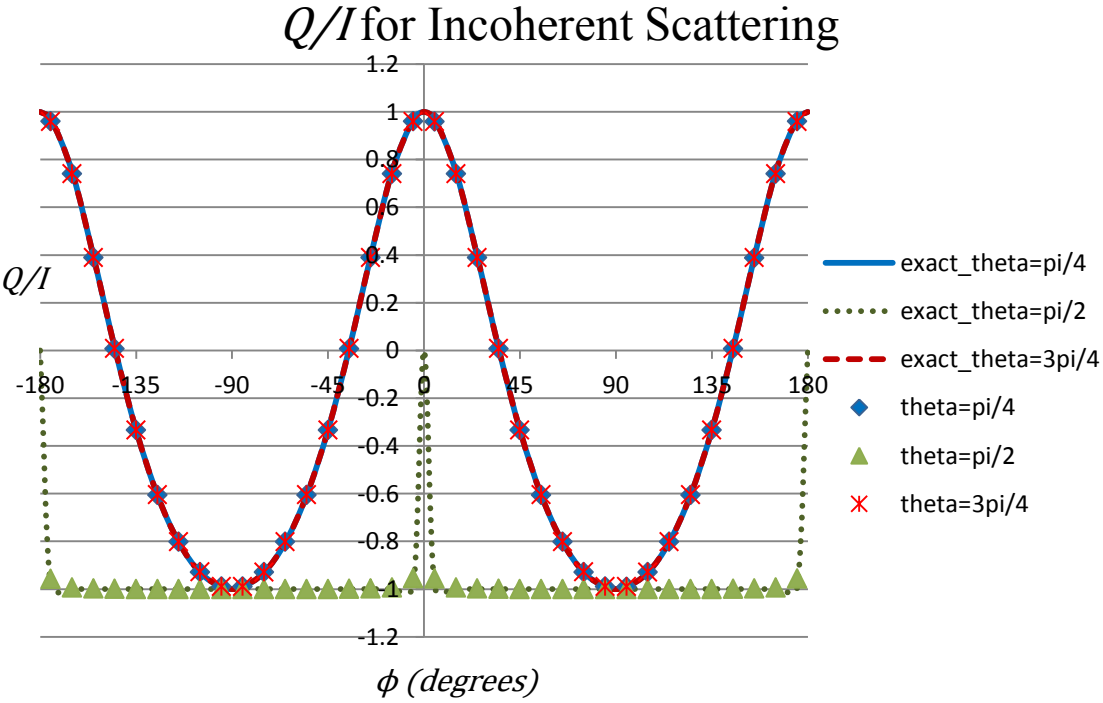

Figure A.46. Q/I for the incoherently scattered portion of a 5 keV photon beam with a source Stokes vector of $[\varphi_I, \varphi_Q, \varphi_U, \varphi_V] = [1,1,0,0]$.

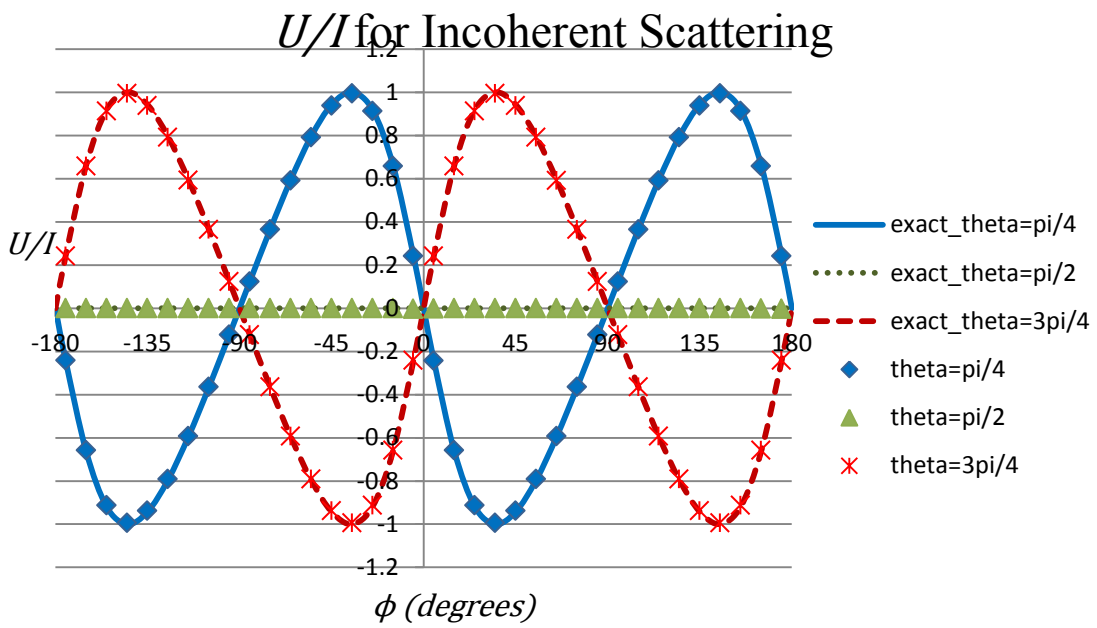

Figure A.47. *U/I* for the incoherently scattered portion of a 5 keV photon beam with a source Stokes vector of $[\varphi_I, \varphi_Q, \varphi_U, \varphi_V] = [1,1,0,0]$.

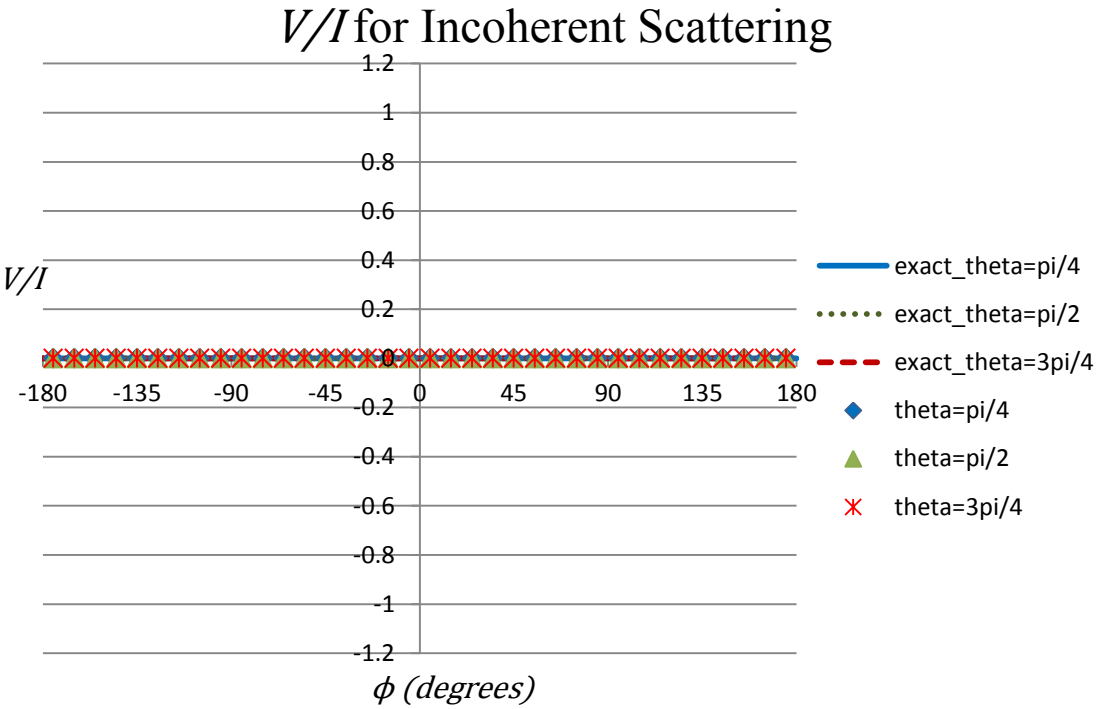

Figure A.48. *V/I* for the incoherently scattered portion of a 5 keV photon beam with a source Stokes vector of $[\varphi_I, \varphi_Q, \varphi_U, \varphi_V] = [1,1,0,0]$.

A.3, $\Gamma = [1,0,-1,0]$

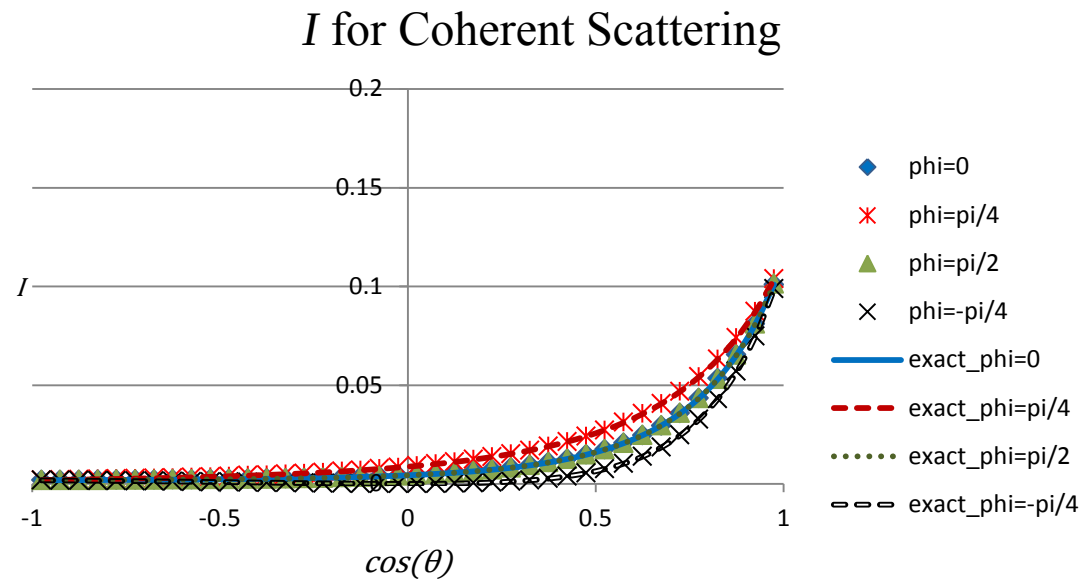

Figure A.49. I for the coherently scattered portion of a 5 keV photon beam with a source Stokes vector of $[\varphi_I, \varphi_Q, \varphi_U, \varphi_V] = [1,0,-1,0]$.

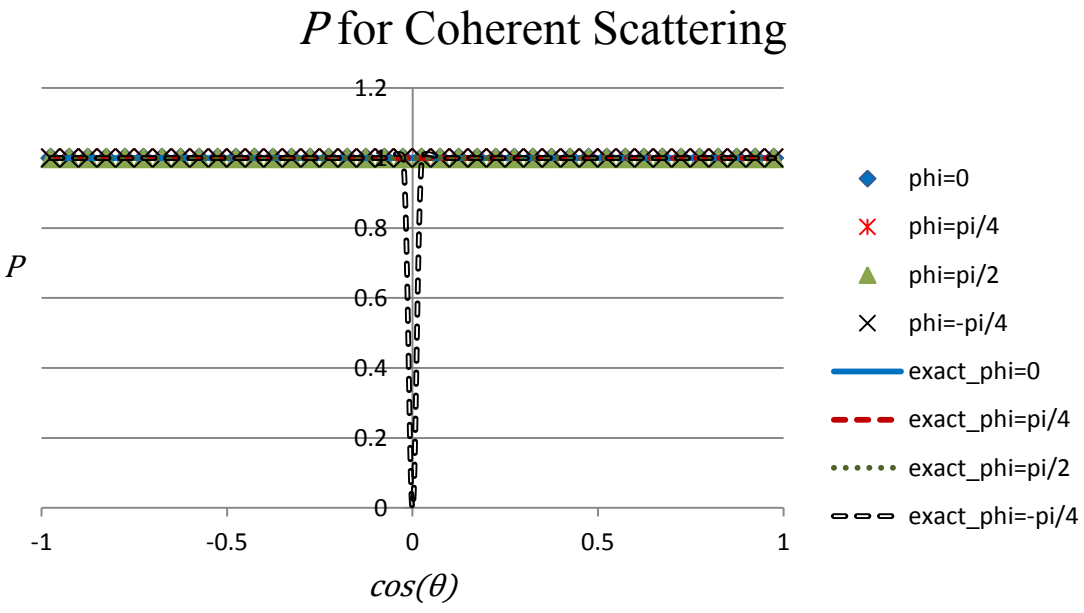

Figure A.50. P for the coherently scattered portion of a 5 keV photon beam with a source Stokes vector of $[\varphi_I, \varphi_Q, \varphi_U, \varphi_V] = [1,0,-1,0]$.

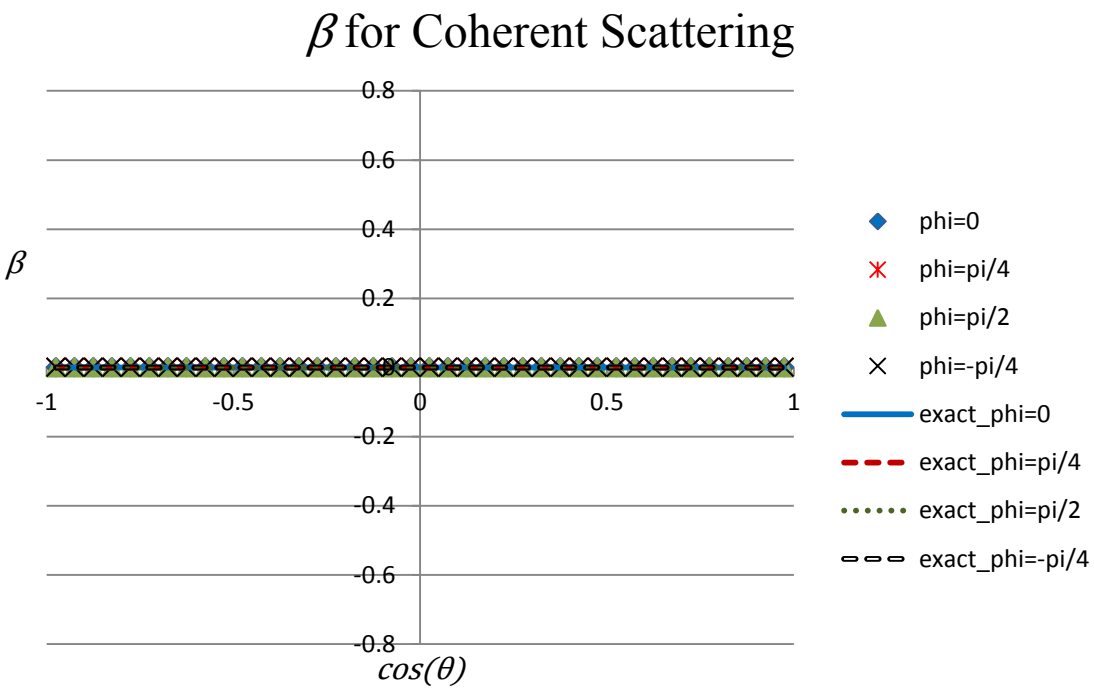

Figure A.51. β for the coherently scattered portion of a 5 keV photon beam with a source Stokes vector of $[\varphi_I, \varphi_Q, \varphi_U, \varphi_V] = [1,0,-1,0]$.

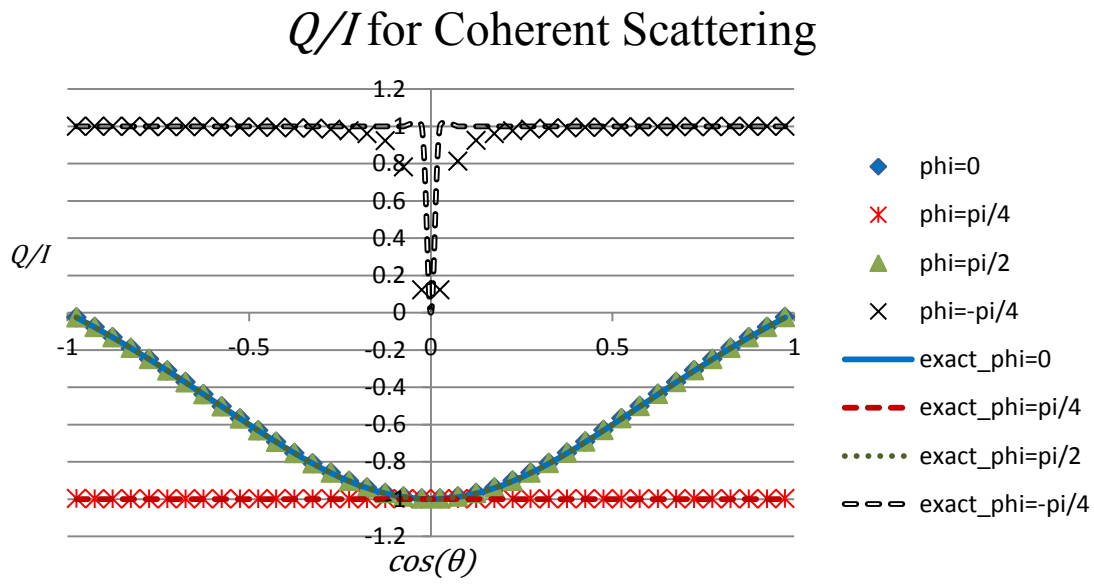

Figure A.52. Q/I for the coherently scattered portion of a 5 keV photon beam with a source Stokes vector of $[\varphi_I, \varphi_Q, \varphi_U, \varphi_V] = [1,0,-1,0]$.

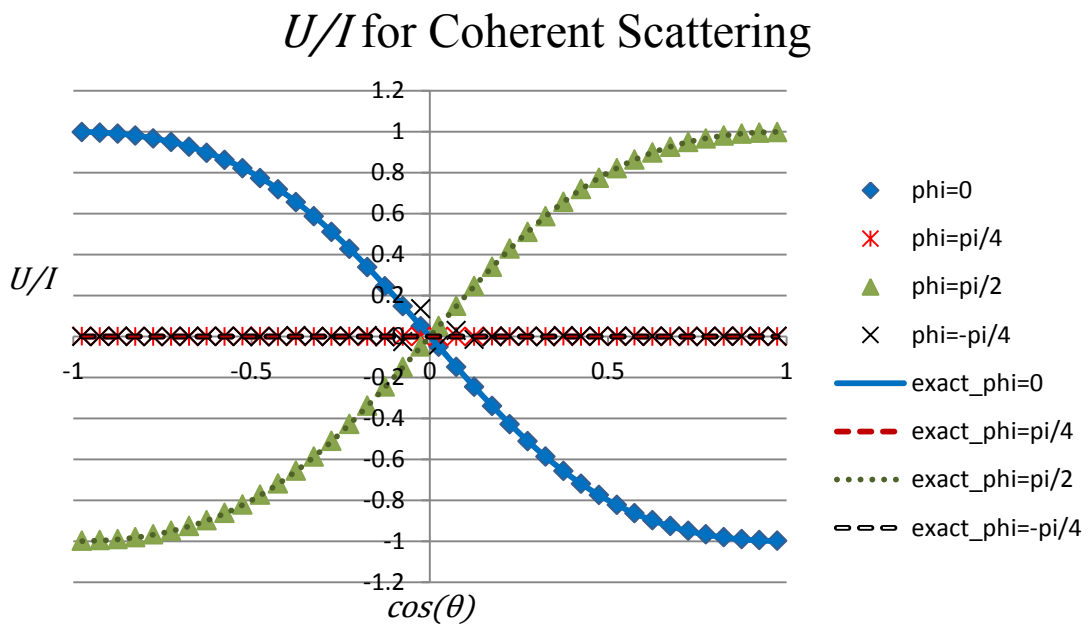

Figure A.53. U/I for the coherently scattered portion of a 5 keV photon beam with a source Stokes vector of $[\varphi_I, \varphi_Q, \varphi_U, \varphi_V] = [1,0,-1,0]$.

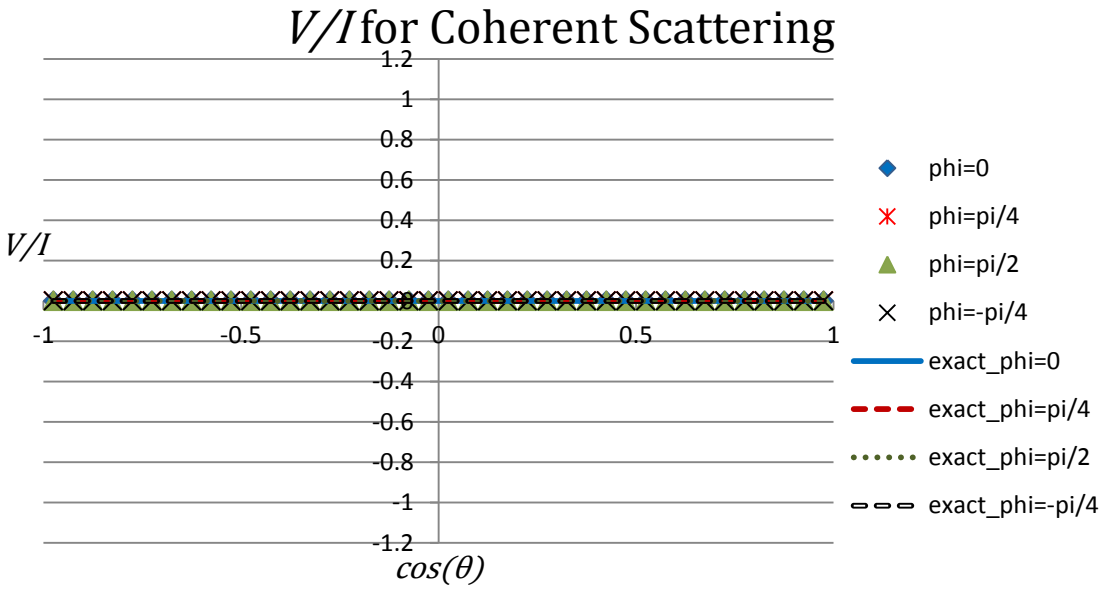

Figure A.54. V/I for the coherently scattered portion of a 5 keV photon beam with a source Stokes vector of $[\varphi_I, \varphi_Q, \varphi_U, \varphi_V] = [1,0,-1,0]$.

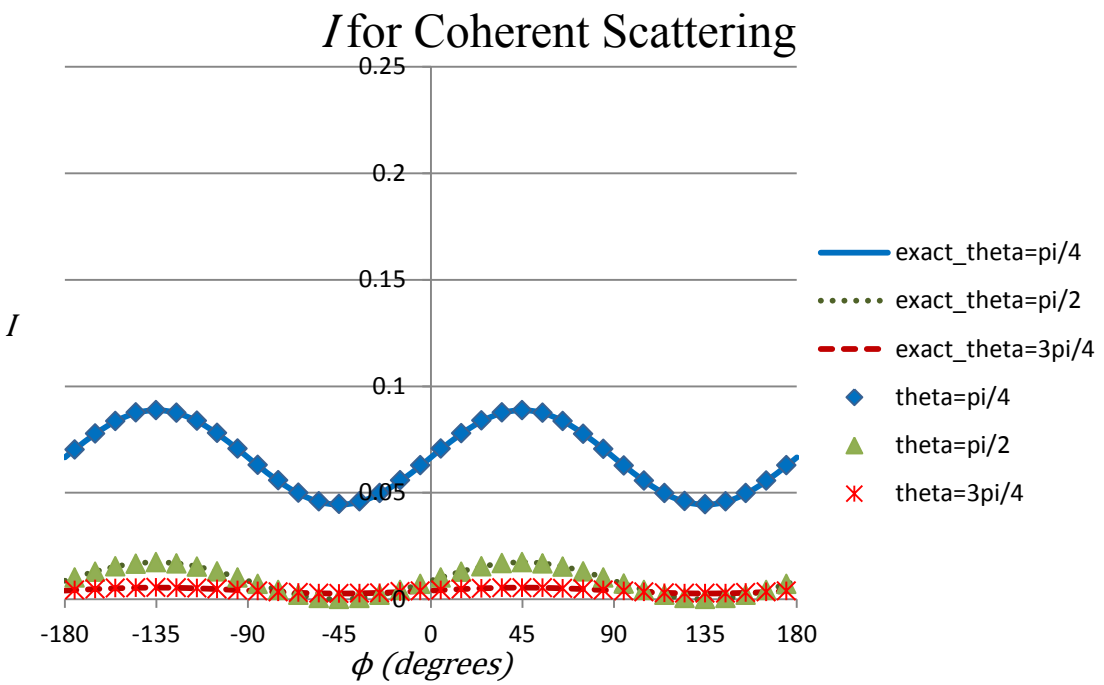

Figure A.55. *I* for the coherently scattered portion of a 5 keV photon beam with a source Stokes vector of $[\varphi_I, \varphi_Q, \varphi_U, \varphi_V] = [1,0,-1,0]$.

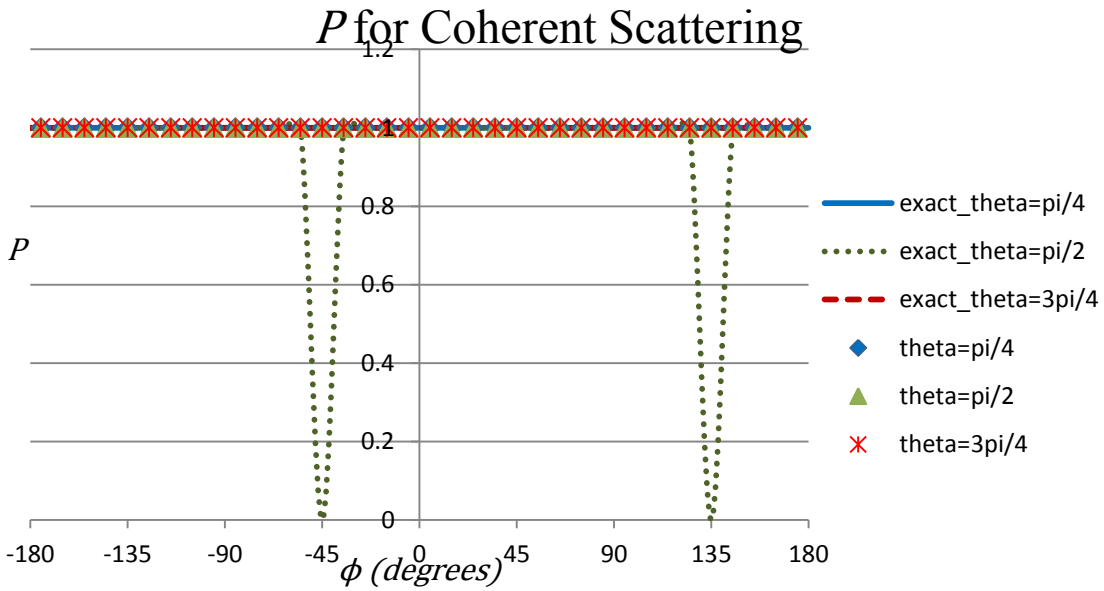

Figure A.56. *P* for the coherently scattered portion of a 5 keV photon beam with a source Stokes vector of $[\varphi_I, \varphi_Q, \varphi_U, \varphi_V] = [1,0,-1,0]$.

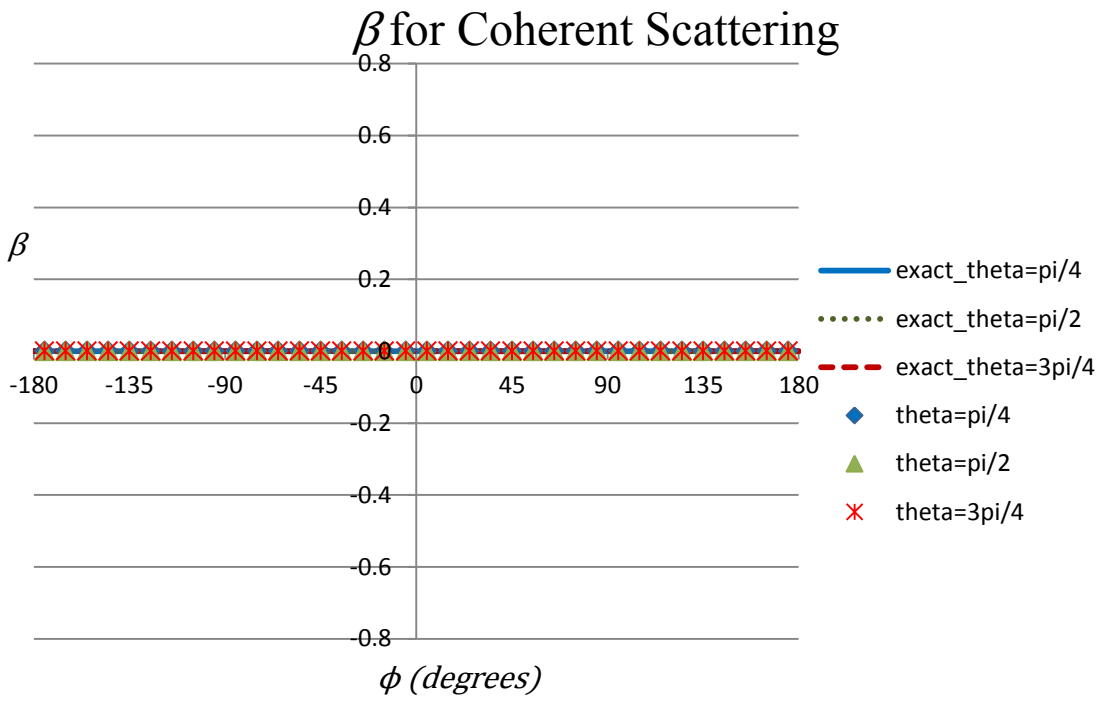

Figure A.57. β for the coherently scattered portion of a 5 keV photon beam with a source Stokes vector of $[\varphi_I, \varphi_Q, \varphi_U, \varphi_V] = [1,0,-1,0]$.

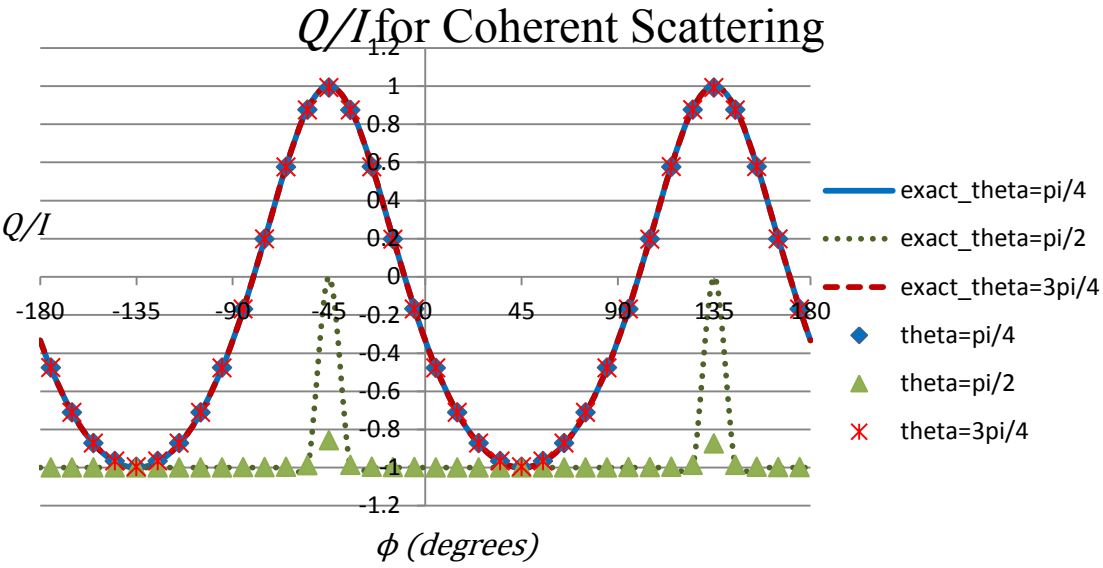

Figure A.58. Q/I for the coherently scattered portion of a 5 keV photon beam with a source Stokes vector of $[\varphi_I, \varphi_Q, \varphi_U, \varphi_V] = [1,0,-1,0]$.

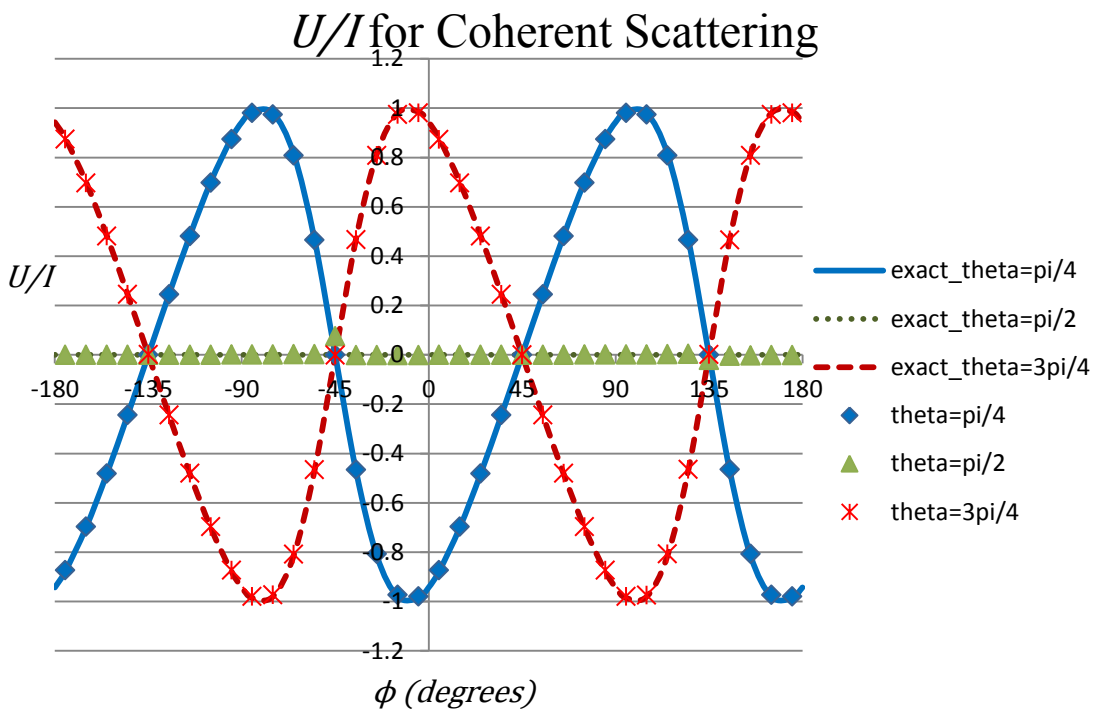

Figure A.59. *U/I* for the coherently scattered portion of a 5 keV photon beam with a source Stokes vector of $[\varphi_I, \varphi_Q, \varphi_U, \varphi_V] = [1,0,-1,0]$.

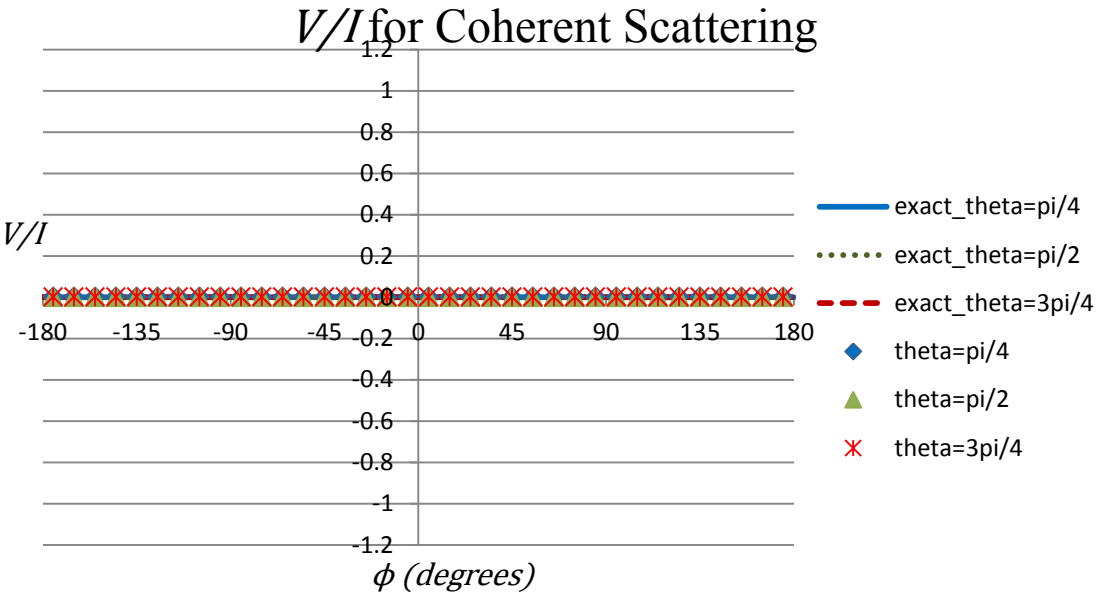

Figure A.60. *V/I* for the coherently scattered portion of a 5 keV photon beam with a source Stokes vector of $[\varphi_I, \varphi_Q, \varphi_U, \varphi_V] = [1,0,-1,0]$.

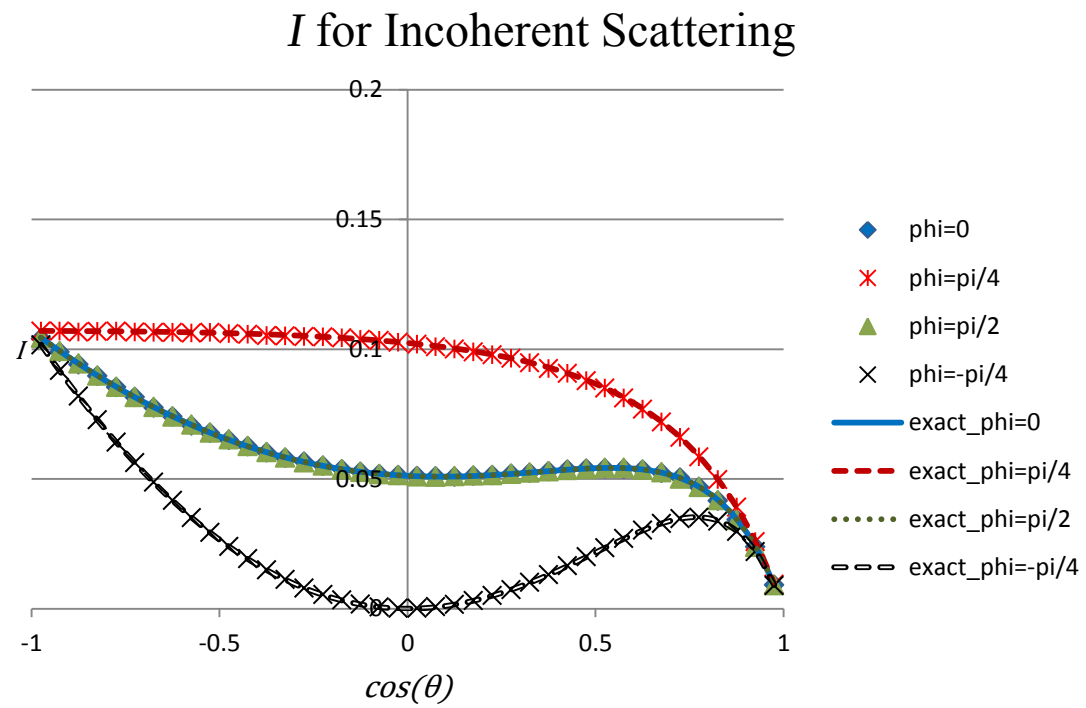

Figure A.61. I for the incoherently scattered portion of a 5 keV photon beam with a source Stokes vector of $[\varphi_I, \varphi_Q, \varphi_U, \varphi_V] = [1,0,-1,0]$.

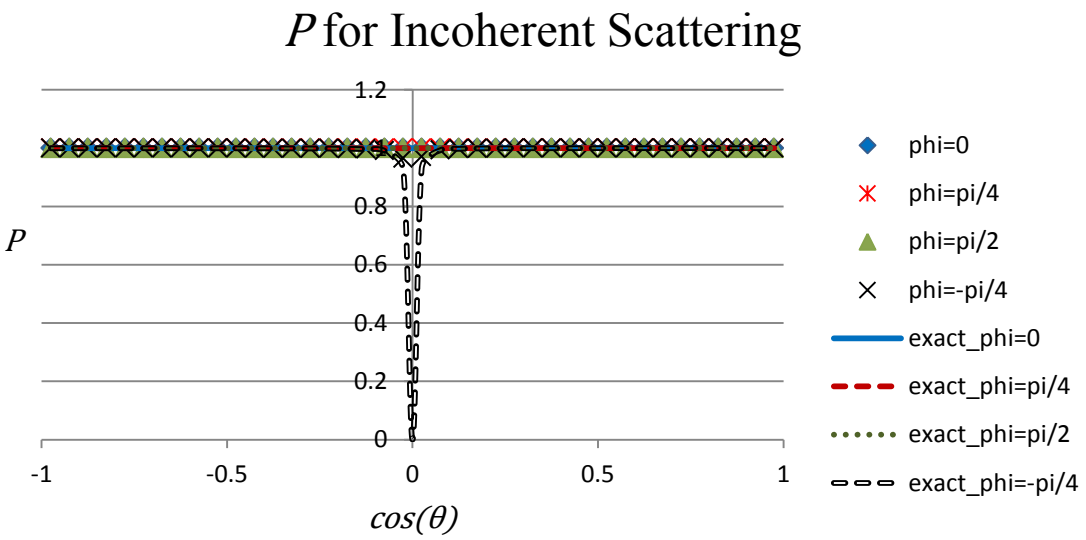

Figure A.62. P for the incoherently scattered portion of a 5 keV photon beam with a source Stokes vector of $[\varphi_I, \varphi_Q, \varphi_U, \varphi_V] = [1,0,-1,0]$.

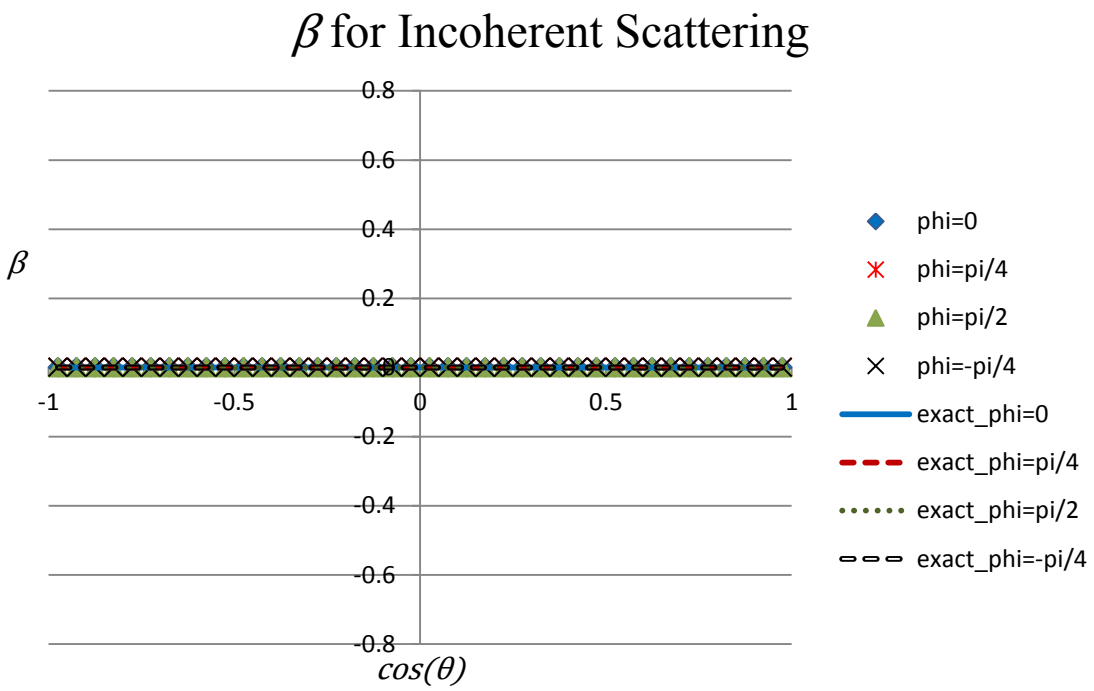

Figure A.63. β for the incoherently scattered portion of a 5 keV photon beam with a source Stokes vector of $[\varphi_I, \varphi_Q, \varphi_U, \varphi_V] = [1,0,-1,0]$.

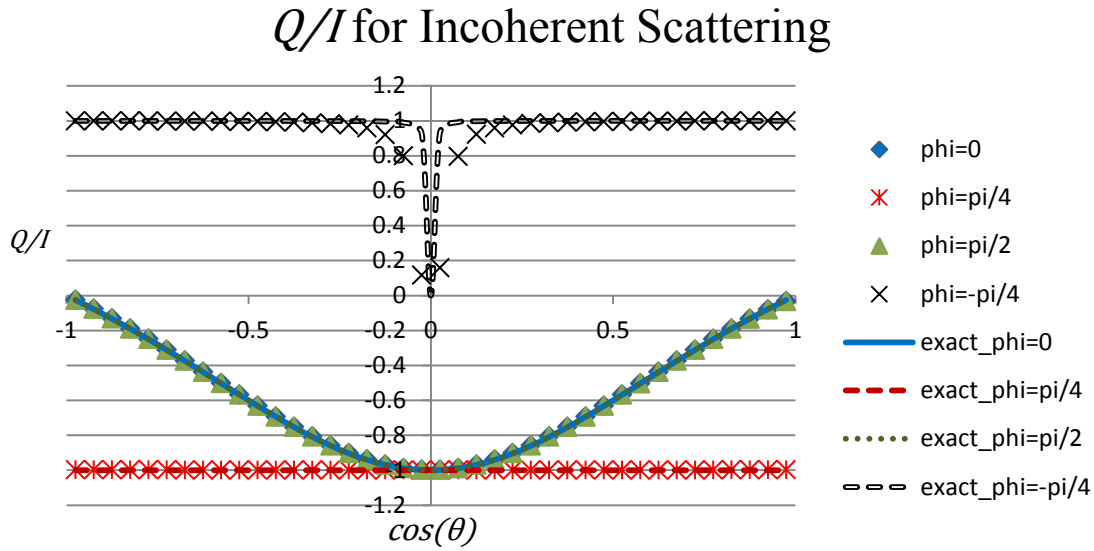

Figure A.64. Q/I for the incoherently scattered portion of a 5 keV photon beam with a source Stokes vector of $[\varphi_I, \varphi_Q, \varphi_U, \varphi_V] = [1,0,-1,0]$.

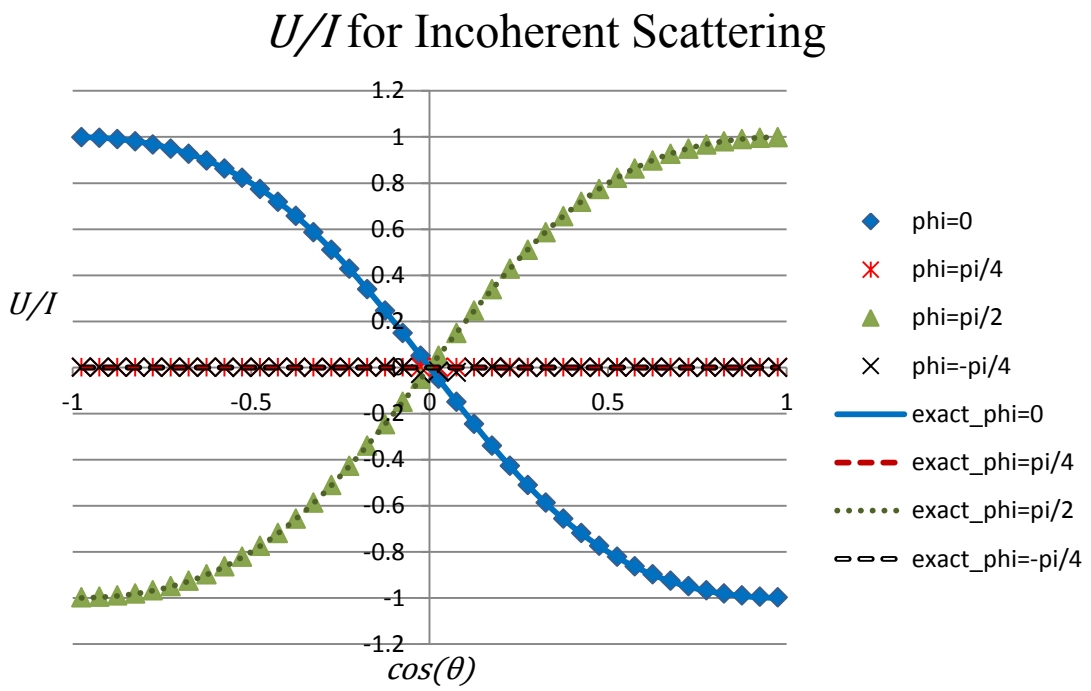

Figure A.65. *U/I* for the incoherently scattered portion of a 5 keV photon beam with a source Stokes vector of $[\varphi_I, \varphi_Q, \varphi_U, \varphi_V] = [1,0,-1,0]$.

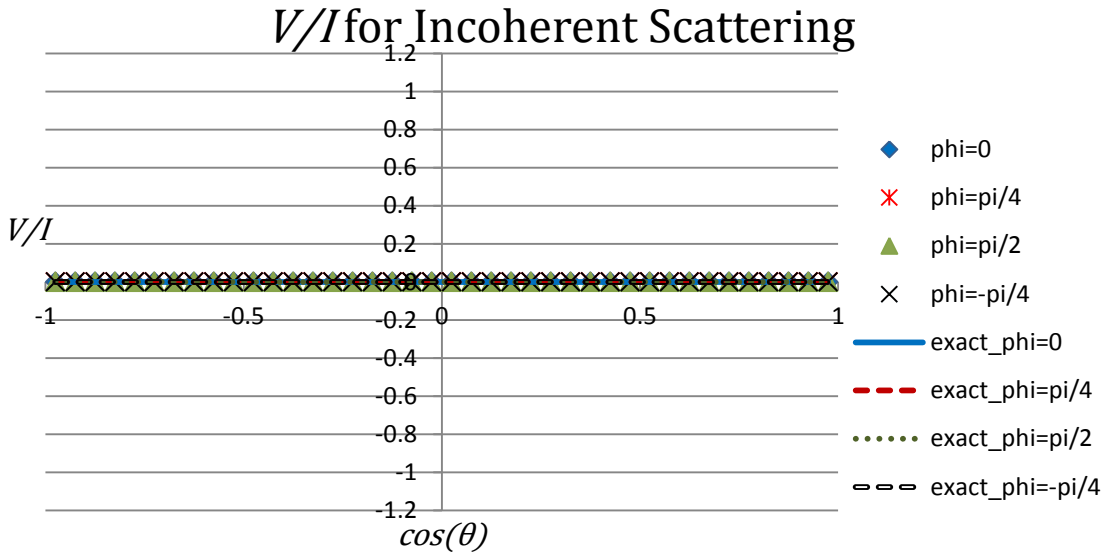

Figure A.66. *V/I* for the incoherently scattered portion of a 5 keV photon beam with a source Stokes vector of $[\varphi_I, \varphi_Q, \varphi_U, \varphi_V] = [1,0,-1,0]$.

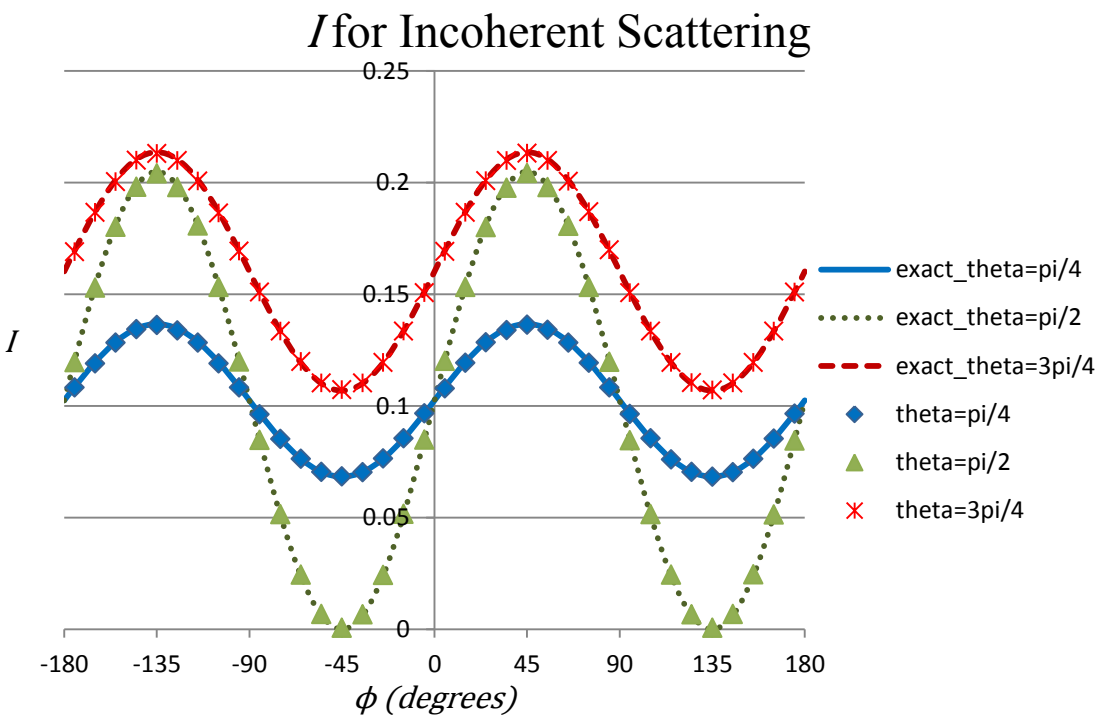

Figure A.67. *I* for the incoherently scattered portion of a 5 keV photon beam with a source Stokes vector of $[\varphi_I, \varphi_Q, \varphi_U, \varphi_V] = [1,0,-1,0]$.

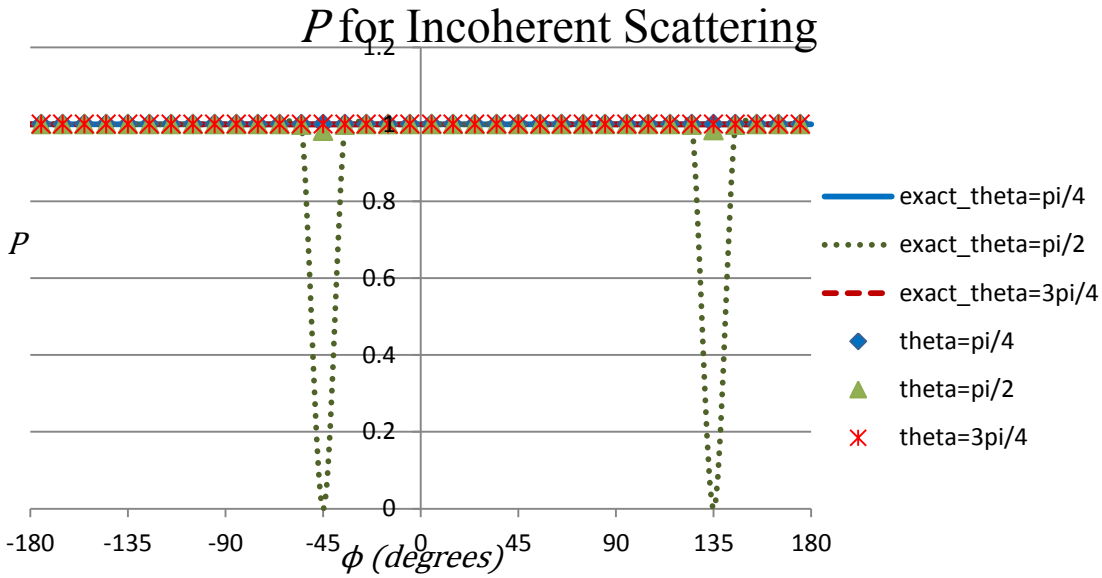

Figure A.68. *P* for the incoherently scattered portion of a 5 keV photon beam with a source Stokes vector of $[\varphi_I, \varphi_Q, \varphi_U, \varphi_V] = [1,0,-1,0]$.

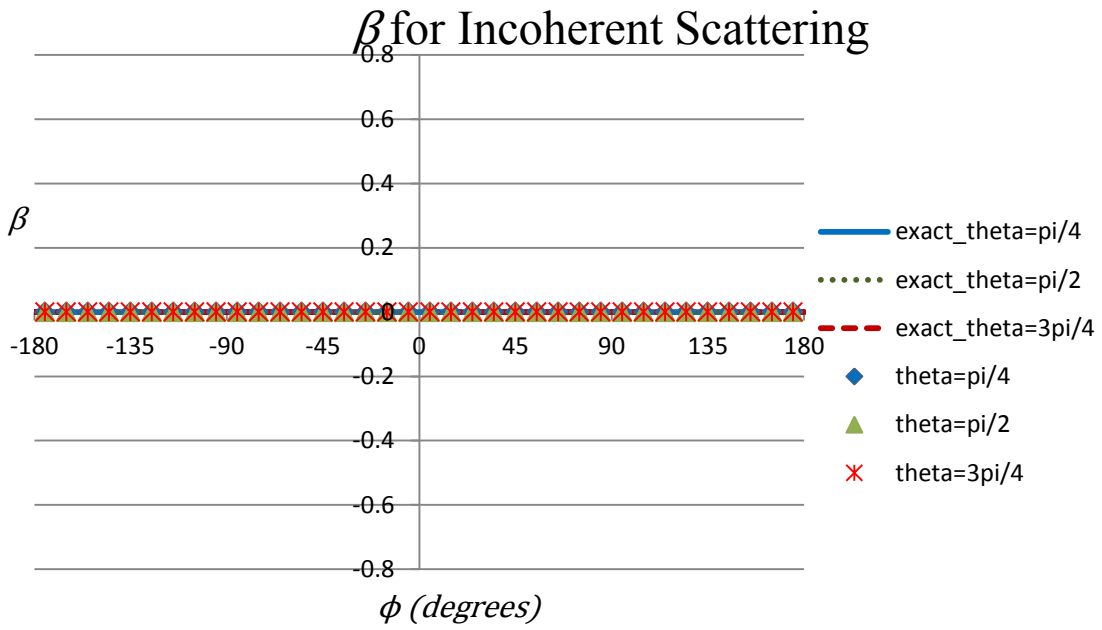

Figure A.69. β for the incoherently scattered portion of a 5 keV photon beam with a source Stokes vector of $[\varphi_I, \varphi_Q, \varphi_U, \varphi_V] = [1,0,-1,0]$.

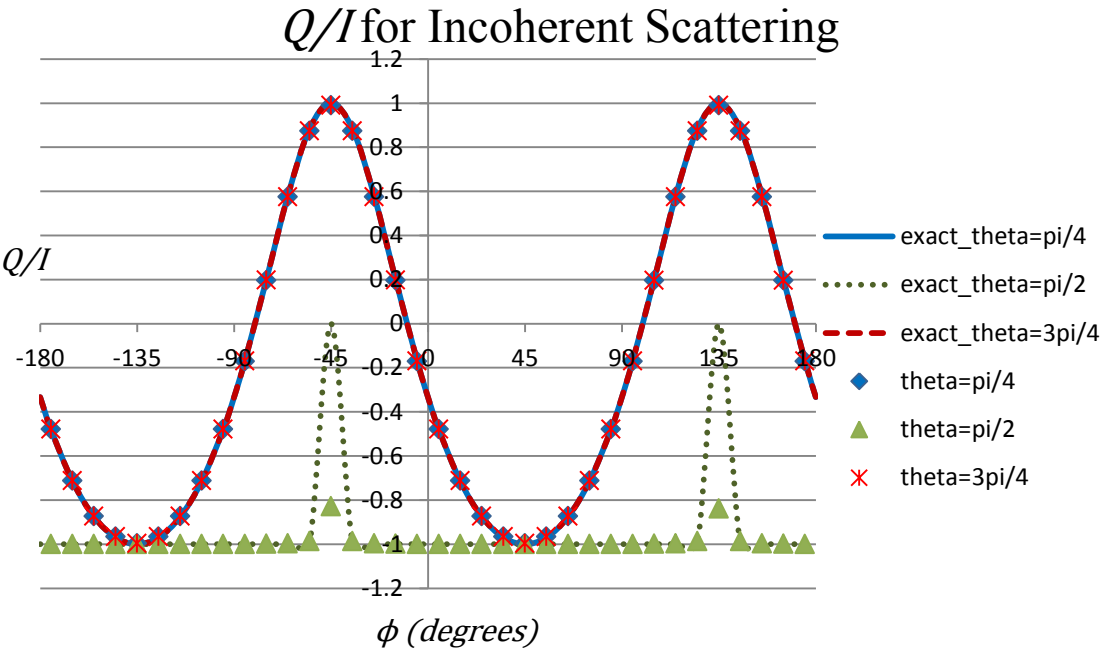

Figure A.70. Q/I for the incoherently scattered portion of a 5 keV photon beam with a source Stokes vector of $[\varphi_I, \varphi_Q, \varphi_U, \varphi_V] = [1,0,-1,0]$.

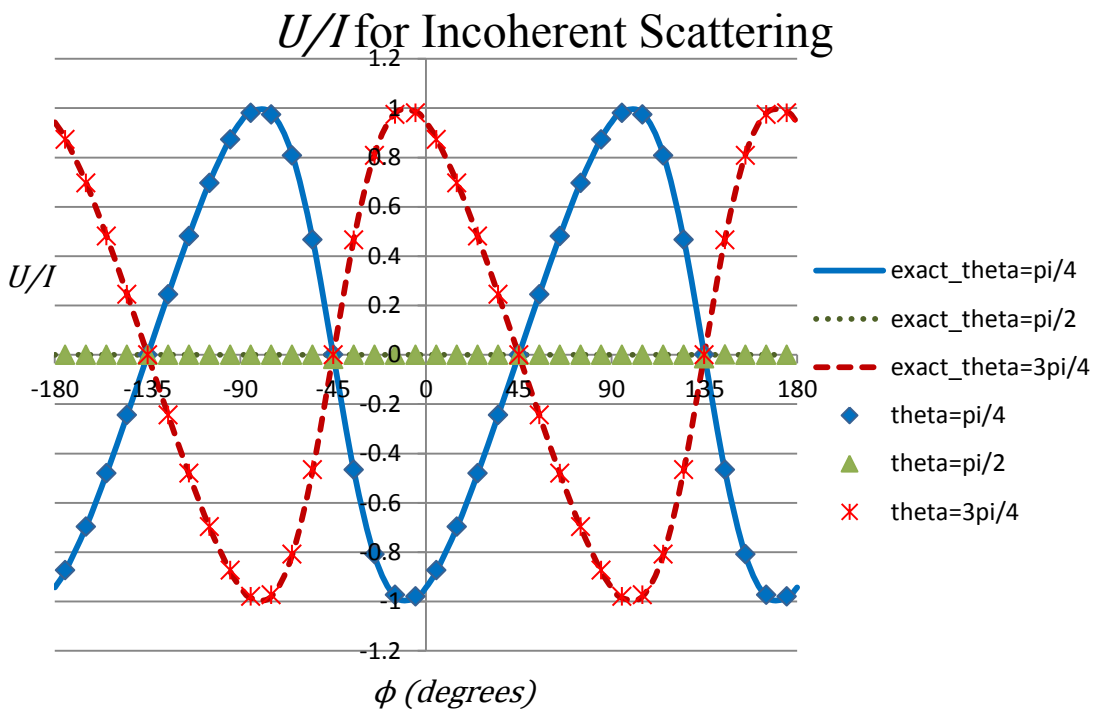

Figure A.71. *U/I* for the incoherently scattered portion of a 5 keV photon beam with a source Stokes vector of $[\varphi_I, \varphi_Q, \varphi_U, \varphi_V] = [1,0,-1,0]$.

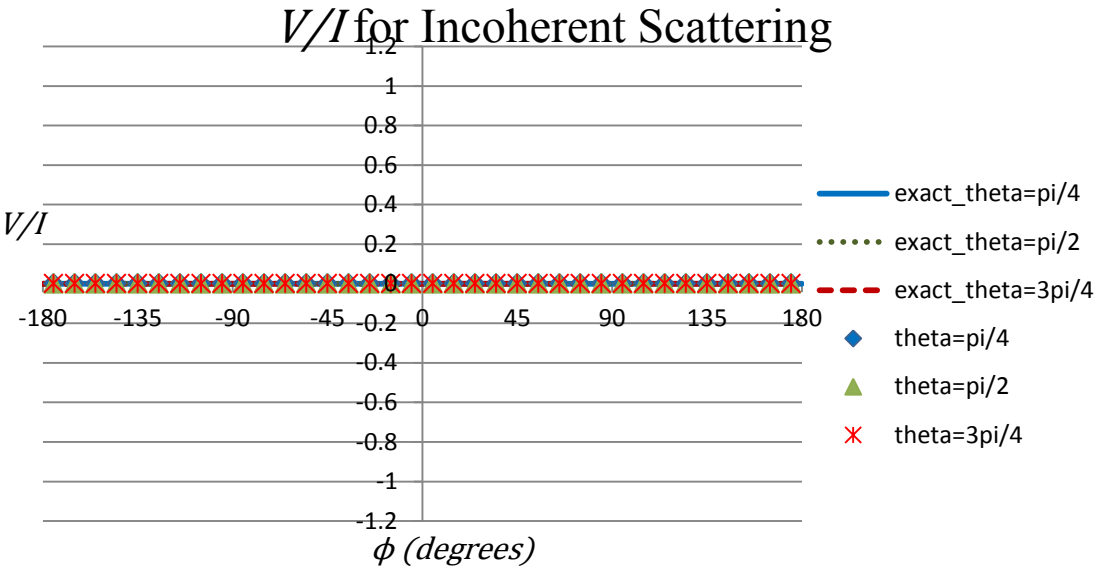

Figure A.72. *V/I* for the incoherently scattered portion of a 5 keV photon beam with a source Stokes vector of $[\varphi_I, \varphi_Q, \varphi_U, \varphi_V] = [1,0,-1,0]$.

A.4, $\Gamma = [1,0,0,1]$

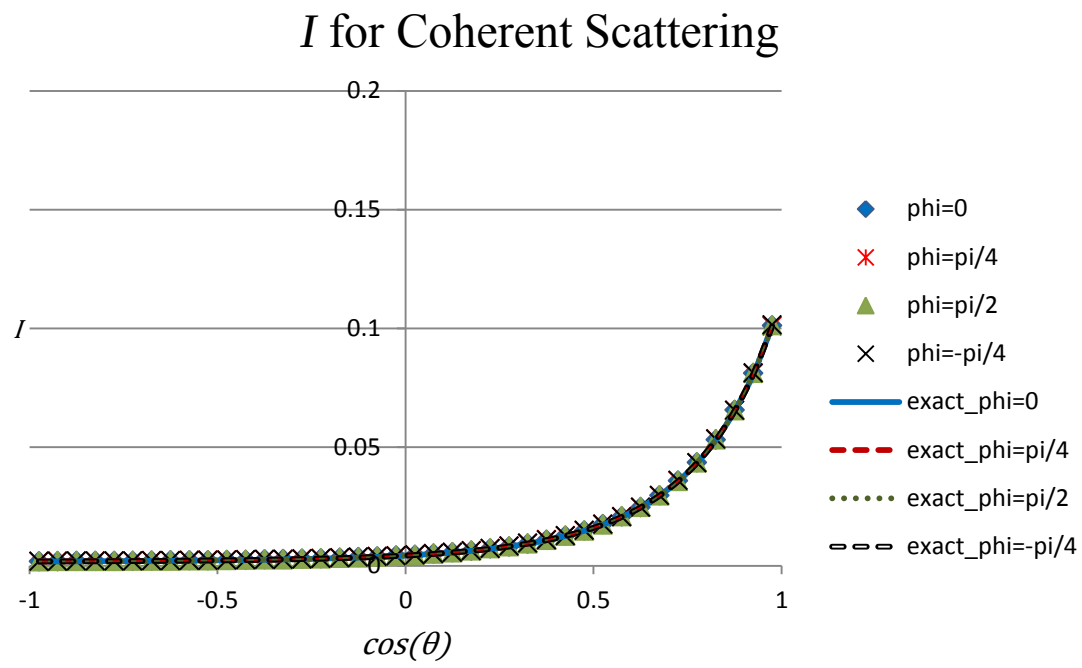

Figure A.73. I for the coherently scattered portion of a 5 keV photon beam with a source Stokes vector of $[\varphi_I, \varphi_Q, \varphi_U, \varphi_V] = [1,0,0,1]$.

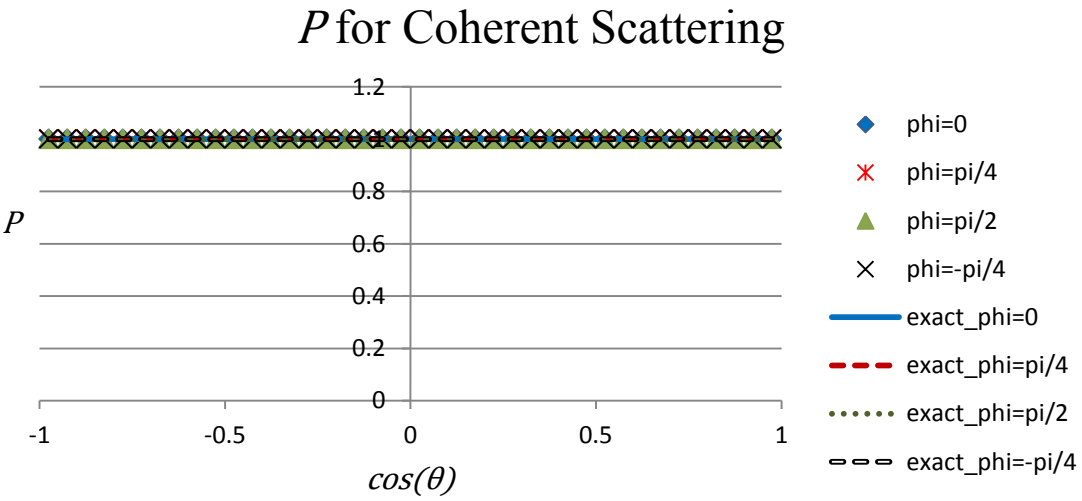

Figure A.74. P for the coherently scattered portion of a 5 keV photon beam with a source Stokes vector of $[\varphi_I, \varphi_Q, \varphi_U, \varphi_V] = [1,0,0,1]$.

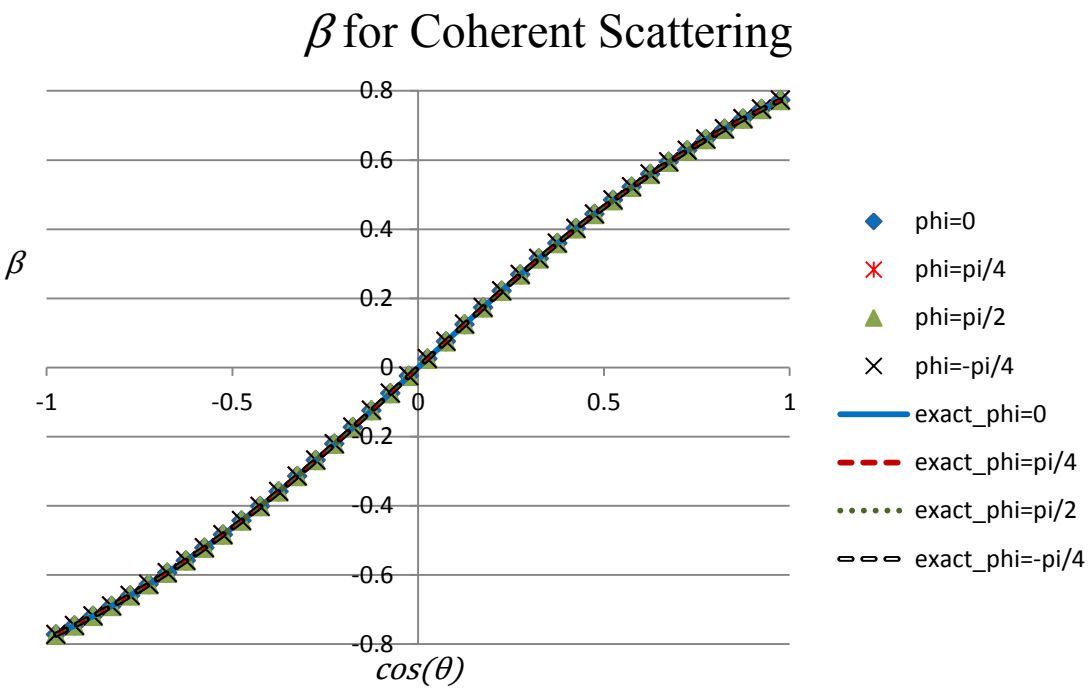

Figure A.75. β for the coherently scattered portion of a 5 keV photon beam with a source Stokes vector of $[\varphi_I, \varphi_Q, \varphi_U, \varphi_V] = [1,0,0,1]$.

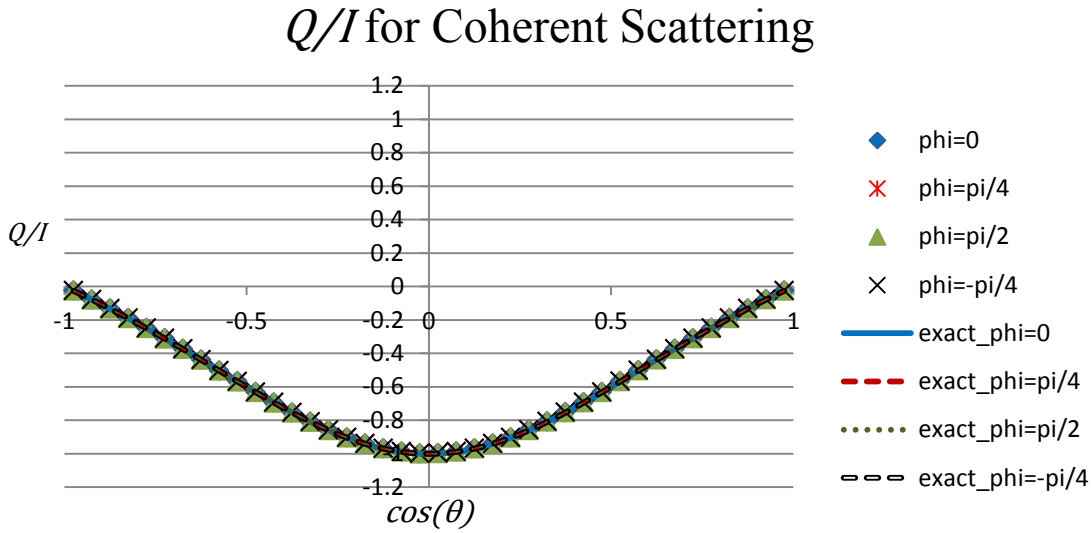

Figure A.76. Q/I for the coherently scattered portion of a 5 keV photon beam with a source Stokes vector of $[\varphi_I, \varphi_Q, \varphi_U, \varphi_V] = [1,0,0,1]$.

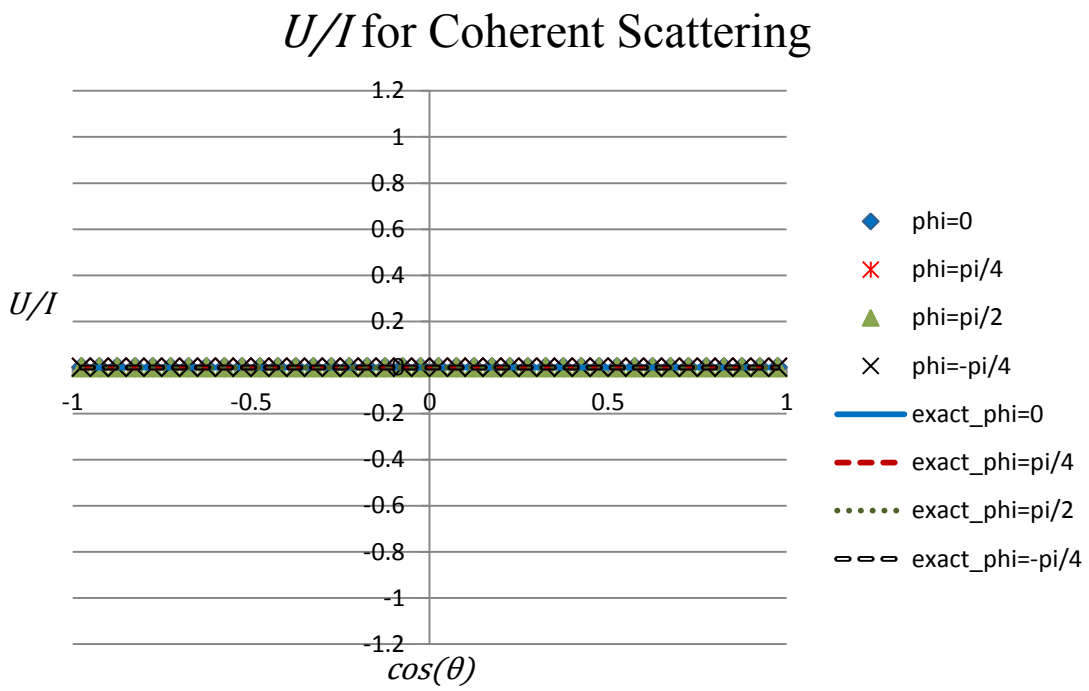

Figure A.77. *U/I* for the coherently scattered portion of a 5 keV photon beam with a source Stokes vector of $[\varphi_I, \varphi_Q, \varphi_U, \varphi_V] = [1,0,0,1]$.

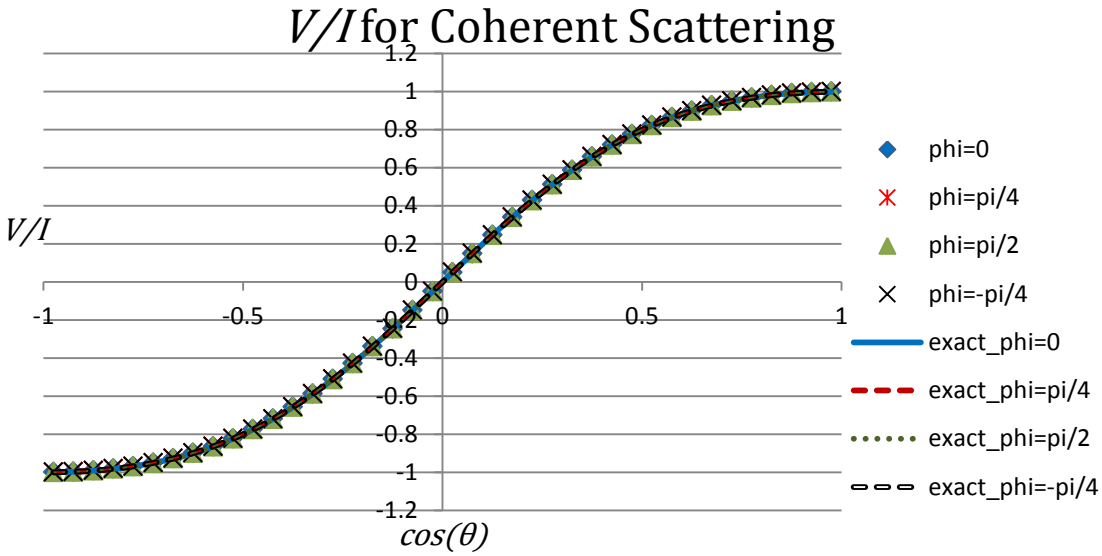

Figure A.78. *V/I* for the coherently scattered portion of a 5 keV photon beam with a source Stokes vector of $[\varphi_I, \varphi_Q, \varphi_U, \varphi_V] = [1,0,0,1]$.

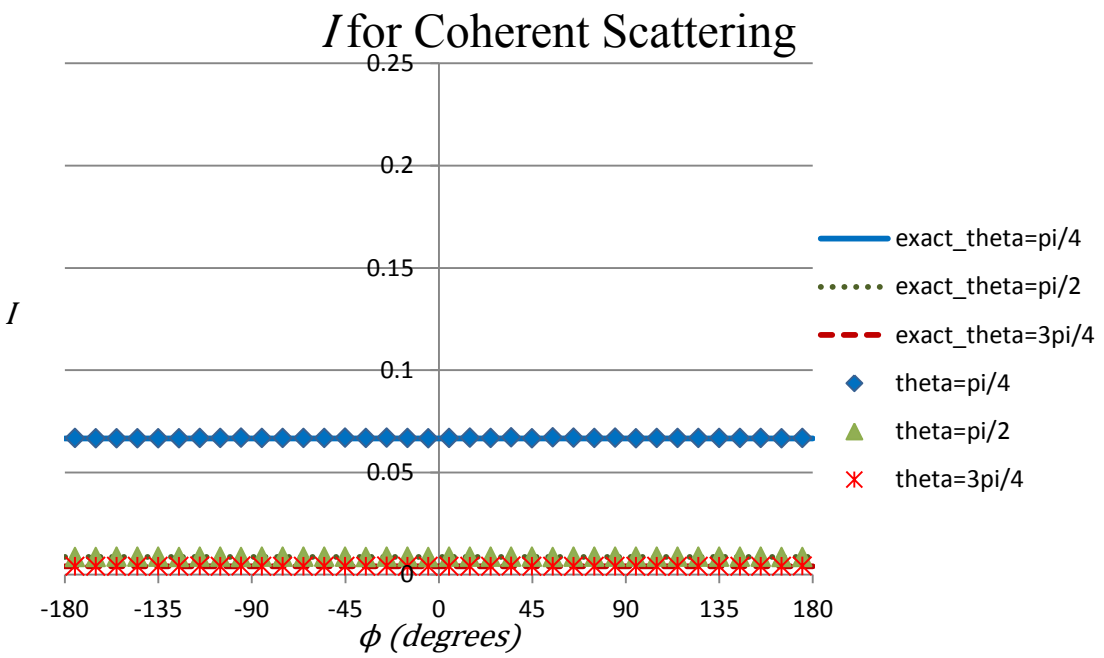

Figure A.79. *I* for the coherently scattered portion of a 5 keV photon beam with a source Stokes vector of $[\varphi_I, \varphi_Q, \varphi_U, \varphi_V] = [1,0,0,1]$.

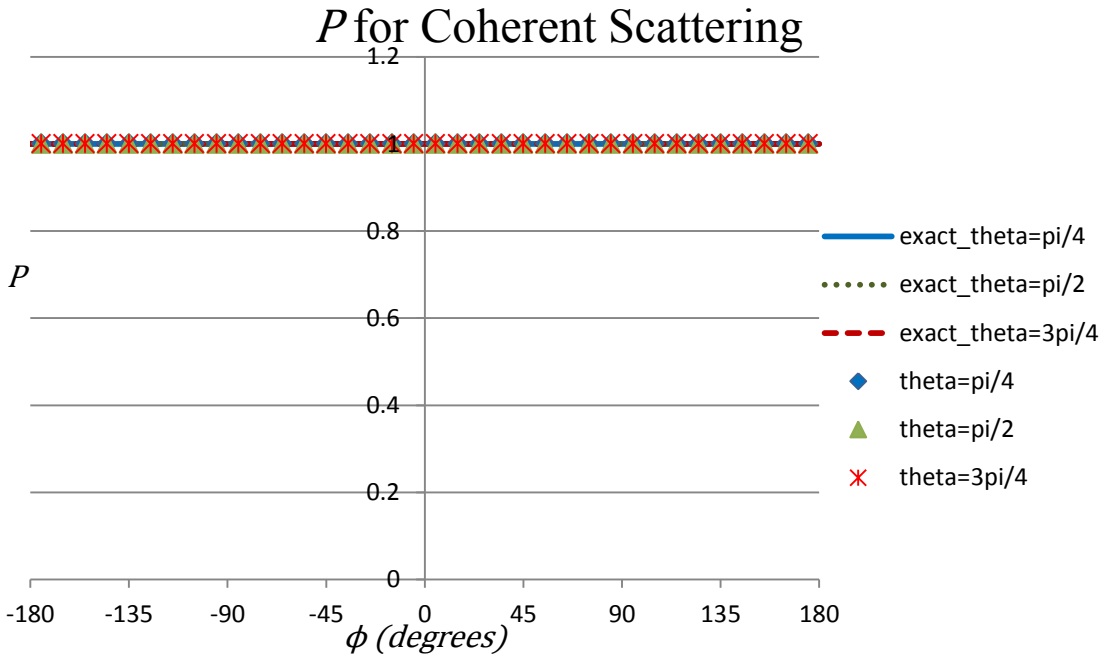

Figure A.80. *P* for the coherently scattered portion of a 5 keV photon beam with a source Stokes vector of $[\varphi_I, \varphi_Q, \varphi_U, \varphi_V] = [1,0,0,1]$.

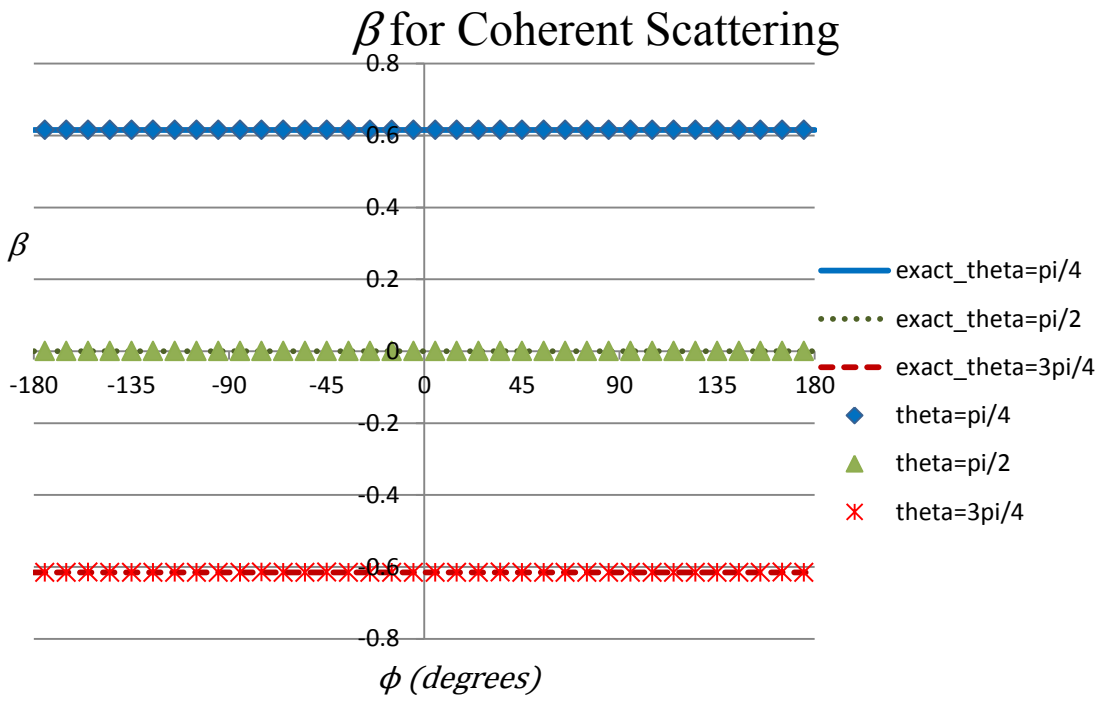

Figure A.81. β for the coherently scattered portion of a 5 keV photon beam with a source Stokes vector of $[\varphi_I, \varphi_Q, \varphi_U, \varphi_V] = [1,0,0,1]$.

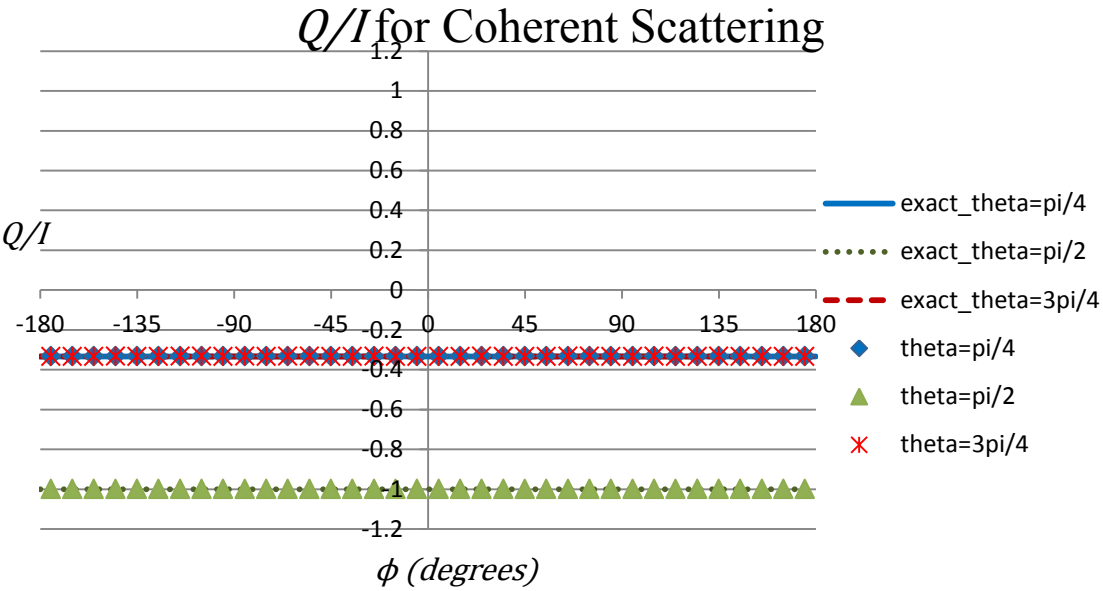

Figure A.82. Q/I for the coherently scattered portion of a 5 keV photon beam with a source Stokes vector of $[\varphi_I, \varphi_Q, \varphi_U, \varphi_V] = [1,0,0,1]$.

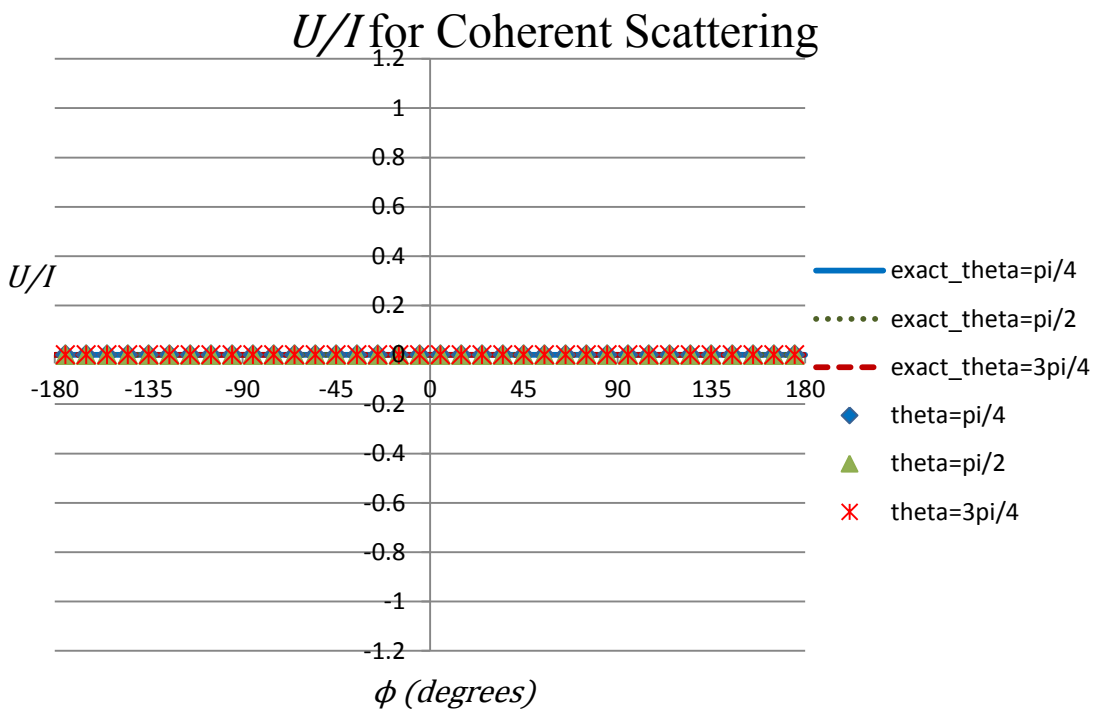

Figure A.83. U/I for the coherently scattered portion of a 5 keV photon beam with a source Stokes vector of $[\varphi_I, \varphi_Q, \varphi_U, \varphi_V] = [1,0,0,1]$.

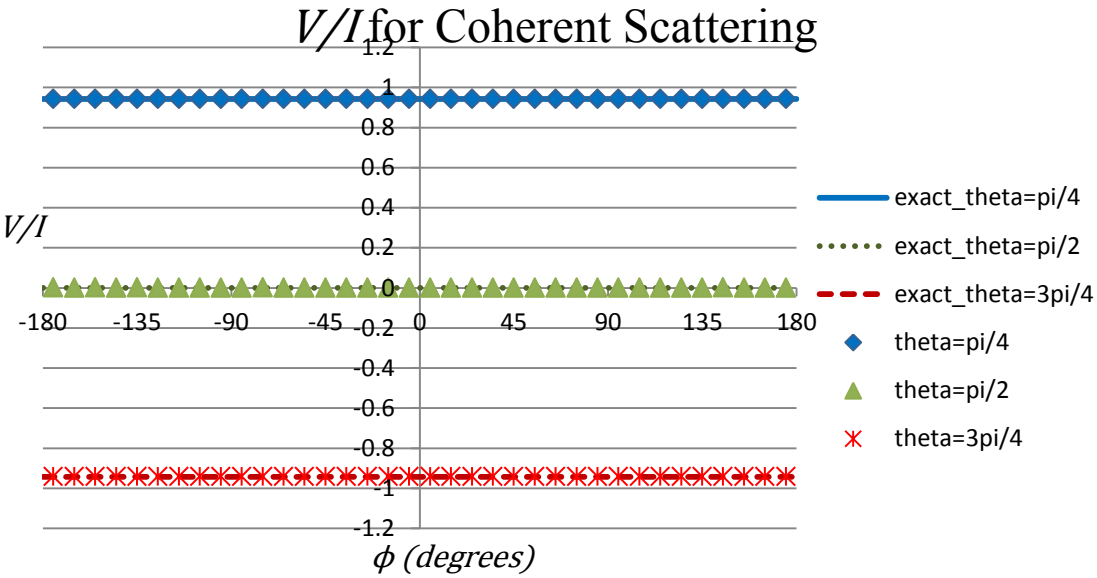

Figure A.84. V/I for the coherently scattered portion of a 5 keV photon beam with a source Stokes vector of $[\varphi_I, \varphi_Q, \varphi_U, \varphi_V] = [1,0,0,1]$.

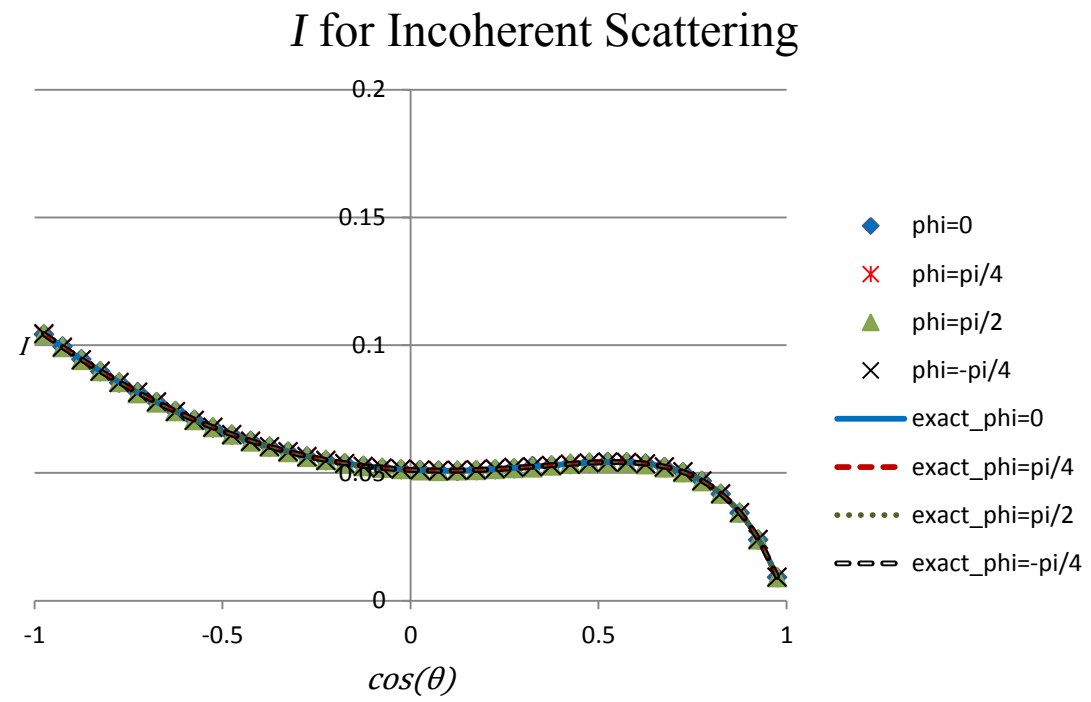

Figure A.85. I for the incoherently scattered portion of a 5 keV photon beam with a source Stokes vector of $[\varphi_I, \varphi_Q, \varphi_U, \varphi_V] = [1,0,0,1]$.

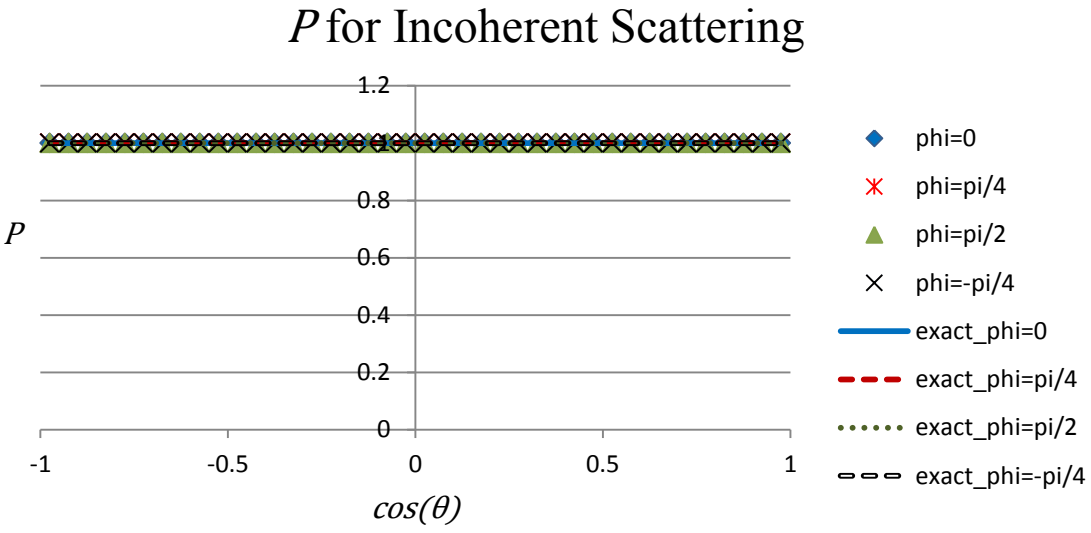

Figure A.86. P for the incoherently scattered portion of a 5 keV photon beam with a source Stokes vector of $[\varphi_I, \varphi_Q, \varphi_U, \varphi_V] = [1,0,0,1]$.

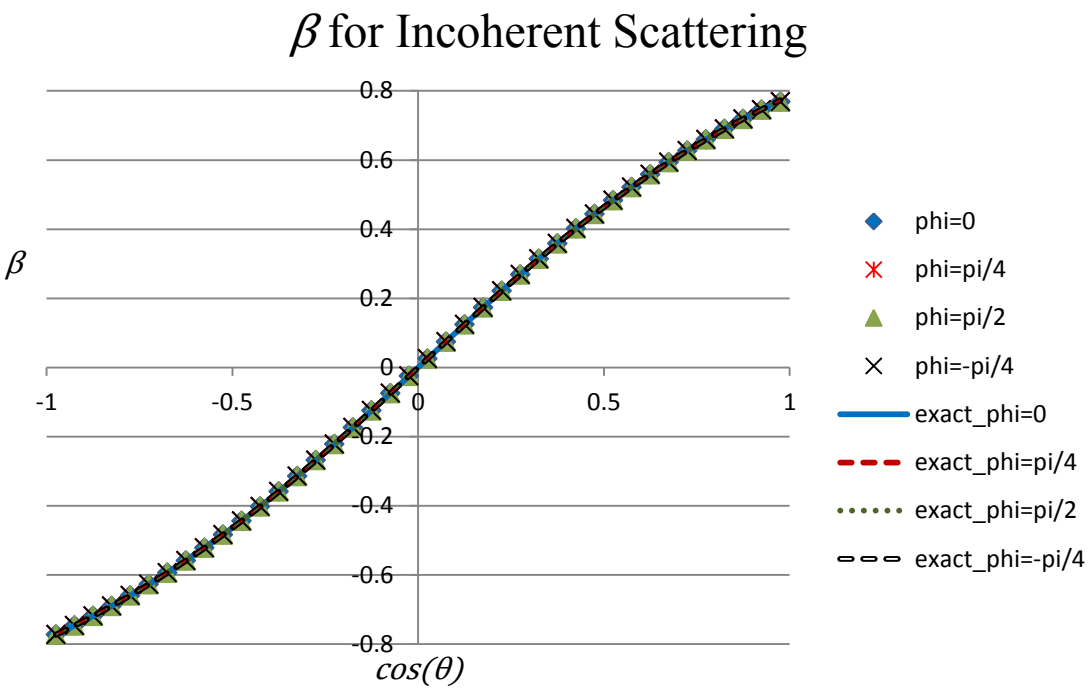

Figure A.87. β for the incoherently scattered portion of a 5 keV photon beam with a source Stokes vector of $[\varphi_I, \varphi_Q, \varphi_U, \varphi_V] = [1,0,0,1]$.

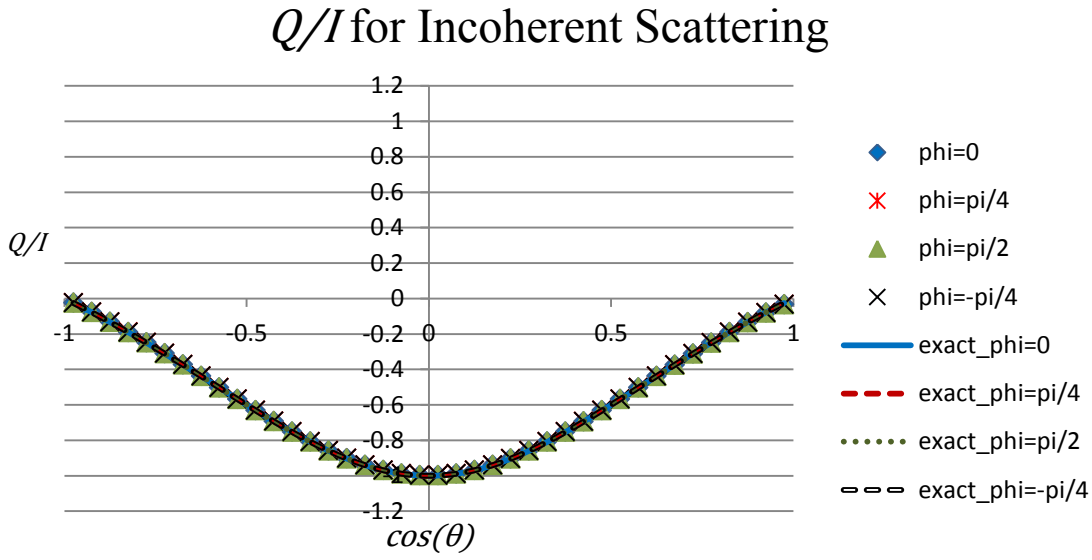

Figure A.88. Q/I for the incoherently scattered portion of a 5 keV photon beam with a source Stokes vector of $[\varphi_I, \varphi_Q, \varphi_U, \varphi_V] = [1,0,0,1]$.

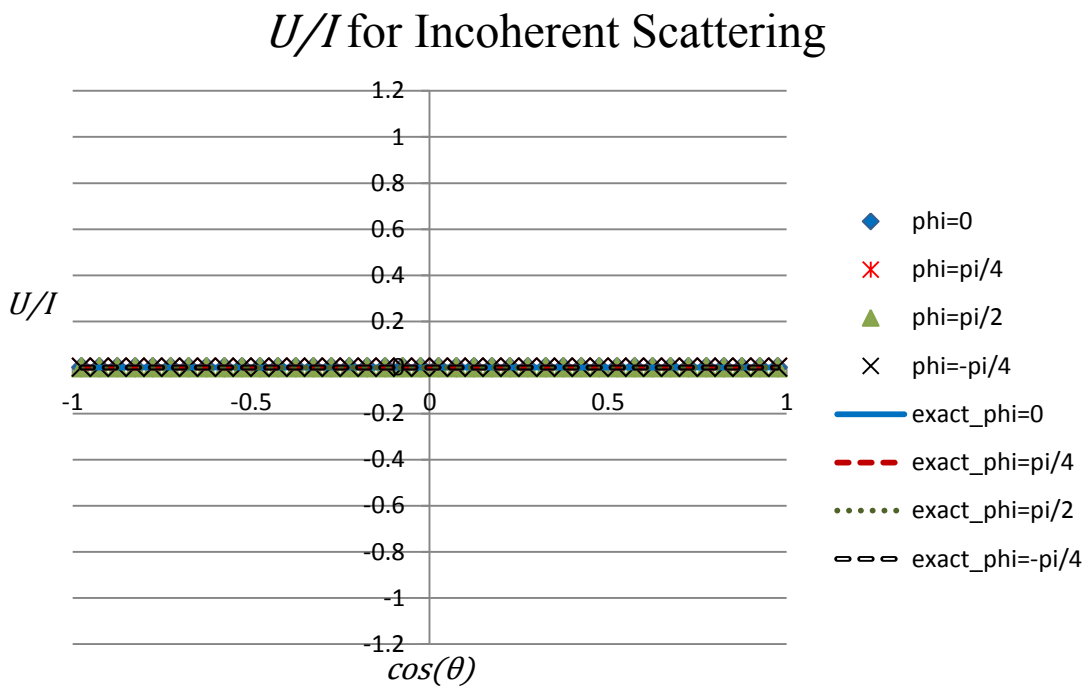

Figure A.89. *U/I* for the incoherently scattered portion of a 5 keV photon beam with a source Stokes vector of $[\varphi_I, \varphi_Q, \varphi_U, \varphi_V] = [1,0,0,1]$.

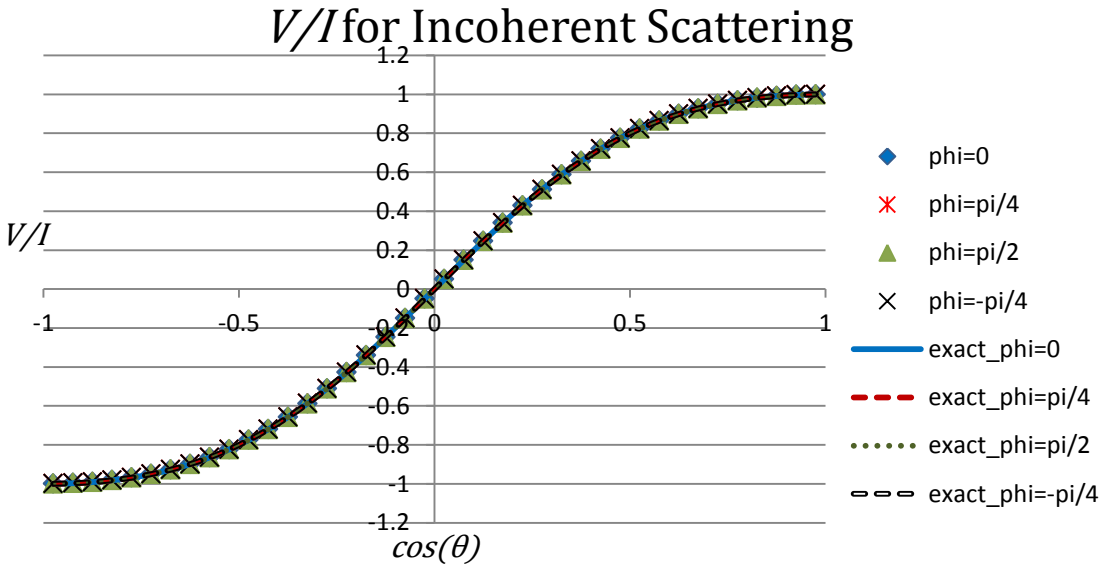

Figure A.90. *V/I* for the incoherently scattered portion of a 5 keV photon beam with a source Stokes vector of $[\varphi_I, \varphi_Q, \varphi_U, \varphi_V] = [1,0,0,1]$.

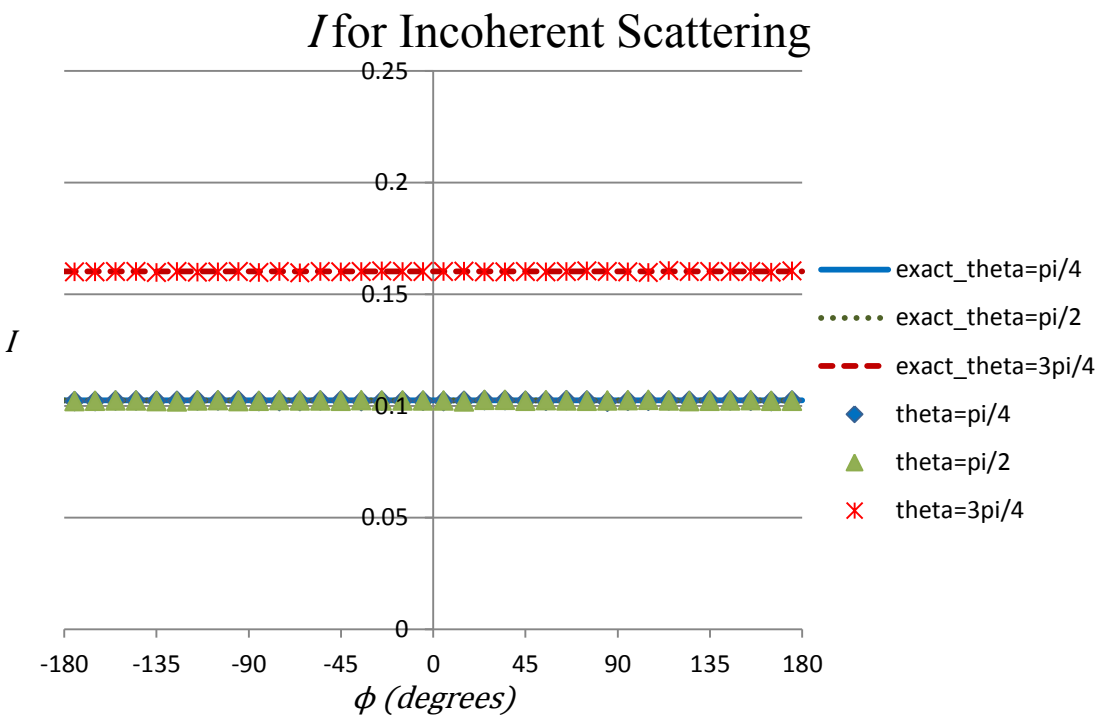

Figure A.91. I for the incoherently scattered portion of a 5 keV photon beam with a source Stokes vector of $[\varphi_I, \varphi_Q, \varphi_U, \varphi_V] = [1,0,0,1]$.

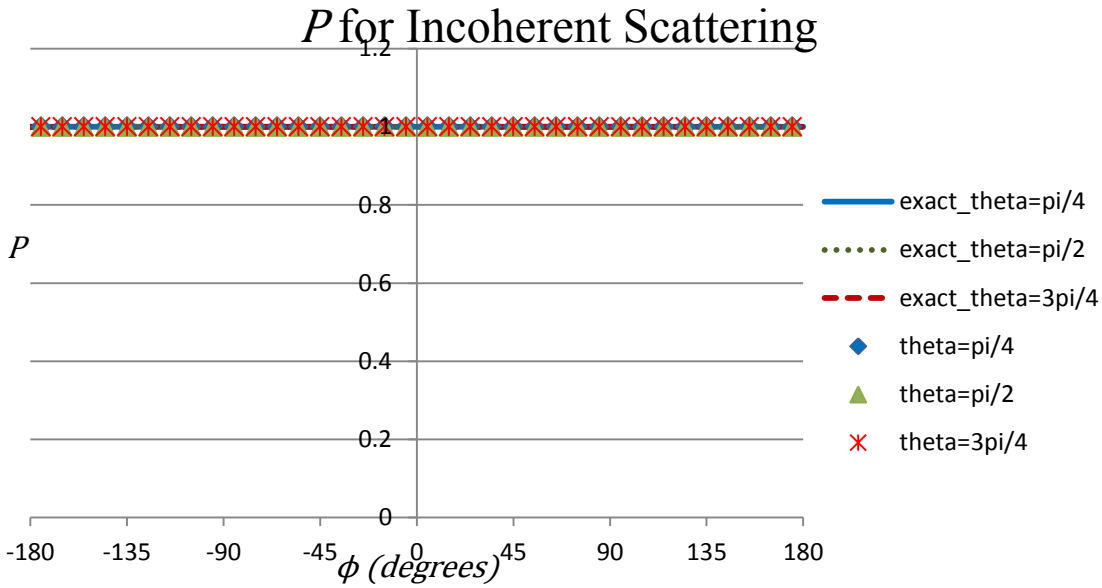

Figure A.92. P for the incoherently scattered portion of a 5 keV photon beam with a source Stokes vector of $[\varphi_I, \varphi_Q, \varphi_U, \varphi_V] = [1,0,0,1]$.

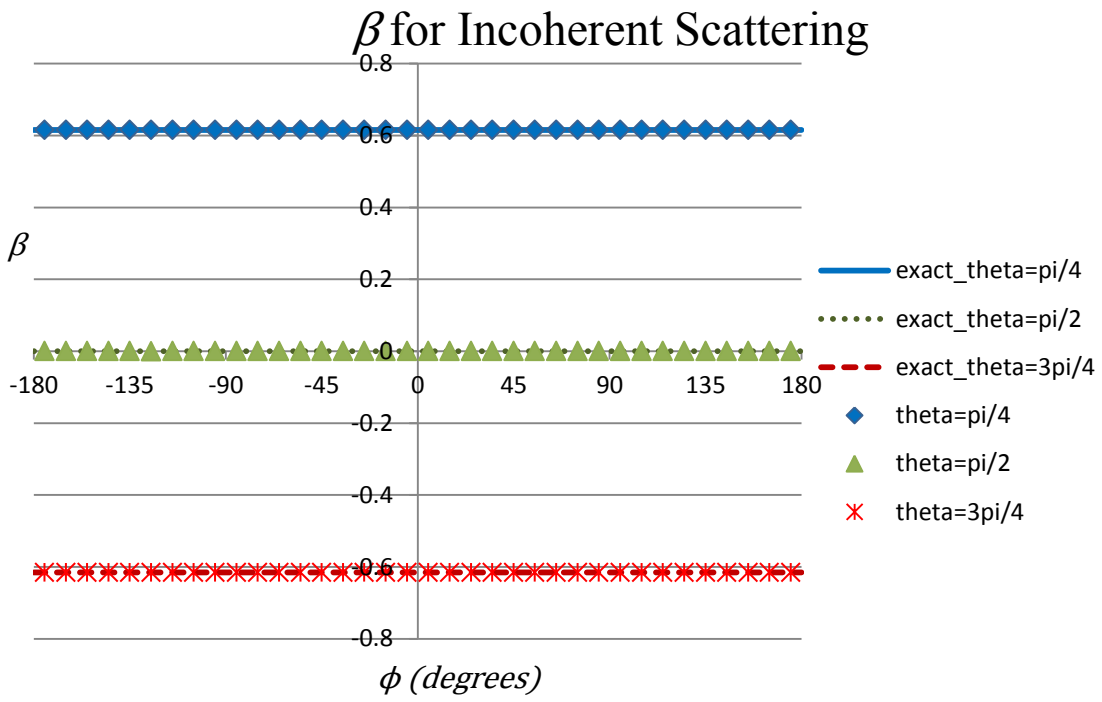

Figure A.93. β for the incoherently scattered portion of a 5 keV photon beam with a source Stokes vector of $[\varphi_I, \varphi_Q, \varphi_U, \varphi_V] = [1,0,0,1]$.

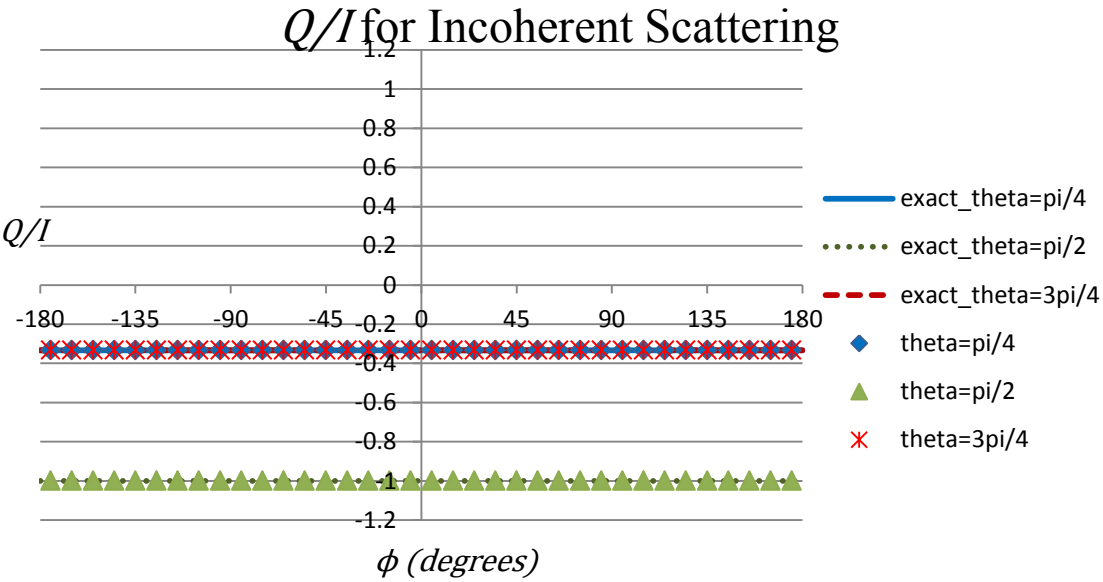

Figure A.94. Q/I for the incoherently scattered portion of a 5 keV photon beam with a source Stokes vector of $[\varphi_I, \varphi_Q, \varphi_U, \varphi_V] = [1,0,0,1]$.

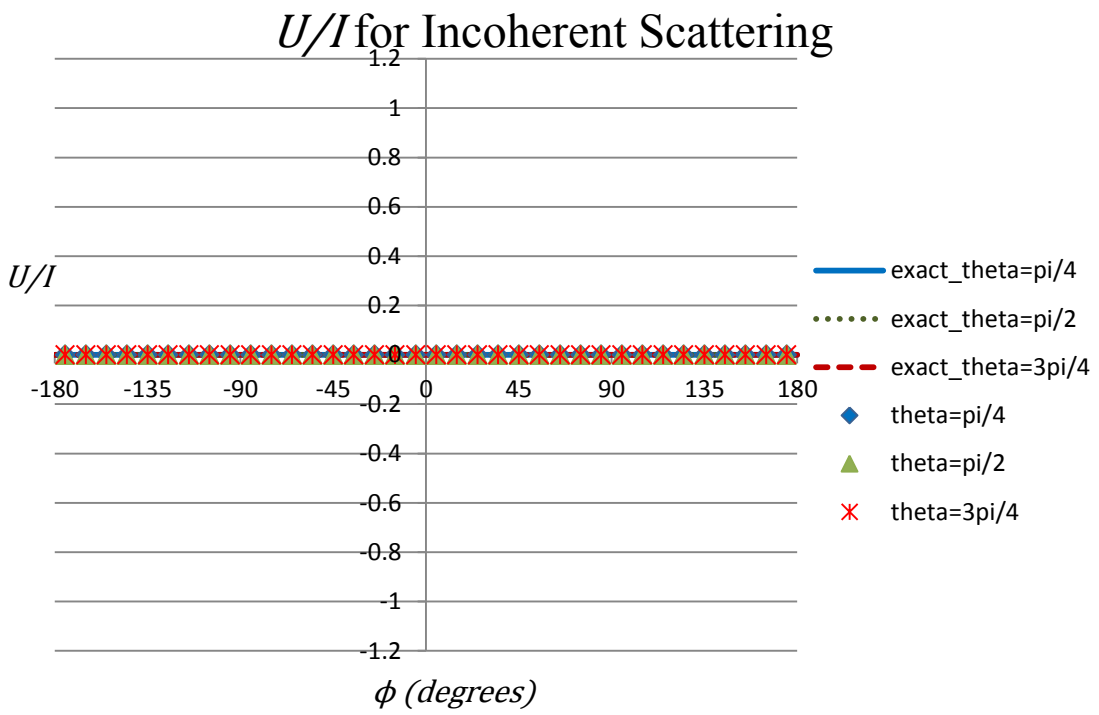

Figure A.95. *U/I* for the incoherently scattered portion of a 5 keV photon beam with a source Stokes vector of $[\varphi_I, \varphi_Q, \varphi_U, \varphi_V] = [1,0,0,1]$.

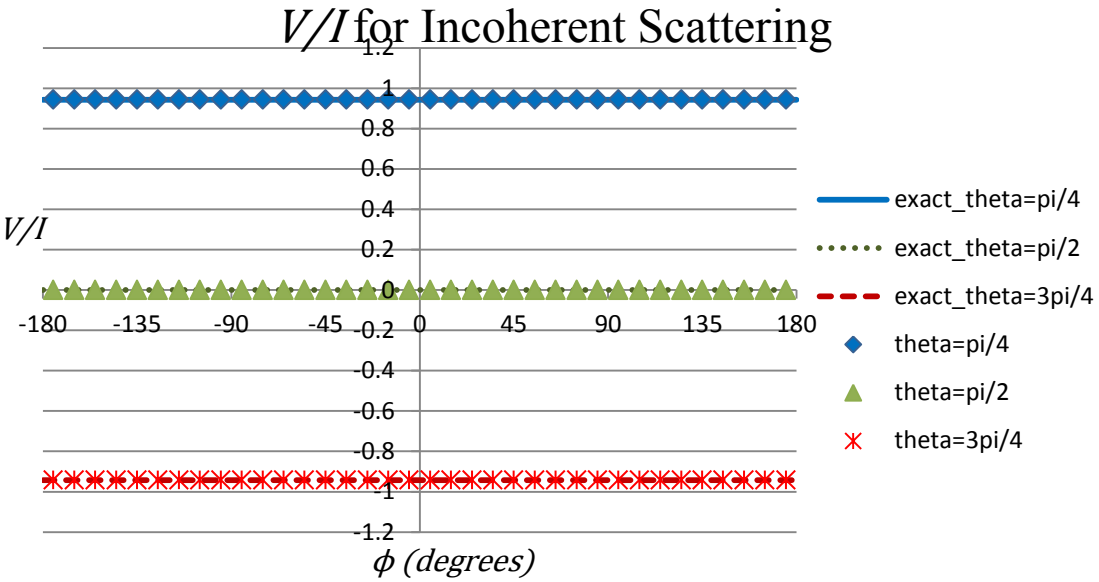

Figure A.96. *V/I* for the incoherently scattered portion of a 5 keV photon beam with a source Stokes vector of $[\varphi_I, \varphi_Q, \varphi_U, \varphi_V] = [1,0,0,1]$.

A.5, $\Gamma = [1,0.5,0.5,0]$

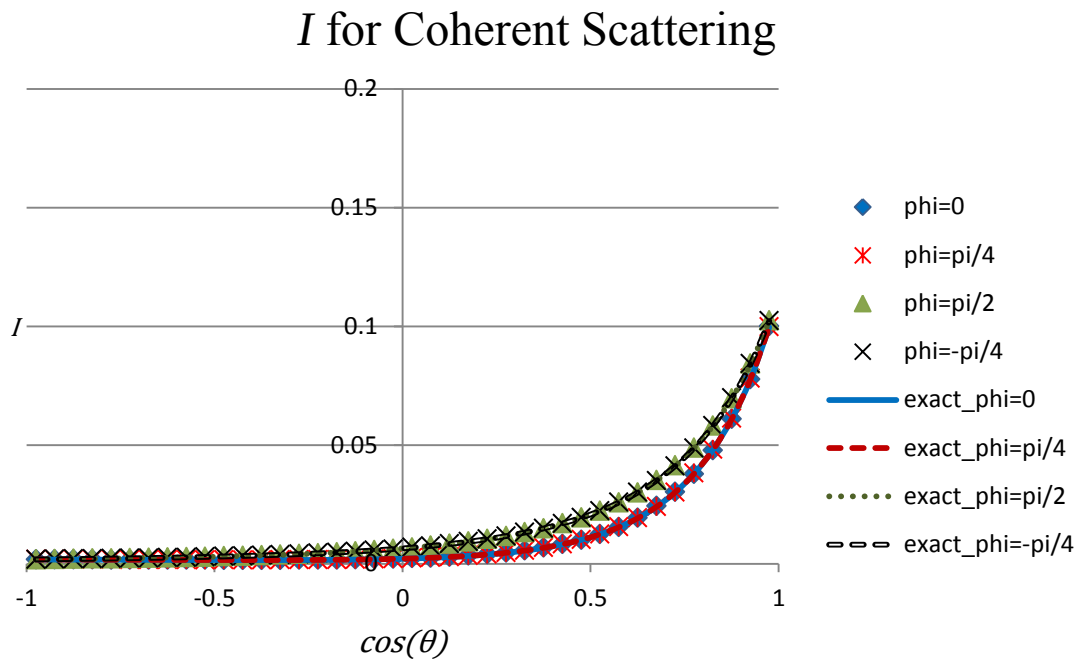

Figure A.97. I for the coherently scattered portion of a 5 keV photon beam with a source Stokes vector of $[\varphi_I, \varphi_Q, \varphi_U, \varphi_V] = [1,0.5,0.5,0]$.

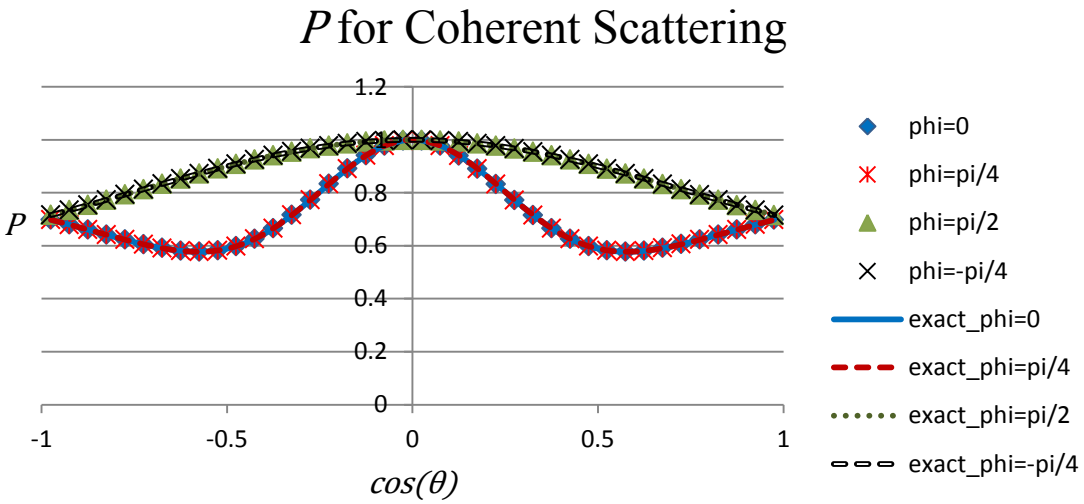

Figure A.98. P for the coherently scattered portion of a 5 keV photon beam with a source Stokes vector of $[\varphi_I, \varphi_Q, \varphi_U, \varphi_V] = [1,0.5,0.5,0]$.

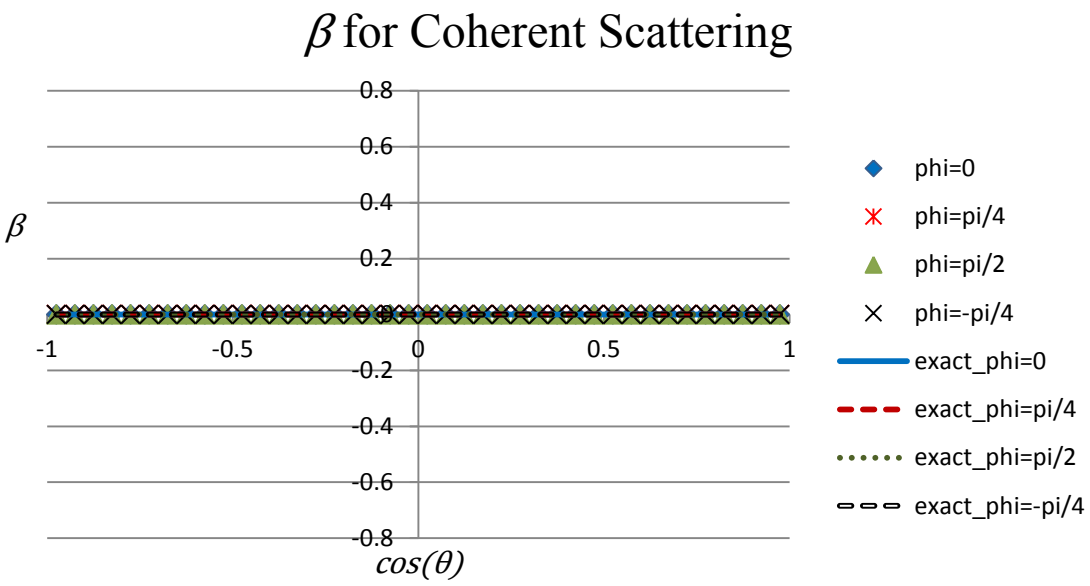

Figure A.99. β for the coherently scattered portion of a 5 keV photon beam with a source Stokes vector of $[\varphi_I, \varphi_Q, \varphi_U, \varphi_V] = [1,0.5,0.5,0]$.

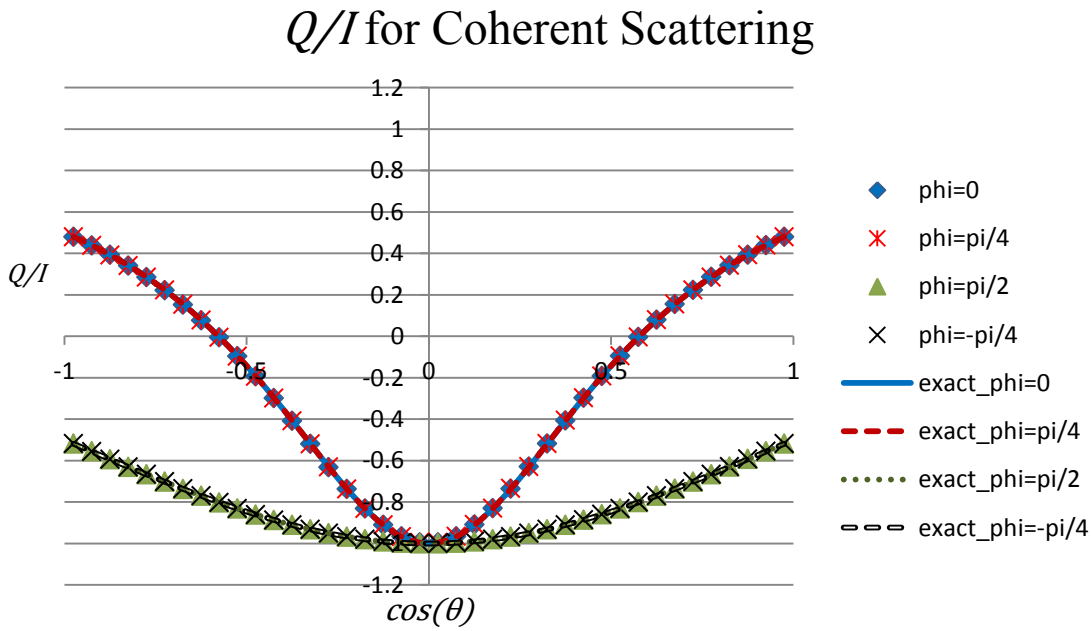

Figure A.100. Q/I for the coherently scattered portion of a 5 keV photon beam with a source Stokes vector of $[\varphi_I, \varphi_Q, \varphi_U, \varphi_V] = [1,0.5,0.5,0]$.

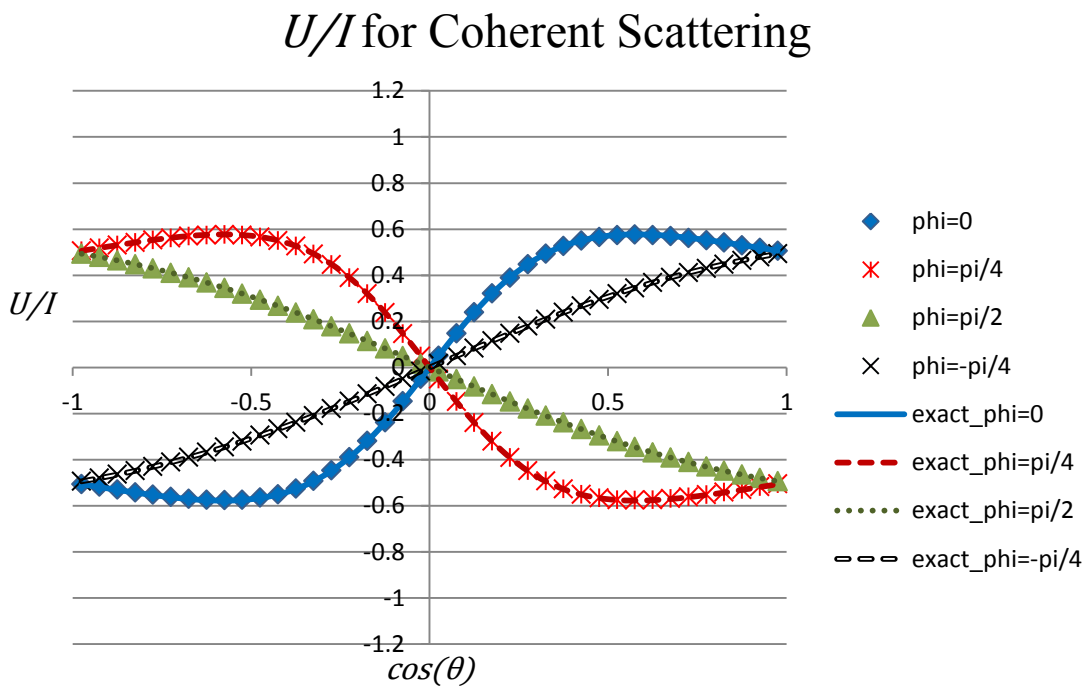

Figure A.101. *U/I* for the coherently scattered portion of a 5 keV photon beam with a source Stokes vector of $[\varphi_I, \varphi_Q, \varphi_U, \varphi_V] = [1,0.5,0.5,0]$.

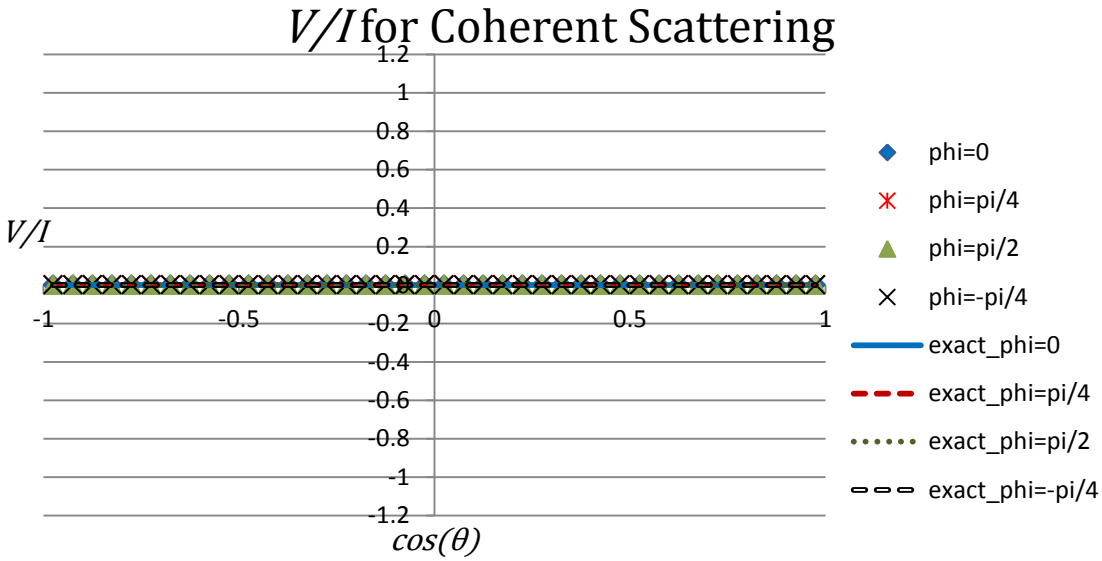

Figure A.102. *V/I* for the coherently scattered portion of a 5 keV photon beam with a source Stokes vector of $[\varphi_I, \varphi_Q, \varphi_U, \varphi_V] = [1,0.5,0.5,0]$.

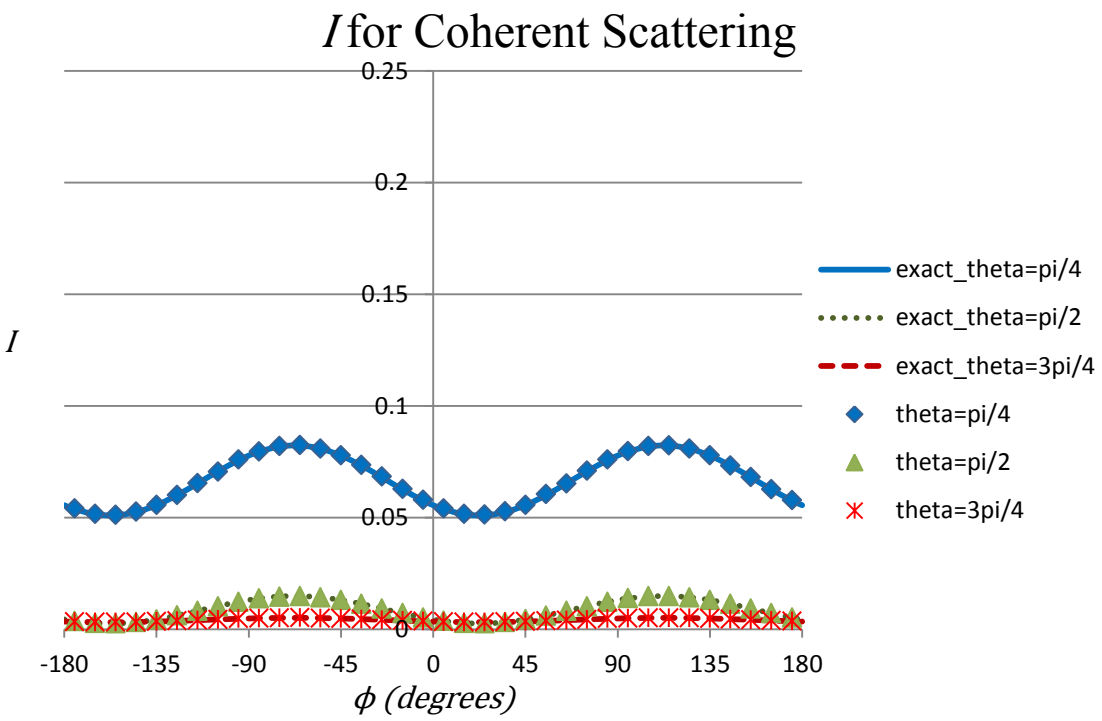

Figure A.103. *I* for the coherently scattered portion of a 5 keV photon beam with a source Stokes vector of $[\varphi_I, \varphi_Q, \varphi_U, \varphi_V] = [1,0.5,0.5,0]$.

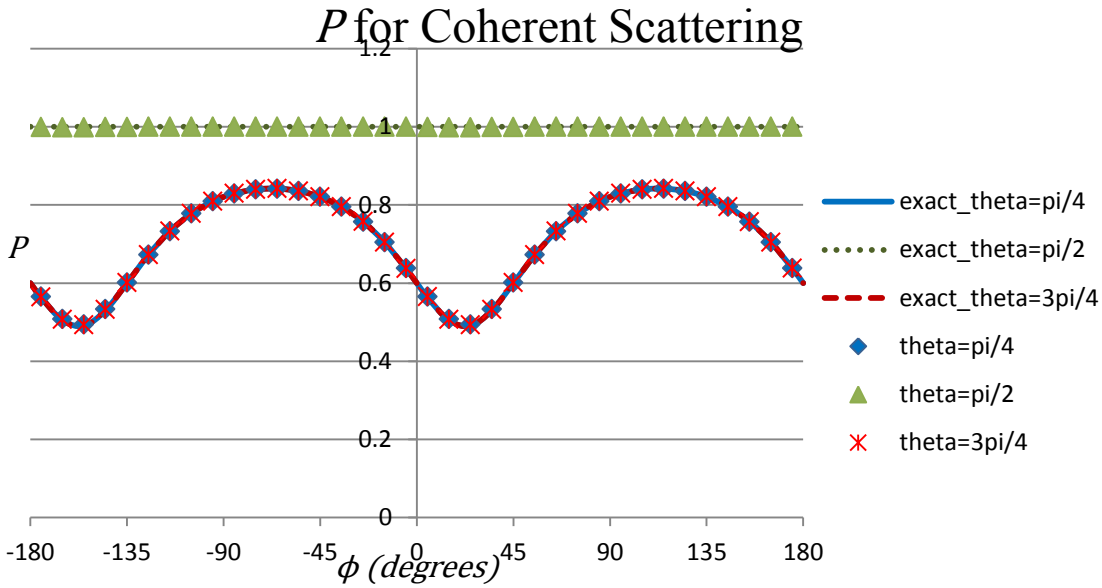

Figure A.104. *P* for the coherently scattered portion of a 5 keV photon beam with a source Stokes vector of $[\varphi_I, \varphi_Q, \varphi_U, \varphi_V] = [1,0.5,0.5,0]$.

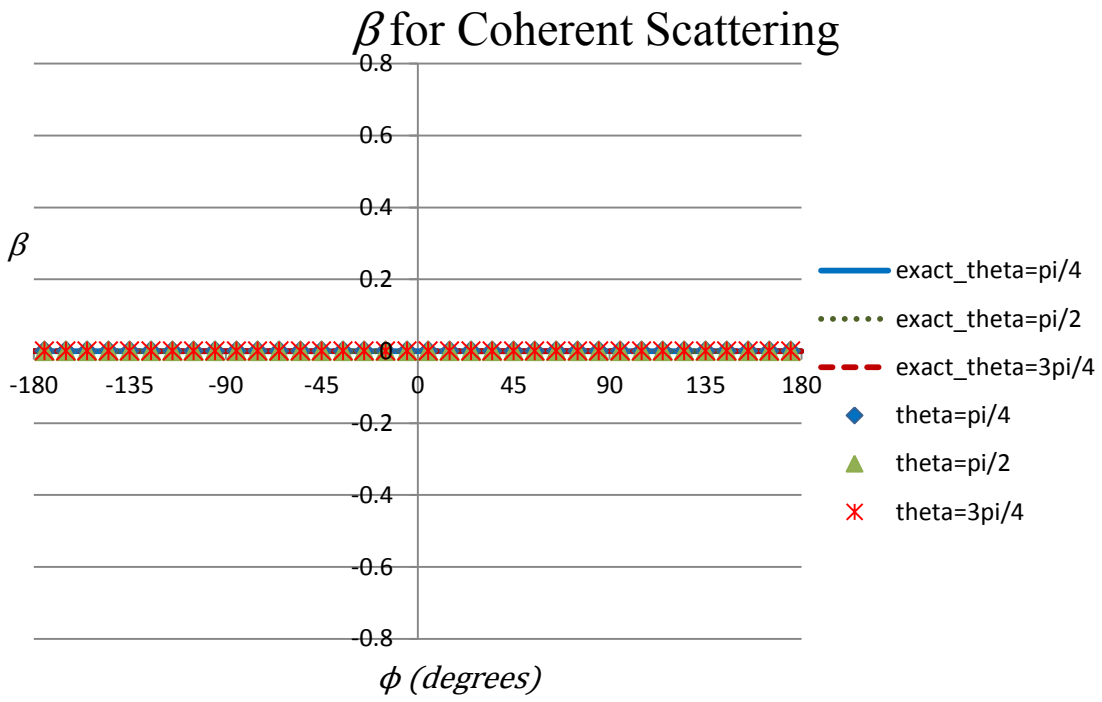

Figure A.105. β for the coherently scattered portion of a 5 keV photon beam with a source Stokes vector of $[\varphi_I, \varphi_Q, \varphi_U, \varphi_V] = [1,0.5,0.5,0]$.

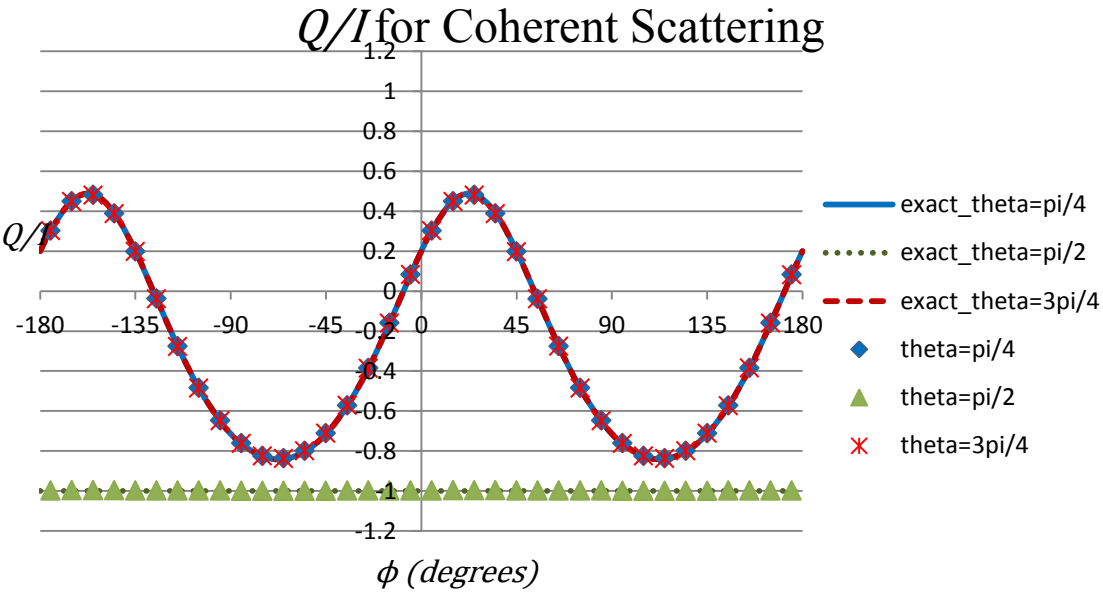

Figure A.106. Q/I for the coherently scattered portion of a 5 keV photon beam with a source Stokes vector of $[\varphi_I, \varphi_Q, \varphi_U, \varphi_V] = [1,0.5,0.5,0]$.

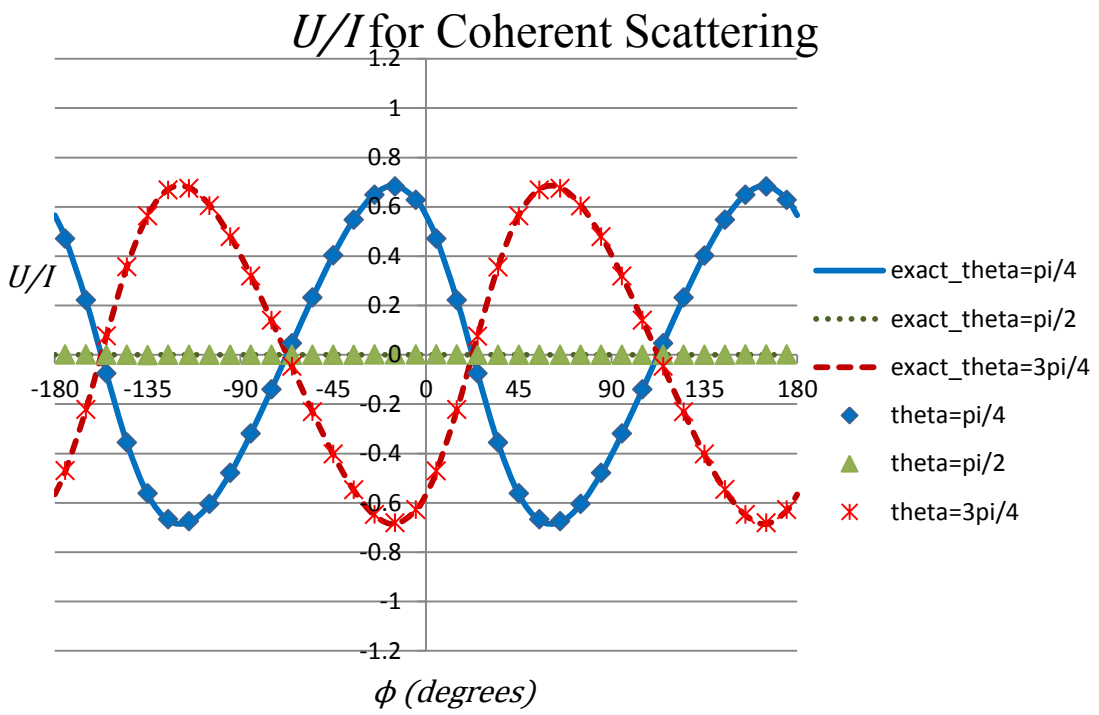

Figure A.107. *U/I* for the coherently scattered portion of a 5 keV photon beam with a source Stokes vector of $[\varphi_I, \varphi_Q, \varphi_U, \varphi_V] = [1,0.5,0.5,0]$.

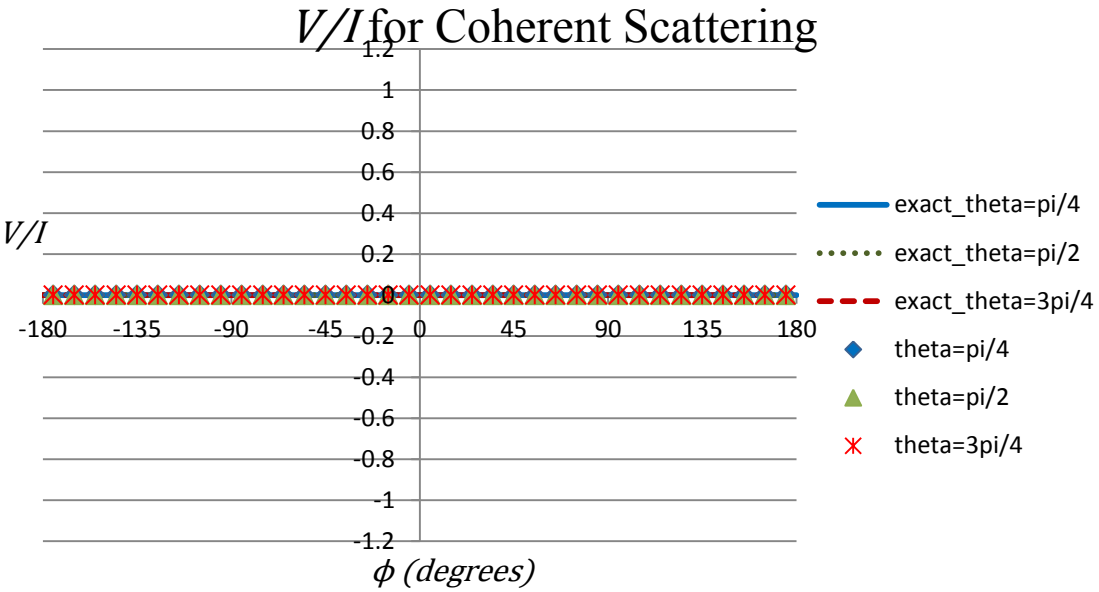

Figure A.108. *V/I* for the coherently scattered portion of a 5 keV photon beam with a source Stokes vector of $[\varphi_I, \varphi_Q, \varphi_U, \varphi_V] = [1,0.5,0.5,0]$.

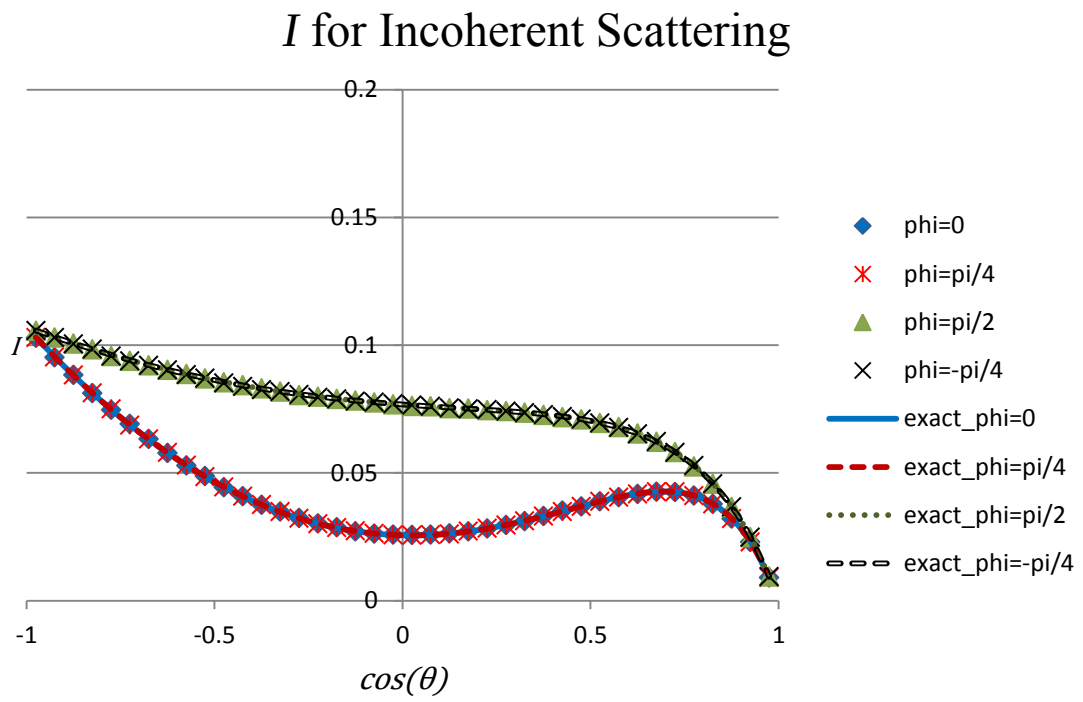

Figure A.109. *I* for the incoherently scattered portion of a 5 keV photon beam with a source Stokes vector of $[\varphi_I, \varphi_Q, \varphi_U, \varphi_V] = [1,0.5,0.5,0]$.

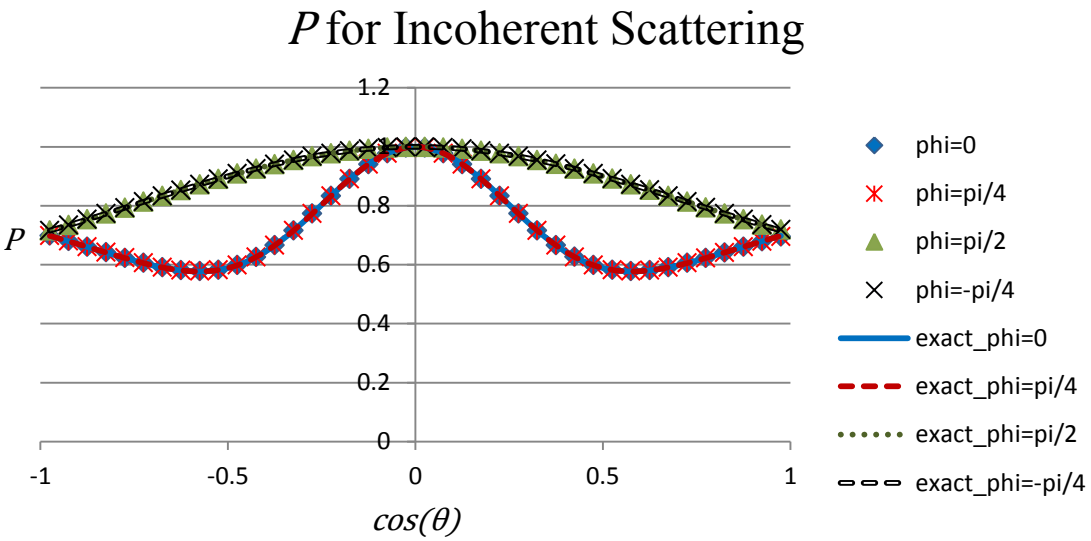

Figure A.110. *P* for the incoherently scattered portion of a 5 keV photon beam with a source Stokes vector of $[\varphi_I, \varphi_Q, \varphi_U, \varphi_V] = [1,0.5,0.5,0]$.

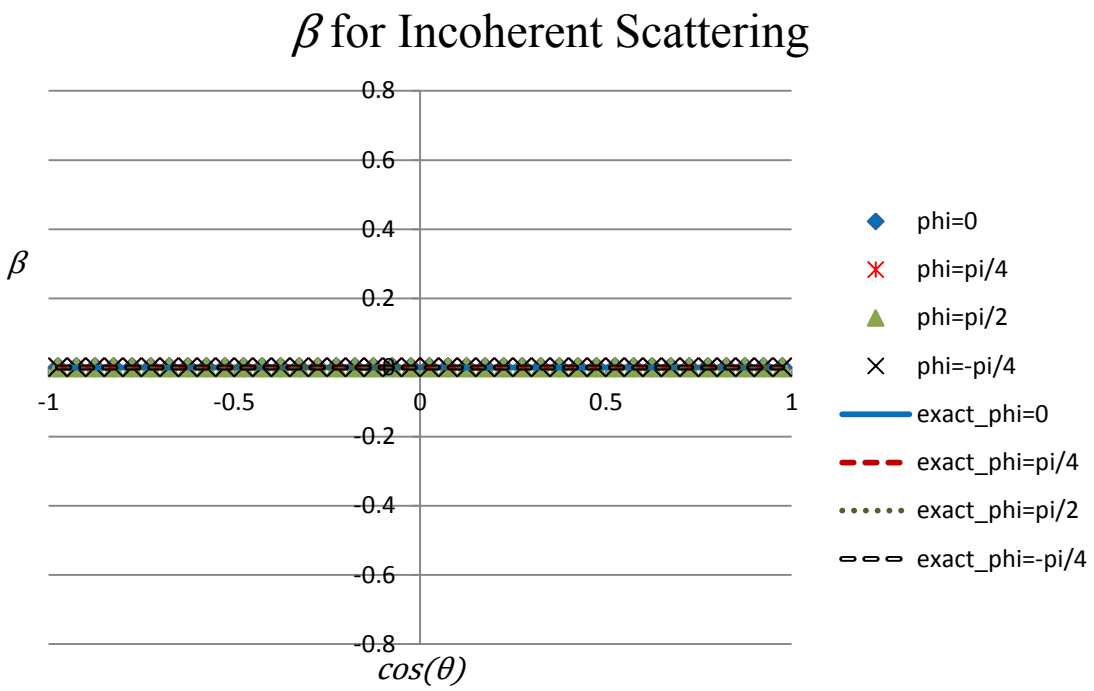

Figure A.111. β for the incoherently scattered portion of a 5 keV photon beam with a source Stokes vector of $[\varphi_I, \varphi_Q, \varphi_U, \varphi_V] = [1,0.5,0.5,0]$.

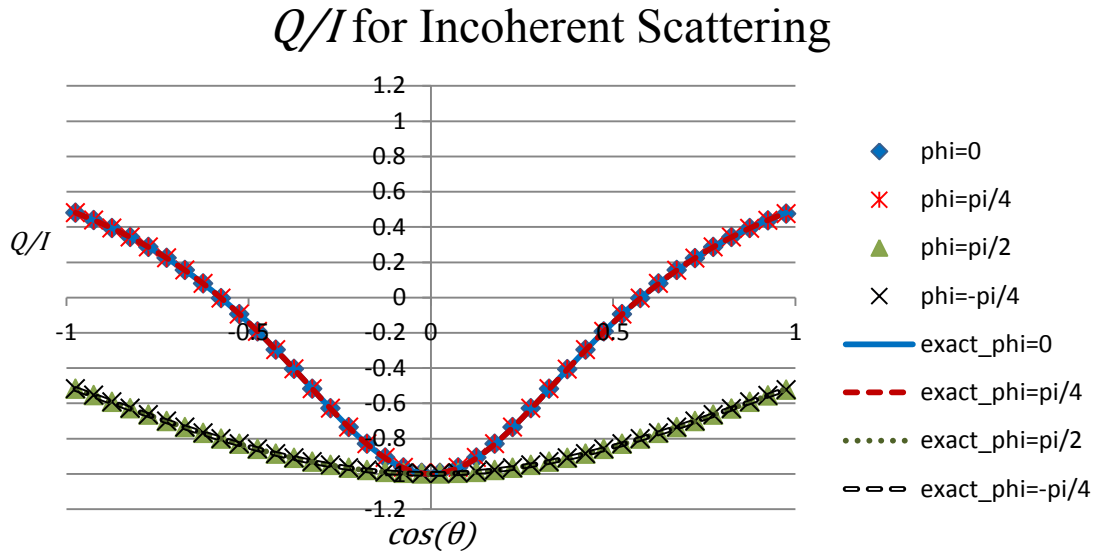

Figure A.112. Q/I for the incoherently scattered portion of a 5 keV photon beam with a source Stokes vector of $[\varphi_I, \varphi_Q, \varphi_U, \varphi_V] = [1,0.5,0.5,0]$.

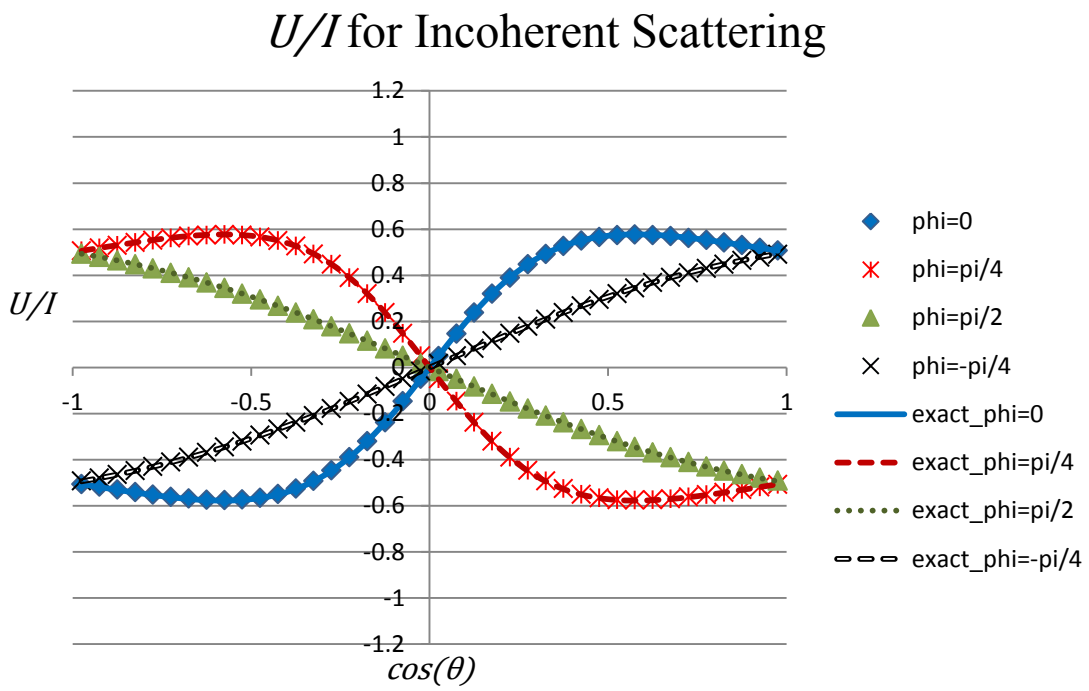

Figure A.113. U/I for the incoherently scattered portion of a 5 keV photon beam with a source Stokes vector of $[\varphi_I, \varphi_Q, \varphi_U, \varphi_V] = [1,0.5,0.5,0]$.

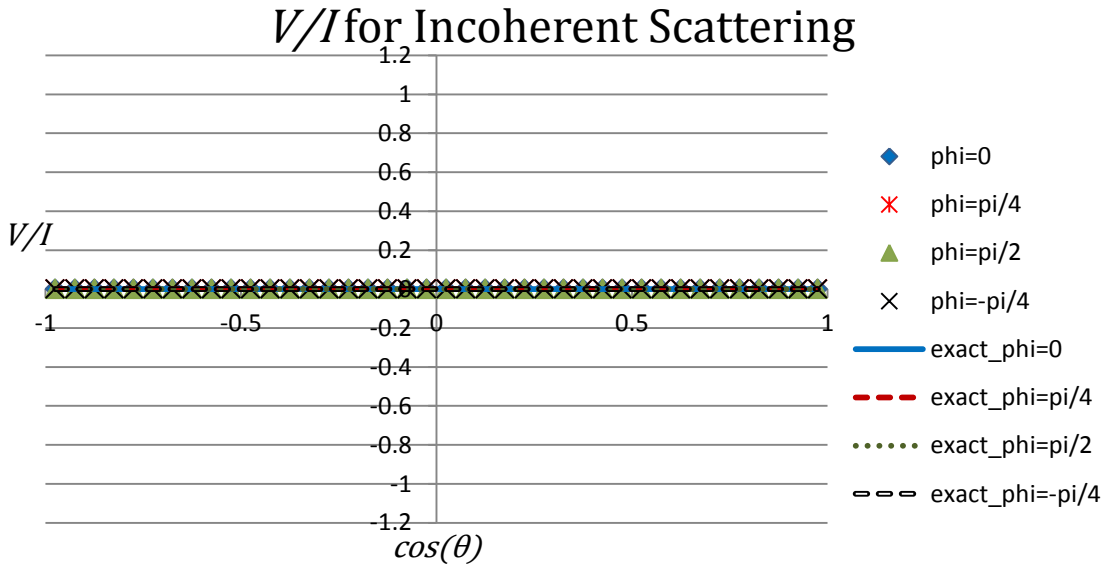

Figure A.114. V/I for the incoherently scattered portion of a 5 keV photon beam with a source Stokes vector of $[\varphi_I, \varphi_Q, \varphi_U, \varphi_V] = [1,0.5,0.5,0]$.

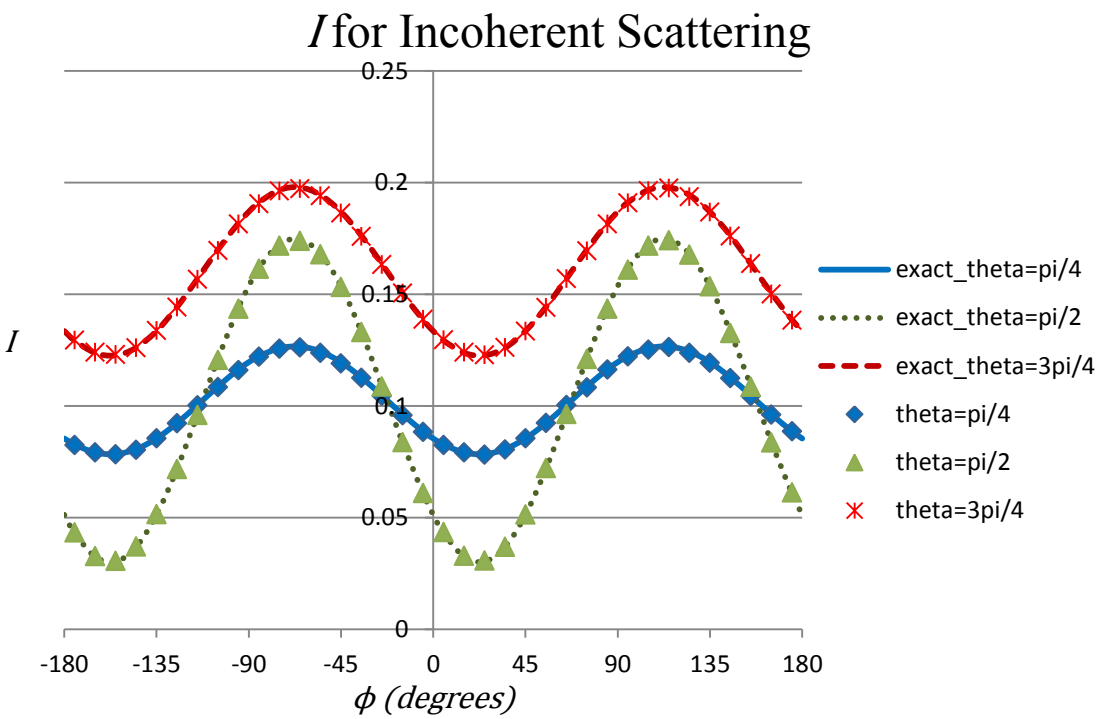

Figure A.115. I for the incoherently scattered portion of a 5 keV photon beam with a source Stokes vector of $[\varphi_I, \varphi_Q, \varphi_U, \varphi_V] = [1,0.5,0.5,0]$.

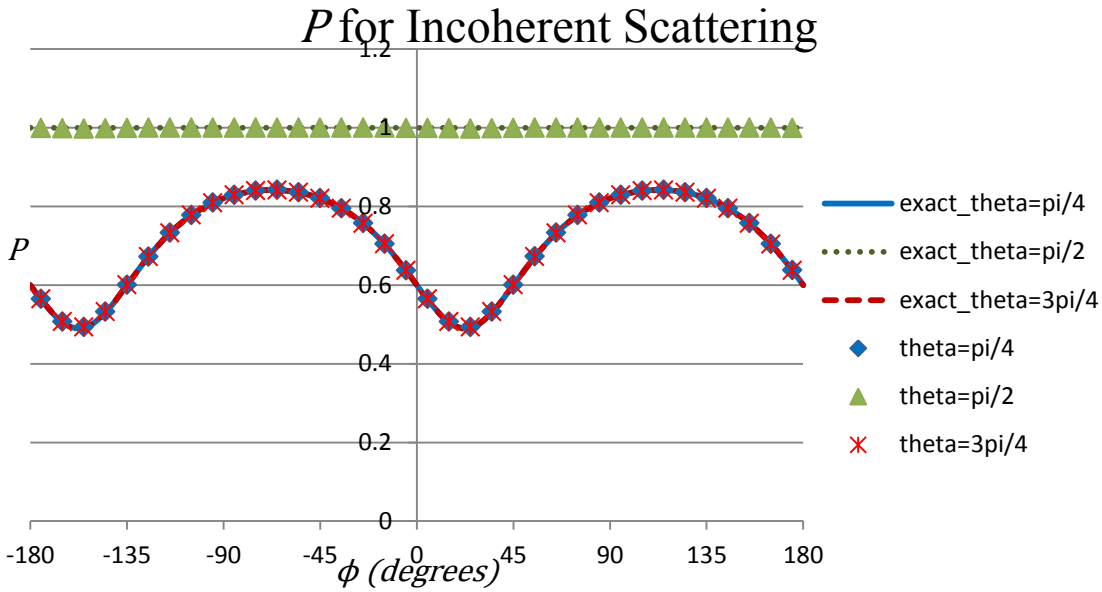

Figure A.116. P for the incoherently scattered portion of a 5 keV photon beam with a source Stokes vector of $[\varphi_I, \varphi_Q, \varphi_U, \varphi_V] = [1,0.5,0.5,0]$.

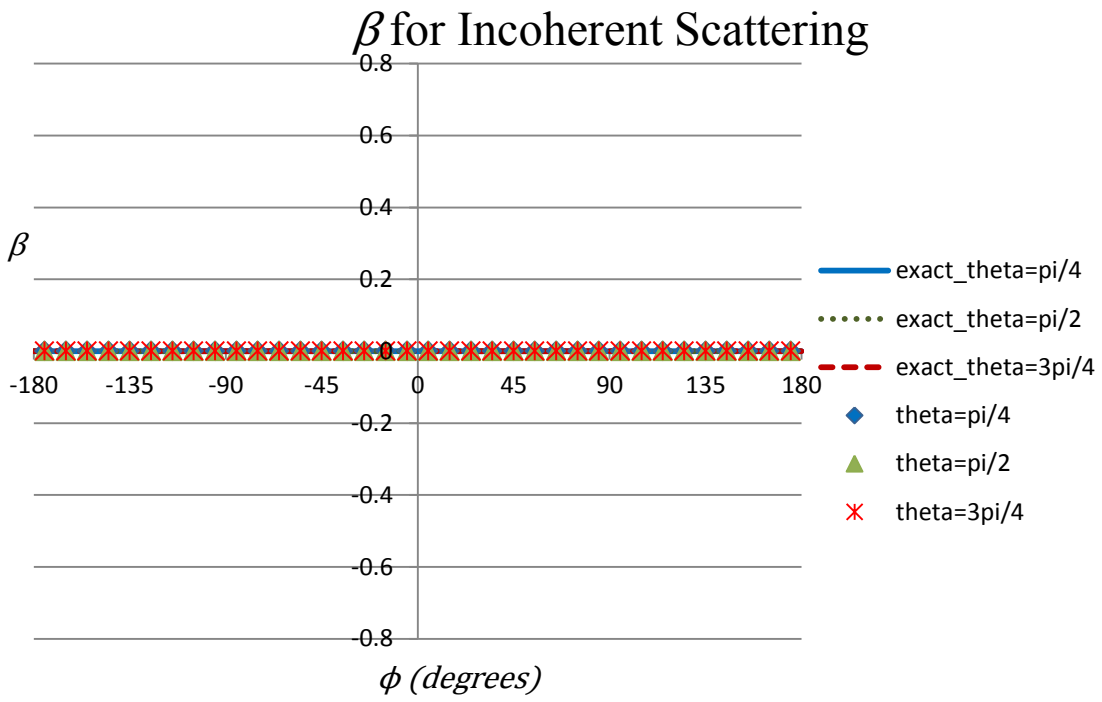

Figure A.117. β for the incoherently scattered portion of a 5 keV photon beam with a source Stokes vector of $[\varphi_I, \varphi_Q, \varphi_U, \varphi_V] = [1,0.5,0.5,0]$.

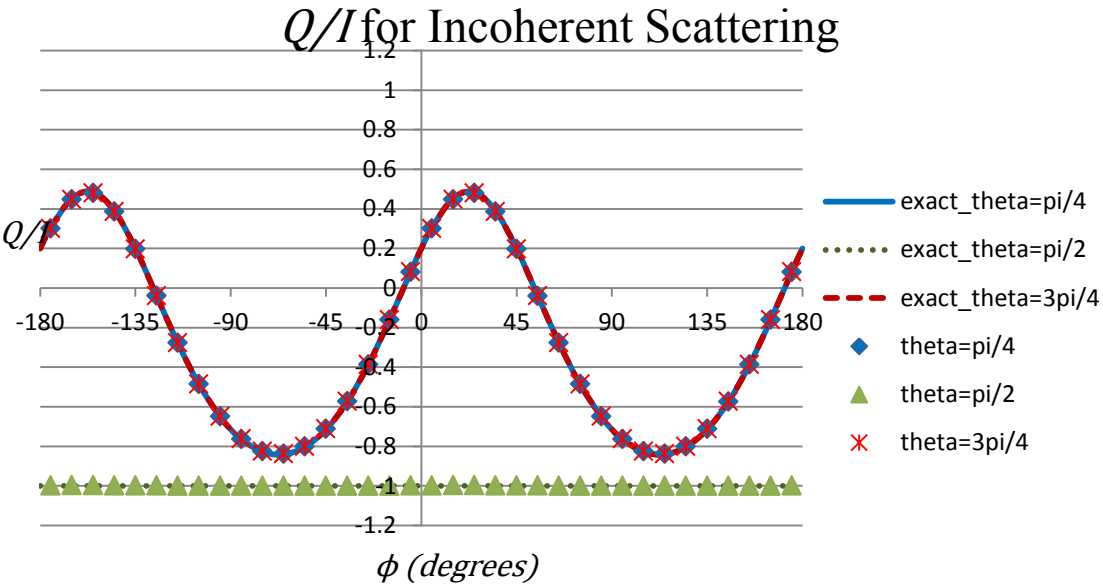

Figure A.118. Q/I for the incoherently scattered portion of a 5 keV photon beam with a source Stokes vector of $[\varphi_I, \varphi_Q, \varphi_U, \varphi_V] = [1,0.5,0.5,0]$.

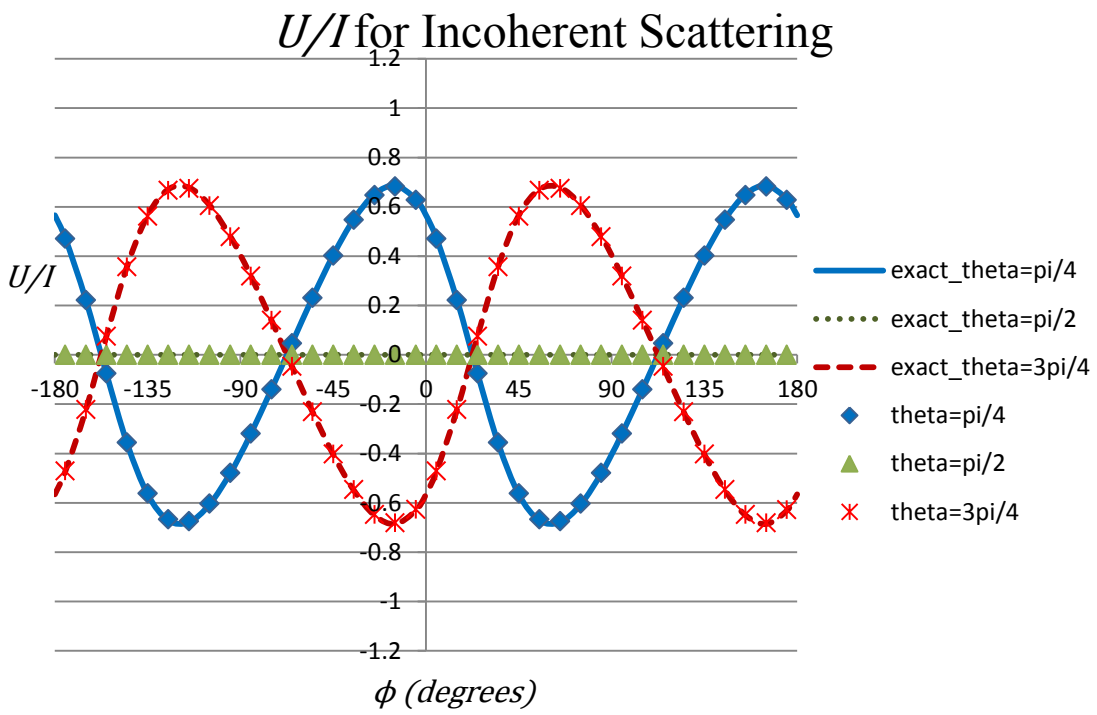

Figure A.119. *U/I* for the incoherently scattered portion of a 5 keV photon beam with a source Stokes vector of $[\varphi_I, \varphi_Q, \varphi_U, \varphi_V] = [1,0.5,0.5,0]$.

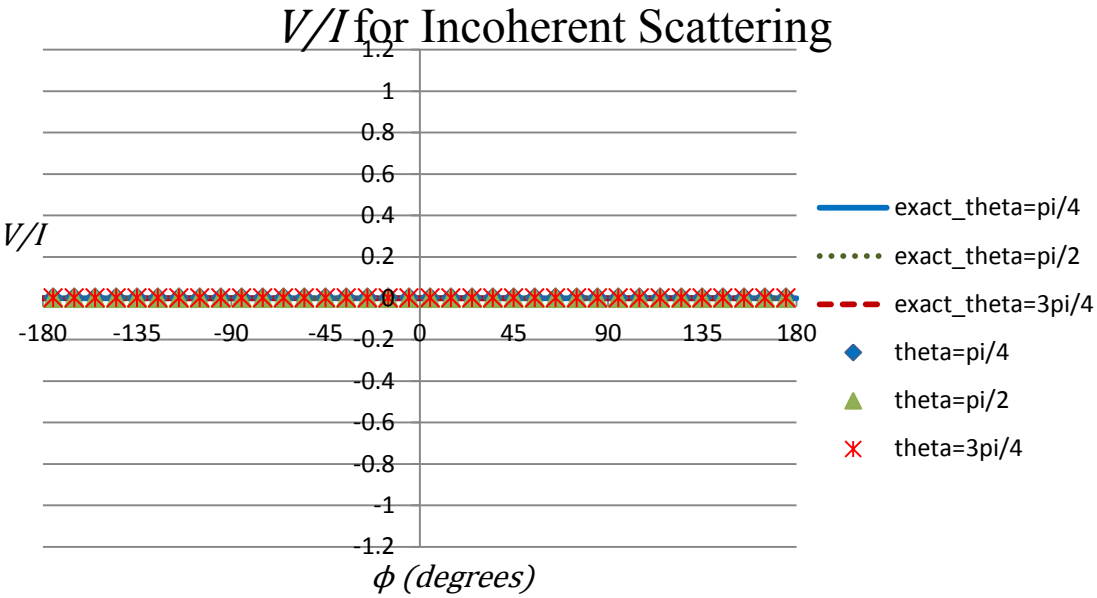

Figure A.120. *V/I* for the incoherently scattered portion of a 5 keV photon beam with a source Stokes vector of $[\varphi_I, \varphi_Q, \varphi_U, \varphi_V] = [1,0.5,0.5,0]$.

APPENDIX B

IMPLEMENTATION INTO A DETERMINISTIC TRANSPORT CODE

While the scope of this project was to implement polarization effects into the Mercury Monte Carlo code, additional work was done to determine how polarization effects could be implemented into a deterministic transport code called PDT (Parallel Deterministic Transport). This work has not been fully completed, but significant progress has been made, and that progress will be detailed in this appendix.

In PDT, the scalar transport equation given in Eq. 2 is solved by discretizing the equation in energy, space, and direction.

$$\vec{\Omega}\cdot\vec{\nabla}I(\vec{r},\vec{\Omega},E)+\ \sigma_t I(\vec{r},\vec{\Omega},E) = \int_0^\infty dE' \int_{4\pi} d\Omega'\,\sigma_s(\overrightarrow{\Omega'},\vec{\Omega},E',E)I(\vec{r},\vec{\Omega}',E')\ +\ \Gamma(\vec{r},\vec{\Omega},E) \quad \text{Eq. 92}$$

In order to implement polarization effects, the vector transport equation given in Eq. 3 needs to be solved.

$$\vec{\Omega}\cdot\vec{\nabla}\boldsymbol{I}(\vec{r},\vec{\Omega},E)+\ \sigma_t \boldsymbol{I}(\vec{r},\vec{\Omega},E) = \int_0^\infty dE' \int_{4\pi} d\Omega'\,\boldsymbol{H}(\overrightarrow{\Omega'},\vec{\Omega},E',E)\boldsymbol{I}(\vec{r},\vec{\Omega}',E')\ +\ \boldsymbol{\Gamma}(\vec{r},\vec{\Omega},E) \quad \text{Eq. 93}$$

This is not as troublesome as it might sound at first. Since PDT already discretizes the equation into multiple energy groups, the solvers in the code are already solving a vector equation of sorts, but instead of a vector of for four different Stokes

parameters the code is solving for a vector of multiple energy groups. Therefore, implementing polarization effects would just consist of expanding the number of groups by a factor of four. So what used to be a 2-group problem would now look like an 8-group problem to the code. From here on out, "groups" will refer to the total number of groups as seen by the code. So in the problem mentioned above, there are eight groups but two energy ranges. Eq. B.1 shows the expansion from the 2-group problem to the 8-group problem.

$$\begin{pmatrix} I_1 \\ I_2 \end{pmatrix} \rightarrow \begin{pmatrix} \boldsymbol{I_1} \\ \boldsymbol{I_2} \end{pmatrix} = \begin{pmatrix} I_1 \\ Q_1 \\ U_1 \\ V_1 \\ I_2 \\ Q_2 \\ U_2 \\ V_2 \end{pmatrix} \qquad \text{Eq. B.1}$$

However this presents its own new set of problems. Since the number of groups is being expanded by four, there are now four times as many groups for which cross sections needs to be known. For the total cross section this is simple because the total cross section affects each Stokes parameter the same way. So the expansion of the total cross section consists of copying each cross section four times. This can be seen in Eq. B.2

$$\begin{pmatrix} \sigma_{t_1} \\ \sigma_{t_2} \end{pmatrix} \rightarrow \begin{pmatrix} \sigma_{t_1} \\ \sigma_{t_1} \\ \sigma_{t_1} \\ \sigma_{t_1} \\ \sigma_{t_2} \\ \sigma_{t_2} \\ \sigma_{t_2} \\ \sigma_{t_2} \end{pmatrix} \qquad \text{Eq. B.2}$$

The scattering term is where all of the difficulties reside. This should not be a surprise since scattering events are where polarization effects are present. Before delving into the approach for including polarization effects, it is useful to demonstrate how PDT treats the scattering term before polarization. The scattering term for a specific group can be seen below.

$$S_g(\vec{\Omega}) = \sum_{g'=1}^{G} \int_{4\pi} d\Omega' \, \sigma_{s,g'g}(\overrightarrow{\Omega'} \rightarrow \vec{\Omega}) I_{g'}(\vec{\Omega}') \qquad \text{Eq. B.3}$$

where S_g is the scattering term for group$g$, $\sigma_{s,g'g}$ is the scattering kernel for scatters that go from group g' to group g, and G is the total number of groups. A simplifying assumption that can be made is to assume that $\sigma_{s,g'g}$ is only dependent on $\overrightarrow{\Omega'} \cdot \vec{\Omega}$ which will be referred to as μ_0 from here on out. From here PDT expands the cross section using the Legendre polynomials as a basis for expansion. The expansion can be seen below.

$$\sigma_{s,g'g}(\mu_0) = \sum_{l=0}^{\infty} \frac{(2l+1)}{2} \sigma_{s,g'g,l} P_l(\mu_0) \qquad \text{Eq. B.4}$$

$$\sigma_{s,g'g,l} = \int_{-1}^{1} d\mu_0 \sigma_{s,g'g}(\mu_0) P_l(\mu_0) \qquad \text{Eq. B.5}$$

where $\sigma_{s,g'g,l}$ are cross section moments that are part of the input deck for PDT and P_l are Legendre polynomials. The summation in Eq. B.4 goes to infinite, but in reality the summation is truncated to whatever order the user desires to run the problem. The intensity is also expanded, but since it ranges over the entire unit sphere it is expanded in terms of spherical harmonics.

$$I_{g'}(\overrightarrow{\Omega'}) = \sum_{k=0}^{\infty} \sum_{n=-k}^{k} I_{g',kn}\, Y_{kn}(\overrightarrow{\Omega'}) \qquad \text{Eq. B.6}$$

$$I_{g',kn} = \int_{4\pi} d\Omega' I_{g'}(\overrightarrow{\Omega'})\, Y_{kn}^{*}(\overrightarrow{\Omega'}) \qquad \text{Eq. B.7}$$

where $I_{g',kn}$ are intensity moments, Y_{kn} are spherical harmonic functions, and the * represents the complex conjugate. Using these expansions the scattering term can be written as seen in Eq. B.8.

$$S_g = \sum_{g'=1}^{G} \sum_{l=0}^{\infty} \sum_{k=0}^{\infty} \sum_{n=-k}^{k} \frac{(2l+1)}{2} \sigma_{s,g'g,l} I_{g',kn} \int_{4\pi} d\Omega'\, P_l(\mu_0) Y_{kn}(\overrightarrow{\Omega'}) \qquad \text{Eq. B.8}$$

Using the Spherical Harmonic Addition theorem, the Legendre polynomial in Eq. B.8 can be expressed in terms of spherical harmonics.

$$P_l(\mu_0) = P_l(\overrightarrow{\Omega'} \cdot \overrightarrow{\Omega}) = \sum_{m=-l}^{l} \frac{4\pi}{2l+1} Y_{lm}^{*}(\overrightarrow{\Omega'}) Y_{lm}(\overrightarrow{\Omega}) \qquad \text{Eq. B.9}$$

Now the scattering term can be expressed in a way that utilizes the orthonormality of spherical harmonic functions.

$$S_g = \sum_{g'=1}^{G} \sum_{l=0}^{\infty} \sum_{m=-l}^{l} \sum_{k=0}^{\infty} \sum_{n=-k}^{k} 2\pi \qquad \text{Eq. B.10}$$

$$* \sigma_{s,g'g,l} I_{g',kn}\, Y_{lm}(\overrightarrow{\Omega}) \int_{4\pi} d\Omega'\, Y_{lm}^{*}(\overrightarrow{\Omega'}) Y_{kn}(\overrightarrow{\Omega'})$$

$$S_g(\vec{\Omega}) = 2\pi \sum_{g'=1}^{G} \sum_{l=0}^{\infty} \sum_{m=-l}^{l} \sigma_{s,g'g,l} I_{g',lm} Y_{lm}(\vec{\Omega}) \qquad \text{Eq. B.11}$$

A similar but more complex approach to the scattering term must be taken when dealing with polarization effects. The difficulty arises from the fact that the assumption that the scattering kernel only depends on $\overrightarrow{\Omega'} \cdot \vec{\Omega}$. This assumption is incorrect when polarization effects are considered. Instead the scattering kernel is dependent on $\vec{\Omega}$ and $\overrightarrow{\Omega'}$ separately. Each of these direction vectors can be described by the cosine of their polar angles μ and μ' and their azimuthal angles ϕ and ϕ'. Recall the scattering term from Eq. 3 in the main text.

$$\boldsymbol{S}(\vec{\Omega}, E) = \int_0^{\infty} dE' \int_{4\pi} d\Omega' \, \boldsymbol{H}(\overrightarrow{\Omega'}, \vec{\Omega}, E', E) \boldsymbol{I}(\vec{\Omega}', E') \qquad \text{Eq. B.12}$$

Using Eq. 6-11 from the main text, $\boldsymbol{H}(\overrightarrow{\Omega'}, \vec{\Omega}, E', E)$ can be written in the following way.

$$\boldsymbol{H}(\overrightarrow{\Omega'}, \vec{\Omega}, E', E) = \sigma_s(\mu_0, E', E) \begin{bmatrix} 1 & h_{12} & h_{13} & 0 \\ h_{21} & h_{22} & h_{23} & 0 \\ h_{31} & h_{32} & h_{33} & 0 \\ 0 & 0 & 0 & h_{44} \end{bmatrix} \qquad \text{Eq. B.13}$$

Each h_{ij} term is dependent on μ, μ', E', E, and α, where $\alpha = \cos(\phi' - \phi)$, and using Eq. 6-11, the expression for each term can be determined. The term $\sigma_s(\mu_0, E', E)$ is the same scattering kernel used when polarization effects are not considered. It should also be noted that μ_0 can be expressed in terms of μ, μ', and α.

$$\mu_0 = \mu\mu' + \alpha\sqrt{1-\mu^2}\sqrt{1-\mu'^2} \qquad \text{Eq. B.14}$$

Since PDT deals with discreet energy groups instead of a continuous energy spectrum, the next step is to determine the values of the matrix in each energy range.

$$H_{g'g,ij}(\mu,\mu',\alpha) = \frac{\int_{E_{g-1}}^{E_g} dE \int_{E_{g'-1}}^{E_{g'}} dE'\, \sigma_s(\mu_0,E',E) h_{ij}(\mu,\mu',E',E,\alpha) w(E')}{\int_{E_{g'-1}}^{E_{g'}} dE' w(E')} \quad \text{Eq. B.15}$$

The input deck of PDT already gives the value of $\sigma_s(\mu_0,E',E)$ in each energy range, so Eq. B.15 can be simplified.

$$H_{g'g,ij}(\mu,\mu',\alpha) = \frac{\sigma_{s,g'g}(\mu_0) \int_{E_{g-1}}^{E_g} dE \int_{E_{g'-1}}^{E_{g'}} dE'\, h_{ij}(\mu,\mu',E',E,\alpha) w(E')}{\int_{E_{g'-1}}^{E_{g'}} dE' w(E')} \quad \text{Eq. B.16}$$

Returning to the example of a 2-group problem turning into an 8-group problem, the scattering matrix from the 2-group problem would be transformed from a 2x2 matrix to an 8x8 matrix.

$$\begin{pmatrix} \sigma_{s,1\to1} & \sigma_{s,2\to1} \\ \sigma_{s,1\to2} & \sigma_{s,2\to2} \end{pmatrix} \to \begin{pmatrix} H_{11,11} & H_{11,12} & H_{11,13} & H_{11,14} & \\ H_{11,21} & H_{11,22} & H_{11,23} & H_{11,24} & \boldsymbol{H_{21}} \\ H_{11,31} & H_{11,32} & H_{11,33} & H_{11,34} & \\ H_{11,41} & H_{11,42} & H_{11,43} & H_{11,44} & \\ & \boldsymbol{H_{12}} & & & \boldsymbol{H_{22}} \end{pmatrix} \quad \text{Eq. B.17}$$

$$\to \begin{bmatrix} \sigma_{s,11} & \cdots & \sigma_{s,81} \\ \vdots & \ddots & \vdots \\ \sigma_{s,18} & \cdots & \sigma_{s,88} \end{bmatrix}$$

The scattering term for polarization effects can now be rewritten similarly to Eq. B.3.

$$S_g(\vec{\Omega}) = \sum_{g'=1}^{G} \int_{4\pi} d\Omega'\, \sigma_{s,g'g}(\mu,\mu',\alpha) I_{g'}(\vec{\Omega}') \quad \text{Eq. B.18}$$

The same process of expanding the cross section and intensities in terms of Legendre polynomials and spherical harmonics is now used except this time the cross section is dependent on three variables instead of just one. The intensity is expanded in the same way as before.

$$\sigma_{s,g'g}(\mu,\mu',\alpha) = \sum_{l=0}^{\infty}\sum_{m=0}^{\infty}\sum_{a=0}^{\infty}\frac{(2l+1)(2m+1)(2a+1)}{8}\sigma_{s,g'g,lma}P_l(\mu)P_m(\mu')P_a(\alpha) \quad \text{Eq. B.19}$$

$$\sigma_{s,g'g,lma} = \int_{-1}^{1}d\mu\int_{-1}^{1}d\mu'\int_{-1}^{1}d\alpha\,\sigma_{s,g'g}(\mu,\mu',\alpha)P_l(\mu)P_m(\mu')P_a(\alpha) \quad \text{Eq. B.20}$$

The scattering term now looks similar to Eq. B.8

$$S_g = \sum_{g'=1}^{G}\sum_{l=0}^{\infty}\sum_{m=0}^{\infty}\sum_{a=0}^{\infty}\sum_{k=0}^{\infty}\sum_{n=-k}^{k}\frac{(2l+1)(2m+1)(2a+1)}{8}\sigma_{s,g'g,lma}I_{g',kn} \times P_l(\mu)\int_{4\pi}d\Omega'\,P_m(\mu')P_a(\alpha)Y_{kn}\left(\overrightarrow{\Omega'}\right) \quad \text{Eq. B.21}$$

The Spherical Harmonic Addition theorem can be used to expand $P_a(\alpha)$ into spherical harmonics similar to how $P_l(\mu_0)$ was expanded before. The only difference is that α is the dot product of the normalized projections of $\vec{\Omega}$ and $\overrightarrow{\Omega'}$ onto the x-y plane.

$$P_a(\alpha) = \sum_{b=-a}^{a}\frac{4\pi}{2a+1}Y_{ab}^{*}(\mu=0,\phi')Y_{ab}(\mu=0,\phi) \quad \text{Eq. B.22}$$

At this point, it is useful to give the equation for a spherical harmonic function in terms of Associated Legendre polynomials.

$$Y_{ab}(\mu,\phi) = \sqrt{\frac{(2a+1)(a-b)!}{4\pi(a+b)!}}P_{ab}(\mu)e^{ib\phi} \qquad \text{Eq. B.23}$$

Using Eq. B.21-B.23 the scattering term can be rewritten again.

$$S_g = \sum_{g'=1}^{G}\sum_{l=0}^{\infty}\sum_{m=0}^{\infty}\sum_{a=0}^{\infty}\sum_{b=-a}^{a}\sum_{k=0}^{\infty}\sum_{n=-k}^{k}\frac{(2l+1)(2m+1)\pi}{2}\sigma_{s,g'g,lma}I_{g',kn}$$

$$\times Y_{ab}(\mu=0,\phi)P_l(\mu)\int_{4\pi}d\Omega'\,P_m(\mu')Y^*_{ab}(\mu=0,\phi')Y_{kn}\left(\overrightarrow{\Omega'}\right) \qquad \text{Eq. B.24}$$

$$S_g = \sum_{g'=1}^{G}\sum_{l=0}^{\infty}\sum_{m=0}^{\infty}\sum_{a=0}^{\infty}\sum_{b=-a}^{a}\sum_{k=0}^{\infty}\sum_{n=-k}^{k}\frac{(2l+1)(2m+1)\pi}{2}\sigma_{s,g'g,lma}I_{g',kn}$$

$$\times\sqrt{\frac{(2a+1)(a-b)!}{4\pi(a+b)!}}\sqrt{\frac{(2k+1)(k-n)!}{4\pi(k+n)!}}Y_{ab}(\mu=0,\phi')P_l(\mu)P_{ab}(0) \qquad \text{Eq. B.25}$$

$$\times\int_0^{2\pi}d\phi'\int_{-1}^{1}d\mu'\,P_m(\mu')e^{-ib\phi'}P_{kn}(\mu')e^{in\phi'}$$

In Eq. B.25 b and n must be equal to each or the $d\phi'$ integral will be zero.

Therefore Eq. B.25 can be simplified slightly.

$$S_g = \sum_{g'=1}^{G}\sum_{l=0}^{\infty}\sum_{m=0}^{\infty}\sum_{a=0}^{\infty}\sum_{k=0}^{\infty}\sum_{n=-k}^{k}\frac{(2l+1)(2m+1)\pi}{4}\sigma_{s,g'g,lma}I_{g',kn}$$

$$\times\sqrt{\frac{(2a+1)(a-n)!}{(a+n)!}}\sqrt{\frac{(2k+1)(k-n)!}{(k+n)!}}Y_{an}(\mu=0,\phi')P_l(\mu)P_{an}(0) \qquad \text{Eq. B.26}$$

$$\times\int_{-1}^{1}d\mu'\,P_m(\mu')P_{kn}(\mu')$$

The scattering term can be reduced even further because $Y_{an}(\mu = 0, \phi')$ and $P_{an}(0)$ equal zero unless $a = |n|$. The final simplified expression for the scattering term can be seen in Eq. B.27.

$$S_g = \sum_{g'=1}^{G} \sum_{l=0}^{\infty} \sum_{m=0}^{\infty} \sum_{k=0}^{\infty} \sum_{n=-k}^{k} \frac{(2l+1)(2m+1)\pi}{4} \sigma_{s,g'g,lm|n|} I_{g',kn}$$

$$\times \sqrt{\frac{(2|n|+1)(|n|-n)!}{(|n|+n)!}} \sqrt{\frac{(2k+1)(k-n)!}{(k+n)!}} Y_{|n|n}(\mu = 0, \phi') P_l(\mu) P_{|n|n}(0) \quad \text{Eq. B.26}$$

$$\times \int_{-1}^{1} d\mu' \, P_m(\mu') P_{kn}(\mu')$$

While this scattering term is much messier than the one in Eq. B.11, it is still very manageable for the code. The summations are not intractable because they are cut off at whatever order the problem is being run at, and the moments are only calculated once at the beginning of the run.

Outside of expanding the problem by a factor of four, the scattering term is the only term that is affected by the inclusion of polarization. Any source terms are easy to manage because the source Stokes vector replaces the source intensity for each energy range. After the simulation is completed, some post processing will be necessary to express the solution in terms of Stokes vectors at each original energy range instead of just intensities at four times as many energy ranges. One of the biggest advantages of this formulation is that no additional information is needed in the input file of PDT.

As of the writing of this appendix, this method has not been implemented or tested, but the mathematics is sound and should work with proper implementation.